



The University of
Nottingham

UNITED KINGDOM · CHINA · MALAYSIA

Division of Infrastructure, Geomatics & Architecture
Faculty of Engineering

**Investigation of High Capacity Heat Energy
Storage for Building Applications**

YATE DING

(BEng, MSc)

**Thesis submitted to The University of Nottingham
for the degree of Doctor of Philosophy**

December 2013

To my parents, my wife, my daughter and son

ABSTRACT

The problems of excessive consumption of fossil resources, oil shortages and greenhouse gas emissions are becoming increasingly severe. Research and development work on new methods of thermal energy storage are imminently required. To effectively store seasonal renewable energy, a novel high capacity heat storage system has been designed and evaluated/validated through laboratory experiments and numerical simulations in this research. The system is driven by direct flow evacuated tube solar collector with enhanced PCM tank and intends to be applied in residential and commercial buildings.

Theoretical and experimental approaches and numerical analysis have been employed in this study. Firstly, phase change materials (PCM) with specific heat density, melting point, melting and solidifying time have been investigated. This type of PCMs can maintain a considerable high internal temperature of environment chamber in a frozen ambient temperature. Numerical modelling has been conducted on a passive house (Nottingham H.O.U.S.E) to study whether proposed thermochemical materials can cover relative heating load and be power by solar panel in terms of roof size. Meanwhile, PCMs have been used to give a long duration for temperature-controlled chamber in laboratory, and thermochemical materials have been utilized in closed pumping pipe system for cooling and heating purpose.

Secondly, characteristic experiments have been conducted on a modified solar collector working with an enhanced PCM tank that is integrated with a fan coil heat exchanger. The results show that light radiation of tungsten lamps (as a solar simulator) has approximately 70% efficiency to equate to

solar radiation under the same Pyranometer reading value. At the same time, the solar system can supply over 50°C heating energy and the PCM tank within it can supply higher output temperature with longer duration than water tank. The efficiency of the whole solar collector heating system is over 50% as a heat absorption chamber in sunny days, while only approximately 10% under mostly cloudy weather.

Lastly, proposed thermochemical materials (silica gel, calcium chloride, zeolite 13x, vermiculite and activated carbon) have been evaluated on designed thermochemical absorption chamber to supply fresh high temperature air for space heating. The results show that zeolite holds the highest reacted temperature (over 58°C) and vermiculite has really fast absorbing hydration duration, less than half hour. Silica gel possesses the biggest water absorbing capacity and vermiculite has a worse result. A comparison between experimental and numerical modelling results has been revealed. Considering the complexity of processes in cooling and heating system, the agreement of simulation and experimentation is satisfactory, thus the lumped numerical model is acceptable and significant for investigation of this scaled seasonal high capacity heat storage system.

A full size seasonal heat storage system with a nominal heating capacity of 3kW has been proposed and illustrated in economic and environmental issues section. The results from net present value (NPV) and internal rate of return (IRR) sensitivity analysis both shows it is greatly attractive to develop this novel system for application in both household and commercial buildings in consideration of its about 9 years payback period, 20 years life span and zero gas (CO₂) emissions. An intelligent transpired solar collector system is also introduced and illustrated as future work.

LIST OF PUBLICATIONS

Ding Yate, Riffat Saffa, 2012, Thermochemical Energy Storage Technologies for Building Applications: a State-of-the-art Review, *The International Journal of Low-Carbon Technologies* 2012, 1-11, doi:10.1093/ijlct/cts004.

Riffat Saffa, Su Yuehong, **Ding Yate**, 2013, Thermochemical cooling system based on adsorption pumping pipe, *The International Journal of Low-Carbon Technologies* 2013, 1-7, doi:10.1093/ijlct/ctt055.

Ding Yate, Riffat Saffa, 2013, Experimental Investigation on a Novel Thermochemical Absorption Cooling System, In: *12th International Conferences on Sustainable Energy Technologies (SET-2013)*, 26-29 August, Hong Kong, China.

Ding Yate, Riffat Saffa, 2013, Experimental Investigation of Thermal Controlled Packaging from Phase Change Materials, In: *12th International Conferences on Sustainable Energy Technologies (SET-2013)*, 26-29 August, Hong Kong, China

Ding Yate, Riffat Saffa, Agyenim Francis, 2012, Thermal Energy Storage Technologies with Thermochemical and Phase Change Materials: a state-of-the-art Review, In: *11th International Conferences on Sustainable Energy Technologies (SET-2012)*, 2-5 September, Vancouver, Canada, ISBN: 0-9781236-1-2

Submitted:

Ding Yate, Riffat Saffa, 2014, Experimental Investigation on the Performance of Solar Collector System to Power Desiccant Storage System for Building Application, Submitted for: *13th International Conferences on Sustainable Energy Technologies (SET-2014)*, 25-28 August, Geneva, Switzerland

Ding Yate, Riffat Saffa, 2014, Modelling Passive House for Thermochemical Materials Energy Storage, Submitted for: *13th International Conferences on Sustainable Energy Technologies (SET-2014)*, 25-28 August, Geneva, Switzerland

ACKNOWLEDGEMENTS

First and foremost, I would like to express my sincere thanks and gratitude to Professor Saffa Riffat for his immeasurable and invaluable guidance, support and advice throughout the duration of this research. Further thanks go to Professor Siddig Omer, Dr. Francis Agyenim, Dr. Sean Casey and Dr. Mark Worall, for their technical advice and dedicated involvement. I would also extend my thanks to the staff of the Department of Architecture and Built Environment, the Faculty of Engineering of the University of Nottingham for providing help, information and experiment facilities required for this project, especially to Mr David Oliver, and Mrs Amante-Roberts Zeny. Without their help, I would not have been this far.

I also wish to acknowledge Mr Kevin Simpson and the financial support from European Thermodynamics Ltd. and the project of Interseasonal Thermochemical Renewable Energy Storage Systems (INTRESTS) funded by Technology Strategy Board (TSB) of the UK.

I am greatly indebted to all friends in Nottingham for their precious friendship and sharing their experiences on how to develop an interdisciplinary research work as an independent academic.

Last but not least, I would especially like to thank my parents, sisters and brothers for their endless help and support throughout all of my education. Special thanks go to my wife Dr. Yudan Jia, my daughter Xixi Ding and son Chenbei Ding. Absolutely, without your great love I would not have been here and so confident with myself today.

CONTENT

ABSTRACT	i
LIST OF PUBLICATIONS	iii
ACKNOWLEDGEMENTS	iv
CONTENT	v
NOMENCLATURE	xiv
LIST OF FIGURES	xvii
LIST OF TABLES	xxvi

Chapter 1: Introduction

1.1 Background	1
1.2 Topic of the Study	2
1.3 Global Energy Retrospect and Prospect	2
1.3.1 Energy Resources and Energy Consumption	2
1.3.2 Global Energy Crisis and Climate Change	5
1.3.2.1 Global Energy Crisis and the Move to Alternative	5
1.3.2.2 Climate Change and the Environment	6
1.4 The Fundamentals of High Capacity Heat Storage Technologies	7
1.5 Novelty and Timeliness of the Research	8
1.6 Objectives and Structure of the Research	9
1.6.1 Objectives of the Study	9
1.6.2 Structure of the Research	10

Chapter 2: Literature Review on Thermal Energy Storage and Solar Energy Collection Systems

2.4.5	Chemical Heat Pump (CHP) Storage Systems	46
2.5	Performance of Thermochemical Energy Storage Techniques	50
2.6	Solar Energy Collection Systems	53
2.6.1	Evacuated Tube Collectors	54
2.6.1.1	Heat Pipe Evacuated Tube Collector	56
2.6.1.2	Direct Flow Evacuated Tube Collector	57
2.7	Summary	59
Chapter 3: Theoretical Analysis and Computer Simulation for Thermal Energy Storage		
3.1	Introduction	62
3.2	Introduction to Nottingham H.O.U.S.E	64
3.3	Modelling Passive House	65
3.3.1	Simulation Target Statement	65
3.3.2	Simulation Setting	67
3.3.2.1	Calendar	67
3.3.2.2	Construction Materials	68
3.3.2.3	Zoning	68
3.3.3	Simulation Results Analysis and Discussion	70
3.4	Numeration of Seasonal Thermal Storage System	72
3.4.1	Thermochemical Energy Storage Materials Sizing	72
3.4.2	Solar Thermal Collector Sizing	75
3.5	Summary	78
Chapter 4: Materials Selection and Preliminary Experiment		
4.1	Introduction	79
4.2	PCMs Selection	80
4.2.1	Properties and Characteristics Testing of PCMs	80

4.2.1.1	Experiment Rig Set-up	80
4.2.1.2	PCMs Testing Result Analysis and Discussions	81
4.2.1.3	Summary of Discussions and Results	86
4.2.2	Thermal Energy Storage Testing from PCM	87
4.2.2.1	Experiment Rig Set-up	87
4.2.2.2	Experiment Operation and Procedure	92
4.2.2.3	Experiment Results Analysis and Discussions	93
4.3	Preliminary Experiments to Study PCMs and Thermochemical Materials Energy Storage System	95
4.3.1	Experimental Investigation on Thermal Controlled Chamber from PCMs	95
4.3.1.1	Experiment Rig Set-up	96
4.3.1.2	Experiment Results and Discussion	98
4.3.1.3	Thermal Images Analysis of TCC Chamber	100
4.3.1.4	Conclusion	104
4.3.2	Experimental Investigation on a Closed Thermochemical Absorption Cooling System	104
4.3.2.1	Experiment Rig Set-up	106
4.3.2.2	Experiment Results and Discussion	108
4.3.2.3	Comparison of Experimentation and Simulation	113
4.3.2.4	Conclusion	114
4.4	Summary of Results from Preliminary Experiments	115

**Chapter 5: Experimental Investigation on the Performance of
High Capacity Heat Storage System**

5.1	Introduction	116
5.2	Main Experiment Model Design and Test Rig Set-up	117

5.2.1	Experiment Model Design	117
5.2.2	Experiment Rig Set-up	119
5.2.2.1	Enhanced Solar Collector Heating System	119
5.2.2.2	Open Thermochemical Energy Storage System	123
5.3	Experiment Procedure and Operating Parameters	127
5.3.1	Solar Collector Heating System	127
5.3.2	Open Thermochemical Energy Storage System	128
5.4	Experiment Measurements and Data Acquisition	129
5.4.1	Instrumentation and Measurements	129
5.4.1.1	Temperature Measurement	129
5.4.1.2	Solar Radiation Measurement	130
5.4.1.3	Relative Humidity Measurement	131
5.4.1.4	Measuring the Pressures	132
5.4.1.5	Measuring Weight Change and Air Flow Rates	133
5.4.2	Measurements and the Corresponding Instruments	134
5.4.3	Instruments Calibration	136
5.4.3.1	Calibration of Thermocouples	136
5.4.3.2	Calibration of Weight Sensors (Load Cells)	137
5.5	Summary	139

Chapter 6: Experiment Results and Discussions on Enhanced Solar Collector System

6.1	Introduction	140
6.2	Experiment Results on Fundamental Solar Collector Heating System	140
6.2.1	Solar Collector System Dimensioning	141
6.2.1.1	Selection of Radiation Intensity for Solar Collector System	142

6.2.1.2	Effect of Fan Speed on Heating Temperature	143
6.2.2	Water Tank System Heated by Light Radiation	143
6.2.3	Water Tank System Heated by Solar Energy	144
6.2.4	Comparison of the Light Radiation and Solar Energy on Water Tank Systems	147
6.3	Experiment Results on Solar Collector Heating System Integrated with PCM	149
6.3.1	PCM Tank System Heated by Light Radiation	149
6.3.2	PCM Tank System Heated by Solar Energy	151
6.4	Comparison of Water and PCM System Heated by Solar Energy	152
6.4.1	Experimental Analysis on Differences Between Water and PCM Solar Collector Systems	152
6.4.2	Mathematical Analysis on Heating Storage Capacities of Water and Proposed PCM Solar Collector Systems	155
6.5	Analysis on Efficiency of Solar Collector Heating System	157
6.5.1	Efficiency Change of Solar Collector System in a Sunny Day	159
6.5.2	Efficiency Change of Solar Collector System in a Mostly Cloudy Weather	161
6.6	Summary of Results and Conclusion	163

Chapter 7: Results and Discussions on Seasonal Thermochemical Energy Storage System

7.1	Introduction	164
7.2	Experiment Results on Thermochemical Absorption Systems for Hydration Heat Generation	164
7.2.1	Evaluation of Proposed Thermochemical Materials	164
7.2.1.1	Silica Gel (SiO_2 , white)	164

7.2.1.2	Calcium Chloride (CaCl_2)	169
7.2.1.3	Zeolite 13X	173
7.2.1.4	Vermiculite	176
7.2.1.5	Activated Carbon	180
7.2.2	Comparison of Selected Adsorbents in Hydration Heating Process	183
7.3	Experiment Results on Dehydration Process of Thermochemical Energy Storage System Regeneration	185
7.3.1	Investigation on Thermochemical Energy Storage System with Different Absorbents	185
7.3.1.1	Silica Gel Chamber	185
7.3.1.2	Zeolite 13X Chamber	188
7.3.1.3	Vermiculite Chamber	190
7.3.1.4	Activated Carbon Chamber	192
7.3.2	Comparison of Thermochemical Energy Storage System with Different Absorbents	194
7.4	Comparison of Simulation and Experimentation on Thermochemical Materials Energy Storage Systems	196
7.4.1	Principles for Thermochemical Energy Storage Pumping Pipe System	196
7.4.2	Results Discussion on Experimentation and Simulation	198
7.5	Energy Balance Analysis on Seasonal Thermochemical Energy Storage System Integrated with Solar Collector	200
7.5.1	Heating Energy from Fan Coil Heater Powered by Enhanced Solar Collector	200
7.5.2	Heating Energy Demand on Endothermic Dehydration Process of Absorbents	201
7.6	Summary of Results and Conclusion	202

Chapter 8: Economic, Environmental Analysis and Recommendation	
8.1 Introduction	204
8.2 Economic and Environmental Analysis	204
8.2.1 Economic Analysis	204
8.2.1.1 Capital Cost Comparison with Conventional Heating System of Household	205
8.2.1.2 Estimation of the Cost Payback Period and Life Cycle Cost Saving	207
8.2.2 Environmental Analysis	211
8.3 Recommendation	212
8.3.1 Intelligent Transpired Solar Collector System	212
8.3.2 Seasonal Thermochemical Heat Storage System Integrated with Transpired Solar Collector	213
8.3.2.1 Summer Season Cooling Mode (charging cycle)	213
8.3.2.2 Winter Season Heating Mode (discharging cycle)	214
8.4 Summary	216
Chapter 9: Conclusions and Future Work	
9.1 Summary of the Work	217
9.2 Conclusions	218
9.2.1 Temperature Controlled High Capacity Heat Energy Storage System	218
9.2.2 PCMs Enhanced Solar Collector Heating System	220
9.2.3 Open Thermochemical Energy Storage System	221
9.2.4 3kW Solar-Driven High Capacity Heat Storage System	222
9.3 Potential Improvement and Future Work	222
REFERENCES	224
APPENDICES	239

NOMENCLATURE

Symbol	Term	Units
A	Area	m^2
a_m	Mass fraction	%
B_i	Biot number,	
b_0	Incidence angle modifier constant	
C	Concentration ratio	
C_l	Coefficient of the efficiency	
C_o	Intercept efficiency	%
C_{count}	Counts of water flow per second	
c_p	Specific heat capacity	$\text{kJ/kg}\cdot\text{K}$
d	Diameter	m
F_o	Fourier number	
G	Solar irradiance	W/m^2
G_r	Grashof number	
G_{test}	Flow rate per unit area at test	$\text{kg/s}\cdot\text{m}^2$
g	Acceleration due to gravity	m/s^2
h	Heat transfer coefficient	$\text{W/m}^2\cdot\text{K}$
h_m	Heat of fusion	kJ/kg
H	Specific heat	$\text{J/kg}\cdot\text{K}$
k	Thermal conductivity	$\text{W}/(\text{m}\cdot\text{K})$
k_{pump}	Water pump meter K factor	p/lit
l	Length	m
m	Mass	kg
N_u	Nusselt number	

P_r	Prandtl number	
Q	Energy	J
Q_i	Input energy	J
Q_l	Heat losses	J
Q_u	Useful energy	J
q	Heat flux	W/m ²
R	Thermal resistance	(m ² ·K)/W
R_a	Rayleigh number	
R_e	Reynold number	
r	Radius	m
S_{te}	Stefan number or liquid superheating	
T	Temperature	°C
ΔT	Temperature difference	°C
t	Time	s
T_f	Final temperature	°C
T_i	Initial temperature	°C
T_m	Melting temperature	°C
v	Velocity components	m/s
V	Volume	m ³
Greek Letter	Term	Units
η	Efficiency	%
ε	Emissivity, emmittance	
τ	Transmissivity, or transmittance	
ρ	Density	kg/m ³
ν	Kinematic viscosity	m ² /s
λ	Thermal conductivity	W/(m·K)

Subscripts and superscripts

<i>a, air</i>	Air
<i>c</i>	Can
CHP	Chemical heat pumps
COP	Coefficient of performance
<i>count</i>	Counts of water pipe per second
<i>eq</i>	Equation
<i>f</i>	Fan coil heat exchanger
<i>fin</i>	Final
<i>in</i>	Inlet
<i>l</i>	Liquid phase
<i>mp</i>	melting phase
<i>out</i>	Outlet
<i>p</i>	Phase change materials
<i>pcm</i>	Phase change materials, PCM
<i>ref</i>	reference
<i>s</i>	solid phase or solar
TC	Can and thermocouple
TES	Thermal energy storage
<i>w</i>	water

LIST OF FIGURES

Figure 1.1 Fuel Shares of World Total Primary Energy Supply (OECD/IEA, 2012)	4
Figure 1.2 Evolution from 1971 to 2008 of world total final consumption by region (Mtoe)	4
Figure 1.3 Transforming the global energy mix: the exemplary path until 2050/2100 (WBGU, 2012)	5
Figure 1.4 Schematic of the full research work	11
Figure 2.1 A classification of energy storage methods (Dincer, 2010)	15
Figure 2.2 A classification of thermal energy storage methods (Baylin, 1979, Bales, 2005, Harald, 2008 and Atul Sharma2009)	16
Figure 2.3 The process of PCM charging and discharging	21
Figure 2.4 Classifications of PCMs (Atul, 2009)	22
Figure 2.5 PCMs based on Non-Paraffins and Waxes (Rubitherm® RT) and Latent heat fiber board panels based on Non-Paraffins	23
Figure 2.6 Heat transfer enhancement methods employed in phase change material research (Murat, 2007 and Agyenim, 2010a)	30
Figure 2.7 Classification of chemical & thermochemical storage (Bales 2005)	36
Figure 2.8 Chemical storage and sorption storage classification (Aveyard, 1973, N'Tsoukpoe, 2009 and office, 2012)	37

Figure 2.9 Processes involved in a thermochemical energy storage cycle: charging, storing and discharging (Abedin, 2010 and 2011)	38
Figure 2.10 Different energy storage materials (Hadorn, 2005 Bales, 2006 and N'Tsoukpoe, 2009)	39
Figure 2.11 Adsorption and desorption process of water vapour on solids (Halimeö, 2007)	43
Figure 2.12 Operation principle of closed thermochemical energy storage (Halimeö, 2007 and N'Tsoukpoe, 2009)	45
Figure 2.13 Operation principle of open thermochemical TES (Hauer, 2002; Halimeö, 2007 and N'Tsoukpoe, 2009)	46
Figure 2.14 Classification of chemical heat pumps (Wongsuwan, 2001 and Wang, 2008)	48
Figure 2.15 Solid-gas CHPs (left) and liquid-gas CHPs (right) (Wang, 2008)	49
Figure 2.16 Types of solar energy collectors	54
Figure 2.17 Schematic diagram of an evacuated tube collector (Soteris, 2004 and Ayompe, 2013)	55
Figure 2.18 Heat pipe evacuated tube collectors (Morrison, 2001)	56
Figure 2.19 Direct flow evacuated tube collectors (Morrison, 2001)	58
Figure 3.1 Working principle of seasonal thermal energy storage	63
Figure 3.2 View of Nottingham H.O.U.S.E	65
Figure 3.3 Flow chart of a TAS model process	66
Figure 3.4 The TAS 3D model of Nottingham H.O.U.S.E	67
Figure 3.5 Schematic of zoning on ground floor and first floor	69
Figure 3.6 Annual ambient temperatures of Nottingham (UKCIP 2050)	70
Figure 3.7 Annual internal temperature variation of bed room	71

Figure 4.25 Temperature change during three days with quad PCM Packs	100
Figure 4.26 Fluke TiS Thermal Imaging Scanner	101
Figure 4.27 Temperature change during two days with thermal scanned points under double PCM packs	102
Figure 4.28 Temperature change images by thermal scanner	103
Figure 4.29 Schematic view of the proposed cooling system	107
Figure 4.30 Schematic view of experimental cooling system	107
Figure 4.31 Weight for Lithium Nitrate of before and after testing	109
Figure 4.32 Result for Lithium Nitrate (LiNO_3) with water (H_2O) test	110
Figure 4.33 Silica Gel tank of before and after testing	111
Figure 4.34 Result for Silica Gel (SiO_2) with water (H_2O) test	111
Figure 4.35 Result for Mixture (50% SiO_2 and 50% LiNO_3) with water	113
Figure 4.36 Simulation result on heat sink in zeolite bed (Riffat, 2013)	114
Figure 5.1 Schematic view of the proposed seasonal energy storage system	117
Figure 5.2 Schematic diagram of comprehensive high capacity heat storage system	118
Figure 5.3 Schematic diagram of solar collector heating system with PCM	119
Figure 5.4 Solar collector heating system rig with water and PCM tank	121
Figure 5.5 Tungsten halogen lamps used as a solar simulator	122
Figure 5.6 Schematic diagram of the system with measurement locations	123
Figure 5.7 Open thermochemical energy storage system testing rig	125

Figure 5.8 Testing absorption chamber with air flow baffle	125
Figure 5.9 Detailed view of absorption chamber	126
Figure 5.10 Detailed view of air flow baffle	126
Figure 5.11 Temperature measurements	130
Figure 5.12 RS 53II digital thermometer	130
Figure 5.13 CMP11 Pyranometer (Kipp & Zonen)	131
Figure 5.14 Steam generator and relative humidity evaluation kit (EK-H4)	132
Figure 5.15 Jumo Midas pressure transmitter (type 401001)	132
Figure 5.16 Weight sensors (S220, single point Load Cell)	133
Figure 5.17 Metric thermal anemometer (Testo 405 V1) and five points' measure method	134
Figure 5.18 A standard mercury thermometer	136
Figure 5.19 Temperature calibration of type K thermocouple	136
Figure 5.20 Calibration of six weight sensors (Load cell S220)	138
Figure 6.1 Temperatures change in water tank under light radiation	141
Figure 6.2 Temperatures change in water tank under different radiations	142
Figure 6.3 Outlet temperature change of fan coil heater pipe under different fan speeds	143
Figure 6.4 Temperatures change of fan pipe outlet with water tank under indoor light radiation	144
Figure 6.5 Temperatures change of fan pipe outlet with water tank under outdoor solar radiation	145
Figure 6.6 Solar collector inlet and outlet temperatures change	145
Figure 6.7 Solar inlet temperatures difference between T_{i+1} and T_i and outdoor solar radiation intensity	146
Figure 6.8 Comparison of outdoor solar and indoor lamps light	

radiation	147
Figure 6.9 Water tank internal temperatures and fan pipe outlet temperatures change under different radiations	148
Figure 6.10 PCM tank temperatures change by light radiation	150
Figure 6.11 Fan pipe outlet temperatures change by light radiation	150
Figure 6.12 PCM tank temperatures change by solar radiation	151
Figure 6.13 Fan pipe outlet temperatures change with PCM tank by solar radiation	152
Figure 6.14 Comparison of internal temperatures change between water tank and PCM tank by solar radiation	153
Figure 6.15 Comparison of fan pipe outlet temperatures change between water tank and PCM tank by solar radiation	155
Figure 6.16 Heating gain comparison of water, PCM-RT58 and PCM-55 on different final tank temperature	157
Figure 6.17 Solar collector efficiency (η_s) and fan coil heater efficiency (η_f) in a sunny day	159
Figure 6.18 Solar collector efficiency (η_s), fan coil heater efficiency (η_f) and overall solar system efficiency ($\eta_{overall}$) in a sunny day	160
Figure 6.19 Comparison of light radiation with cloudy day solar radiation	161
Figure 6.20 Solar collector efficiency (η_s) and fan coil heater efficiency (η_f) in a mostly cloudy day	162
Figure 6.21 Solar collector efficiency (η_s), fan coil heater efficiency (η_f) and overall solar system efficiency ($\eta_{overall}$) in a mostly cloudy day	162
Figure 7.1 Weight of silica gel (SiO_2 , white granular) tray	165
Figure 7.2 Water absorption of silica gel (SiO_2)	166

Figure 7.3 Temperature change of absorption chamber with silica gel	167
Figure 7.4 Relative humidity change of internal chamber with silica gel	168
Figure 7.5 Comparison of temperature and relative humidity change of silica gel chamber	168
Figure 7.6 Silica gel tray weight changes during a hydration process	169
Figure 7.7 Weight of calcium chloride (CaCl_2) tray	170
Figure 7.8 Relative humidity change of chamber with calcium Chloride	171
Figure 7.9 Comparison of temperature and relative humidity change of calcium chloride chamber	172
Figure 7.10 Calcium chloride tray weight change during hydration process	172
Figure 7.11 Weight of full zeolite 13x (white granular) tray	174
Figure 7.12 Relative humidity change of internal chamber with zeolite 13x	174
Figure 7.13 Comparison of temperature and relative humidity change of zeolite 13x chamber	175
Figure 7.14 Zeolite 13x tray weight change during the hydration process	176
Figure 7.15 Vermiculite and its weight tray	177
Figure 7.16 Relative humidity change of internal chamber with vermiculite	178
Figure 7.17 Comparison of temperature and relative humidity change of vermiculite chamber	179
Figure 7.18 Vermiculite tray weight change during the hydration	

process	179
Figure 7.19 Activated carbon and its weight tray	180
Figure 7.20 Relative humidity change of with activated carbon	181
Figure 7.21 Comparison of temperature and relative humidity change of activated carbon chamber	182
Figure 7.22 Activated carbon tray weight change during hydration process	183
Figure 7.23 Comparison on internal temperature change of Absorbents	183
Figure 7.24 Comparison on internal relative humidity change of absorbents	184
Figure 7.25 Temperature change of silica gel chamber during a hydration and dehydration process	186
Figure 7.26 Weight change of silica gel chamber during a hydration and dehydration process	187
Figure 7.27 Comparison on internal temperature, relative humidity and silica gel tray weight change	188
Figure 7.28 Temperature change of zeolite 13x chamber during a hydration and dehydration process	189
Figure 7.29 Weight change of zeolite 13x chamber during a hydration and dehydration process	190
Figure 7.30 Temperature change of vermiculite chamber during a hydration and dehydration processes	191
Figure 7.31 Weight change of vermiculite chamber during a hydration and dehydration process	192
Figure 7.32 Temperature change of activated carbon chamber during a hydration and dehydration process	193
Figure 7.33 Weight change of activated carbon chamber	

during a hydration and dehydration process	194
Figure 7.34 Comparison on hydrated and dehydrated mass	
change of absorbents of an equal tray weight	195
Figure 7.35 Water absorption ratios of absorbents (1000g)	195
Figure 7.36 Mechanism of adsorption on composite adsorbent	196
Figure 7.37 Working principle of absorption heat pipe for	
thermal storage	197
Figure 7.38 Simulation on temperature change of adsorption	
pumping pipe with zeolite 13x (Riffat, 2013)	199
Figure 7.39 Temperature change of zeolite 13x absorption	
chamber during experimental testing	199
Figure 7.40 Fan pipe outlet and ambient temperature with heating	
energy from PCM tank solar collector system	201
Figure 7.41 Silica gel chamber outlet and ambient temperatures	
change with heating energy from absorption	
chamber system	202
Figure 8.1 Schematic working principle of a transpired solar collector	213
Figure 8.2 Schematic charging cycle (summer) in combined	
thermochemical energy storage system with a transpired	
solar collector	214
Figure 8.3 Schematic discharging cycle (winter) in combined	
thermochemical energy storage system with a transpired	
solar collector	215

LIST OF TABLES

Table 2.1 Thermal capacities of sensible heat storage materials (20°C)	17
Table 2.2 Requirements for latent heat energy storage materials	19
Table 2.3 Comparison of phase change materials for heat storage	23
Table 2.4 Definitions of common dimensionless parameters for PCMs	25
Table 2.5 Controlled heat transfer of phase change problem by References	26
Table 2.6 Classification of software in simulation LHTES	31
Table 2.7 Classification of solution and validation on phase change problems (ref)	34
Table 2.8 Thermochemical energy storage materials (Perry, 1984 and Darkwa, 2006)	40
Table 2.9 Characteristics of thermochemical materials investigated by different authors	42
Table 2.10 Summary of numerical, experimental and analytical studies on thermochemical energy storage	52
Table 3.1 Day type classification	67
Table 3.2 Detail materials' layers and corresponding thermal properties	68
Table 3.3 Dimension of zones of Nottingham HOUSE	69
Table 3.4 Potential material sizing	75
Table 3.5 Solar panel specifications	76
Table 3.6 Average insolation in Nottingham	76
Table 3.7 Thermal output from solar panel for available space	78

Table 4.1 The amount of materials (R5365A, R52, R65, R4117 and 8676A)	86
Table 4.2 Comparisons characteristics of Materials	87
Table 4.3 The experimental details in two stages	98
Table 4.4 Amount of LiNO_3 and H_2O for experiment testing	108
Table 4.5 Amount of SiO_2 and H_2O for experiment testing	110
Table 4.6 Amount of materials for experiment testing	112
Table 5.1 Description of thermocouples position	120
Table 5.2 Measurement Description of thermochemical system	124
Table 5.3 Instruments' measurement range and uncertainty	135
Table 5.4 Weight sensors original reading value under different weights	137
Table 5.5 Weight sensors actual calibrated value under different weights	138
Table 6.1 Thermophysical properties of PCM (RT58)	149
Table 6.2 Thermophysical properties of Water, PCM-RT58 and PCM-55	156
Table 7.1 Weight of silica gel and water during hydration process	166
Table 7.2 Typical chemical analysis properties of vermiculite	177
Table 8.1 Calculation of the capital cost of a 3kW seasonal thermochemical energy storage system integrated with evacuated solar collector	206
Table 8.2 List of input parameters of heat storage system	209
Table 8.3 The net present value (NPV) analysis method calculation	209

CHAPTER 1

Introduction

1.1 Background

Globally, the problems of excessive consumption of fossil resources, oil shortages and greenhouse gas (GHG) emissions are becoming increasingly severe. All these problems take a large impact on sustainable development of human society. At present, a very important and reasonable solution is to adopt renewable energy as much as possible. Research and development work on new methods of thermal energy storage are required to minimise energy consumption by harvesting renewable energy sources. The crucial challenge is to effectively store excessive energy and bridge the gap between energy generation and consumption. Both phase change materials (PCM) and thermochemical materials energy storage are promising technologies that can help minimise global environmental pollution and reduce energy consumption. The key role of energy storage

systems is to reduce the time or rate mismatch between energy supply and energy demand (Garg HP, 1985). PCMs and thermochemical materials energy storage are particularly attractive techniques because they provide a high capacity energy storage density. Recently, more and more researchers concentrate on the development of high capacity heat storage systems in low/zero carbon building applications.

1.2 Topic of the Study

This study focuses on the integration of high capacity heat storage systems in building applications. High capacity heat storage systems are based on thermochemical materials and phase change materials which is integrated with an evacuated tube solar collector. PCMs are ideal for latent heat storage in thermal management solutions. Thermochemical materials have high specific heat storage density suitable for the energy storage in building application. Direct flow evacuated tube solar collector is a zero carbon dioxide (CO₂) heating system to transform direct and diffuse solar radiation into useful heat energy. Specifically, PCMs can be used in the building sector with the purpose of improving the thermal comfort by reducing the temperature fluctuation of the indoor environment and to decrease the energy consumption. Thermochemical energy storage system is utilized to meet heating load by absorbing moisture from bathroom or kitchen in winter. During summer period, the solar collector is employed to heat and dry thermochemical materials in dehydration reaction. PCMs can be used as a thermal storage tank to improve energy storage capacity and output temperature of the solar system.

1.3 Global Energy Retrospect and Prospect

1.3.1 Energy Resources and Energy Consumption

Energy is necessary in the development of human society. Civilization and standard of living of human being built upon a sufficient supply of energy. Energy is used to light and heat homes, to cook food, to drive transport and power people's communications and to provide the motive force that drives the factories (Hodgson, 2010). Energy can be defined as the capacity, or ability, to do work. Energy is subject to the law of conservation of energy. According to this law, energy can neither be created (produced) nor destroyed by itself. It can only be transformed. Most of the world's energy resources are from the sun via solar radiation, some of which has been preserved as fossil energy, and some is directly or indirectly usable. Energy can be classified as renewable energy and non-renewable energy. Renewable energies are derived from natural processes that do not involve the consumption of exhaustible resources such as fossil fuels and uranium. Renewable energy sources would be sources that are easily replaced, such as solar, water, geothermal and biomass. Non-renewable energies are in limited supply and cannot be replaced again, such as oil, gas and coal.

The International Energy Agency (IEA) estimated in January 2012 that renewable energy only supplies approximately 13% of the world's energy consumption. The Figure 1.1 represents the main fuels in the world total primary energy supply. Renewable energies accounted for 13.1% of the 11,059 Mtoe of world total primary energy supply (OECD/IEA, 2012). About 97% of combustible renewable and waste is biomass, both commercial and non-commercial. Other of renewable energies is represented by geothermal, solar, wind and tide.

According to 2012 key world energy statistics by the international energy agency, total worldwide energy consumption was about 8,428 Mtoe in 2008 with about 180 percent increased from 4,676 Mtoe in 1973 during 35 years.

Figure 1.2 provides the exact percentage contribution of regions to world total final consumption between 1973 and 2008 (OECD/IEA, 2012).

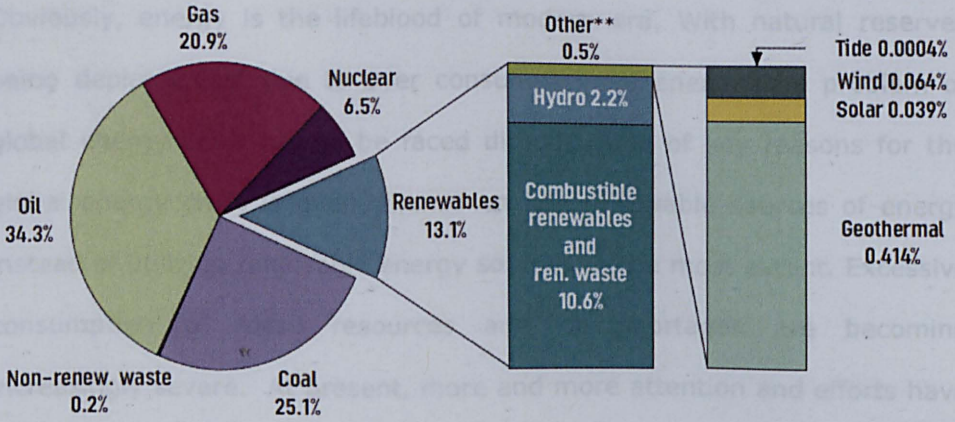


Figure 1.1 Fuel Shares of World Total Primary Energy Supply (OECD/IEA, 2012)

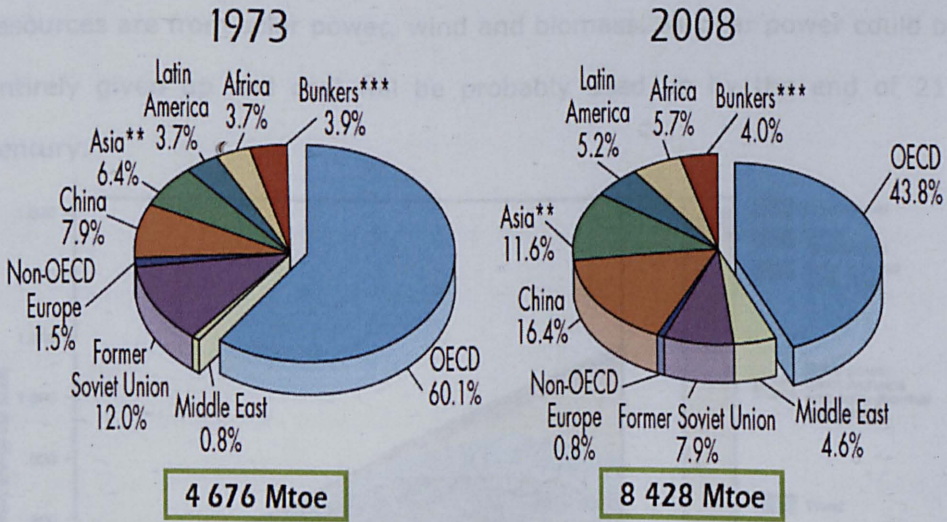


Figure 1.2 Evolution from 1973 to 2008 of world total final consumption by region (Mtoe). ** Asia excludes China. *** Includes international aviation and international marine bunkers. OECD represents the Organization for Economic Co-operation and Development, includes 34 member countries (OECD/IEA, 2012).

1.3.2 Global Energy Crisis and Climate Change

1.3.2.1 Global Energy Crisis and the Move to Alternative

Obviously, energy is the lifeblood of modern era. With natural reserves being depleted fast due to over consumption of energy, the problem of global energy crisis has to be faced directly. One of key reasons for the global energy crisis is over reliance on non-renewable sources of energy instead of utilizing renewable energy sources to the most extent. Excessive consumption of fossil resources and oil shortages are becoming increasingly severe. At present, more and more attention and efforts have been put onto new technologies and developments to exploit renewable energy sources. Figure 1.3 shows an exemplary path of transforming the global energy mix to 2050 and 2100. It can be seen that contribution of renewable energies rapidly increases in future. Most of renewable resources are from solar power, wind and biomass. Nuclear power could be entirely given up and coal will be probably used up by the end of 21st century.

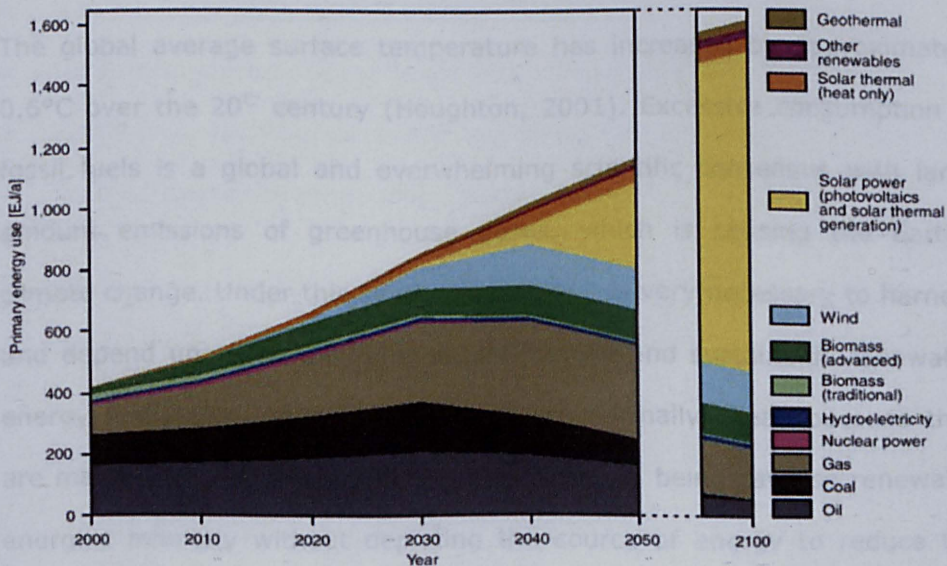


Figure 1.3 Transforming the global energy mix: the exemplary path until 2050/2100 (WBGU, 2012).

1.3.2.2 Climate Change and the Environment

Climate, as an important part of the Earth's system, is the long-term prevalent weather conditions of an area, determined by latitude, position relative to oceans or continents, altitude, etc (Jeremy, 2003). The climate is always in constant flux on the Earth. The main reason can be summed up into two categories: natural climate fluctuations and human activities. The former has direct impacts on drivers of ecosystem change, which includes changes in solar radiation, volcanic eruptions; drought, forest fire, flooding, permafrost melt, forest pest outbreaks, timing of vegetation greening and so on. The latter includes human burning of fossil fuels and deforestation, which results in the increase of greenhouse gases and sulfur aerosol concentration in the atmosphere, the change of land surface cover and land utilization, etc. Climate change normally leads to some negative things. Rising global temperatures, one of key climate change phenomenon, will bring changes in weather patterns, rise up sea levels and increase frequency and intensity of extreme weather.

The global average surface temperature has increased by approximately 0.6°C over the 20th century (Houghton, 2001). Excessive consumption of fossil fuels is a global and overwhelming scientific consensus with large amount emissions of greenhouse gases, which is causing the Earth's climate change. Under this severe situation, it is very necessary to harness and depend upon the environmentally friendly and sustainable renewable energy resources. Renewable energies are normally cheap because they are made from sun directly or indirectly. Human being can use renewable energies infinitely without depleting the source of energy to reduce the dependence on conventional energy sources for a clean Earth system.

1.4 The Fundamentals of High Capacity Heat Storage Technologies

Over the past several decades, studies of high capacity heat storage systems have investigated design fundamentals, components and process optimization, materials selection, transient and long-term behaviour, and field performance. High capacity energy storage system can provide with some advantages over conventional thermal energy storage, which is summarized as follows:

- Reduced energy consumption, initial and maintenance costs,
- Reduced equipment size,
- Increased flexibility of operation,
- Improved indoor air quality,
- Conservation of fossil fuels, by utilizing renewable energy,
- Reduced CO₂ and CFC_s emissions,
- Increased efficiency and effectiveness of equipment utilization,
- Has higher specific energy storage density
- Long-term storage as reactants with smaller thermal loss
- Easily transmitted to generate heat at another location
- Wide temperature range and characteristics.

Currently, there are some challenges and barriers/obstacles that need to be addressed so that high capacity heat storage technologies can be widely used. Thermochemical and phase change materials energy storage for building sectors are still at an experimental stage and the technologies have not been applied abundantly in practice although many patents have filed. Both technical and economical questions about thermochemical energy storage systems have yet to be answered. More research and

development work as well as large scale demonstration projects are required to prove the viability and long term performance of PCMs and thermochemical energy storage systems.

1.5 Novelty and Timeliness of the Research

In order to meet a low/zero carbon building, this research has developed a novel high capacity heat storage system, which is benefited from both phase change and thermochemical materials with specific storage density (SSD). The detailed innovative features of the current proposed research project include the following:

- Experiment investigation on properties (including melt temperature, melt and solidification time during phase change process) of some new PCMs (R5365A, R52, R65, R4117A and 8676A) supplied by proposed manufacturers,
- A unique modelling via software EDSL TAS on actual passive house (Nottingham HOUSE) is presented to size thermochemical materials and solar panel,
- A unique experiment method to evaluate performance of PCM on low temperature range, thermal images analysis method is introduced by employing Fluke TiS thermal imaging scanner,
- Proposed thermochemical materials (lithium nitrate, silica gel and their mixture) are tested on unique well-designed closed thermochemical absorption system (quite low pressure), which achieves the same results as referenced simulation,
- Some advanced and specific measurements (weight sensor, humidity sensor and anemometer) are firstly introduced to illustrate

thermochemical process from multiple aspects. Calibration and uncertainty of measurements are tested and presented,

- Experiment evaluation proposed materials: silica gel (SiO_2), calcium chloride (CaCl_2), zeolite 13x, vermiculite and activated carbon on a unique well-designed open thermochemical absorption system in terms of hydration and dehydration processes,

This research will lead to a novel seasonal high capacity heat storage system integrated with solar collector, which has reduced annual heating load and increased solar efficiency relative to the conventional solar heating systems. It is, therefore, timely in terms of its considerable capability of saving energy and reducing the amount of CO_2 released to the environment.

1.6 Objectives and Structure of the Research

1.6.1 Objectives of the Study

The overall aim of this study is to provide an opportunity to design an efficient, cost-effective, and environmentally friendly seasonal high capacity heat storage system for building applications. More precisely, this project concentrates on the thermochemical and phase change materials energy storage aspect of the heating system and has following objectives:

- Comprehensive literature review on thermal energy storage from PCMs which are usable for medium temperature range (between 0°C and 100°C) in current market.
- Literature review on the specifications of the current state of thermochemical materials usable for low temperatures ($\leq 70^\circ\text{C}$) renewable heat, and comparison with alternative indirect competition on methods of thermal energy storage system.

- To understand and investigate solar energy collection systems for heating purpose and reform solar system to heat and dry the thermochemical energy storage system
- To develop and assess suitable thermochemical absorption chamber model, which is used to select and identify appropriate adsorbents for seasonal thermochemical energy storage system.
- To validate theoretical findings with experimental results from both solar collector and thermochemical materials system.
- To explore theoretical improvements to the thermochemical energy storage systems integrated with transpired solar collector and propose the further stage of development to improve the building envelope.
- To propose and evaluate cost reduction methods and explore the impact on the performance with physical data.
- To discuss and address the technical, economic and environmental benefits of systems.

1.6.2 Structure of the Research

Based on theoretical and experimental methodologies, this project is divided into four stages. The following eight chapters explain and illustrate research process on seasonal renewable energy storage system from PCMs and thermochemical materials. The overall structure of the research work is shown in Figure 1.4.

STAGE I, relevant information has been quoted to explain present situation and background about this topic and future direction. Aims and objectives, methodology and structure of this study have been illustrated. To gain a better understanding of whole study, literature review of previously published theories have been conducted on thermal energy storage, the

performance of phase change and thermochemical materials energy storage and solar energy collector system.

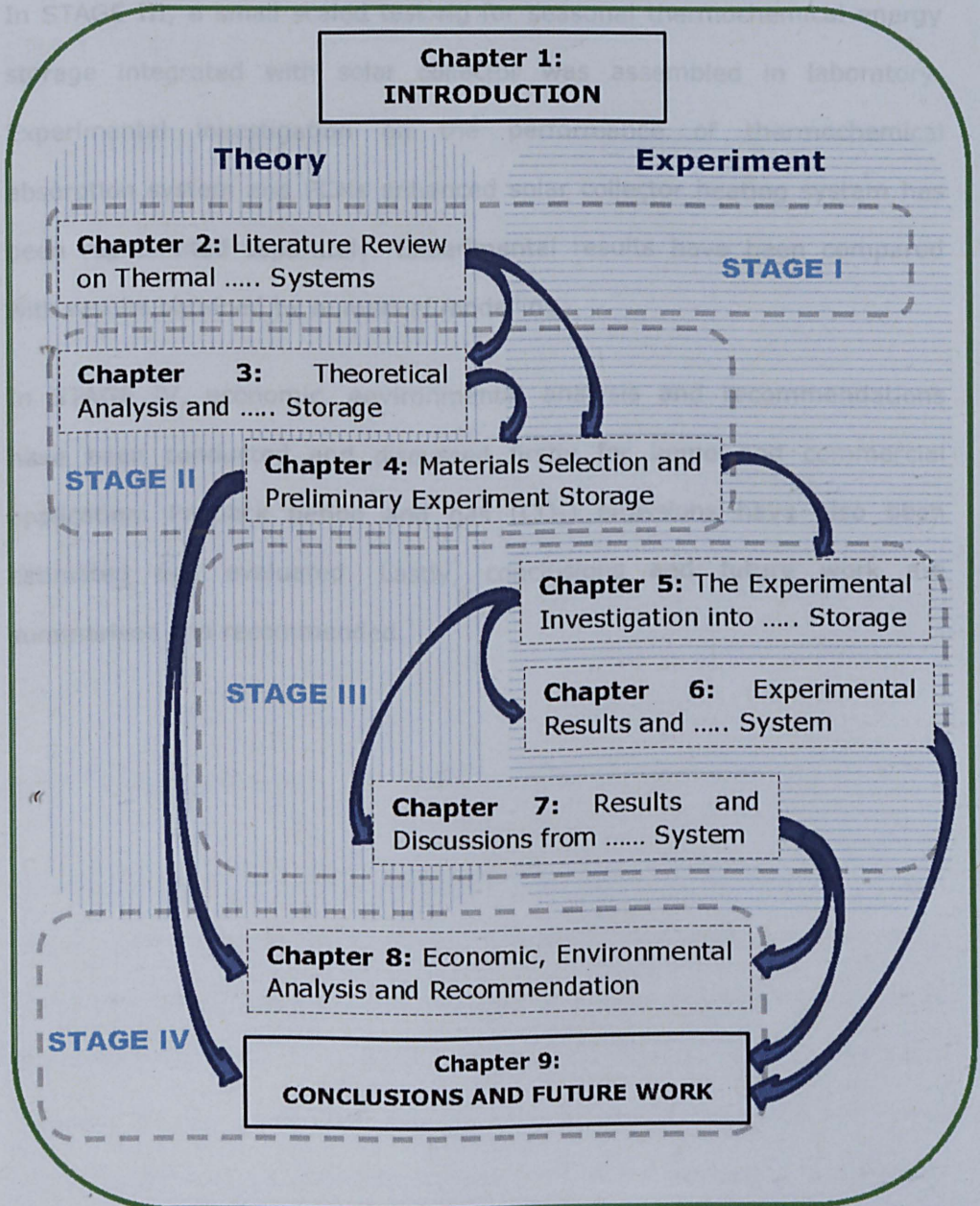


Figure 1.4 Schematic of the full research work

STAGE II is a crucial research stage to service main experiment testing in later stage. Theoretical analysis and computer simulation for thermal energy storage has been discussed in Chapter 3. Selection, development,

synthesis and optimisation of thermal materials and relevant preliminary experiments have been illustrated and discussed in Chapter 4.

In STAGE III, a small scaled test rig for seasonal thermochemical energy storage integrated with solar collector was assembled in laboratory. Experimental investigation on the performance of thermochemical absorption system and PCMs enhanced solar collector heating system has been represented separately. Experimental results have been compared with results obtained by numerical modelling.

In STAGE IV, economic, environmental analysis and recommendations have been conducted and discussed firstly for home and commercial application. Payback period and gas (CO₂) emissions have also been estimated and evaluated. Lastly, conclusions and future work are summarised and recommended.

CHAPTER 2

Literature Review on Thermal Energy Storage and Solar Energy Collection Systems

2.1 Introduction

Research and development work on new methods of thermal energy storage are required to minimise energy consumption by harvesting renewable energy sources. The key role of energy storage systems is to effectively store excess energy and reduce the time or rate mismatch between energy supply and energy demand (Garg HP, 1985). Thermal energy storage is a particularly attractive technique because it can provide a high energy storage density. Recent developments in low/zero carbon buildings have promoted the development of thermal energy storage systems. In order to propose seasonal high capacity heat storage system, a comprehensive literature review of what has been done is presented in this chapter. This is important to establish a combined experimental model

that is not only applicable for household heating but also accurate and able to provide thermal performance prediction for those solar collectors with PCM, and cooling systems working with advanced thermal cycles.

In this literature review, an overview of the studies conducted on phase change materials and thermochemical energy storage technologies for various applications have been reviewed. A particular emphasis has been put on their thermal application and complex heat transfer process due to the study of method (analytical, numerical and experimental). The purpose of this section is to identify appropriate categories of thermal working materials for a long term solar driven by a thermochemical heating system. On the other hand, a review on solar energy collection system has also been studied based on its all kinds of available types. The prime advantage of solar energy compared with other forms of energy is that it is clean and can be supplied without any environmental pollution (Soteris, 2004). A direct flow evacuated tube collector called DF100 will be introduced to integrate with thermochemical adsorption system in further stage.

2.2 Thermal Energy Storage

2.2.1 Types of Energy Storage

Nowadays, energy storage systems can be accomplished by devices or physical media. Energy storage is vitally significant to any intermittent energy source to meet variable demand. It is difficult to evaluate energy storage properly without a detailed understanding of energy supplies and end-use considerations in term of complex properties of energy storage (Jason and Jeff, 2002). Advanced energy storage systems can be integrated with other technologies to provide feasible innovation solutions in energy storage fields. Methods of energy storage devices can be

classified and categorized. Dincer and Rosen (2010) have classified and discussed energy storage devices into forms of mechanical, thermal, chemical, biological, and magnetic (Dincer, 2010), as shown in Figure 2.1.

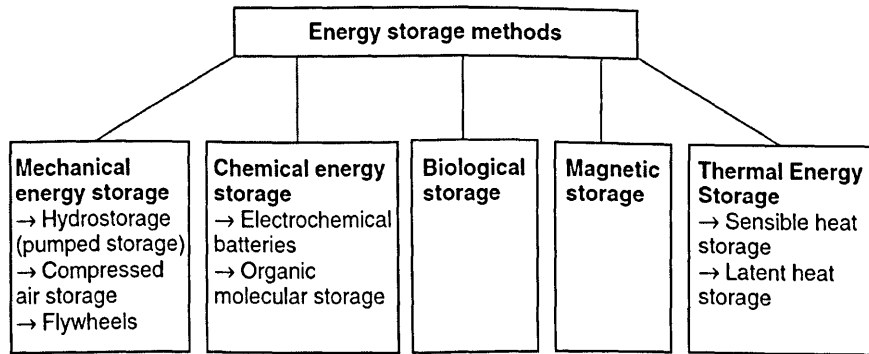


Figure 2.1 A classification of energy storage methods (Dincer, 2010)

2.2.2 Classification of Thermal Energy Storage

Thermal energy storage commonly is defined as an important energy conservation technology. As an advanced energy technology, Thermal energy storage has attracted increasing interest for thermal applications such as space heating, hot water, cooling, and air-conditioning. Thermal energy storage systems have the potential for increasing the effective use of thermal energy equipment and for facilitating large-scale fuel switching, which is significantly useful for addressing the mismatch between the supply and demand of energy (Dincer, 2002b). Thermal energy can be stored as sensible heat, latent heat and thermochemical or combination of these heats. Therefore, some possible methods to study thermal energy storage can be divided into physical and chemical processes. Figure 2.2 shows an overview of major technique of thermal energy storage. Thermal energy storage can be divided into thermochemical pipeline and chemical heat pump and heat of reaction in chemical processes.

Although thermal energy storage is a mature technology to some extent and used in wide variety of commercial and industrial applications today, it still has been required to renew through interdisciplinary collaboration in research. In 2002, Dincer revealed out that advanced modern thermal energy storage technology has been successfully applied throughout the word, particularly in some developed countries (Dincer, 2002a).

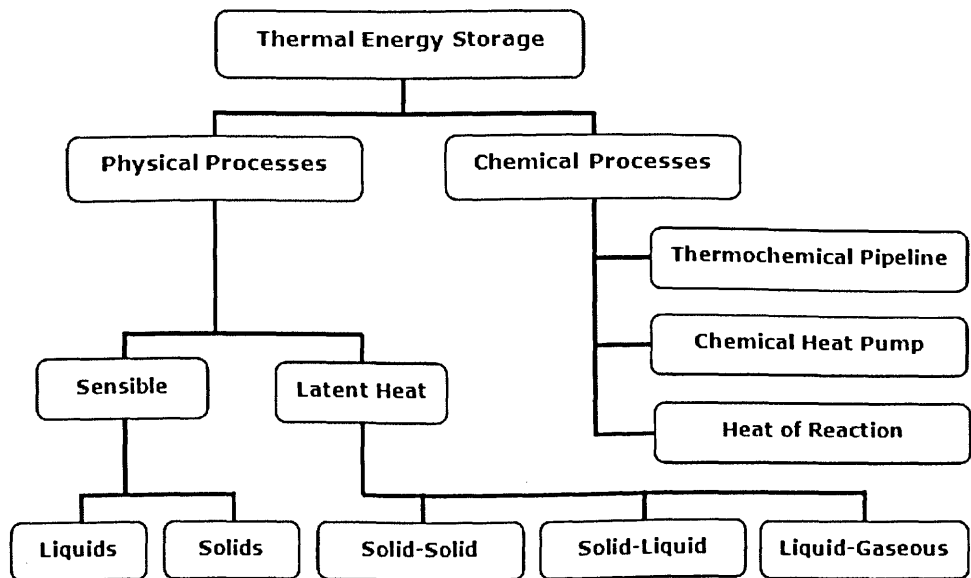


Figure 2.2 A classification of thermal energy storage methods
(Baylin, 1979, Bales, 2005, Harald, 2008 and Atul Sharma 2009)

2.2.3 Physical Energy Storage Processes

2.2.3.1 Sensible Heat Storage

In physical energy storage processes, thermal energy storage can be divided into two principal types as sensible type (e.g., wood, rock) and latent type (e.g., water/ice, salt hydrates). Sensible heat is defined as the heat absorbed or released when a substance just undergoes a temperature change. The sensible heat storage is a thermodynamic process, which can be calculated mathematically. The given equation 2.1 expresses the

amount of heat (Q) stored in a mass of material (m) with respect the specific heat of the material (c_p), the temperature change (ΔT), the volume of storage material (V) and the density of the material (ρ).

$$Q = \int_{T_i}^{T_f} mc_p dT = mc_p \Delta T \quad \text{or} \quad Q = \rho c_p V \Delta T \quad (2.1)$$

Sensible heat storage systems usually employ liquids as storage media such as water and oil but in some cases solids such as molten salts, iron, rock, concrete and bricks are also used as thermal energy storage media. But, normally these materials are not used as sensible energy storage systems in term of their very low volumetric heat capacity of gases (Harald, 2008). Some selected and common sensible heat storage materials and their properties are shown in Table 2.1. A suitable sensible heat material normally should be inexpensive and has a good thermal capacity (Dincer, 2002b). For example, the specific heat of water is approximately twice of those of rock and soil. Compared with other sensible heat materials, higher heat capacity of water often makes water as useful thermal tank liquid in a low temperature range (between 0°C and 100°C).

Table 2.1 Thermal capacities of sensible heat storage materials (20°C)

Material (sensible heat)	Density (kg/m³)	Specific heat (J/kg K)	Volumetric thermal capacity (10⁶J/m³K)
Clay	1458	879	1.28
Brick	1800	837	1.51
Sandstone	2200	712	1.57
Wood	700	2390	1.67
Concrete	2000	880	1.76
Glass	2710	837	2.27
Aluminum	2710	896	2.43
Iron	7900	452	3.57
Steel	7840	465	3.68
Gravelly earth	2050	1840	3.77
Magnetite	5177	752	3.89
Water	988	4182	4.17

Source: (Norton, 1992; Dincer, 2010)

Basically, there are some barriers to effect the development and application in most sensible heat storage system: (Agyenim, 2007):

- a) Low heat storage capacity per unit volume of the storage medium
- b) Non-isothermal behaviour during heat storage and release processes
- c) Large storage size requiring a large occupancy space
- d) Large temperature difference by charging and discharging, not suitable for most practical applications with a narrow temperature range.

2.2.3.2 Latent Heat Storage

In latent heat storage, heat is released or absorbed by a chemical substance during a phase change from solid to liquid or liquid to gas vice versa without a change in temperature. The storage capacity (Q) of the latent heat storage system with a phase change materials (m) can be given by equations 2.2 and 2.3 with respect the heat of fusion per unit mass (Δh_m , J/kg) and specific heat (c_p , J/kg K) (Atul, 2009).

$$Q = \int_{T_i}^{T_m} mc_p dT + ma_m \Delta h_m + \int_{T_m}^{T_f} mc_p dT \quad (2.2)$$

$$Q = m[c_{sp}(T_m - T_i) + a_m \Delta h_m + c_{lp}(T_f - T_i)] \quad (2.3)$$

Where, T_f is final temperature ($^{\circ}\text{C}$), T_i is initial temperature ($^{\circ}\text{C}$), T_m is melting temperature ($^{\circ}\text{C}$), c_{lp} is average specific heat between T_m and T_f (J/kg K), c_{sp} is average specific heat between T_i and T_m (kJ/kg K), a_m is fraction melted.

Compared with sensible heat storage, latent heat storage system is particularly attractive. Usually, the latent heat change is much higher than the sensible heat change for a given medium, which is related to its specific heat. Therefore, latent heat storage is able to provide a considerable storage density and store heat at a constant temperature corresponding to the phase transition temperature of the heat storage medium (Dincer, 2002 and 2010). In common, a latent heat energy storage system should not be less than following three major components (Abhat, 1983):

- 1) Appropriate phase change materials with its melting point in the desired temperature range,
- 2) Fittings of heat exchange surface,
- 3) Suitable configuration of container compatible with the phase change storage materials.

Table 2.2 Requirements for latent heat energy storage materials

Thermal Properties	a. Suitable phase change temperature, b. High latent heat of transition, c. Good heat transfer
Physical Properties	a. Favorable phase equilibrium, b. High density, c. Small volume change, d. Low vapour pressure
Kinetic Properties	a. No or little subcooling (supercooling), b. Sufficient crystallization rate
Chemical Properties	a. Long-term chemical stability, b. Compatibility with materials of construction, c. No toxicity, d. No fire hazard
Economics	a. Abundant, b. Good recyclability, c. Cost effective

Source: (Harald, 2008 and Atul, 2009)

A suitable phase change temperature and a large melting enthalpy are two manifest requirements on a PCM. However, for PCMs, still some

requirements have to be followed so that PCMs can be used in the design of latent heat thermal energy storage (Harald, 2008). These requirements can be divided into thermal properties, physical properties, kinetic properties, chemical properties and economics (Atul, 2009) as shown in Table 2.2.

2.3 Phase Change Material (PCM)

An ideal product of storage materials for thermal management solutions is called Phase Change Material, or short PCM.

2.3.1 Background

The pioneer of research phase change materials were Maria Telkes and Eleanor Raymond in the 1940s, but not much reflection produced at that time until the energy crisis of late 1970s. (Agyenim, 2010a). The first experimental application of PCMs for cool storage occurred in the early 1970s at the University of Delaware, which was led by Dr. Maria Telkes. During the late 1970s and 1980s, some organizations employed phase change materials in different applications, especially for solar heat storage (Dincer, 2002b). After the energy crisis of 1970s, there have been fewer attentions to focus on phase change storage field until it emerged recently. Despite decades of development of PCMs for building purposes, PCMs are still not mainstream interior architecture. Based upon current this energy crisis, it is commonly acknowledged that increasing people apply their mind to seek some innovative methods and new phase change materials in the required operating temperature ranges to save energy.

Basically, a phase change material is a chemical substance with a high heat of fusion, which can melt (condenses) and solidify (crystallizes) at a certain

temperature (Dincer, 2002b). More exactly, PCM is capable of storing and releasing large amounts of latent energy through changing from one phase to another. These phase changes take place at a constant or near constant temperature. Heat is absorbed or released when the material changes from solid to liquid and vice versa, which can be repeated over an unlimited number of cycles with no change to PCM's physical or chemical properties. Water is one of the most common phase change materials. Figure 2.3 is a typical process of PCM charging and discharging.

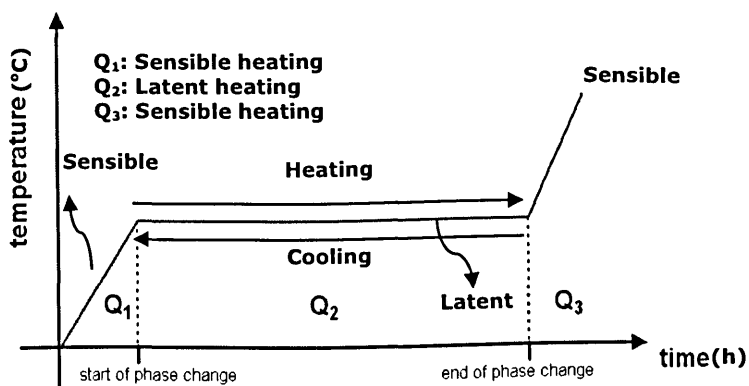


Figure 2.3 The process of PCM charging and discharging (Harald, 2008)

In Figure 2.3, the solid PCM is sensible heating during Q_1 , and then it starts absorbing heat to melt during Q_2 . The process of Q_2 is called phase change storage. At the end of phase change, liquid PCM enters in Q_3 sensible heating. By contrary, from Q_3 to Q_1 , it is a freezing process. This cycle can be repeated unlimited times with no change to PCM's physical and chemical properties. That is why PCM can be classified as latent heat storage material and also called a revolutionary form of insulation material.

2.3.2 Classification and Characteristics of PCMs

Abhat (1983) made a helpful classification of all materials applied for thermal energy storage, which were divided into sensible heat storage

material, latent heat material and chemical energy material (Abhat, 1983). For the purpose of thermal energy storage, more research is focused on latent heat material, especially solid-liquid of phase change materials. Among these references related with PCM, Abhat, Lane, Dincer and Rosen supplied numerous discussions and reviews on PCMs' characteristics, advantages and disadvantages, and various experimental techniques.

Currently, there are numbers of phase change materials in any required temperature ranges. A classification of PCMs is drawn in Figure 2.4, including organic, inorganic and eutectic PCMs. Generally, inorganic compounds usually have higher volumetric latent heat storage capacity ($250\sim400\text{ kg/dm}^3$) than organic compounds ($128\sim200\text{ kg/dm}^3$) (Atul, 2009). Figure 2.5 is showing typical organic PCMs based on non-paraffins and waxes (Rubitherm® RT) and latent heat fiber board panels also based on non-paraffins.

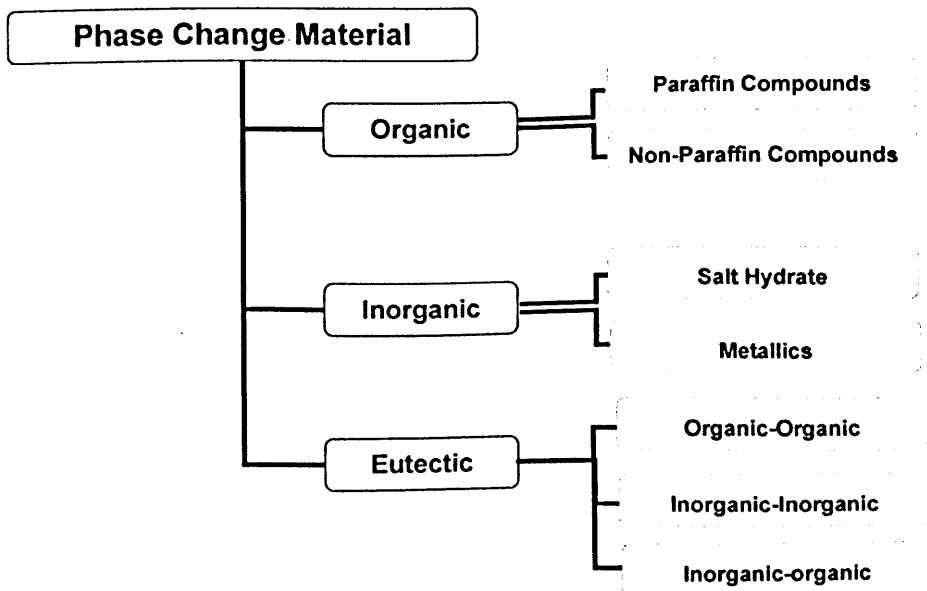


Figure 2.4 Classifications of PCMs (Atul, 2009)



Figure 2.5 PCMs based on non-paraffins and Waxes (Rubitherm® RT) (left) and Latent heat fiber board panels based on non-paraffins (right)

Based upon characterized about all kinds of available phase change materials, a comparison form of these materials for heat storage is generated as shown in Table 2.3. Briefly, salt-based phase change materials with higher phase change enthalpy are cheaper than organic materials. Organic PCMs are simple to use and low or none super cooling compared with inorganic and eutectics PCMs.

Table 2.3 Comparison of phase change materials for heat storage

	Advantages	Disadvantages
Organic	<ul style="list-style-type: none"> Simple to use Non-corrosive Low or none super cooling No nucleating agent 	<ul style="list-style-type: none"> Generally more expensive Lower latent heat/density Often give quite broad melting range Inflammability
Salt-Based (inorganic, eutectics)	<ul style="list-style-type: none"> Generally cheap Good latent heat/density Well defined phase change temperature Non-flammable 	<ul style="list-style-type: none"> Need careful preparation Need additives to stabilize for long term use Undercooling Can be corrosive to some metals

Source (Belén, 2003, Cabeza, 2005 and 2011)

2.3.3 Definition and Correlation Analysis of PCMs

2.3.3.1 Basic Physics of Heat Transfer from Latent Heat Thermal Energy Storage (LHTES) Systems

Basically, it is almost impossible to read some journals or periodicals or understand some fundamental heat transfer processes without appropriate knowledge of Biot, Nusselt, Rayleigh, Stefan, etc. These names are related to dimensionless numbers for heat transfer in LHTES systems. A dimensionless number is defined to represent a property of a physical system, but not measured on a scale of physical units (as of time, mass, or distance). Dimensionless numbers allow people to experiment with relevant model to predict their behaviours under actual sizes. Dimensionless numbers are universally employed to model engineering research projects. Various correlations among LHTES have been revealed to evaluate thermal performance of LHTES systems in both experimental and numerical directions (Agyenim, 2007). Table 2.4 is defined mathematically of some common dimensionless numbers applied in the analysis of LHTES systems.

Table 2.4 Definitions of common dimensionless parameters for PCM

Number	Formula	Significance/determination
Biot, Bi	$Bi = \frac{hl}{k}$	Ratio of conductive to convective heat transfers resistance. Determines uniformity of temperature in solid. (Fukai, 2002)
Dimensionless time or Fourier number, $ Fo$	$\tau = \frac{kt}{\rho C_p l^2}$	Characterizes heat flux into a body or system. (Hamada, 2003)
Grashof number, $ Gr$	$Gr = \frac{g\beta\Delta T l^3}{\nu^2}$	Approximates the ratio of buoyancy force to the viscous force. (El-Dessouky, 1997)
Nusselt, $ Nu$	$Nu = \frac{hd}{k}$	Ratio of the conductive thermal resistance to convective thermal resistance. Determines the ratio of actual heat transferred. (Wang, 1999, Hamada, 2003)
Rayleigh, $ Ra$	$Ra = \frac{g\beta\Delta T l^3}{\alpha\nu}$	Determines the onset of convection. Below a critical value, heat transfer is primarily conduction. (Wang, 1999)
Reynolds number, $ Re$	$Re = \bar{v}$	Ratio of inertial forces to viscous forces. Determines. Whether flow is laminar or turbulent. (Liu, 2005)
Prandtl, $ Pr$	$Pr = \frac{\nu}{\alpha}$	Approximates the ratio of momentum diffusivity to thermal diffusivity. Low Pr means effective heat conduction with dominant thermal diffusivity. High Pr means effective heat. (Wang, 1999)
Stefan, $ Ste$	$Ste = \frac{C_{p,l}\Delta T}{\lambda}$	Ratio of thermal capacity of the melted solid to the latent heat. (Henze, 1981)

Source: (Kreith, 1980, Agyenim, 2007 and 2010a)

2.3.3.2 Analysis of Heat Transfer Mechanisms to Control Insulating Capacity of PCMs

Theoretically, there are three ways to transfer heat in phase change processes (conduction, convection and radiation). Radiation is neglected in term of its inappreciable effect. Heat transfer characteristics of phase change problems can be classified as follows:

- a) Conduction controlled phase change
- b) Convection controlled phase change
- c) Conduction and convection controlled phase change

In phase change problems, some relevant references relating to this classification of heat transfer is shown in Table 2.5. Basically, most of PCMs have low thermal conductivities. At the beginning, many people focused on phase change processes as pure conduction controlled problems. Recently, increasing number of people and research institutes have moved to investigate phase change problems in some complex combinations with conduction and convection controlled.

Table 2.5 Controlled heat transfer of phase change problem by references

Reference	PCM	Control Classification
Halford and Beoham (2007)	Perlite Matrix (salt)	Conduction
Sari and Kaygusuz (2002)	95% purity lauric acid	Conduction
Ahmad et al (2006)	Polyethylene glycol	Conduction
Ng et al (1998)	n - octadecane	Convection
Hamdan and Elwerr (1995)	n - octadecane	Conduction/ Convection
Ismail (2009)	mixtures (water, glycol)	Conduction/ Convection
Agyenim (2011)	Erythritol	Conduction/ Convection

Source: (Kreith, 1980, Agyenim, 2007 and 2010)

2.3.3.3 Melt Time of PCMs

In order to evaluate or select PCMs as energy supply in LHTES systems, melt time of PCMs is a fundamental criteria to check thermal properties of PCMs. Generally, the amount of stored heat within material is determined by the melt temperature and latent heat enthalpy (Agyenim, 2007).

A relationship between the total melt time and average surface heat flux for a volume of a PCM has been revealed by Solomon in 1979. This kind of PCM was subjected to a constant temperature at its boundary and initially at melting temperature of 27.67°C. The simple phase change process can be formulated by equation 2.4.

$$\frac{\partial T}{\partial r} = \frac{\alpha}{r^w} \frac{\partial}{\partial r} \left(r^w \frac{\partial T}{\partial r} \right), \quad r(t) \leq r \leq l \quad T = T_{cr} \quad r \leq r(t) \quad (2.4)$$

Where w is a dimensionless parameter defined by $1 + w = lA/V$, with $w = 0$ for a PCM slab, $w = 1$ for a PCM cylinder, $w = 2$ for a PCM sphere. The duration of melting process t_s is related to the total heat input per unit surface area Q and average heat flux \bar{q} at over $r = l$, the exact expressions has been drawn by Solomon (1979) as shown in equations: 2.5, 2.6 and 2.7 for $0 \leq Ste \leq 4$, where Stefan number was also involved in these equations.

$$t_s = \frac{l^2}{2\alpha(1+w)Ste} \{1 + (0.25 + 0.17w^{0.7})Ste\} \quad (2.5)$$

$$\bar{q} = \frac{-2k\Delta T}{l} \{1 + (0.1210 + 0.0424w)Ste^{(0.7645-0.2022w)}\} \quad (2.6)$$

$$Q = \bar{q}t \quad (2.7)$$

Where Stefan number, $Ste = \frac{C_p(T_{\infty} - T_m)}{\lambda}$, $C = C_{p,l}$ for melting process, $C = C_{p,s}$ for solidification process.

In equation 2.5, the geometric configuration in term of cylinder or sphere radius and the length of slab represented by l were emphasized during this direct relationship, which mean that melt time depended on the length of the constructor. In order to account for the thermal properties, a dimensionless parameter (Stefan number) was used in equation 2.6. The Stefan number is associated to the specific heat capacity (melting and solidification), latent heat enthalpy and the melting temperature of PCM.

2.3.4 Enhanced Heat Transfer Techniques from PCMs

Generally, most of PCMs have quite low thermal conductivities, which will significantly slow down charging and discharging rates of PCMs during phase change. Heat transfer enhancement techniques therefore are essentially required nowadays. There are two ways to enhance heat transfer processes in latent heat thermal energy storage. First method is to improve heat transfer through convection, which only occurs in a liquid phase. Hence, heat can be transferred into PCM by using some liquid mass. On the other hand, increasing the thermal conductivity of materials is also an effective method. This allows employing some available substance with large thermal conductivities into PCM for overall high conductivity (Halime, 2007).

Several studies have been conducted to promote heat transfer enhancement in phase change materials. Most reviewed researches concern on positioning of fixed, stationary high conductivity inserts or structures. A number of materials can be applied as the thermal conductivity promoters, such as, copper, aluminum, nickel, stainless steel and carbon fiber. These materials can be in various forms of fins, honeycomb, wool, brush, etc (Fan, 2011). Figure 2.6 illustrates that some common images and drawings are involved in heat transfer enhancement

techniques. Ettouney et al (2004) found out that the gained enhancement of heat transfer in Fourier and Nusselt number was nearly three times by inserting metal screens or spheres. Zhao et al (2010) used metal foams embedded within PCMs and the result implied that the addition of metal foam could increase the overall heat transfer rate by 3 to 10 times during the melting process (two phase zone) and the pure liquid zone. Akhilesh (2005) utilized composite heat sinks (CHS) with highly conductive base material (BM) to enhance heat transfer in LHTES. Robak (2011) revealed that embedded heat pipes could increase PCM melting rates by approximately 60% and transfer approximately twice the energy between a heat transfer fluid and the PCM by experiment.

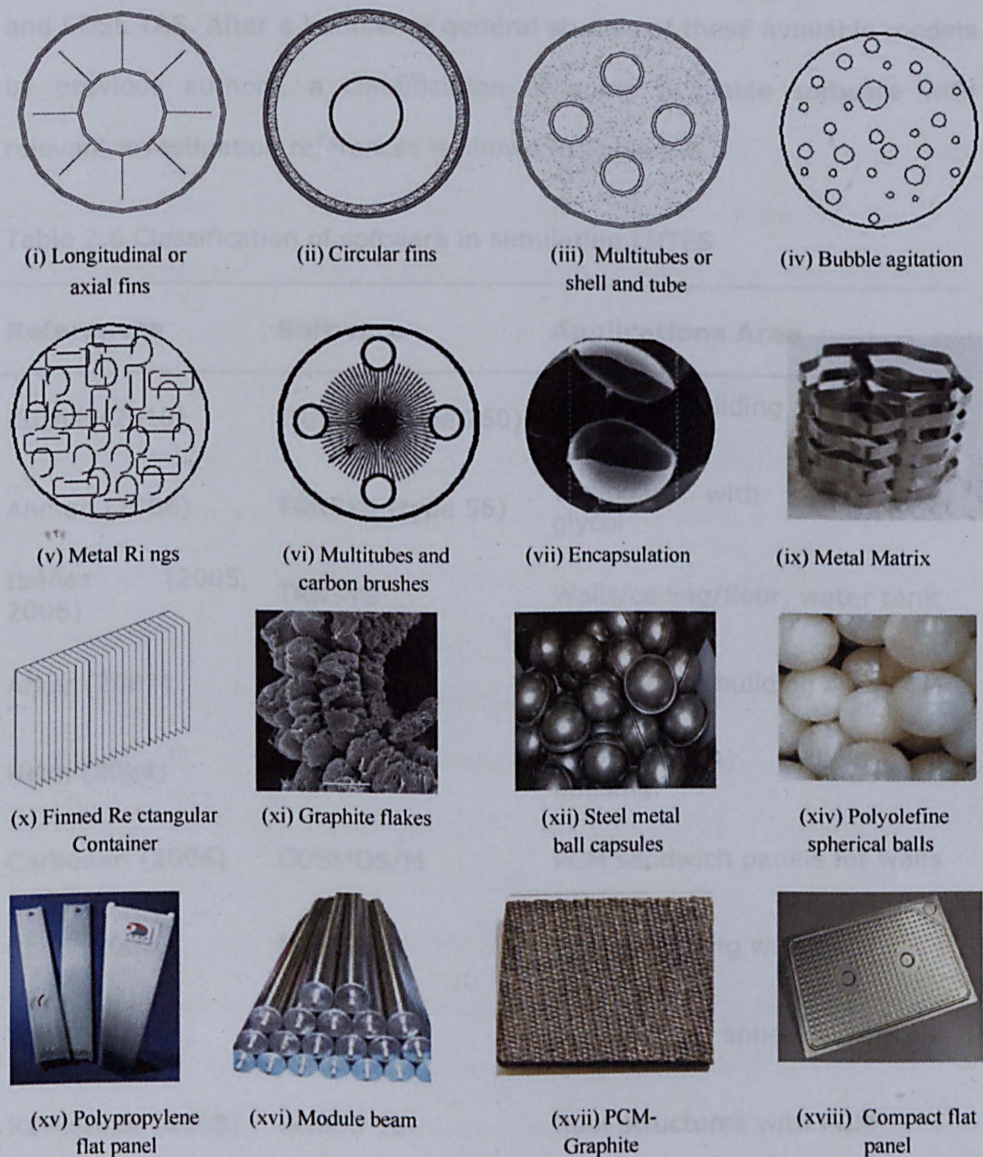


Figure 2.6 Heat transfer enhancement methods employed in phase change material research (Murat, 2007 and Agyenim, 2010a)

2.3.5 Modellization of Heat Transfer in PCMs Using Available Software

Simulation of heat transfer in a PCM system with a simple geometry can be done with many available mathematical and engineering software tools like TRNSYS, ESP-r, EnergyPlus, COMSOL, COSMOS/M, PCM express, ANSYS

and EDSL TAS. After a number of general studies of these available models by previous authors, a classification of some available software with relevant investigation references is shown in Table 2.6.

Table 2.6 Classification of software in simulating LHTES

References	Software	Applications Area
Kuznik (2010)	TRNSYS (type 260)	External building walls with PCM
Ahmad (2006)	TRNSYS (type 56)	Wallboard with polyethylene glycol
Ibáñez (2005, 2006)	TRNSYS	Walls/ceiling/floor, water tank
Arkar (2007)	TRNSYS	Free cooling building with PCM
Heim (2004)	ESP-r	PCM-gypsum panels in building
Carbonari (2006)	COSMOS/M	PCM sandwich panels for walls
Chen (2008)	MATLAB	Energy-storing wallboard
Tan (2009)	CFD	PCM inside a spherical capsule
Ravikumar (2008)	ANSYS 10	Roof structures with PCM
Zhang (2007)	COMSOL	Concrete with solid-solid PCM
Zhuang (2010)	EnergyPlus	Wallboard with PCM
Lucelia (2013)	EDSL TAS	Ceiling gypsum board with PCM

Some basic knowledge on numerical methods for heat transfer is required in using simulation software, especially on heat transfer in LHTES system. However, disadvantages of using simulation software cannot be ignored. It is sometime difficult to understand what the software actually does and

outputs (Harald, 2008). At the same time, the accuracy of result is often and highly overestimated in terms of the colourful and fancy graphs. As is known, it is totally different from ordinary one when heat is transferred by convection with PCM. The reason for this is that abundant amounts of latent heat can be transported by PCM in its melting temperature range, which brings much stronger convection with quite little fluid movement and density changes. Another main disadvantage of using software is that when a large difference occurs in the scale problem. This is because a numerical procedure is normally only used for simulating the large scale (house heat size) or small scale (shipping packages with PCM). For example, if any of the boundary conditions is changed, the results will not illustrate well and truly as a function anymore. In this situation, the previous numeric procedure has to be rewritten for this specific storage system and then combine them for next model simulation (Harald, 2008).

For thermal analysis, TAS (thermal analysis software) is an ideal building thermal analysis software developed by EDSL (environmental design solutions limited). Further simulations of Nottingham House will be performed using EDSL TAS software. The software has been validated by means of empiric case comparisons and it is scientific and professionally recognized for building dynamic thermal analysis (Edsl, 2013).

2.3.6 Classification of Experimental, Numerical and Analytical Investigations on PCMs

A review on analytical, theoretical, numerical and experimental work in the field of phase change materials, especially in melting and solidification processes in 2005, was carried out by Goldstein et al (2010). Recent years, heat transfer associated with phase change materials has been formed an

active area of research. Relevant studies include heat transfer enhancement, thermal insulation and regulation, mathematical models, finned PCMs (tubes, ducts and heat sinks) and variable wall temperature with PCM. Hence, to analyze heat transfer problems with phase change materials can be complicated processes, because the solid-liquid boundary moves depending on the speed at which the latent heat is absorbed or lost at the boundary.

Generally, the study of phase change problems includes analytical, numerical and experimental methods in terms of one-dimensional, two-dimensional or three-dimensional models.

Table 2.7 gives a list of some latter authors for various solutions and methods employed in some applications with PCMs. From these surveys, the main advantages of the analytical model are simplicity and short computation times. Using numerical modelling normally is time consuming. However, in analytical model a classical Stefan-type problem, nonlinearity is the source of difficulties and it destroys the validity of generally-used solving methods such as the superposition method and the separation of variables method (Alexiades, 1993). Some kinds of two-dimensional heat transfer problems with phase change process have to appeal numerical models via the enthalpy method or the effective heat-capacity method to figure out.

Table 2.7 Classification of solutions and validation on phase change problems

References	Nature of Study	Applications & Solution/Validation/Results
Xiao, et al (2009)	Analytical	Passive solar building with interior PCM panels; Formula derivation and sinusoidal approximation method.
Nayak, et al (2006)	Numerical	Heat sink models with three types: porous matrix, plate-type fins and rod-type fins, enthalpy based mathematical formulation and numerical model; A transient finite volume method with enthalpy based formulation and numerical
Lamberg (2004)	Analytical and Numerical	Two-phase solidification problem with finned PCM; 1D analytical method based on Stefan problem and 2D accuracies of different and effective heat-capacity numerical methods
Tay, et al (2011)	Experimental	a tube-in-tank with PCM for cold storage; experimentally derived equation based on the effectiveness-number of transfer unit (ϵ -NTU)
Zhao, et al (2011)	Experimental	LHTES composites with PCM and metal foams and expanded graphite; enthalpy based method shown metal foams and expanded graphite reducing the charging and discharging period
Agyenim, et al (2010b)	Experimental	Shell and tube heat exchanger with medium temperature PCM; 2D convection controlled heat transfer compared to conduction, and the onset of natural convection
Agyenim, et al (2009)	Experimental	horizontal concentric tube heat exchanger with PCM: Erythritol; Analysis by isotherm plots and temperature-time curves based on two heat transfer enhancement methods: circular finned and longitudinal finned
Riffat, et al (2001)	Experimental	Heat pipes and phase change materials for thermoelectric refrigeration; Thermodynamics and enthalpy based, encapsulated PCM given an improvement in cooling storage capability.
Cerón, et al (2011)	Experimental	Room floor tiles with PCM and pavement combined with PCM; DSC tests and temperature difference measurement, the prototype has been proved this solution improving the energy performance of sunny locals.
Zhao, et al (2010)	Experimental and Numerical	PCM with embedded metal foams; temperature difference method and 2D numerical analysis based on Finite Difference Method (FDM)
Ismail and Moraes (2009)	Numerical and Experimental	PCM encapsulated in spherical and cylindrical shells for cold storage; 2D finite difference approximation with a moving grid scheme numerical method

2.4 The State of the Art of Thermochemical Energy Storage

The study of thermochemical energy storage using chemical heat pump was pioneered by Swedish and Swiss researchers in the 1970s (Wettermark G., 1979 and Taube M., 1980). In Germany, a long distance thermal energy transportation system, named EVA-ADAM, was proposed in 1970s and the technology was demonstrated in 1980s. This was the first practical example of thermochemical heat storage (Hanneman et al., 1974). A project on super heat pump and energy integrated system was conducted in Japan during 1984~1992, in which several ammoniate /ammonia and halogenated inorganic reactant/water materials were investigated as working pair of chemical heat pump as part of this project (NEDO, 1993). In 1991, an enhanced thermal heat transfer was examined using CaO/H₂O chemical heat pump system (Ogura H., 1991). Different reactant mixtures to enhance the thermal heat transfer of adsorbent bed were examined in Japan (Fujioka k., 1998), France (Croizat G., 1988) and the UK (Tamainot-Telto Z., 2001).

2.4.1 Classification of Chemical Storage and Sorption Storage

Chemical thermal energy storage can be categorised into chemical storage and thermochemical storage in general. Thermochemical storage systems can be divided into open and closed systems (Bales, 2005). Open storage system is based on the adsorption process to complete the sorption processes with desiccant and heat storage systems. Closed systems work with a closed working fluid cycle which is isolated from the atmosphere. There are two processes to be defined in a closed system; adsorption and

absorption. Figure 2.7 illustrates a classification of chemical and thermochemical storage.

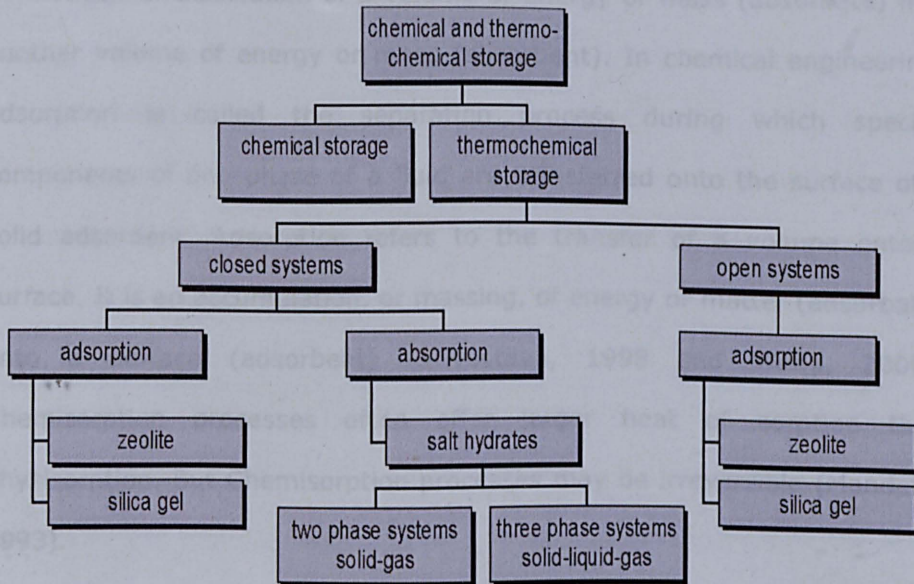


Figure 2.7 Classification of chemical & thermochemical storage (Bales 2005)

On the other hand, usually, it is difficult to make clear boundary distinctions between these expressions, such as chemical storage, thermochemical storage and sorption storage (N'Tsoukpoe, 2009). As shown in Figure 2.8, it is a classification of chemical storage and sorption storage. Chemical energy storage is defined that a chemical substance can be transformed to other forms of energy by a chemical reaction (Garg, 2009). Sorption can be used to describe a phenomenon of fixation or capture of a gas or a vapour (sorbate) by a substance in condensed state (solid or liquid) called sorbent (Hauer, 2007). Depending on the type of bonding involved, sorption can be classified as physical and chemical sorption. Generally, sorption includes both absorption and adsorption (Aveyard, 1973, Inglezakis, 2006 and Wang, 2009). Absorption and Adsorption refer to different phenomena but their commonality is that both

involve the physical transfer of a volume of mass or energy. Specifically, absorption is related to a transfer of a volume into a volume. It is a permeation or dissolution of a volume of energy or mass (absorbate) into another volume of energy or mass (absorbent). In chemical engineering, adsorption is called the separation process during which specific components of one phase of a fluid are transferred onto the surface of a solid adsorbent. Adsorption refers to the transfer of a volume onto a surface. It is an accumulation, or massing, of energy or matter (adsorbate) onto a surface (adsorbent) (Srivastava, 1998 and Wang, 2009). Chemisorption processes often offer larger heat of sorption than physisorption. But Chemisorption processes may be irreversible (Mandelis, 1993).

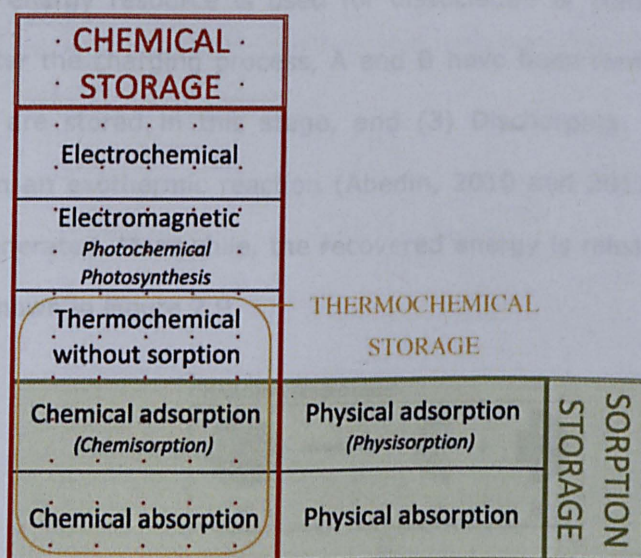


Figure 2.8 Chemical storage and sorption storage classification (Aveyard, 1973, N'Tsoukpoe, 2009 and office, 2012)

2.4.2 Principles of Thermochemical Energy Storage

Sorption and thermochemical storage systems are based on performing a reversible chemical reaction (or desorption), which allows absorption of

heat in the course of the decomposition (desorption) process that is endothermic. A reverse synthesis reaction is exothermic and results in giving stored heat back (Kawasaki, 1999 and Kato, 2007). In this reversible physic-chemical reaction, C is the thermochemical material. With a heat supplement, C can be dissociated into components A and B, which can be any phase and stored separately. A and B are reactants as working pair or sorption couple, C will be formed with a heat release when A and B are put together (Kato, 2007).



A general thermochemical energy storage cycle includes three main processes: (1) Charging: the charging process is an endothermic reaction. A required energy resource is used for dissociation of compound C. (2) Storing: after the charging process, A and B have been formed. Materials (A and B) are stored in this stage, and (3) Discharging, A and B are combined in an exothermic reaction (Abedin, 2010 and 2011). Material C will be regenerated. Meanwhile, the recovered energy is released from this phase, as shown in Figure 2.9.

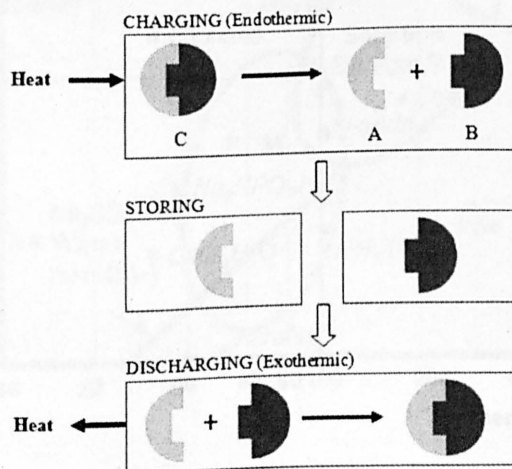


Figure 2.9 Processes involved in a thermochemical energy storage cycle: charging, storing and discharging (Abedin, 2010 and 2011)

2.4.3 Thermochemical Materials Currently Used or Studied

Thermochemical materials (TCMs) are a promising new alternative for long term heat storage. The process concerned is based on a reversible chemical reaction, which is energy demanding in one direction and energy yielding in the reverse direction. Normally, thermochemical materials have the higher storage density with repetitive storage properties to use in sorption storage systems and some of materials may even offer storage density close to properties of biomass (Hastings, 2007). Because of higher energy density, thermochemical thermal energy storage systems can provide more compact energy storage relative to latent and sensible thermal energy storage, as shown in Figure 2.10.

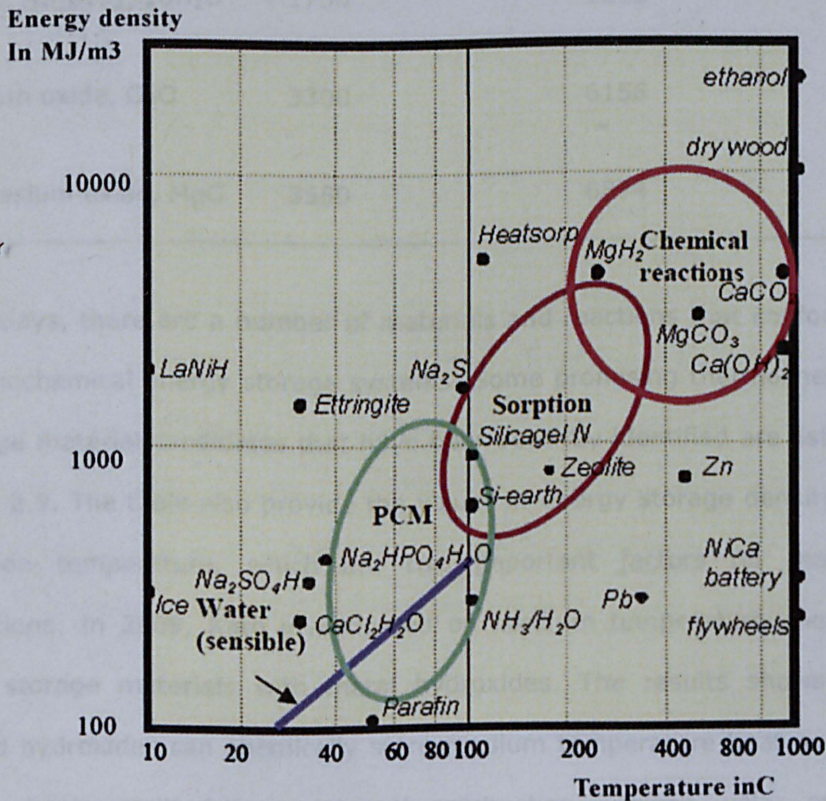


Figure 2.10 Different energy storage materials (Hadorn, 2005 Bales, 2006 and N'Tsoukpoe, 2009)

Numerous research work and experiments on various storage methods has shown that thermochemical energy storage systems has the potential to become probably the most effective and economic method of storing and utilising waste heat (Perry, 1984 and Darkwa, 2006), as shown in Table 2.8.

Table 2.8 Thermochemical energy storage materials (Perry, 1984 and Darkwa, 2006)

Material	Density(ρ), kg/m³	Energy Density, MJ/m³
Aluminium oxide, Al ₂ O ₃	3970	4320
Barium oxide, BaO	5720	4906
Borax, Na ₂ B ₄ O ₇ · 10H ₂ O	1730	1218
Calcium oxide, CaO	3300	6158
Magnesium oxide, MgO	3580	6874

Nowadays, there are a number of materials and reactions that conform to thermochemical energy storage systems. Some promising thermochemical storage material candidates that have been recently identified are listed in Table 2.9. The table also provide the values of energy storage density and reaction temperature, which are two important factors for material selections. In 2009, Kato investigated on medium temperature chemical heat storage materials with metal hydroxides. The results shows that mixed hydroxides can chemically store medium temperature heat such as waste heats emitted from internal combustion engines, solar energy system and high temperature system (Kato, 2006). Visscher revealed that the group of salt-hydrates in general are considered to be suitable

thermochemical materials (Visscher, 2004). Magnesium sulfate heptahydrate ($\text{MgSO}_4 \cdot 7\text{H}_2\text{O}$) is specifically popular as thermochemical materials. It is essential that salt-hydrates can incorporate large amounts of water into the crystal lattice. When a hydrated salt is heated, the crystal water is driven off. In a long term seasonal storage system, solar heat can be employed to dehydrate the salt-hydrate in summer. Subsequently the anhydrous salt is stored until needed. In winter, this salt experiences reverse reaction and yields energy in the form of heat, which can be used for building applications such as hot tap water and central heating. Magnesium sulfate heptahydrate ($\text{MgSO}_4 \cdot 7\text{H}_2\text{O}$), commonly known as epsom salt, can be used for such energy storage applications. Recent Essen (2009) and Posern (2008) have assessed the capability of $\text{MgSO}_4 \cdot 7\text{H}_2\text{O}$ as an ideal material for thermochemical energy storage. The results were similar to Stach's findings using experimental measurements (Stach, 2005, Posern, 2008 and Essen, 2009). In 2010, Balasubramanian, et al investigated the capability of $\text{MgSO}_4 \cdot 7\text{H}_2\text{O}$ to store thermochemical energy via mathematical model (Balasubramanian, 2010). This simulated method can help identify optimal materials for thermochemical storage within practical constraints. In 2011, Abedin investigated a closed thermochemical TES using bromide strontium ($\text{SrBr} \cdot 6\text{H}_2\text{O}$) as the reactant and water as the working fluid (Abedin, 2011). In 2006, Lahmidi simulated a sorption process based on the use of bromide strontium ($\text{SrBr} \cdot 6\text{H}_2\text{O}$), which is adapted to solar thermal systems (Lahmidi, 2006).

Table 2.9 Characteristics of thermochemical materials investigated by different authors

Compound	References	Dissociation reaction			Energy storage density of C GJ/m ³	Turnover Temp. °C
		C	A	B		
Magnesium sulphate	(Visscher, 2005; Van, 2007; Essen, 2008; Hongois, 2008; Balasubramanian, 2010; Ghommem, 2011)	MgSO ₄ ·7H ₂ O	MgSO ₄	H ₂ O	2.8	122
Silicon oxide	(Visscher, 2005; Van, 2007)	SiO ₂	Si	O ₂	37.9	1700
Iron carbonate	(Visscher, 2005; Van, 2007)	FeCO ₃	FeO	CO ₂	2.6	180
Iron hydroxide	(Visscher, 2004 and 2005; Van, 2007)	Fe(OH) ₂	FeO	H ₂ O	2.2	150
Calcium sulphate	(Visscher, 2005; Van, 2007)	CaSO ₄ ·2H ₂ O	CaSO ₄	H ₂ O	1.4	89
Sodium sulphide	(Boer, 2004; Iammak, 2004)	Na ₂ S·5H ₂ O	Na ₂ S	H ₂ O	2.8	110
Bromide strontium	(Lahmidi, 2006; Mauran, 2008; Abedin, 2011a and 2011b)	SrBr ₂ ·6H ₂ O	SrBr ₂ ·H ₂ O	H ₂ O	0.22	43
Calcium hydroxide	(Fujimoto, 2002; Ogura, 2003; Darkwa, 2000 and 2006)	Ca(OH) ₂	CaO	H ₂ O	2.2	25

2.4.4 Sorption Storage Systems

Chemisorption processes can be realized by utilizing reversible chemical reactions. The sorption storage systems can be explained for solid adsorbents and the results can be transferred to liquid absorbents (Halimeö, 2007). The process of adsorption and desorption on solid materials show in Figure 2.11. Adsorption refers to the binding of a gaseous or liquid phase of component on the inner surface of a porous material. Basically, sorption thermal energy storage can be divided into open and closed systems. Soutullo (2011) presented a comparative study of the performance of absorption cooling systems with internal storage and also external storage and the results shown conventional system has a greater room requirement than an internal absorption system (Soutullo, 2011). In 2011, Liu et al evaluated a seasonal storage system for house heating and revealed that the storage capacity of the absorption process increases with the evaporator temperature and the storage temperature before the absorption phase, and decreases with the absorber temperature (Liu, 2011). Generally, sorption storage systems can be divided into open and closed systems.

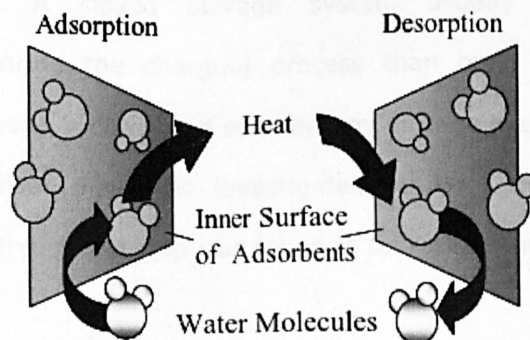


Figure 2.11 Adsorption and desorption process of water vapour on solids
(Halimeö, 2007)

2.4.4.1 Closed Thermochemical Energy Storage

A closed sorption system is based on the same physical effect as the open storage, but the engineering is quite different from open sorption systems. In closed systems, the components cannot be exposed to the atmosphere and sorption process can use water vapour as adsorptive and the operation pressure of the working fluid can be adjusted, see Figure 2.12. The heat energy from system needs to be transferred to and from the adsorbent using a heat exchanger. Comparing with open storage, the expected energy density of closed systems is reduced. The main reason for this is that the adsorbent (water vapour) is the part of the storage system and has to be stored as well (Halimeö, 2007). Adedin and Rosen (2011) used energy and exergy method to assess closed thermochemical energy storage (Adedi, 2011b). Exergy analysis can be used to identify the locations and reasons of thermodynamic losses and evaluate efficiencies for the various processes of closed storage systems. In 2008, Hauer has given a comparison on sorption storage systems, which means that internal substances of closed system are separate from the heat transport stream and can provide higher output temperatures than open storage. Meanwhile, closed systems can be used to supply low temperatures for building cooling (Hauer, 2008). A closed storage system usually requires higher temperatures during the charging process than open systems (Hauer, 2007). Furthermore, a combined solar energy storage system with a closed loop chemical heat pipe was investigated by Levy et al. The overall performance of the closed loop was found to be satisfactory (Hauer, 2002).

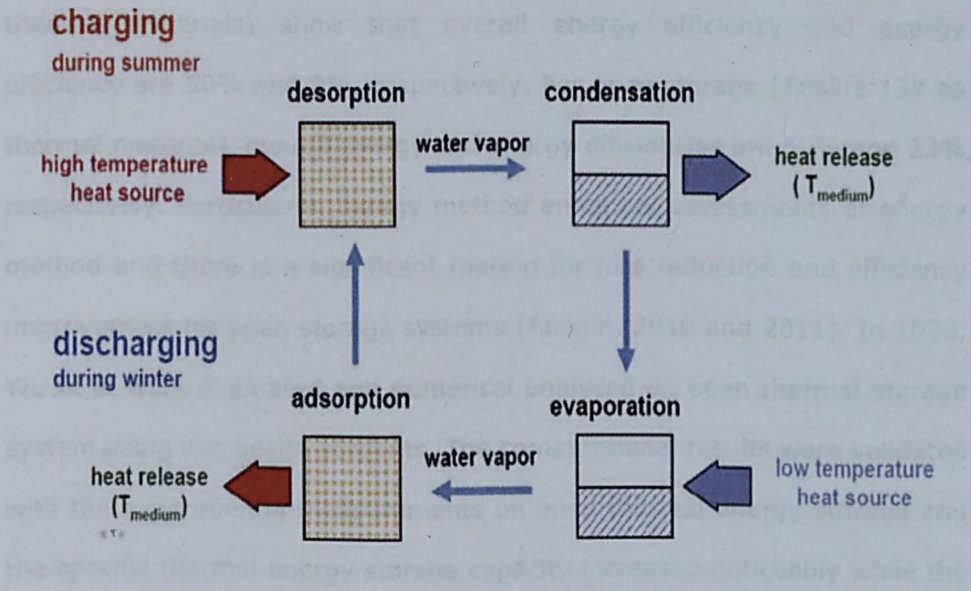


Figure 2.12 Operation principle of closed thermochemical energy storage
(Halimeö, 2007 and N'Tsoukpoe, 2009)

2.4.4.2 Open Thermochemical Energy Storage

In an open sorption storage system, air is carrying water vapour and heat energy in and out of the packed bed of solid adsorbents or a reactor where the air is in contact with a liquid desiccant as shown in Figure 2.13 (Halimeö, 2007). An open sorption system is composed of a working fluid and a thermochemical material. Gaseous working fluid of open system is directly released to the environment and operates at atmospheric pressure (Abedin, 2010). Therefore, normally only water is a possible candidate as the working fluid. Also, materials are required to be non-toxic and non-flammable in open systems. In open storage systems, separated desorption step (charging process) and adsorption step (discharging process) are used to store thermal energy without any thermal energy losses. Closed and open thermochemical energy storage systems were investigated by Abedin and Rosen through based on energy and exergy methods (Abedin, 2011). The results for closed storage ($SrBr_2 \cdot 6H_2O$ as

thermal materials) show that overall energy efficiency and exergy efficiency are 50% and 9%, respectively. For open storage (Zeolite 13X as thermal material), overall energy and exergy efficiencies are 69% and 23%, respectively. Particularly, exergy method enhances assessments of energy method and there is a significant margin for loss reduction and efficiency improvement for open storage systems (Abedin, 2010 and 2011). In 2009, Wu et al were evaluated and numerical analysed an open thermal storage system using composite sorbents. The computational results were validated with the experimental measurements on open thermal energy storage and the specific thermal energy storage capacity increased noticeably while the COP of the thermal energy storage system decreased (Wu, 2009).

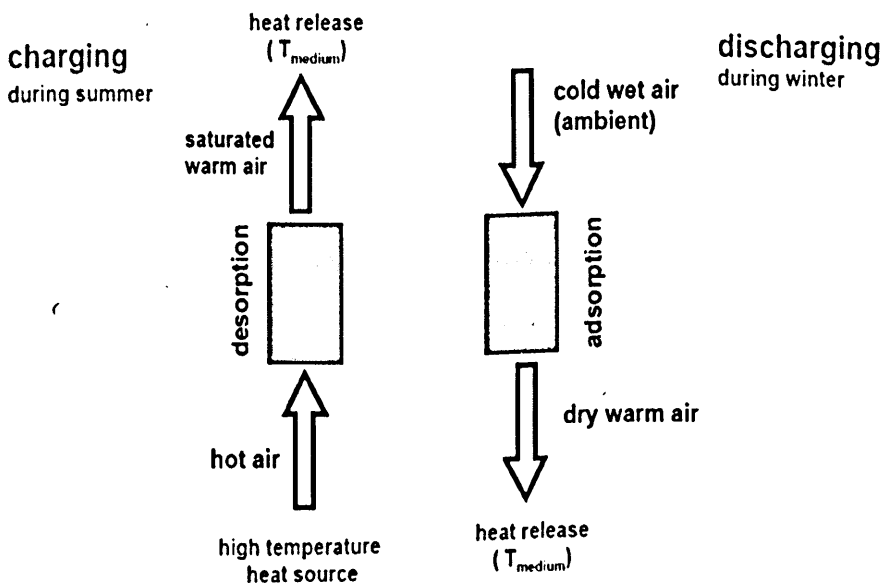


Figure 2.13 Operation principle of open thermochemical TES (Hauer, 2002; Halimeö, 2007 and N'Tsoukpoe, 2009)

2.4.5 Chemical Heat Pump (CHP) Storage Systems

Chemical heat pump (CHPs) is a representative of chemical thermal energy conversion and storage systems (Kato, 2007). Basically, chemical heat

pump makes use of transformation between thermal power and potential energy (Wang, 2008). Specifically, chemical heat pump systems utilize the reversible chemical reaction and sorption to change temperature level of the thermal energy, which is stored by chemical substances (Kawasaki, 1999; Wongsuwan, 2001). These chemical materials play a significant role in absorbing and releasing heat (Kato, 1996). According to the characteristic of the chemical reaction, various chemical materials could be involved in chemical heat pumps. Chemical heat pump system can be sorted as mono-variant system and di-variant system (Wongsuwan, 2001 and Wang, 2008). The general classification of chemical heat pumps is illustrated in Figure 2.14.

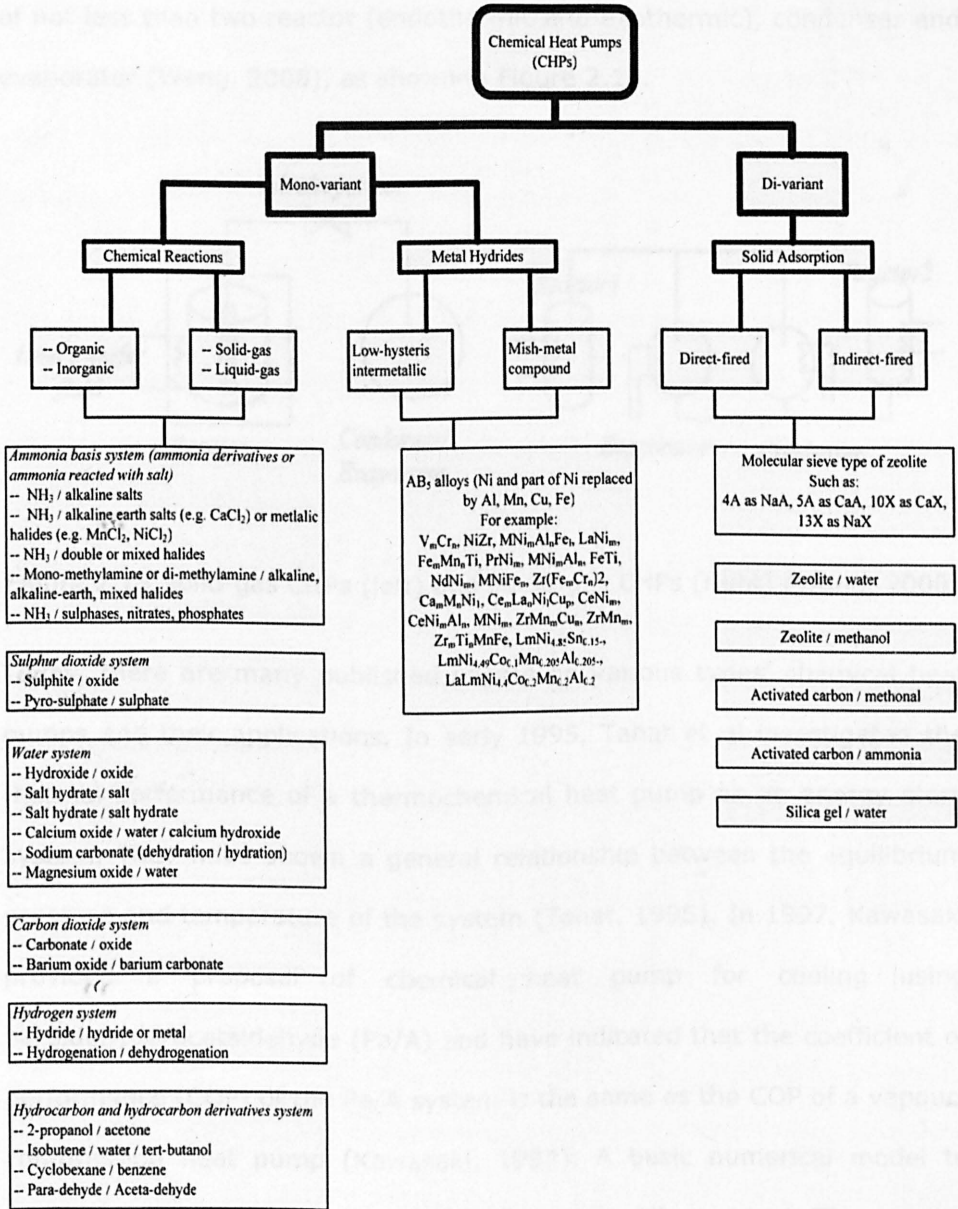


Figure 2.14 Classification of chemical heat pumps (Wongsuwan, 2001 and Wang, 2008)

On the other hand, chemical heat pump could be categorized into two types commonly: solid to gas and liquid to gas in term of the phase of working pairs. Solid-gas systems normally are composed of reactor, condenser and evaporator. Liquid-gas chemical heat pumps are consisted

of not less than two reactor (endothermic and exothermic), condenser and evaporator (Wang, 2008), as shown in Figure 2.15.

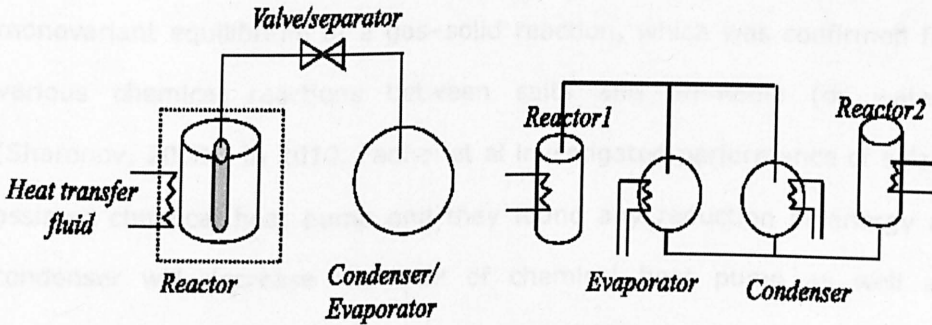


Figure 2.15 Solid-gas CHPs (left) and liquid-gas CHPs (right) (Wang, 2008)

Today, there are many published papers on various types' chemical heat pumps and their applications. In early 1995, Tahat et al investigated the thermal performance of a thermochemical heat pump as an energy store system. They have shown a general relationship between the equilibrium pressure and temperature of the system (Tahat, 1995). In 1997, Kawasaki provided a proposal of chemical heat pump for cooling using paraldehyde/acetaldehyde (Pa/A) and have indicated that the coefficient of performance (COP) of the Pa/A system is the same as the COP of a vapour-compression heat pump (Kawasaki, 1997). A basic numerical model to analyse chemical heat pump was developed by Mbaye et al. The source-based method (which is a fixed grid enthalpy approach) was employed (Mbaye, 1998). Kato was examined experimentally a packed bed reactor of magnesium oxide/water chemical heat pump system to evaluate the contribution of the chemical heat pump to decentralised cogeneration. This type of chemical heat pump enhanced the energy utilisation efficiency of the cogeneration system by storing and utilising surplus exhaust heat from the cogeneration system (Kato, 2001). In 2002, Fujimoto published his

work on dynamic simulation of an experimental prototype $\text{CaO}/\text{Ca}(\text{OH})_2$ chemical heat pump system (Fujimoto, 2002). Sharonov found the Carnot efficiency can be obtained for a chemical heat pump that results from monovariant equilibrium of a gas–solid reaction, which was confirmed for various chemical reactions between salts and ammonia (or water) (Sharonov, 2008). In 2010, Fadhel et al investigated performance of solar-assisted chemical heat pump and they found any reduction of energy at condenser will decrease the COP of chemical heat pump as well as decrease the efficiency of drying (Fadhel, 2010 and 2011). Kim et al evaluated a chemical heat pump with reactivity enhancement of chemical materials (EMC), which is a mixed materials comprising expanded graphite, $\text{Mg}(\text{OH})_2$ and calcium chloride (CaCl_2). Enhancement of chemical materials was concluded to have higher dehydration rate and hydration reactivity at temperatures of up to 200 °C than the other materials (Kim, 2011).

2.5 Performance of Thermochemical Energy Storage Techniques

Thermochemical energy storage systems utilise renewable energy sources and waste energy recovery over a wide range of temperatures. Table 2.10 provides a list of some recent analytical, numerical and experimental studies for different solution methods employed in investigating the thermochemical energy storage. From these recent surveys, the main advantages of the analytical model are simplicity and short computation times.

Thermochemical energy storage could be investigated using analytical, numerical and experimental methods in terms of one-dimensional, two-dimensional or three-dimensional models. An up to date three dimensional

hydrogen absorption model is developed by Nam et al (2011). This 3D model is first experimentally validated against the temperature evolution data available in the literature (Nam, 2011).

Table 2.10 Summary of numerical, experimental and analytical studies on thermochemical energy storage

References	Nature	Working pairs	Applications & Solution/Validation/Results
Abedin and Rosen, 2011	Analytical	SrBr ₂ ·6H ₂ O	Energy and exergy methods, closed and open thermochemical energy storage
Liu et al, 2011	Analytical	CaCl ₂ /H ₂ O, etc	Seasonal storage of solar energy for house heating, the storage capacity changing with evaporator and absorber temperature
Sharonov et al, 2008	Analytical	MgCl ₂ ·2H ₂ O, etc	Chemical and adsorption heat pumps, the second law efficiency, degradation of the efficiency due to the thermal entropy production
Nam et al, 2011	Numerical	LaNi ₅ H ₆	3D hydrogen absorption model, heat and mass transport phenomena in metal hydride hydrogen storage vessels
Ghommem et al, 2011	Numerical	MgSO ₄ ·7H ₂ O	Modelling the heat release during a thermochemical hydration reaction, dimensionless parameters have influence on heat release process
Balasubramanian et al, 2010	Numerical	MgSO ₄ ·7H ₂ O	Mathematical model to investigate the capability of salt hydrates to store thermochemical energy, employing a finite difference scheme
Darkwa et al, 2006	Numerical	Na ₂ B ₄ O ₇ ·10H ₂ O, etc	Agitated fluidised bed thermochemical reactor system, enhanced adsorption capacities and heat transfer rates
Sapienza et al, 2012	Experimental	LiNO ₃	Low regeneration temperature (<70°C), the cycle performance depends on the cycle time, duration of the isobaric adsorption and desorption
Stitou et al, 2011	Experimental	BaCl ₂ ·8NH ₃	Solar air-conditioning pilot plant for housing, collectors operating at 70 °C, solar COP of thermochemical sorption process is around 18%
Aristov et al, 2010	Experimental	LiNO ₃	intermittent cooling cycle with adsorption & desorption, the duration of desorption phase has efficient on the cycle COP and SCP
Posern and Kaps, 2010	Experimental	MgSO ₄ & MgCl ₂	Isothermal heat of sorption and thermogravimetry (TG), reduced the deliquescence relative humidity and increased the capacity of condensation
Fadhel et al, 2010, 2011	Experimental & numerical	CaCl ₂ ·8NH ₃	Solar-assisted chemical heat-pump dryer, reduction of energy at condenser will decrease the COP and the efficiency of drying
Kim et al, 2011	Experimental & Analytical	Mg(OH) ₂	Reactivity enhancement of chemical materials (EMC), EMS have potential in MgO/H ₂ O chemical heat pump

2.6 Solar Energy Collection Systems

A solar thermal collector is a device designed to basically absorb and capture incoming solar energy in form of heat through a heat transfer medium and convert it into a usable or storable energy form. This usable or storable energy can be used for various applications. It can be used for electric power generation using an expander or turbine, for hot water supply, for cooling, industrial process heat and most importantly for desalination facilities.

Solar collectors can be divided into two types of sun tracking concentrating and non-concentrating or stationary solar collectors. A sun tracking concentrating solar collector usually has concave reflecting surfaces (reflectors) to focus and concentrate the solar radiation onto a smaller receiving area (absorber). Whereas, a non-concentrating solar collector does not focus the solar radiation but only uses the flat surface area absorbers to capture the solar energy. A comprehensive list is to catalogue the solar collectors in the available market, which is shown in Figure 2.16.

In 2013, Tian and Zhao presented a review on solar collectors and thermal energy storage in solar thermal applications, which are the two core components. Their paper focuses on various types of solar collectors including both non-concentrating collectors (low temperature) and concentrating collectors (high temperature), and various types of thermal energy storage systems including sensible heat storage and latent heat storage, chemical storage (Tian and Zhao, 2013).

Nowadays, one challenge for the widespread use of solar energy is a reduced or curtailed energy production when the sun sets or is blocked by

clouds. Thermal energy storage provides a workable solution to this challenge.

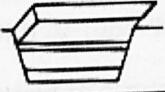
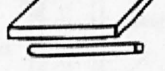
		Collector Type		Concentration Ratio, C_1 for Direct Insolation	Indicative Temperature Obtained T (K)	
		Name	Schematic Diagram			
Motion	Stationary	Non-convecting Solar Pond		$C \leq 1$	$300 < T < 360$	
		Flat-plate Absorber				
		Evacuated Envelope		$C \leq 1$	$320 < T < 460$	
		Compound Parabolic Reflector		$1 \leq C \leq 5$	$340 < T < 510$	
	Solar Tracking	Single Axis	Parabolic Reflector		$5 \leq C \leq 15$	$340 < T < 560$
			Fresnel Refractor		$15 < C < 40$	$340 < T < 560$
			Cylindrical Refractor		$10 < C < 40$	$340 < T < 540$
		Two Axis	Parabolic Dish Reflector		$10 < C < 50$	$340 < T < 540$
			Spherical Bowl Reflector		$100 < C < 1000$	$340 < T < 1200$
			Heliostat Field		$100 < C < 300$	$340 < T < 1000$
				$100 < C < 1500$	$400 < T < 3000$	

Figure 2.16 Types of solar energy collectors (Source: thermopedia.com)

2.6.1 Evacuated Tube Collectors

Evacuated tube collectors are the most efficient as solar thermal collection systems. The collectors are usually made of parallel rows of transparent

glass tubes. Each tube contains a glass outer tube and inner glass or metal tube attached to a fin as the absorber (Figure 2.17). Air is removed, or evacuated, from the space between the two tubes to form a vacuum, which eliminates conductive and convective heat loss. Evacuated tube collectors, based on single envelope vacuum tubes with heat-pipe energy removal and all-glass evacuated tubes with U-tube heat removal system, both have been commercialised in the world (Morrison, 2001).

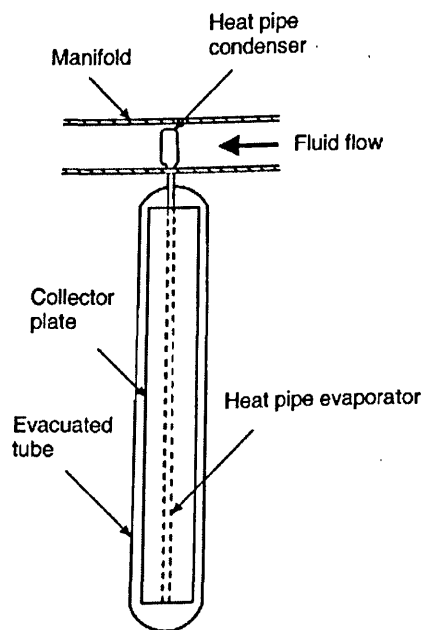


Figure 2.17 Schematic diagram of an evacuated tube collector (Soteris, 2004 and Ayompe, 2013)

Normally, evacuated tube collectors can be classified in two main groups as direct flow tubes and heat pipe tubes, which are being used for both lower and higher temperature applications. Lower temperature (70°C to 150°C) applications comprise of water heating for domestic and commercial purposes, steam generation for cooking and refrigeration. Higher temperature (up to 400°C) applications are mainly for power generation. There have been many reference publications about evacuated tube solar

collectors. In 2004, some common characteristics of a typical evacuated tube collector system were summarised by Soteris, as shown in Table 3.2. Tang et al (2009) presented a paper on optimal tilt-angles of all-glass evacuated tube solar collectors in China and results implied that collector types, central distance between tubes, size of solar tubes, tilt and azimuth angles were main factors to affect the annual collectible radiation on a tube (Tang, 2009). A comparative performance study (Ayompe, 2011) on flat plate and heat pipe evacuated tube collectors for domestic heating systems in a temperate climate was conducted by Ayompe in 2011. Caglar and Yamali theoretically and experimentally investigated the performance of a solar-assisted heat pump with an evacuated tubular collector (Caglar, 2012).

2.6.1.1 Heat Pipe Evacuated Tube Collector

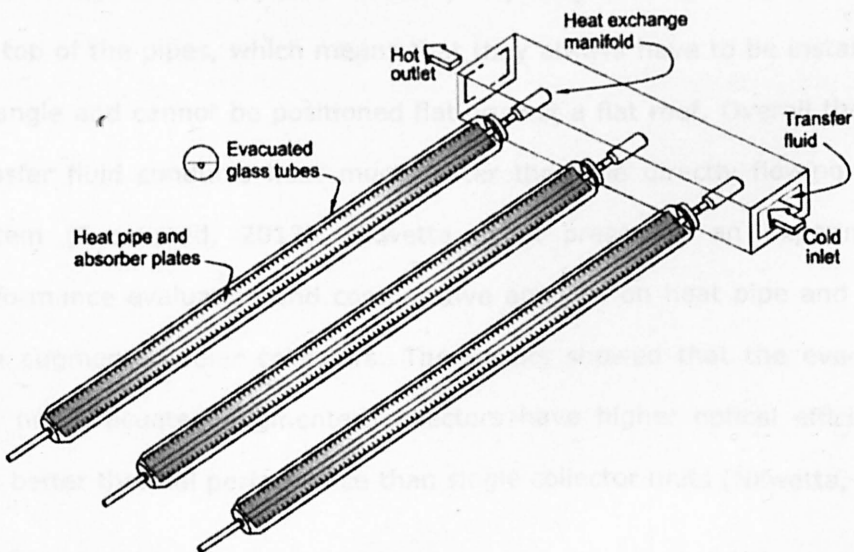


Figure 2.18 Heat pipe evacuated tube collectors (Morrison, 2001)

Heat pipe evacuated tube collectors are widely and commonly used in the UK. It combines a heat pipe solar collector and a storage tank into one system. The condenser of the heat pipe tube is directly inserted into the

non-corroding copper protection tube within the water tank (Figure 2.18). The heat pipe evacuated tubes collect heat with high efficiency transforming of the incoming solar irradiation into heat. The condenser transfers the generated heat to the manifold where the water is heated. Thereafter, the hot water is circulating in the system until the system attains the required temperature (Evacuated, 2013).

A direct flow evacuated tube collectors is a very simple system that works in a similar fashion to a conventional flat plate collector but with the benefit of vacuum insulation. There is a key problem about tubes maintenance, which is difficult for future replacement. On the other hand, heat pipes evacuated tube collectors can be easily disconnected from the manifold and replaced or maintained without fear of damaging water pipes. Heat pipe systems do tend to cost a little more than direct flow systems. But, disadvantage of heat pipes is that they rely on gravity to move the heat to the top of the pipes, which means that they always have to be installed at an angle and cannot be positioned flat against a flat roof. Overall the heat transfer fluid conducts heat much faster than the directly flowing water system (Evacuated, 2013). Nkwetta et al presented an experimental performance evaluation and comparative analysis on heat pipe and direct flow augmented solar collectors. The results showed that the evacuated and non-evacuated augmented collectors have higher optical efficiencies and better thermal performance than single collector units (Nkwetta, 2013).

2.6.1.2 Direct Flow Evacuated Tube Collector

A direct flow evacuated solar collector consists of a row or solar tubes and a highly insulated manifold. Heat transfer fluid is circulated in a coaxial manner through the manifold and tubes. Water is the heat transfer fluid and circulates through the pipes, one for inlet fluid and the other for outlet

fluid (as shown in Figure 2.19). Direct flow evacuated tube collector systems have a loop of pipe that runs through the evacuated tubes. The water is directly heated by the sun and pumped around the tubes and eventually passes through the secondary coil into the hot water cylinder.

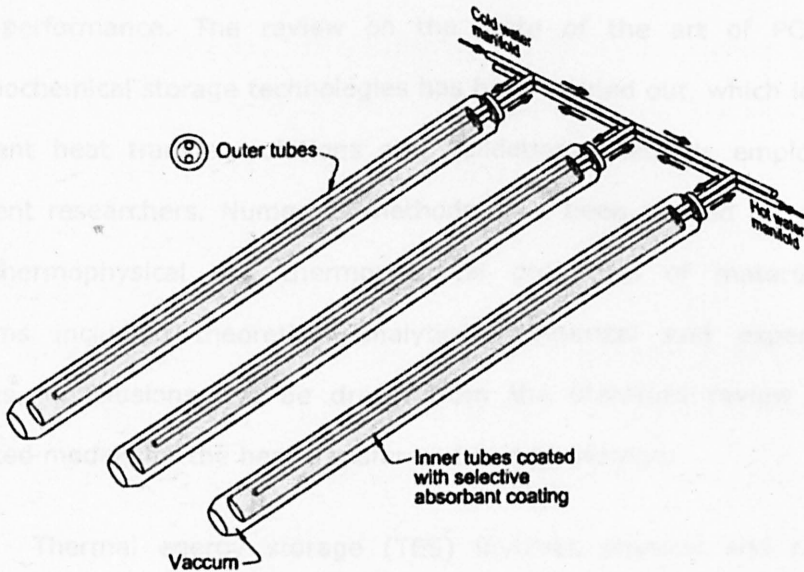


Figure 2.19 Direct flow evacuated tube collectors (Morrison, 2001)

According to the distribution of these pipes, there are several types of collectors classified as glass-metal collector, glass-glass collector and evacuated tube with CPC (Zhang, 2010). Glembin et al conducted a simulation on the direct flow coaxial vacuum tube collectors (Glembin, 2010). Their results showed an efficiency reduction of 10% if reducing the flow rate from $78 \text{ kg/m}^2 \text{ h}$ to $31 \text{ kg/m}^2 \text{ h}$ for a collector group with 60 parallel vacuum tubes with a coaxial flow conduit at one-sided connection. Kingspan has introduced a very common glass-metal direct flow evacuated tube collector called DF100. DF100 is recommended for a wet environment especially for industrial and commercial use and ideal for UK weather conditions. This versatile system can be installed on facades or flat roofs both horizontally and vertically (Kingspan, 2013).

2.7 Summary

Over the past several decades, studies of thermal energy storage systems have investigated design fundamentals, components and process optimization, materials selection, transient and long-term behaviour, and field performance. The review on the state of the art of PCMs and thermochemical storage technologies has been carried out, which identifies different heat transfer solutions and validations methods employed by different researchers. Numerous methods have been applied for studying the thermophysical and thermochemical properties of materials and systems including theoretical analytical, numerical and experimental studies. Conclusions can be drawn from the literature review on the reported models for the heat transfer and energy storage:

- Thermal energy storage (TES) involves physical and chemical processes. Most of potential TES systems are latent heat (solid-liquid phase change process) thermal energy storage and thermochemical energy storage.
- PCMs include organic, inorganic and eutectic materials. Organic materials are simple to use and non-corrosive, inorganic and some eutectic materials are generally cheap and good for latent heat. Solar powered system can be combined with PCMs.
- Most PCMs have quite low thermal conductivities. In order to improve these PCMs' rates of charging and discharging, heat transfer enhancement techniques are introduced by inserting special materials as thermal conductivity promoters. These special materials include Copper, aluminium, nickel, stainless steel and carbon fiber with various forms of fins, honeycomb, wool, and brush, etc.

- Melt time of PCMs is a basic criterion to check their thermal properties, which depends on length of constructor and is related to Stefan number.
- Many available mathematical and engineering software tools, such as TRNSYS, ESP-r, EnergyPlus, COMSOL, COSMOS/M, PCM Express and ANSYS, have been employed to simulate heat transfer with PCMs. The disadvantages to use these tools are that the result is often overestimated and a large difference could occur in the scale problem (Harald, 2008). In addition, leakages and corrosion cannot be numerically simulated.
- Phase change problems can be studied by analytical, numerical and experimental methods in terms of one-dimensional, two-dimensional or three-dimensional models. Analytical models are usually simple with short computation time. Numerical and experimental processes are time consuming. In experimental models, positioning thermocouples sometimes is a challenge.
- Chemical thermal energy storage in general can be categorised into chemical storage and thermochemical storage. Thermochemical storage systems can be divided into open and closed systems.
- Energy and exergy method is employed to assess closed and open thermochemical energy storage systems. Closed system can be used to supply low temperatures for building cooling. Open system is directly operated at atmospheric pressure. Therefore, water is usually a possible candidate as its working fluid.
- Chemical heat pump (CHPs) is a representative of chemical thermal energy conversion and storage systems. CHP can be

categorized into two types: (solid to gas and liquid to gas in term of the phase of working pairs).

- Compared with physical change, thermochemical energy storage system has the following advantages: having higher energy density, long-term storage as reactant with smaller thermal loss, easily to be transmitted to generate heat at another location, having wider temperature range and characteristics.

Meanwhile, this chapter has also reviewed and illustrated types of solar energy collectors in terms of their motion on solar tracking concentrating or stationary (non-concentrating). Evacuated tube collectors can be divided into direct flow solar collector and heat pipe solar collectors. The glass-metal direct flow evacuated tube collector is an ideal for UK wet weather conditions supplied by Kingspan Renewables Ltd, which is investigated and discussed in the following chapters.

CHAPTER 3

Theoretical Analysis and Computer Simulation for Thermal Energy Storage

3.1 Introduction

In order to propose and build a state of the art high capacity heat storage system, a modelling passive house is represented by the EDSL TAS building thermal analysis software for a thermochemical materials energy storage system. This thermochemical materials energy storage system is proposed to integrate with a solar collector with PCM store tank.

Theoretically, seasonal high capacity thermal energy storage is a novel technology using thermochemical materials to store the excessive solar heat gained during summer time to apply for heating in winter, which can not only avoid overheating in summer but also reduce space heating cost in winter. A seasonal thermochemical energy storage system is composed

of four parts including high density thermochemical materials energy storage system, solar collectors, air to air heat exchanger and some associated auxiliary equipment. Thermal energy captured from high efficient roof-integrated solar collectors and energy recovery system inside building will be transferred to the underground thermal energy storage. With chemical reaction and removal of moisture, energy can be stored in a stable state for a long time. And in winter, when space heating is required, thermal energy will be generated through a reversing process, as shown in Figure 3.1.

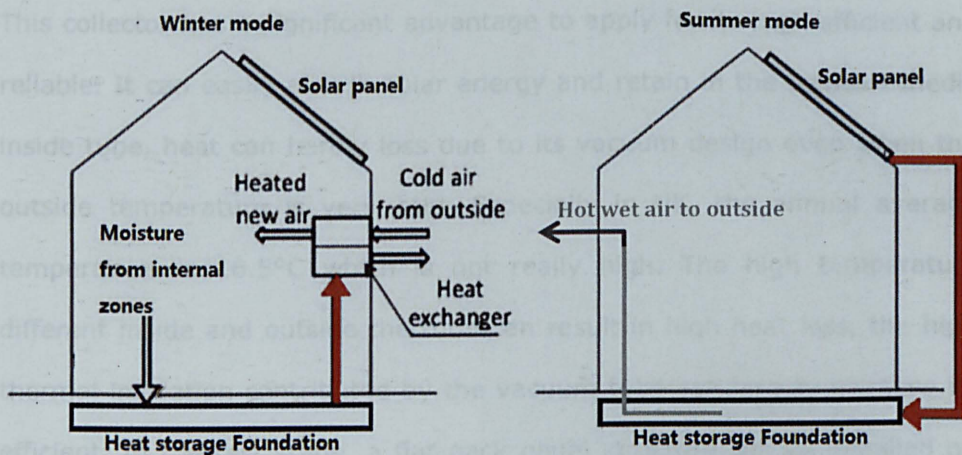


Figure 3.1 Working principle of seasonal thermal energy storage

In practice implementation, high thermal storage density, acceptable space requirements and low associate costs are the considerations that should take during design stage. In area where annual heating load is really high, like United Kingdom, the amount of material that need to satisfy it heating demands will usually occupy large volume, which therefore has high mass. So, structure foundation of a building is an ideal place to install it. The foundation supports should be excavated or impacted piers of concrete or concrete columns. And a good container which has a high thermal

resistance and good air tightness for adsorbent installation is required to reduce heat loss for long term energy storage.

Roof-integrated solar collector takes the role as a "heat generator" in this system and is the main way thermal energy comes from. Large amount of solar energy that reaches the roof will be collected by it every year. Heat will then be transferred from the roof to the modular foundation via a media, like water, and finally be absorbed by the thermal energy with aid of heat exchanger. Evacuated tube solar collector is a common type of solar collector used for water heating and solar air conditioning purpose. This collector has a significant advantage to apply for its high efficient and reliable. It can easily absorb solar energy and retain in the transfer media inside tube, heat can hardly loss due to its vacuum design even when the outside temperature is very cold. Especially in UK, the annual average temperature is 16.5°C which is not really high. The high temperature different inside and outside the tube can result in high heat loss, the high thermal insulation contributed by the vacuum tube can largely increase its efficient. In the test stage, a flat pack panel structure will be installed on the roof of a zero carbon house at the University of Nottingham, UK.

3.2 Introduction to Nottingham H.O.U.S.E

The Nottingham HOUSE is a Zero-Carbon Modular Home at the University of Nottingham, as shown in Figure 3.2, which is built following the world's most stringent energy-saving house design codes of German Passivhaus Institute Design and Code 6 of UK for sustainable homes (Zero Carbon Emission). Priorities include achieving zero carbon targets where all the energy used in the house is produced by the solar collector system on the roof.

This is a two-floor flat roof house, with a big skylight set on the roof to obtain enough daylight for the ground and the first floor. The total construction area of two floors is 75.34 m², which is comprised of 9 rooms: entrance lobby, toilet, living room (including the kitchen), stair, two bedrooms, bathroom, circulation space and a plant room on the ground floor. Since the plant room locates outside the external door and no ventilation and thermal requirement are needed there, it will not be considered during simulation.



Figure 3.2 View of Nottingham H.O.U.S.E

3.3 Modelling of Passive House

3.3.1 Simulation Target Statement

Nottingham HOUSE will be applied to test the actual thermal performance of this seasonal storage system. However, in design stage, the interior environment situations should be assessed at design stage. With the accurate values of annual cooling load and heating load, the system can be

sized with different materials and to achieve energy performances of different types.

In this stage, EDSL TAS software has been applied to simulate the proposed Nottingham HOUSE. TAS (Thermal Analysis Software) is building thermal analysis software developed by EDSL (Environmental Design Solutions Limited). TAS provides an analysis of a building's energy consumption and assesses summer peak temperatures. There are usually five key steps to build up and simulate a comprehensive model in TAS simulator. Figure 3.3 is the flow chart showing what exact five steps are.

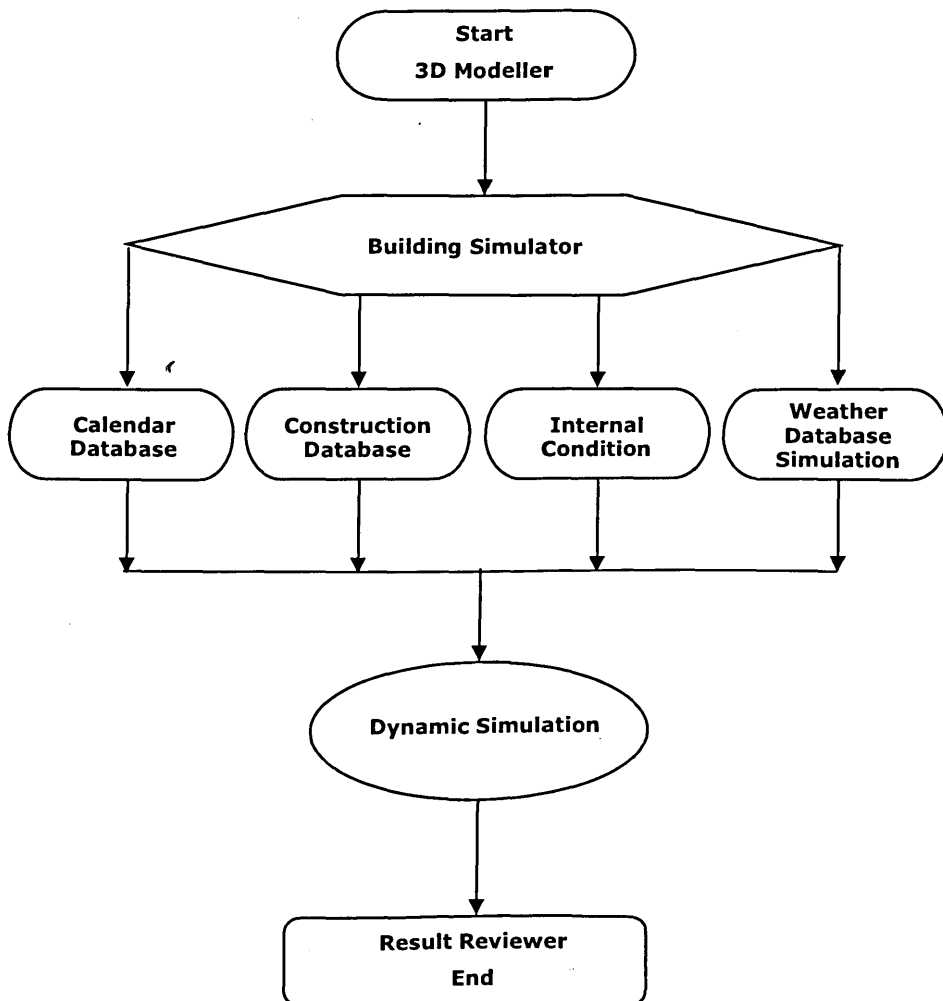


Figure 3.3 Flow chart of a TAS model process

3.3.2 Simulation Setting

Core parameters settings in EDSL TAS software include year calendar, local weather, zoning of house, construction materials, internal conditions of each zone and operation schedules. Figure 3.4 is a 3D model of Nottingham HOUSE in EDSL TAS.

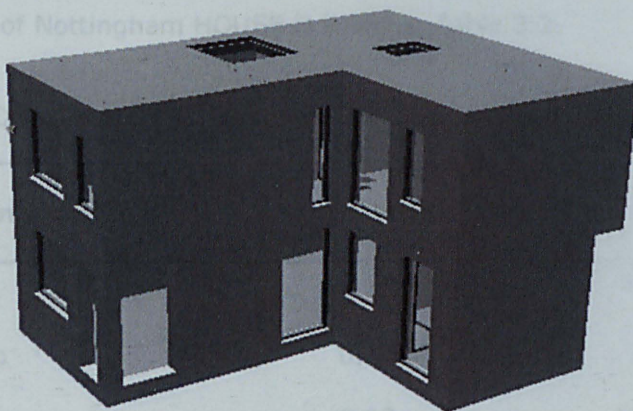


Figure 3.4 The TAS 3D model of Nottingham H.O.U.S.E

3.3.2.1 Calendar

Calendar setting is a key function in TAS. As the annual weather condition varies day by day, the occupants of house will have different responses on different weather. Four season days are simple as shown in Table 3.1. It is based on the annual climate variation in United Kingdom which is recommended by CIBSE.

Table 3.1 Day type classification

Day type	Year days number
Spring days	81 - 123
Summer days	124 - 247
Autumn days	248 - 334
Winter days	1 - 80, 335 - 365

3.3.2.2 Construction Materials

Heat loss through building envelop take a large proportion of total energy loss. To minimize such loss, attention should pay on both design and construction stage: thermal resistance of construction materials and airtightness of envelop. Materials with low U-Value will significantly reduce unexpected heat transfer through the fabric. The U-value of main construction of Nottingham HOUSE is listed in Table 3.2.

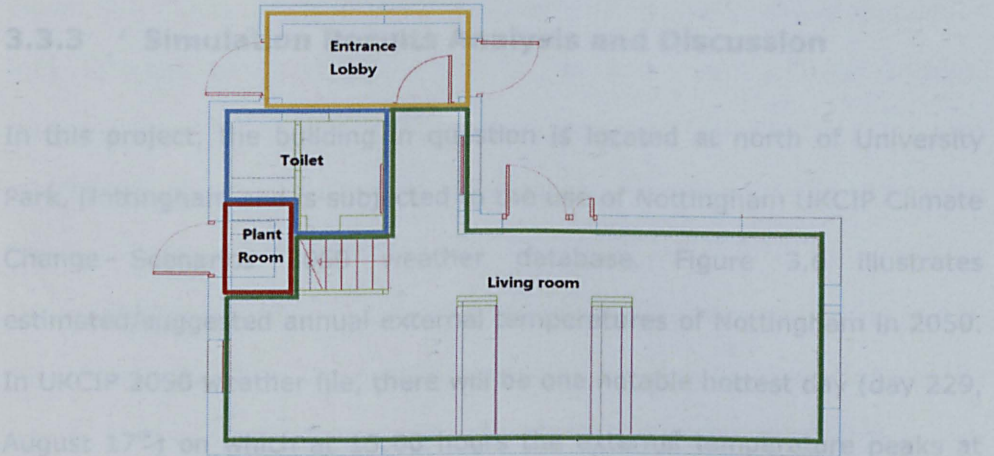
Table 3.2 Detail materials' layers and corresponding thermal properties

Construction materials	U-value (W/m ² k)
Wall Build up	0.10
Floor build up	0.10
Roof build up	0.13
Skylight	0.46
Normal window	2.20
Door	0.16
Frame	0.54

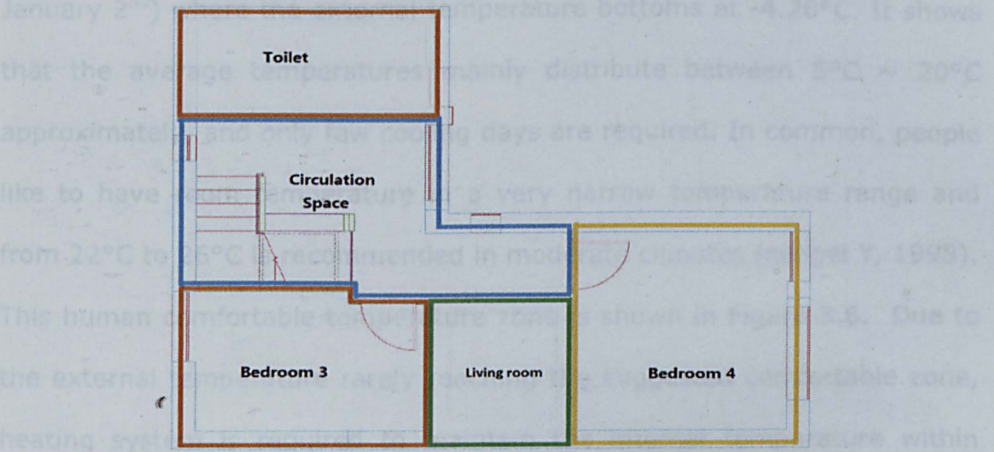
(Source: *Nottingham House, 2013*)

3.3.2.3 Zoning

Zone function is the basic unit for a building to simulate in TAS, and the modelling result will be displayed in zone format. Figure 3.5 shows the Nottingham HOUSE zone setting on ground floor and first floor. With different function classification of rooms, the whole house is divided into seven zones: bedroom 3, bedroom 4, toilet, entrance lobby, living room, circulation and plant room. The detail parameters of zones of Nottingham HOUSE are listed in Table 3.3.



A: Ground floor



B: First floor

Figure 3.5 Schematic of zoning on ground floor and first floor

Table 3.3 Dimension of zones of Nottingham HOUSE

Zone	Area (m ²)	Volume (m ³)
Entrance lobby	4.006	9.214
Toilet	8.149	18.481
Plant room	0.619	1.424
Living room	31.863	84.389
Bedroom 3	7.865	17.680
Bedroom 4	10.749	24.163
Circulation space	12.704	28.659

3.3.3 Simulation Results Analysis and Discussion

In this project, the building in question is located at north of University Park, Nottingham and is subjected to the use of Nottingham UKCIP Climate Change Scenarios 2050 weather database. Figure 3.6 illustrates estimated/suggested annual external temperatures of Nottingham in 2050. In UKCIP 2050 weather file, there will be one notable hottest day (day 229, August 17th) on which at 15:00 hours the external temperature peaks at 33.60°C. At the same time, there is a remarkable coolest day (day 2, January 2nd) where the external temperature bottoms at -4.20°C. It shows that the average temperatures mainly distribute between 5°C ~ 20°C approximately, and only few cooling days are required. In common, people like to have room temperature in a very narrow temperature range and from 22°C to 26°C is recommended in moderate climates (çengel Y, 1998). This human comfortable temperature zone is shown in Figure 3.6. Due to the external temperature rarely reaching the suggested comfortable zone, heating system is required to maintain the internal temperature within thermal comfort zone.

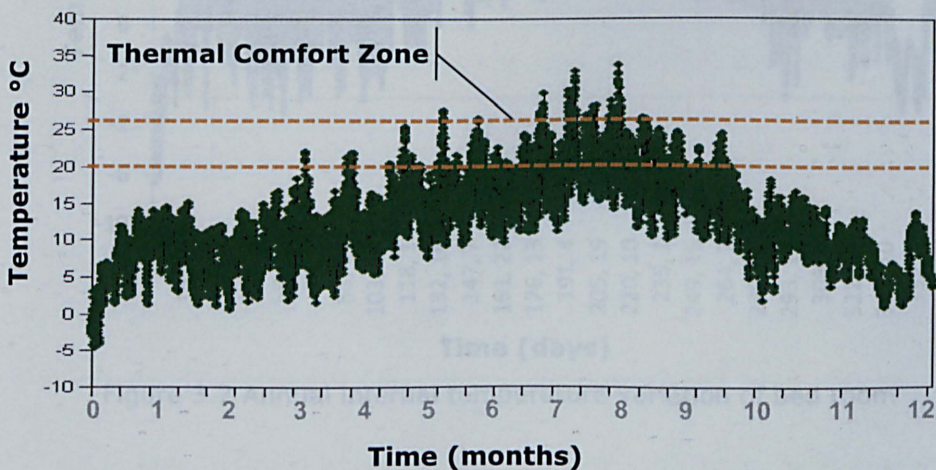


Figure 3.6 Annual ambient temperatures of Nottingham (UKCIP 2050)

Figure 3.7 shows the comparison between outdoor temperature fluctuation and internal temperature variations in bed room. These internal temperatures are around 20°C at the beginning of year, and increase slowly following the outdoor temperature variation trend. Except the toilet room, all other rooms have temperature points below 20°C during winter. This is because the zones have been set an operational schedule for energy saving purpose. Thus, the heating system in a specific zone is controlled to switch on only when the zone is occupied. It will be pre-heated one hour before the arrival of occupants, and will stop being heated till all occupants leave. As this building has a high thermal insulation, little heat loss through fabric occurs during off-schedule period and temperature fluctuation is therefore small.

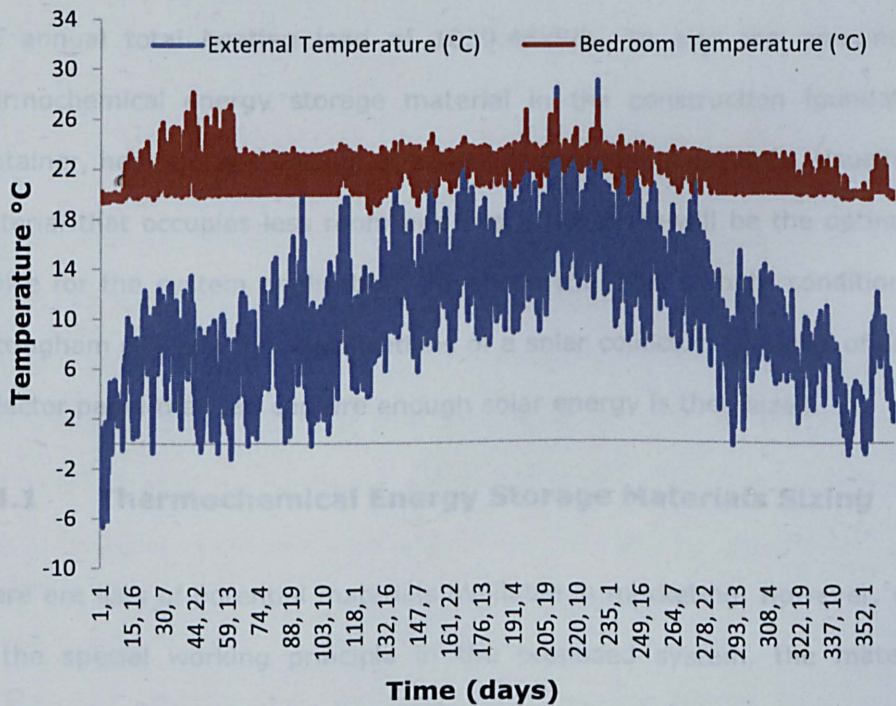


Figure 3.7 Annual internal temperature variation of bed room

Annual cooling and heating load assessments are another core aspect to evaluate the energy performance of Nottingham HOUSE. As seen from the

simulation results, the annual heating and cooling loads are about 1039.46kWh and 46.70kWh, respectively. As the total heating floor area is aforementioned 75.34m², the heating load for average square meter is 13.80kWh/m².yr. According to the Passivhaus standard of UK, the annual heating load per square meter should be less than 15kWh/m².year. Hence, the Nottingham HOUSE performs in low energy consumption and satisfies the requirement as a Passive House. A designed seasonal thermal energy storage system is therefore recommended for winter heating task in this building to reduce annual energy consumption.

3.4 Numeration of Seasonal Thermal Storage System

Based on above simulation results, a seasonal thermal energy storage system can then be sized for winter heating in Nottingham HOUSE to meet the annual total heating load of 1039.46kWh. To size the amount of thermochemical energy storage material in the construction foundation container, heat storage density of a specific material is required. Usually, a material that occupies less room and has a low price will be the optimum choice for the system application. Based on the local climate condition in Nottingham city and the specifications of a solar collector, the area of solar collector panel that can capture enough solar energy is then sized.

3.4.1 Thermochemical Energy Storage Materials Sizing

There are lists of potential materials available in marketing. However, due to the special working principle in the proposed system, the material selected should satisfy the following four requirements:

- A high thermal storage density, which leads to less amount of material to store the same required heat.

- Heat storing in a hydration reaction and releasing in a dehydration way. With water taking part in the reaction, the system can be easily controlled as water vapour can be added or removed in a simple way. The running cost will also be very low as the water vapour required can be captured as moisture from all zones inside the building.
- Temperature of heat absorption reaction occurring over 35°C.
- A low price. Large amount of storage material will be required, and cheap material can save lots of money.

Calcium chloride (CaCl₂) and calcium nitrate (Ca(NO₃)₂) are two promising materials for application.

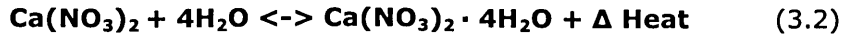
Calcium chloride / CaCl₂ processes heat stores in a reaction as below equation:



The salt content: 50~70 wt. %. The water sorption capacity (T = 35°C, P_{H₂O} = 12 mbar): W = 0.4~0.5 g/g (the hydration phase). The water sorption capacity (T = 80°C, P_{H₂O} = 30 mbar): W = 0.1~0.15 g/g (the dehydration phase). The heat storage density of CaCl₂: Q ≈ 1000 J/g ≈ 500 J/cm³. Cost of the expanded vermiculite is about 80~800 dollar/tonne. Cost of the calcium chloride (China) is about 150~200 Euro/tonne.

To store 1039.463kWh thermal energy during reaction, 3.74 tonne calcium chloride will be applied 7.48m³ in volume. As the ground floor area is 53.60m², if the material is fully distributed underground in 53.60m², the thickness will be 14cm, i.e., it is applicable.

For calcium nitrate / $\text{Ca}(\text{NO}_3)_2$, the corresponding heat storage reaction is shown as below:



The salt content: 50~70 wt. %. The water sorption capacity ($T = 35^\circ\text{C}$, $P_{\text{H}_2\text{O}} = 12 \text{ mbar}$): $W = 0.30 \text{ g/g}$ (the hydration phase). The water sorption capacity ($T = 80^\circ\text{C}$, $P_{\text{H}_2\text{O}} = 30 \text{ mbar}$): $W = 0.03 \text{ g/g}$ (the dehydration phase). The heat storage density: $Q \approx 750 \text{ J/g} \approx 400 \text{ J/cm}^3$. Cost of the expanded vermiculite is about 80~800 dollar/tonne. Cost of the calcium nitrate (China) is about 300~400 Euro/tonne.

To store 1039.463kWh thermal energy during reaction, 4.99 tonne calcium chloride will be applied 9.36m³ in volume. As the ground floor area is 53.60m², if the material is fully distributed underground in 53.60m², the thickness will be 17.50cm.

In terms of capital cost, the prices of CaCl_2 and $\text{Ca}(\text{NO}_3)_2$ are 150~200 Euro/tonne and 300~400 Euro/tonne (imported from China), respectively. Initial investments on CaCl_2 and $\text{Ca}(\text{NO}_3)_2$ are about 1309.70 Euro and 3274.25 Euro. Thus, CaCl_2 , calcium chloride is the optimal material based on volume and price calculation. Besides, several other potential materials can also be applied here. The materials with thermal storage density and sized volume or mass are listed in Table 3.4. Comparatively speaking, the simplest method is to use more materials in heat energy storage system. However, if some kind of cheap material is available, it should be most attractive. The composite material is simple to prepare, inexpensive and may be up scaled in future.

Table 3.4 Potential material sizing

Name / Chemical formula	Thermal storage density	Volume (m³)	Mass (ton)
MgSO ₄	2.8 GJ/m ³	1.34	N/A
FeO	2.2 GJ/m ³	1.70	N/A
CaSO ₄	1.4 GJ/m ³	2.67	N/A
E 30	201.0 kJ/kg	N/A	18.60
Climsel C32	212.0 kJ/kg	N/A	17.65
E 32	186.0 kJ/kg	N/A	20.12
Na ₂ SO ₄	234.0 kJ/kg	N/A	15.99
CaBr ₂	115.5 kJ/kg	N/A	32.40
Zn(NO ₃) ₂	146.9 kJ/kg	N/A	25.47
Na ₂ CO ₃	246.0 kJ/kg	N/A	15.20

3.4.2 Solar Thermal Collector Sizing

It has been carried out that 1039.46kWh thermal energy is required for space heating during autumn and winter in Nottingham House. As the heat is captured and stored inside thermal storage material during summer time, it is necessary to check by software if the solar panel installed on the roof has enough area to collect enough heat during that period. The solar insulation and dimensions of the roof can be used to calculate and size solar thermal collector for Nottingham HOUSE. Evacuate tube solar collector is a type of high efficient solar collector and the efficiency can be high up to 86%. Specifications of the selected solar panel are shown in Table 3.5. The average insolation in Nottingham input is shown in Table 3.6, which shows that the insolation in spring and summer (from March to September) is much stronger than that in autumn and winter (from

October to February) which takes about 83.96% of the annual total insolation.

Table 3.5 Solar panel specifications (Kingspan DF100 vacuum collector)

Specifications	DF100 (3m²)
Number of tubes	30
Dimensions (gross) [mm]	1996 x 2127 x 97
Absorber Area [m ²]	3.02
Weight (empty) [kg]	81.40
Fluid Content [Ltr]	5.60
Max. Operating Pressure [bar]	8
Flow Rate [l/min/tube]	0.10 - 0.25
Vacuum level [mbar]	10 ⁻⁵
Glass Specification	Low Iron Solar Glass
Efficiency (Absorber) η_s	0.832
a1 [W/m ² K]	1.140
a2 [W/m ² K ²]	0.014
Heat Capacity [kJ/m ² /K]	9.200

Table 3.6 Average insolation in Nottingham

Month	Ave. Insolation kWh/m²/day
January	0.65
February	1.32
March	2.22
April	3.39
May	4.42
June	4.50
July	4.48
August	3.85
September	2.64
October	1.57
November	0.82
December	0.51
Annual Total	30.37

Roof dimension of Nottingham HOUSE is shown in Figure 3.8. It can be seen that two skylights are located on this flat roof which are not permitted to be covered by solar panel. The rest area of roof is approximate 39.60m^2 , which can be fully installed panels.

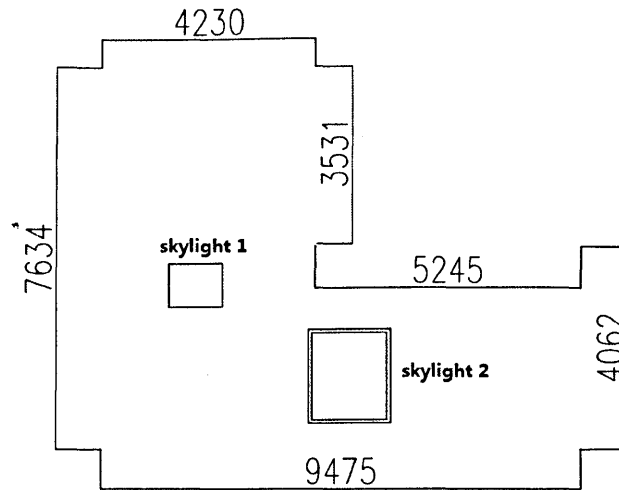


Figure 3.8 Roof dimension of Nottingham H.O.U.S.E

Based on relevant parameters of solar panel are shown in Table 3.4, fourteen panels can be installed on the available area on the roof as a maximum value. Meanwhile, REOPT software is employed to calculate thermal output of solar panels, which is copyright to Dr. Matiwaza Ncube. The result of monthly thermal energy output from solar panel when the roof is fully occupied, which is listed in Table 3.7 in term of the solar insolation and parameters of building roof. It shows that approximate 30362KWh thermal energy will be output annually from fourteen solar panels. However, as the annual heating load for this house is just 1039.40 kWh (Section 3.3.3), one panel of 2.83 m^2 areas will supply enough heat for the storage system. Considering the working principle of seasonal thermal energy storage, thermal energy should be collected from March to September. Heat output from one panel during that period is 1831.16kWh.

Table 3.7 Thermal output from solar panel for available space

Month	Monthly thermal output (KWh/m ²)	Thermal Output for available space (KWh)
Jan	16.185	640.926
Feb	30.951	1225.648
Mar	57.121	2261.976
Apr	84.411	3342.676
May	113.727	4503.573
Jun	112.050	4437.180
Jul	115.271	4564.708
Aug	99.061	3922.796
Sep	65.736	2603.146
Oct	39.093	1548.083
Nov	20.418	808.553
Dec	12.699	502.881
Total	766.721	30362.140

3.5 Summary

Theoretical analysis and computer simulation of a passive house has been stated in the chapter. The results show that some thermochemical materials can be sized in construction foundation container of household to store solar energy in summer and to meet annual heating load of Nottingham HOUSE. On the other hand, proposed solar collector panel can also be sized due to a limited roof space to power thermochemical materials. Both of these data can give a strong reference for further research stage. Therefore, some relevant preliminary experiments on selection, development, synthesis and optimisation of thermal materials will be illustrated and investigate in the following Chapter 4.

CHAPTER 4

Materials Selection and Preliminary Experiment

4.1 Introduction

Selection, development, synthesis and optimisation of thermal materials and some relevant preliminary experiments are a crucial research stage, which will help to propose and build a state of the art high capacity heat storage system. In this chapter, properties and characteristics of some new phase change materials have been firstly investigated in term of their applicable purpose. Then, a preliminary experiments investigation on thermal controlled chamber with PCM is carried out to understand the mechanism and performance of this technology on behalf of ambient temperature respect. Lastly, a closed thermochemical absorption cooling system is conducted to investigate heat capacity and hydration reaction temperature of thermochemical materials, which may give a good idea for winter room heating system as renewable energy strategy.

4.2 PCMs Selection

4.2.1 Properties and Characteristics Testing of PCMs

Materials are one of key elements of a high capacity heat storage system. In order to select appropriate materials (temperature around 60°C) for solar collector energy storage tank, some proposed phase change materials (R5365A, R52, R65, R4117A and 8676A) have been synthesised by manufactory (Figure 4.3). Therefore this experiment aims to investigate properties (melting and solidifying temperature) of these phase change materials in laboratory.

4.2.1.1 Experiment Rig Set-up

Figure 4.1 shows the schematic of experimental rig, which consists of main components as illustrated in Figure 4.2. There are a 1.4kW digital thermostat water heater, a DT80 data taker and a type K thermocouple.

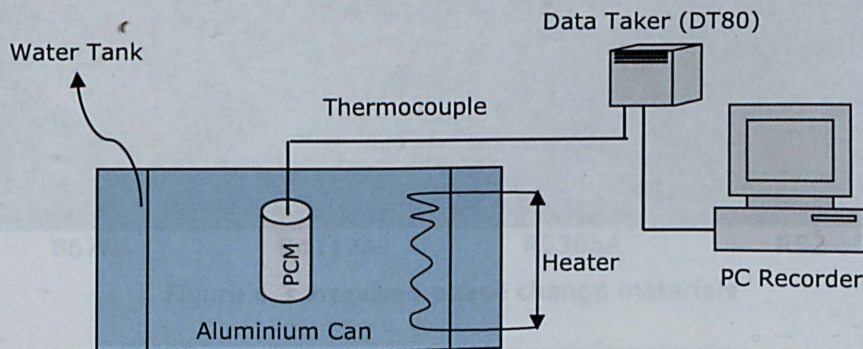


Figure 4.1 Schematic of experiment rig for PCMs testing

In order to obtain exact melting temperatures of these materials and duration of melt and solidification, a thermostat water heater is used to maintain a constant temperature supply to the test water rig, and thermocouples and a DT80 data taker are employed to record materials temperature change.



Figure 4.2 Measurement instruments

4.2.1.2 Phase Change Materials Testing Result Analysis and Discussions

Figure 4.3 shows proposed phase change materials: 8676A, R4117A, R5365A and R52. These phase change materials are filled up into special designed aluminium cans and weighed by types and groups before test (Figure 4.4).



Figure 4.3 Proposed phase change materials



Figure 4.4 Weight of PCMs by groups and types

● **Material: R5365A**

Materials are heated and cooled by hot or cold water during the experiment. The temperature of hot water is maintained at about 72°C. Material R5365A is kept at room temperature (about 25°C) before being put into hot water. Figure 4.5 shows exact melting process of the material R5365A in the hot water. It can be seen that melting point of R5365A is approximate 58°C with phase change from solid to liquid. The duration of this change is about 12 minutes, which will be changed in term of water temperature, structure of the amount of material and aluminium cans (inside with or without fins). For example, the melting time will be reduced if aluminium cans is with inside fins, which means the heat transfer is enhanced between water and material.

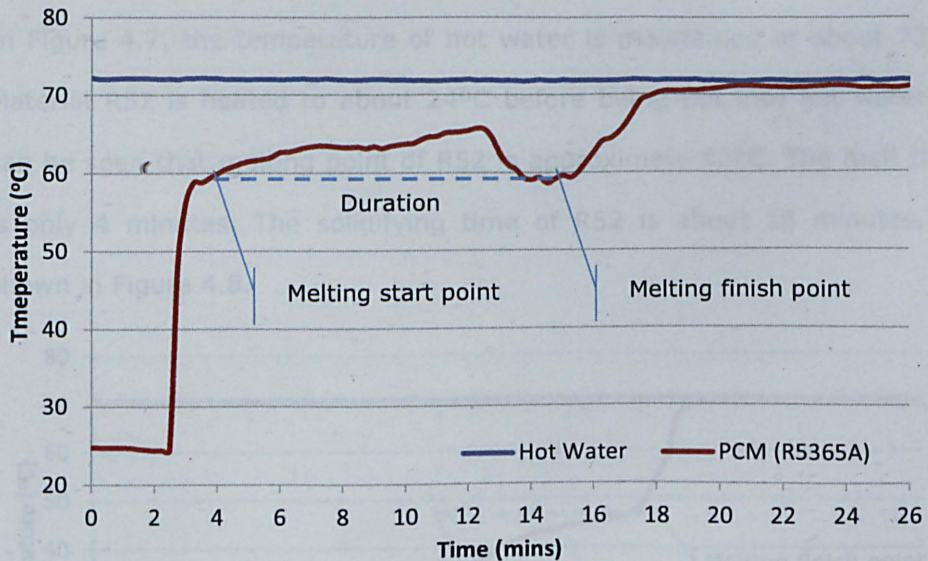


Figure 4.5 Phase change of PCM-R5365A melting process

Figure 4.6 illustrates a solidifying process of the material of R5365A. Liquid R5365A with a temperature of approximate 72°C is put into cold water (temperature around 22°C), which rapidly solidifies to reach the

temperature of cold water. The whole duration of solidification is around 14 minutes.

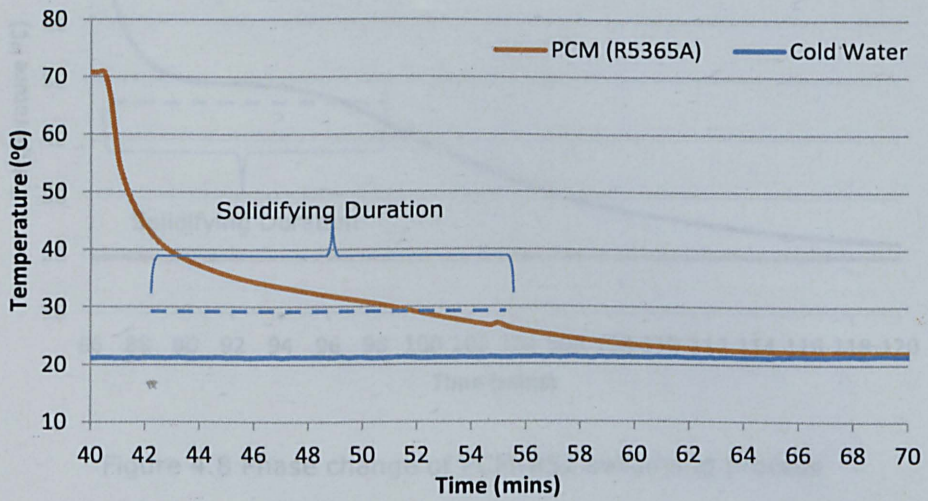


Figure 4.6 Phase change of PCM-R5365A solidifying process

● **Material: R52**

In Figure 4.7, the temperature of hot water is maintained at about 72°C. Material R52 is heated to about 24°C before being put into hot water. It can be seen that melting point of R52 is approximate 42°C. The melt time is only 4 minutes. The solidifying time of R52 is about 18 minutes, as shown in Figure 4.8.

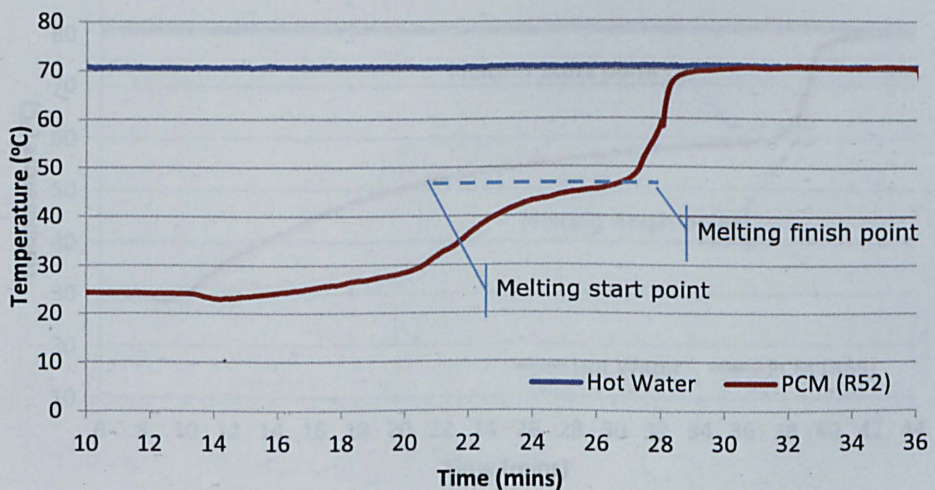


Figure 4.7 Phase change of PCM-R52 melting process

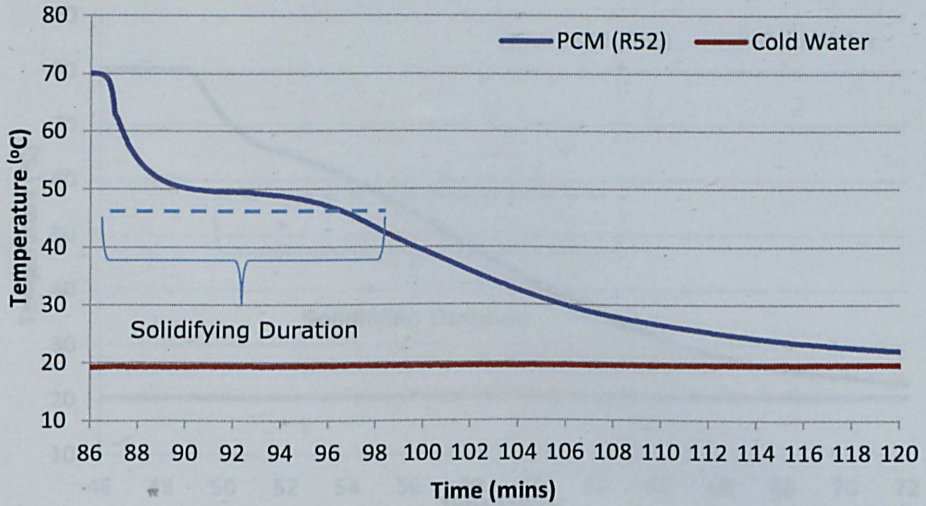


Figure 4.8 Phase change of PCM-R52 solidifying process

- **Materials: R65**

In Figure 4.9, the temperature of hot water is maintained at about 82°C. Material R65 is heated to 30°C before being put into hot water. It can be seen that melting point of R52 is approximate 59°C. The melt time is as short as 3 minutes. The melt time of R52 is about 15 minutes, as shown in Figure 4.10.

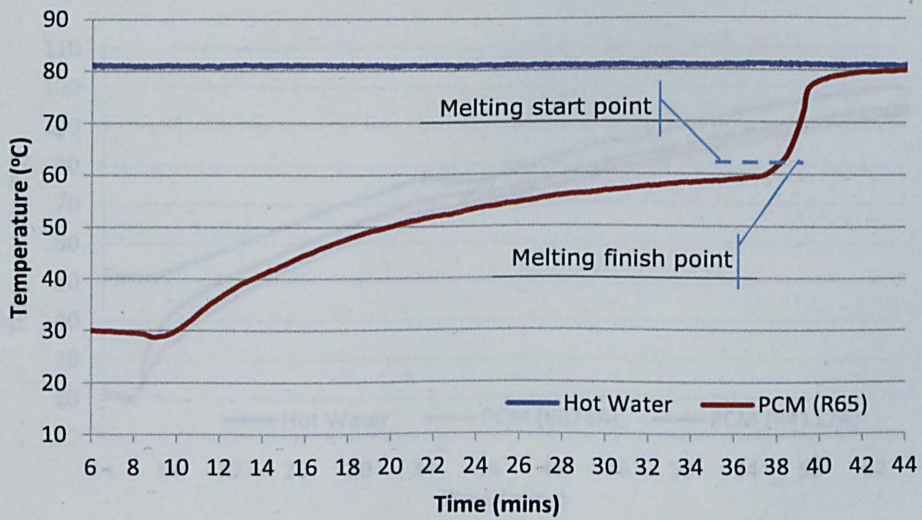


Figure 4.9 Phase change of PCM-R65 melting process

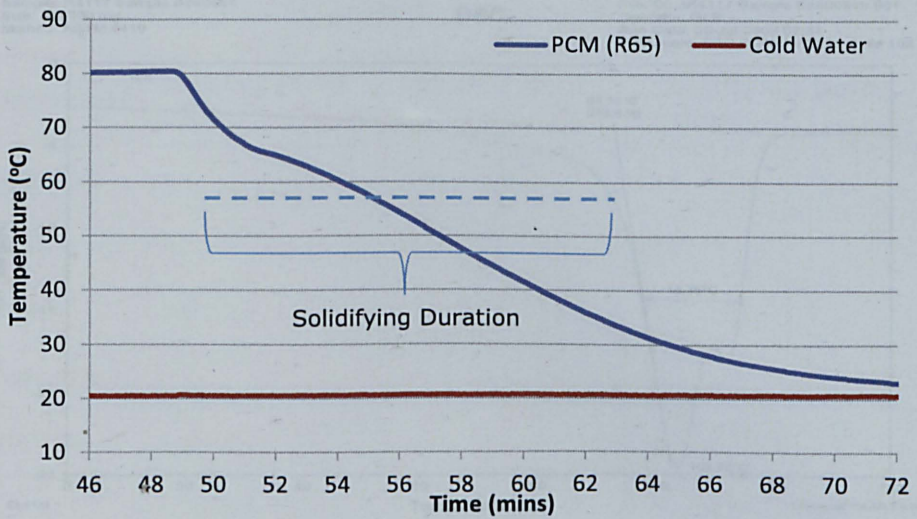


Figure 4.10 Phase change of PCM-R65 solidifying process

● **Materials: R4117A and 8676A**

Figure 4.11 shows test results of R4117 and 8676A. As it can be seen, their temperatures just increase with water temperature and no phase change happens so far, which means their melting points must be over 100°C. This situation will be sorted out by other high temperature liquid (such as oil) in a further stage. Figure 4.12 shows the DSC testing result for R4117A from manufacturer with a peak melting point around 103.75°C.

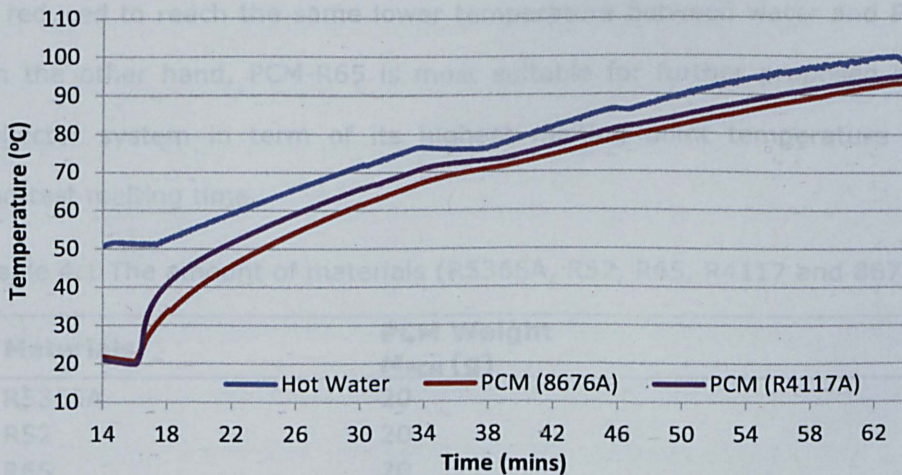


Figure 4.11 PCM-8676A and PCM-R4117A with hot water

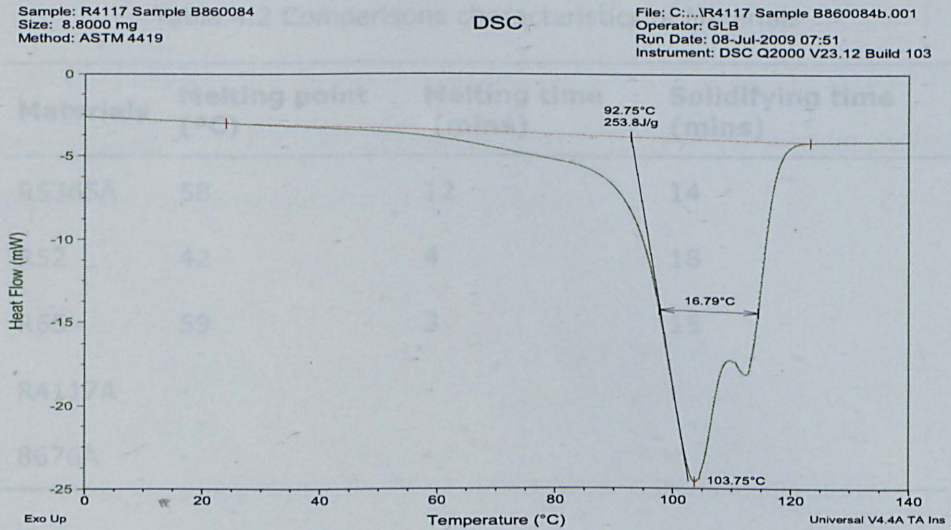


Figure 4.12 DSC testing result for PCM-R4117 (from the manufacturer)

4.2.1.3 Summary of Discussions and Results

Table 1 shows the amount of materials tested (R5365A, R52, R65, R4117A and 8676A) in this experimental testing. Based on above temperatures analysis and discussions, a summarised Table 4.2 can be generated. As can be seen, the solidifying time of materials is longer than the melting time of materials. The main reason for this is that the aluminium cans of PCMs are keeping into small water tank and there is no water flow, the heat transfer is reduced to reach the same lower temperature between water and PCM. On the other hand, PCM-R65 is most suitable for further proposed solar collector system in term of its highest melting point temperature and shortest melting time.

Table 4.1 The amount of materials (R5365A, R52, R65, R4117 and 8676A)

Materials	PCM Weight M_{PCM} (g)
R5365A	20
R52	20
R65	20
R4117A	17
8676A	16

Table 4.2 Comparisons characteristics of Materials

Materials	Melting point (°C)	Melting time (mins)	Solidifying time (mins)
R5365A	58	12	14
R52	42	4	18
R65	59	3	15
R4117A	-	-	-
8676A	-	-	-

4.2.2 Thermal Energy Storage Testing from PCM

4.2.2.1 Experiment Rig Set-up

This experiment is designed to investigate the problem of heat transfer in well-designed building device (high melt temperature PCMs tank) in environmental laboratory. The aim of this experiment is to examine PCMs' energy storage capacity, which leads to maintain a considerable internal temperature in a low ambient temperature.

Figure 4.13 shows the main schematic diagram of PCMs energy storage test rig. A flow indicator is installed vertically and connected by copper tubes and fittings via pump valves, which is used to measure the volume flow of the circuit, controlled by a flow control valve. The temperature of the oil between the valve and heater is measured by a type K thermocouple (T1). Copper pipes connect the control valve to a 12kW heater unit. A 12 kW immersion heater element, (Incoloy 825 industrial immersion heater) is connected to a flange and located within the tube. All of the thermocouples are connected to a 12 channels selector switch and the values displayed with a Kubler Codix 532 temperature indicator. An

electrical panel contains relays and switches required for the supply and control of power to the heater. An isolator switch is sited on the side of the panel. Figure 4.14 shows a photograph of PCMs energy storage system with the control panel and the electrical panel.

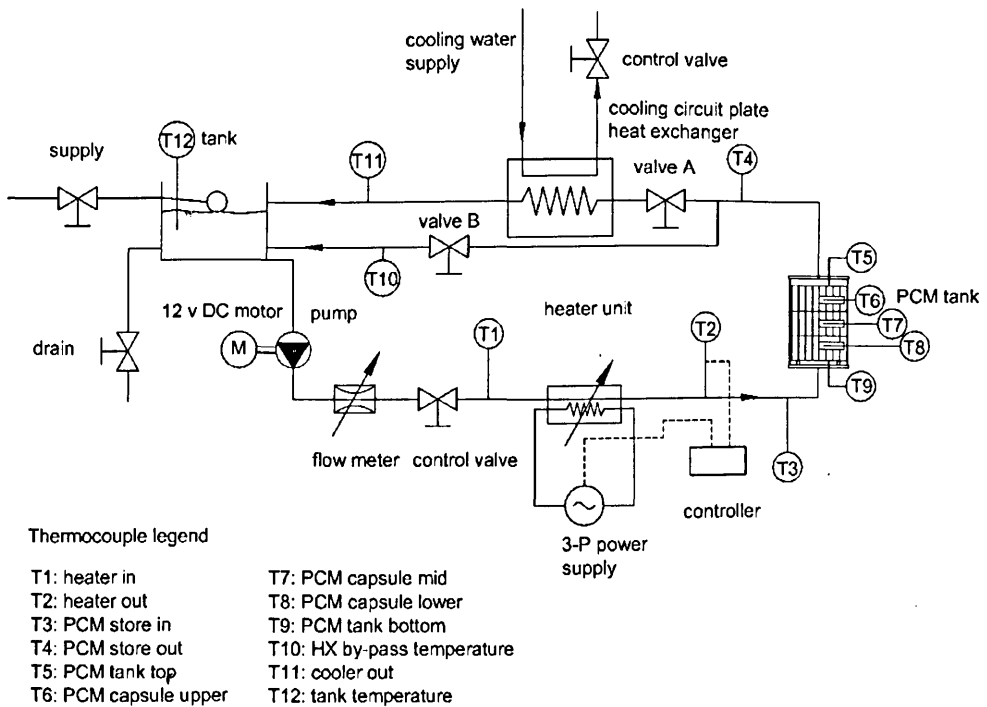


Figure 4.13 Schematic diagram of PCMs energy storage test rig

The heater element is powered by a 32A 3 phase 400V AC power supply. The heater unit is located in the vertical plane with the element in the upward direction. The inlet of the pump is connected to the bottom of the unit, with the flow direction vertically upwards. The outlet is connected via copper tubes elbows and tees to the bottom of the PCM tank. A type K thermocouple (T3) is sited downstream of the PCM tank inlet. The PCM tank consists of a 210mm ID x 3mm thick 316 stainless steel tube, 310mm in length, with 275mm x 210mm flanges welded to the ends of the tube.

Blanking flanges were manufactured with drillings for fittings and thermocouple fittings. 3mm thickness gaskets fit between the flanges and end plates to provide a seal. If the end plates are disassembled then it is recommended that replacement gaskets and sealing compound are used on reassembly. Thermocouple fittings are provided at three points along the axial length of the tube. The PCM tank is orientated vertically so that the flow from the heater unit enters at the bottom of the tank and flows upward through the bed of PCM capsules. Type K thermocouples are sited at the PCM top (T5), PCM bottom (T9), PCM upper (T6), PCM mid (T7) and PCM lower (T8). A Type K thermocouple (T4) is sited to measure the temperature at the outlet from the PCM tank. The PCM tank is designed to contain a number of PCM capsules, which consist of copper tubes cut to 90mm in length, and are filled with PCMs and capped with push fit end stops. Three capsules are constructed to house type K thermocouples corresponding to T6, T7 and T8 and alighted horizontally.

Figure 4.13 shows two valves, valve A and valve B upstream of the PCM tank. A cooling circuit plate heat exchanger is fitted so that the temperature into the tank and inlet to the heater unit can be controlled. Flow is directed to the plate heat exchanger when valve A is open and valve B is closed. A type K thermocouple (T11) is sited between the plate HX outlet and tank return to measure the temperature at outlet from the plate heat exchanger.

The flow through the cooling circuit plate heat exchanger can be by-passed by opening valve B and closing valve A. A type K thermocouple (T10) is attached to the pipe to measure temperature of oil entering the oil tank. A type K thermocouple (T12) measures the temperature of the oil in the tank.

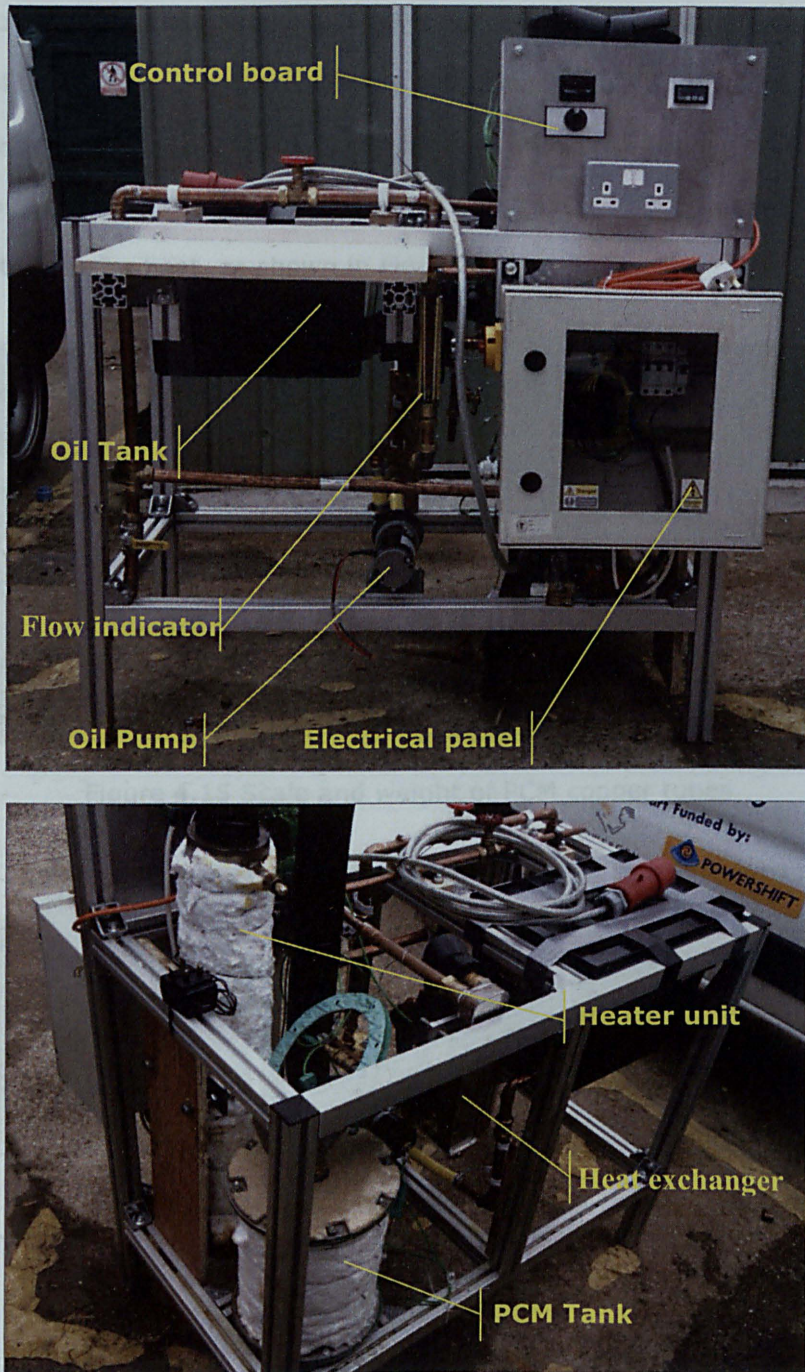


Figure 4.14 Schematic view of PCMs energy storage system

In the experiment, PCM R5365A is used as the thermal energy storage material. R5365A (Figure 4.3) composes of small white particles and its melting point obtained in this research is 58°C (Table 4.2). R5365A is

heated till phase changing from solid to liquid in the oven and filled up into special designed copper tubes. Figure 4.15 shows scale and weight of these well sealed copper tubes. Figure 4.16 shows PCM tank insider construction set up with copper tubes. Engine oil (Total Quartz 7000) is used as flow liquid to transfer heat, as shown in Figure 4.17.

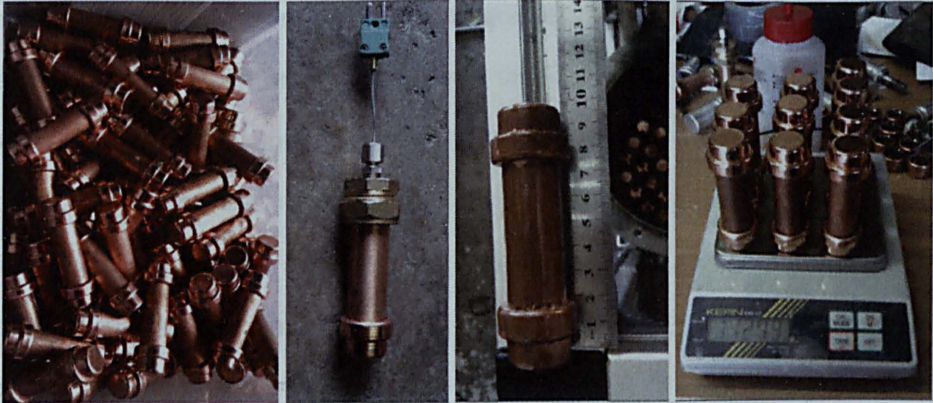


Figure 4.15 Scale and weight of PCM copper tubes

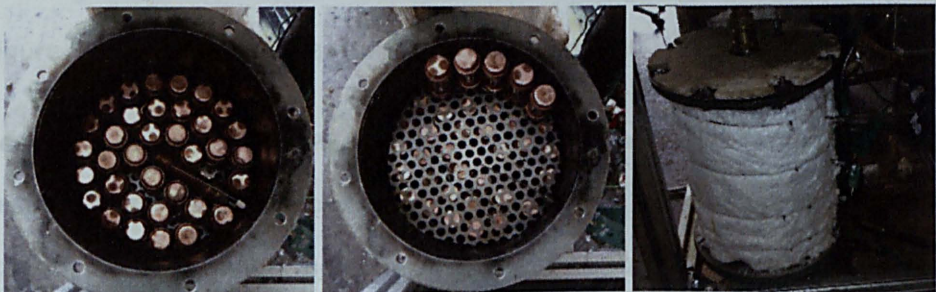


Figure 4.16 PCM tank insider set-ups with copper tubes



Figure 4.17 Engine oil (Total Quartz 7000) for flow liquid

4.2.2.2 Experiment Operation and Procedure

First of all, ensure that all electrical supplies to the test rig are switched off and isolated. Connect supply and return hoses to the cooling circuit. Connect the plug from the double socket on the control board into a 230V AC supply and switch on. Connect the power supply for the pump and the temperature indicator into the double socket. Ensure that the flow control valve is open. Switch on the pump and slowly adjust the flow control valve to a desired value. Open the cooling water control valve. Switch on the power to the temperature indicator. After a couple of seconds, the indicator will show the values of the thermocouples connected to the channels. With power to the heater unit, the outlet temperature (T2) it will increase until reaches the set point temperature. The circulation flow rate can be varied using the flow control valve and the temperature of the circulation flow rate entering the tank (T11) can be varied by controlling the cooling water valve. Figure 4.18 gives a full view of PCM testing rig with water inlet and outlet.

Secondly, to carry out a PCM melting test, change the set point value to a desired temperature above the PCM phase transition temperature in standby mode. Change the controller to active and "CV" will show a green flashing light. The outlet temperature of the heater unit should begin to increase. When the outlet temperature reaches the set value the controller will automatically maintain the set value. The temperatures around the circuit can be monitored through the selector switch and indicator as the experiment progresses.

Thirdly, to carry out a PCM freezing test, change the set point value to a desired temperature below the PCM phase transition temperature in standby mode. Change the controller to active and "CV" will show a green

flashing light. The outlet temperature of the heater unit will begin to decrease. When the outlet temperature reaches the set value the controller will automatically maintain the set value. The temperatures around the circuit can be monitored through the selector switch and display as the experiment progresses.

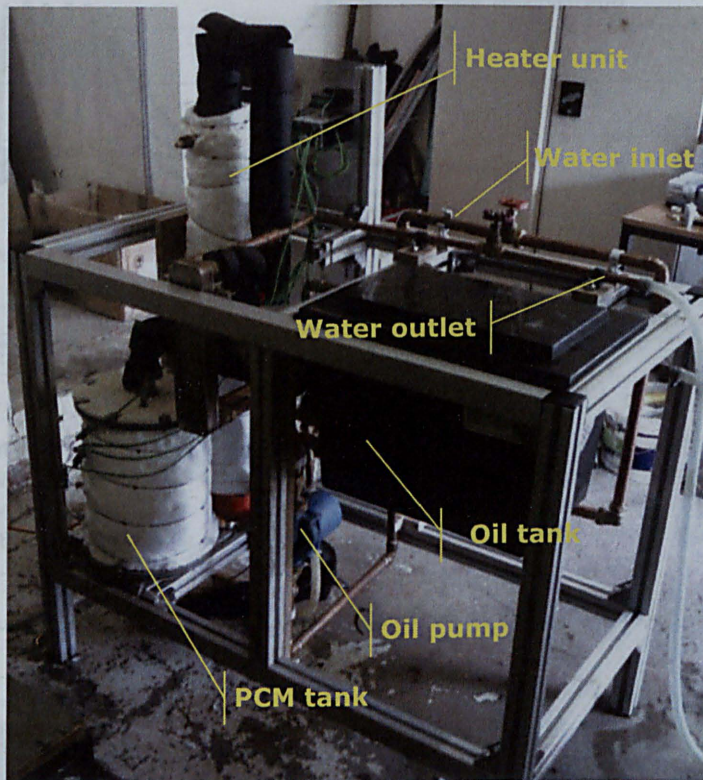


Figure 4.18 PCM testing full rig with water inlet and outlet

4.2.2.3 Experiment Results Analysis and Discussions

The thermal energy storage is a technology not only for building application, but also can be used for thermal efficiency of motor vehicle engines. In 2010, Kauranen et al investigated temperature optimisation of automotive diesel engine with PCM high capacity heat energy storage using exhaust gas heat recovery system (Kauranen, 2010). However, automotive PCM

energy storage has not become a commercial success due to the extra mass and space required for the accumulator. The experiment in this research has employed PCM to maintain a considerable internal temperature of building application tank in a low temperature ambient.

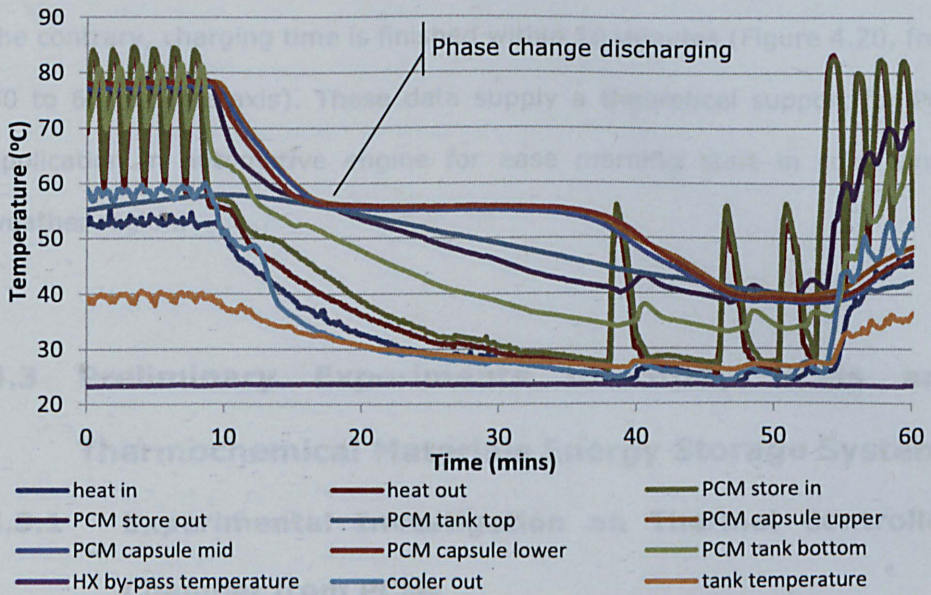


Figure 4.19 Temperatures change of PCM test rig (discharging)

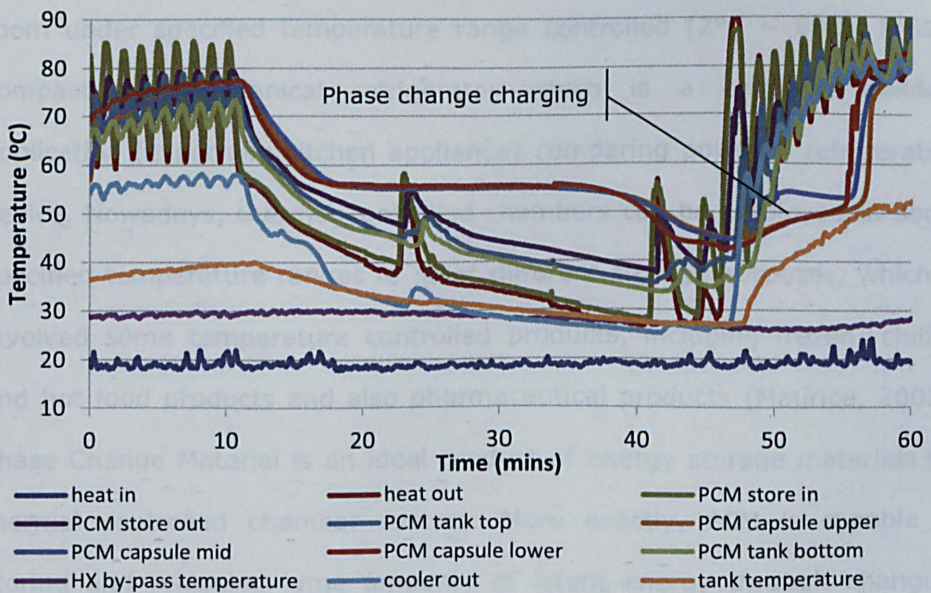


Figure 4.20 Temperatures change of PCM test rig (charging)

Figure 4.19 and Figure 4.20 show temperatures change of PCM energy storage system. When the system is heated to about 78°C and PCM R5365A is fully charged, cold water is used to discharge it. Solidify point of R5365A is around 58°C and it takes approximately 30 minutes to finish phase change, as shown in Figure 4.19 (from 10 to 40 in Time axis). On the contrary, charging time is finished within 10 minutes (Figure 4.20, from 50 to 60 in Time axis). These data supply a theoretical support for PCM application in automotive engine for ease morning start in cold winter weather region.

4.3 Preliminary Experiments to Study PCMs and Thermochemical Materials Energy Storage System

4.3.1 Experimental Investigation on Thermal Controlled Chamber from PCMs

Basically, cold closet, or called refrigerating chamber is a special freezing room under specified temperature range controlled (2°C ~ 8°C). It is a compact non-mechanical refrigerator which is a common building application (especially kitchen appliance) comparing powered refrigeration device. Nowadays, thermal controlled chambers can be employed at some specified temperature ranges to meet different storage purposes, which is involved some temperature controlled products, including frozen, chilled and hot food products and also pharmaceutical products (Maurice, 2003). Phase Change Material is an ideal product of energy storage materials for thermal controlled chamber system. More exactly, PCM is capable of storing and releasing large amounts of latent energy through changing

from one phase to another. These phase changes take place at a constant or near constant temperature.

The experiment described in this section is the first of many steps to develop and test a temperature controlled chamber system for some temperature controlled products in order to maintain an internal temperature within a specified low range between 2°C and 8°C as long as possible even ambient high temperature over 30 °C.

4.3.1.1 Experiment Rig Set-up

The original experiment is established to explain the work that has been conducted in an environmental laboratory regarding to an investigation of heat transfer in TCC chamber (with PCMs). This experiment aims to examine performance of TCC chamber with double and quad PCM packages to maintain a constant internal temperature of 2°C ~ 8°C in a high temperature ambient. At the same time, how long the TCC chamber can maintain an internal temperature in 2°C ~ 8°C has also been investigated. The target chamber called thermal controlled chamber as TCC, has external dimensions of 351mm x 266mm x 241mm and internal dimensions of 235mm x 64mm x 132mm, and is insulated with PCM.

Figure 4.21 shows schematically the exact experiment rig. The environmental testing room is used to maintain temperatures as simulated and required ambient temperature range. The TCC chamber has been set up into the environmental room. Five thermocouples are embedded in the chamber to measure temperature at different positions in the TCC chamber. Data taker (DT80) is used to record relevant temperature readings during experiment. Experimental data can be collected by linked PC.

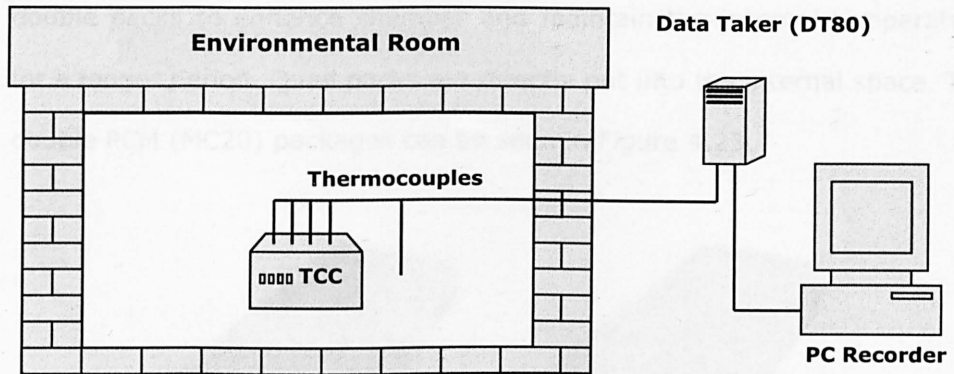


Figure 4.21 Schematic of experiment rig

More specifically, five thermocouples are at different positions into TCC chamber. Thermocouple 1 and 2 are located internal high level and low level positions, respectively. Thermocouple 3 and 4 are set up at two sides of PCM packages. The thermocouple 5 is stood at external section. The exact positions of thermocouples setup can be seen in Figure 4.22.

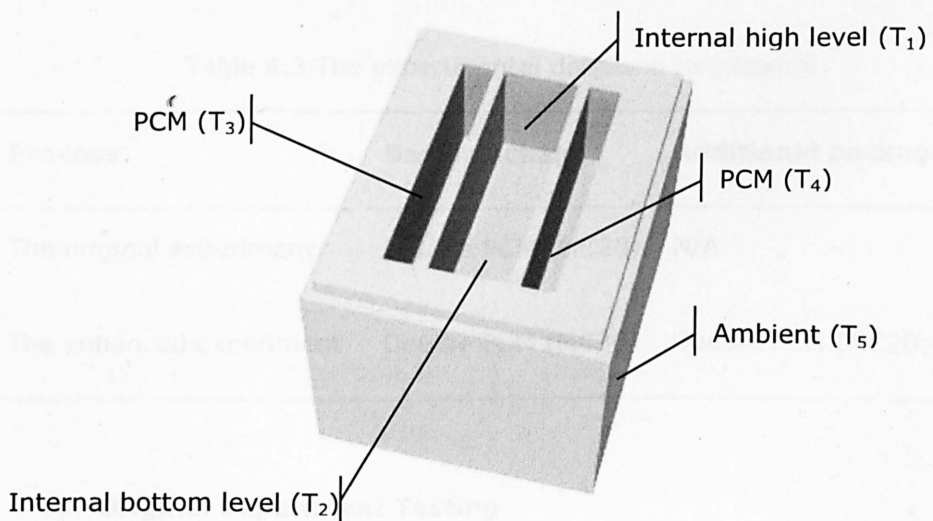


Figure 4.22 Schematic of TCC chamber and thermocouples positions

In this experiment, the first examination is based on the original TCC chamber with double PCM (MC20) packs, which are located at two separated spaces. The second stage is taking advantage of additional

double packs to enhance chamber and maintain the internal temperature for a longer period. Quad packs are directly put into the internal space. The double PCM (MC20) packages can be seen in Figure 4.23.

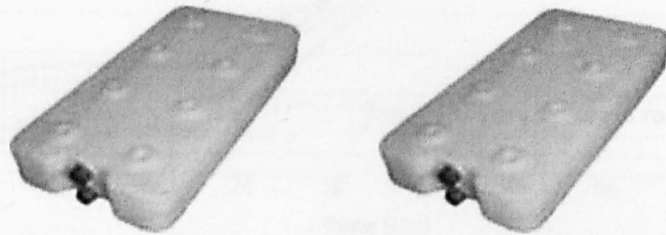


Figure 4.23 Phase change material (MC20) Packs

4.3.1.2 Experiment Results and Discussion

The experiment has been divided into two stages (original and enhanced) to evaluate the performance of TCC chamber as shown in Table 4.3.

Table 4.3 The experimental details in two stages

Process	Basic package	Additional package
The original experiment	Double PCM (MC20)	N/A
The enhanced experiment	Double PCM (MC20)	Double PCM (MC20)

● Original Experiment Testing

In the first stage, the TCC chamber is put into environmental test room and inside double PCM packs of chamber has been discharged already. The external temperature is kept over 25°C. The experiment runs over three days (72 hours).

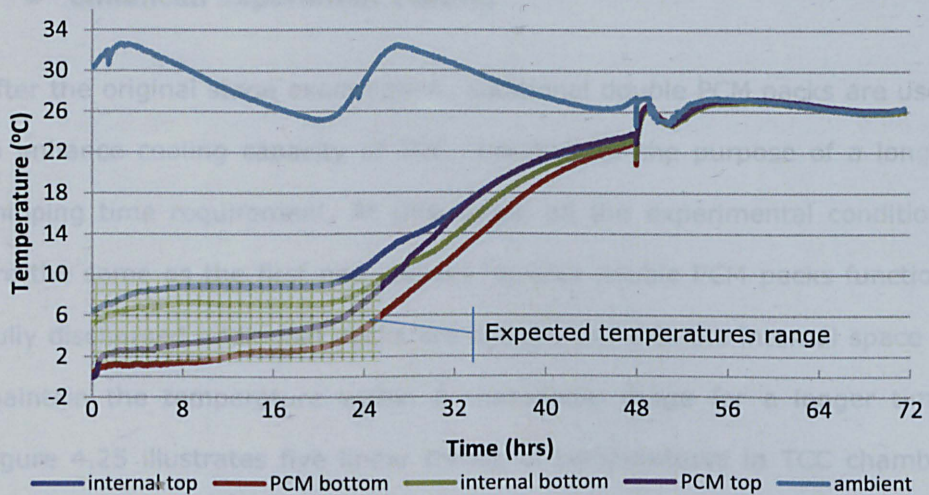


Figure 4.24 Temperature change during three days with double PCM packs

Figure 4.24 is plotting the collected temperature data. As mentioned before, thermocouple 5 (light blue one) represents the external temperatures of TCC chamber, over 25°C during 72 hours. Thermocouple 4 (purple line) and thermocouple 3 (red line) are linked to two PCM packs. The experiment was running after PCM was fully discharged, temperatures of PCM package started from around zero. With time went by, PCM were melting and storing energy to maintain the internal temperature within the expected temperatures range (2°C ~ 8°C). About 24 hours later, PCM have been fully charged. Green and blue lines started to increase to catch up with the external high temperatures. The slight difference between green and blue line is due to thermocouple's location, which can be seen in Figure 4.30. With PCM packages, green line and blue line (thermocouple 1 and 2) experienced the same linear trend during these 72 hours. Black and red lines represent exact internal target temperatures. Black line was at an internal high level position and temperature was slight over 8°C during first 24 hours, it means that the internal high level appears to be a weak space, which needs to be enhanced for perfect shipping package chamber.

- **Enhanced Experiment Testing**

After the original stage examination, additional double PCM packs are used to enhance cooling capacity of TCC chamber for the purpose of a longer shipping time requirement. At this stage, all the experimental conditions are the same as the first one, except for plus double PCM packs function. Fully discharged additional packs are directly put into the internal space to maintain the temperature within a reasonable range for a longer time. Figure 4.25 illustrates five linear trends of temperatures in TCC chamber with quad PCM packs. With additional packs effect, the duration of target temperature range is extended to approximate 48 hours from 24 hours. At the same time, both green line and blue line are kept in the expected temperatures range ($2^{\circ}\text{C} \sim 8^{\circ}\text{C}$) about 48 hours.

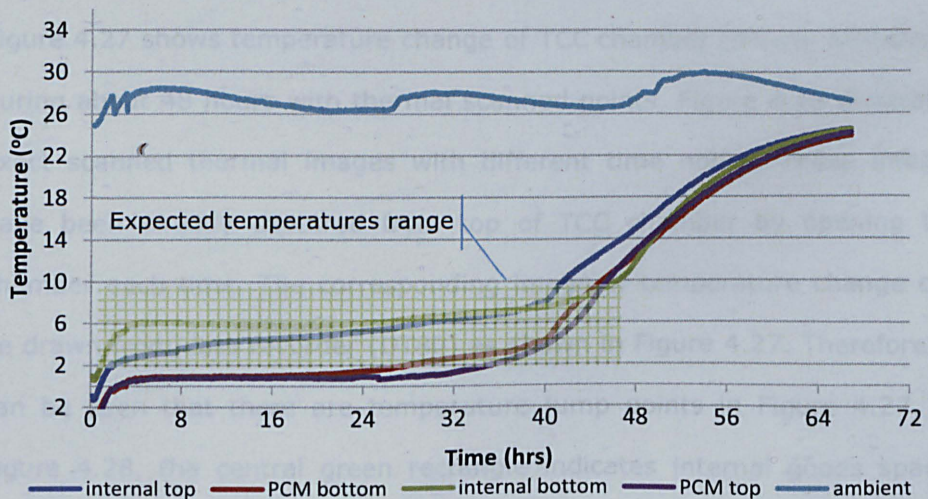


Figure 4.25 Temperature change during three days with quad PCM packs

4.3.1.3 Thermal Images Analysis of TCC Chamber

In order to further analyse the performance of TCC chamber, thermal images analysis method is introduced to at this stage by employing

thermal imaging scanner during this project. Figure 4.26 shows the Fluke TiS thermal imaging scanner, which is for temperature measurement range from -20°C to $+100^{\circ}\text{C}$ and temperature measurement accuracy about $\pm 5^{\circ}\text{C}$ or 5 % at 25°C .



Figure 4.26 Fluke TiS Thermal Imaging Scanner

Figure 4.27 shows temperature change of TCC chamber (double PCM packs) during about 48 hours with thermal scanned points. Figure 4.28 illustrates exact scanned thermal images with different time nodes. These images have been directly captured from top of TCC chamber by opening the chamber each time. The corresponding image of temperature change can be drawn from data recorder (DT80) as shown in Figure 4.27. Therefore, it can be seen that there are temperature jump points in Figure 4.27. In Figure 4.28, the central green rectangle indicates internal goods space. Three type temperatures (average, maximum and minimum) are shown in this rectangle, average temperatures are almost the same as temperature nodes in Figure 4.27. The top and bottom rectangles represent PCM packages. Specifically, each image is related to a time node when the image is scanned and the TCC chamber has to be opened each time. Image (a) shows temperature distribution of TCC chamber before put PCM packs

into it. Image (b) to (f) show temperature distribution after PCM packs have been put into chamber in 5 minutes, 1.5 hours, 5.2 hours and 24 hours, which can be seen that PCM packs are charging during this period. After about 48 hours, PCM is fully charged as shown in image (f) of Figure 4.28 in which the top and bottom rectangles (PCM) are disappeared. At the same time, all temperatures of thermocouple have reached to nearly the same value as shown in Figure 4.27.

Therefore, thermal images analysis method provides an attractive method to analyze some thermal solutions in very simple and quick way than other devices, what you see what you get.

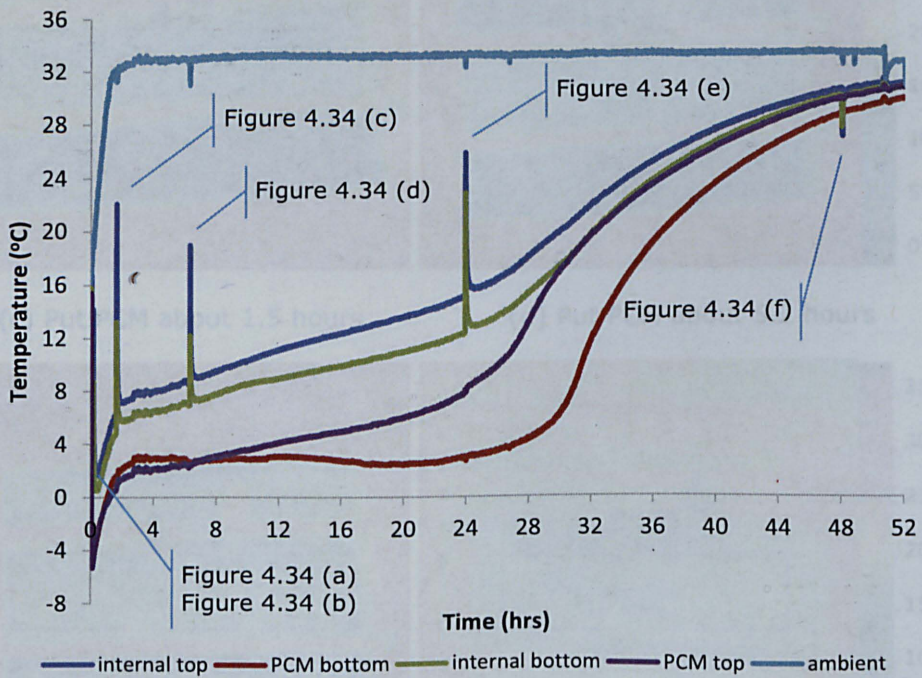
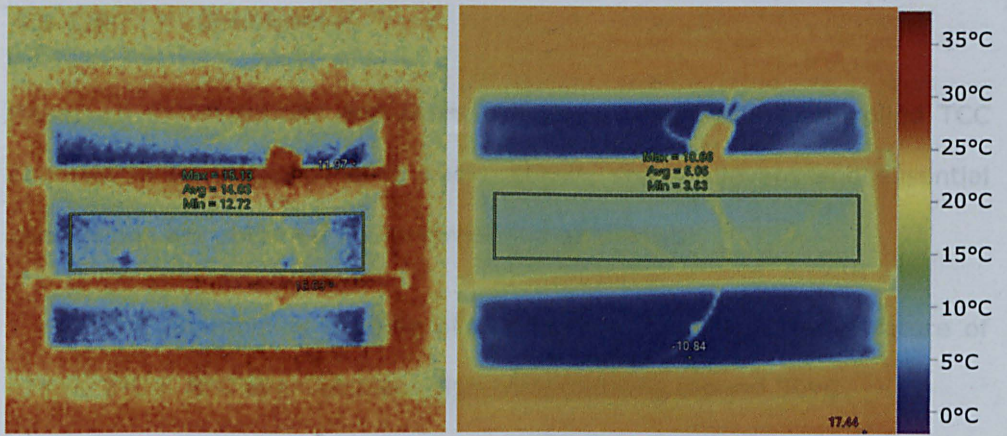
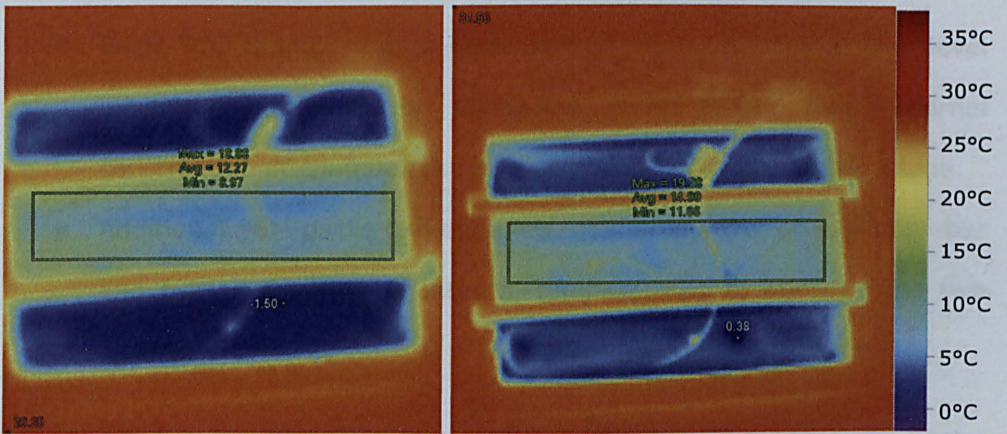


Figure 4.27 Temperature change during two days with thermal scanned points under double PCM packs



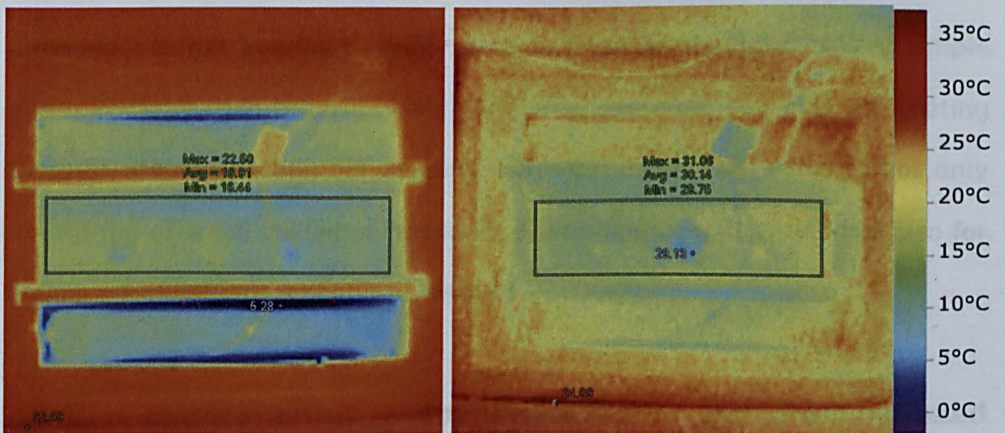
(a) Before put PCM into chamber

(b) Put about 5 minutes



(c) Put PCM about 1.5 hours

(d) Put PCM about 5.2 hours



(e) Put PCM about 24 hours

(f) Put PCM about 48 hours

Figure 4.28 Temperature change images by thermal scanner

4.3.1.4 Conclusion

Based on investigations and assessments on temperature controlled TCC chamber with double or quad packs above, some relevant and essential conclusions are obtained and summarized as follows:

- TCC chamber is capable of maintaining a constant temperature of 2°C ~ 8°C even ambient high temperatures around 30°C
- Original TCC chamber can keep internal temperatures within 2°C ~ 8°C for 24 hours in term of capacity of PCM (MC20) packs
- Basic TCC chamber has a weak cooling space at internal high level position (temperatures increased over 8°C). The internal construction of chamber should be redesigned in the further stage.
- Additional PCM packs can enhance cooling capacity of TCC chamber and extend duration of internal temperatures to approximate two days.

Thermal images analysis method has shown almost the same results as the thermocouples' on the performance of TCC chamber. This novel instrument provides a bright avenue to analyze some thermal solutions in very simple and quick way than other devices, what you see what you get. Integrating thermal controlled chamber system with PCM is a viable concept not only for storing of small chilled or hot food, pharmaceutical products but also for building and industry cooling or heating applications.

4.3.2 Experimental Investigation on a Closed Thermochemical Absorption Cooling System

With the rapid development of economy and the improvement of people's living standard, energy shortage is getting more and more serious.

Research and development work on new methods of thermal energy storage are required to minimize energy consumption by harvesting renewable energy sources. Thermochemical energy storage is a particularly attractive technique because it can provide a high energy storage density (Ding, 2012). Recently the widespread applications of low carbon buildings and energy efficient industry and food chilling have promoted the development of thermochemical energy storage systems. Thermochemical heat pump (CHPs) is a representative of chemical thermal energy conversion and storage systems (Kato, 2007).

There are many published papers on various types CHPs and their applications. In early 1995, Tahat et al investigated the thermal performance of a thermochemical heat pump as an energy store system, which has shown a general relationship between the equilibrium pressure and temperature of the system [Tahat et al, 1995]. Kawasaki (1999) provided a proposal of chemical heat pump for cooling using paraldehyde/acetaldehyde (Pa/A) and had indicated that the coefficient of performance (COP) of the Pa/A system was the same as the COP of a vapour compression heat pump (Kawasaki, 1999). A novel cooling and heating energy storage system technology was presented and patented by the University of Nottingham (Riffat, 2000). This method is based on potential vapour adsorption ability of dry adsorbents (LiNO_3 and SiO_2), in which $10^\circ\text{C} \sim 15^\circ\text{C}$ temperatures drop 500ml water may be available in a short time (about 5 minutes) for cooling purpose.

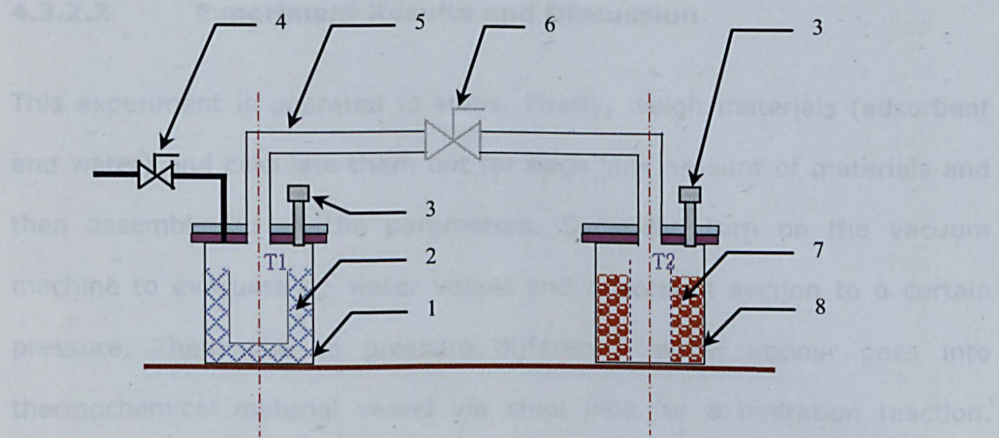
Therefore, a high performance thermochemical energy storage pumping pipe system is proposed for thermal management solutions in cooling/heating applications in this stage. This preliminary experiment is to investigate this novel closed thermochemical energy storage pumping pipe

system and a fast adsorption cooling technique (chilling of food products). The energy release, storage capacity and efficiency of proposed adsorbents, lithium nitrate/ LiNO_3 , silica gel/ SiO_2 , and mixtures have been studied. Experiment work is presented in detailed in this section to describe the performance and design information of the adsorption cooling system. At the same time, heat capacity and hydration reaction temperature of thermochemical materials have been valued, which will give a reference for winter room heating system due to their high reaction temperature.

4.3.2.1 Experiment Rig Set-up

This experiment is composed of two main glass vessels. One of glass vessels is used to hold thermochemical material and another is for water. A scaled cooling system is applied as shown in Figure 4.29. Figure 4.30 is experimental cooling system rig in view of the principle of adsorption pumping pipe. It consists of two vacuumed glass vessels separated with a valve through steel pipe, one contains a wet water wick and the other is filled with dry adsorbent. During this experimental process, as soon as the ball valve is opened, adsorbent will adsorb vapour, and then water in wick begins to evaporate and inside space of water vessel section will be quickly cooled. The reason for this is that water can be evaporated under low temperature (room temperature about 20°C) in term of internal vacuum condition, and the produced vapour is absorbed by adsorbents.

Based upon the investigation of the thermochemical performance of energy release and storage, sorption properties (includes sorption isotherm and kinetics under conditions close to the operating temperature) of adsorbents have been tested. At the same time, the mechanical and hydrothermal stability of selected adsorbents have been tested into multiple cycling.



Item	Description	Item	Description
1	Water vessel (evaporation section)	5	50mm diameter stainless steel pipe
2	Water c/w wick	6	Ball valve
3	Pressure transducer	7	Adsorbent material
4	Ball valve connect to vacuum pump	8	Adsorbent vessel (adsorption section)

Figure 4.29 Schematic view of the proposed cooling system

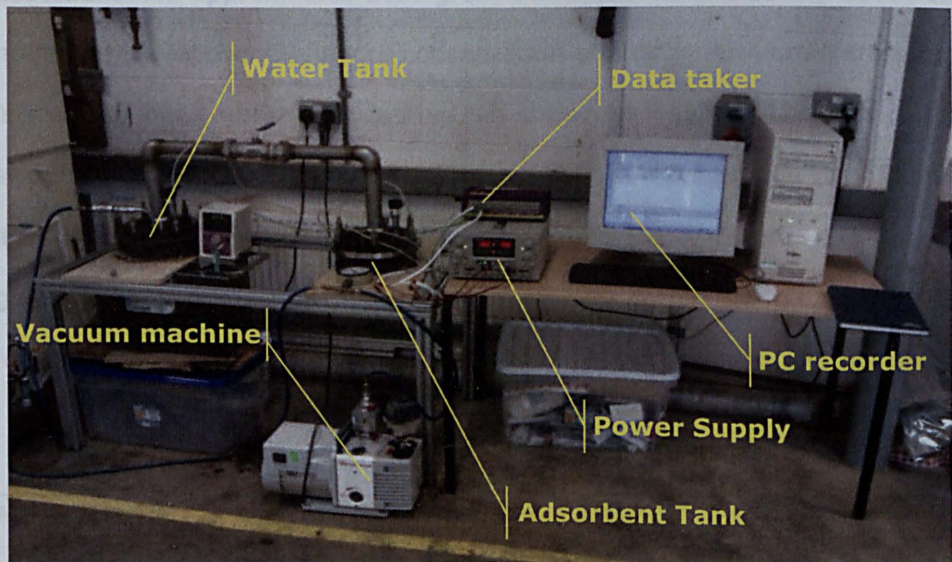


Figure 4.30 Schematic view of experimental cooling system

4.3.2.2 Experiment Results and Discussion

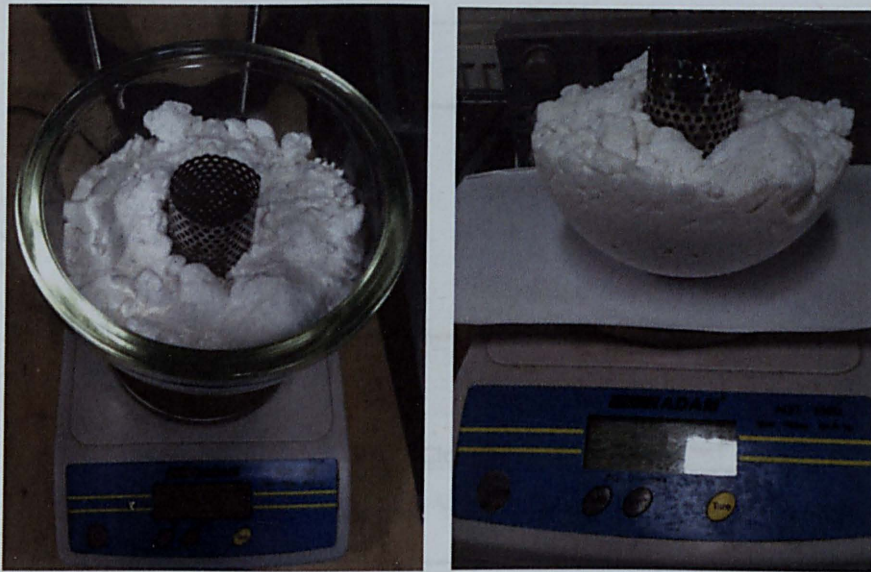
This experiment is operated in steps. Firstly, weigh materials (adsorbent and water) and calculate them out for each side amount of materials and then assemble up all the parameters. Secondly, turn on the vacuum machine to evacuate up water vessel and adsorbent section to a certain pressure. Then, due to pressure difference, water vapour goes into thermochemical material vessel via steel pipe for a hydration reaction. Finally, experimental data will be collected after the reaction is finished and stabilized, and weigh them again to obtain data as shown in Table 4.4 ~ 4.8 and Figure 4.31 ~ 4.34.

- **Lithium Nitrate / LiNO_3**

Lithium nitrate (LiNO_3) is selected as adsorbent due to its high performance of on low thermal source (about 70°C) (Sapienza, 2012). Table 4.4 lists weight transformation of lithium nitrate (LiNO_3) and water (H_2O) during this hydration reaction. About 22.4 gram water is evaporated and adsorbent has approximate 21.4 gram increased weight during about two hours, which follows the law of conservation of energy. Lithium Nitrate tank is weighed before and after testing, as shown in Figure 4.31. As it can be seen, Lithium nitrate has a phase change from powder (image (a) of Figure 4.31 with glass vessel) to solidification (image (b) of Figure 4.31 without glass vessel). A meshed metal tube is located in the middle of tank. Its function is to increase surface and let water vapour going to another side.

Table 4.4 Amount of LiNO_3 and H_2O for experiment testing (unit: gram)

Materials	M_b (Before)	M_a (After)	ΔM_d
LiNO_3	817.5	838.9	21.4
H_2O	345.1	322.7	22.4



(a) Before-with glass vessel

(b) After- without glass vessel

Figure 4.31 Weight for Lithium Nitrate before and after testing

In Figure 4.32, the ball valve is always closed before the experiment is starting, then the vacuum machine is used to suck up air from the water and adsorbent vessel to low pressure. Water temperature and adsorbent temperature are very close to room temperature around 19°C. When the valve is open, dry adsorbent will adsorb vapour and its temperature will rapidly increase due to a hydration reaction. Water section temperature will quickly decrease by evaporation.

Temperatures change of water and Lithium Nitrate are to accompany with main valve status in which valve is closed and opened twice in order to supply enough water vapour (see Figure 4.32). Vacuum machine is turn on both glass vessels when the valve is closed to maintain low pressure all the time. During this testing process, maximum temperature of adsorbent stands up 30.06 °C and water temperature bottom about 6.72 °C.

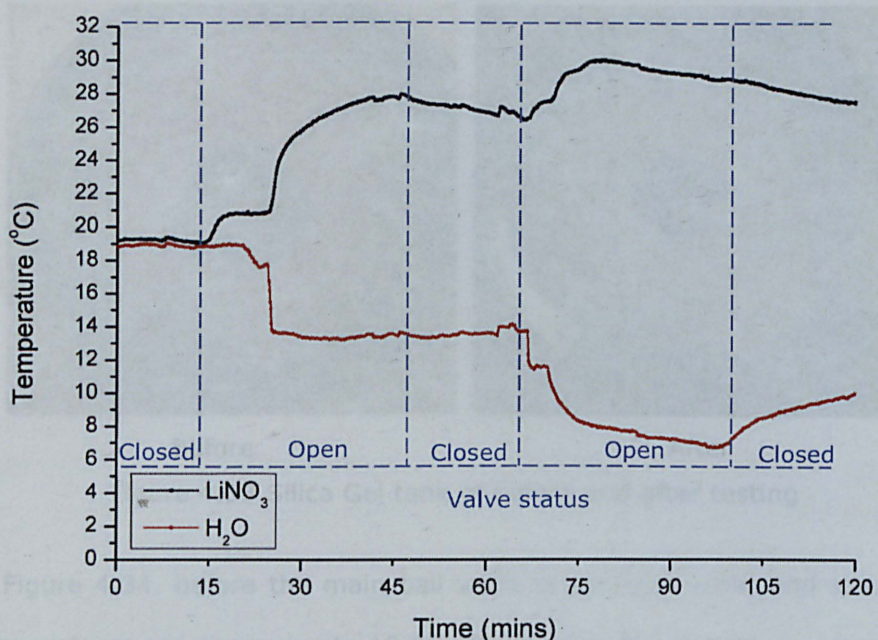


Figure 4.32 Result for Lithium Nitrate (LiNO_3) with water (H_2O) test

- **Silica Gel / SiO_2**

The amount of materials (silica gel and water) change is shown as Table 4.5. About 1kg silica gel participates in chemical reaction and holds about 47.9 gram increased weight. Weight difference has the same trend as that of Lithium Nitrate. Figure 4.33 is silica gal tank before and after testing. As it can be seen, silica gal experienced a colour change from yellow to white. There is no phase change compared with Lithium Nitrate.

Table 4.5 Amount of SiO_2 and H_2O for experiment testing (unit: gram)

Materials	M_b (Before)	M_a (After)	ΔM_d
SiO_2	1019.5	1067.4	47.9
H_2O	397.8	339.1	58.7



Before

After

Figure 4.33 Silica Gel tank of before and after testing

In Figure 4.34, before the main ball valve is opened, water and silica gel temperatures are approximate 19 °C. When the valve is open, vapour goes into silica gel side due to the pressure difference in which the pressure of silica gel vessel is approximate 20 mbar and the pressure of water vessel is about 25 mbar. Silica gel will quickly adsorb vapour and its temperature will rapidly increase to about 50 °C in five minutes. Maximum temperature of silica gel stands up 50.87 °C. On the contrary, water temperature will fast decrease to bottom about 3.69 °C.

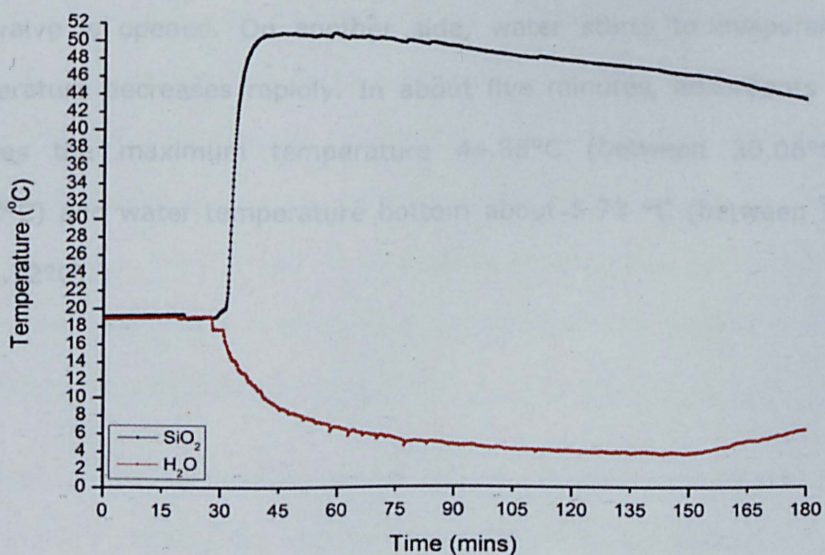


Figure 4.34 Result for Silica Gel (SiO₂) with water (H₂O) test

● **Mixed Materials (50% SiO₂ and 50% LiNO₃)**

At this stage, the adsorbent is compounded materials, which is mixed through silica gel and lithium nitrate by half and half (500 gram each). After the hydration reaction, there is approximate 35.1 gram difference. The details are shown in Table 4.6.

Table 4.6 Amount of materials for experiment testing (unit: gram)

Materials	M_b (Before)	M_a (After)	Δ M_d
SiO ₂	500	1035.1	35.1
LiNO ₃	500		
H ₂ O	416.1	368.9	47.2

Based on above discussions for single phase hydration reaction, silica gel has higher hydrated temperature (approximate 50°C) than lithium nitrate (about 30°C). Figure 4.35 shows that the adsorbents mixture has the similar linear variation as those of lithium nitrate and silica gel (Figures 4.32 and 4.34). Mixed materials temperature quickly increases when main ball valve is opened. On another side, water starts to evaporate and temperature decreases rapidly. In about five minutes, adsorbents vessel reaches the maximum temperature 44.88°C (between 30.06°C and 50.87°C) and water temperature bottom about 5.73 °C (between 3.69°C and 6.72°C).

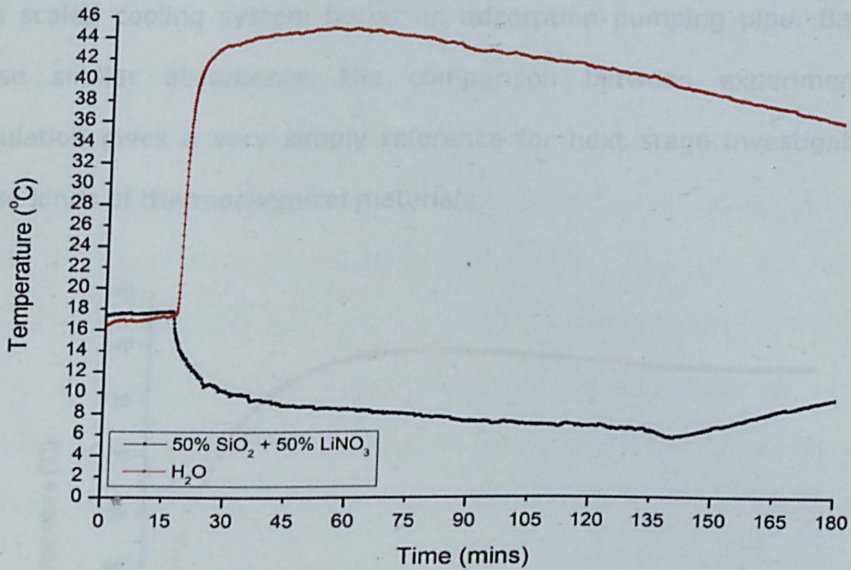


Figure 4.35 Result for Mixture (50% SiO₂ and 50% LiNO₃) with water

4.3.2.3 Comparison of Experimentation and Simulation

A simple comparison of simulation thermochemical absorption system is shown in Figure 4.36, in which Saffa Riffat et al (2013) have evaluated this cooling system based on theoretical principle of the thermochemical energy storage pumping pipe. Simulation was in 330ml water in a water tank, with zeolite 13X as adsorbent and water as refrigerant. The result shows that a total of 250g zeolite 13X could decrease the temperature of 330 ml by about 15°C in 2~3 minutes (Riffat and Ding, 2013). As discussed and mentioned above, the experimental results (Figures 4.32, 4.34 and 4.35) have the same linear trend as simulation as shown in Figure 4.36. This numerical solution is compared with the experimental models and results to validate the proposed cooling system.

Considering the complexity of the process in the cooling system, the agreement of simulation and experimentation is satisfactory, thus the lumped model is acceptable and significant for preliminary investigation of

this scaled cooling system based on adsorption pumping pipe. Based on these similar absorbents, the comparison between experiment and simulation gives a very simply reference for next stage investigation on these kinds of thermochemical materials.

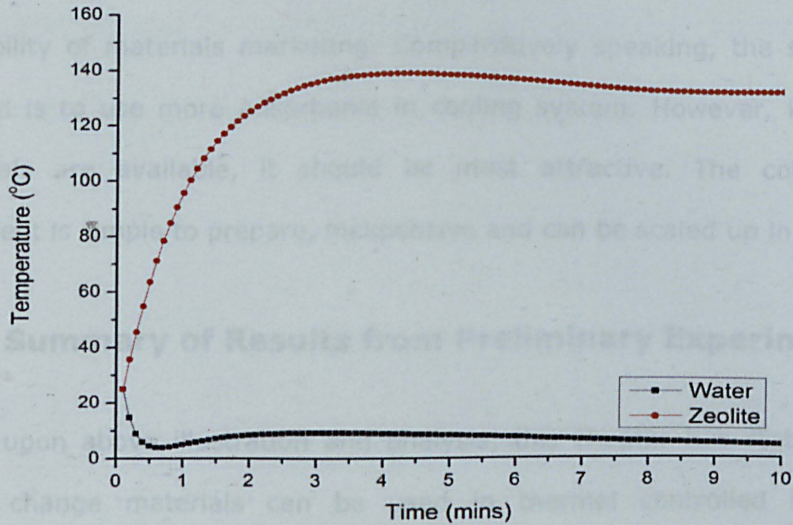


Figure 4.36 Simulation result on heat sink in zeolite bed (Riffat and Ding, 2013)

4.3.2.4 Conclusion

Experimental works with comparison of a similar modeling have been carried out based on a novel closed thermochemical absorption cooling system. The system can be used for building and industry applications. There are some challenges and barriers needed to be addressed. This proposed and tested system is a fully closed system under quite lower internal pressure, which brings more difficulties to apply for building devices. Meanwhile, during experiment processes, the adsorbents vessel side has quite high temperatures (over 50°C) after the hydration reaction. This heat must be removed to ambient or temporarily stored in some methods, such as heat sink and adsorbent own thermal capacity, which

may give a good idea for winter room heating system as renewable energy strategy. On the other hand, materials have different high thermal capacities, and lithium nitrate and silica gel have shown different maximum heat temperatures. Adsorbents selection, development, and optimization are an issue for further works. Its feasibility may depend on the price and availability of materials marketing. Comparatively speaking, the simplest method is to use more adsorbents in cooling system. However, if cheap materials are available, it should be most attractive. The composite adsorbent is simple to prepare, inexpensive and can be scaled up in future.

4.4 Summary of Results from Preliminary Experiments

Based upon above illustration and analysis, this chapter has stated that phase change materials can be used in thermal controlled building application system. At the same time, thermal images analysis method gives an avenue to solve some thermal problems in very simple and quick way than other devices. Heat of hydration reaction from thermochemical materials is attractive to use for winter room heating system due to their high temperature and heat capacity. In the following Chapter 5, the research will illustrate a comprehensive seasonal thermochemical energy storage system integrated with solar collector, define and describe relevant experiment measurements and process.

CHAPTER 5

Experimental Investigation on the Performance of High Capacity Heat Storage System

5.1 Introduction

A novel seasonal high capacity heat storage system is introduced in this chapter based on previous literature review, theoretical analysis and computer simulation, materials selection and preliminary experiments sections. The proposed experiment model involves two independent test rigs: thermochemical absorption system and a solar collector system, to set up the experiment. The aim of this experiment is to evaluate the performance of this seasonal high capacity heat storage system for building application, which is driven by a solar collector with a PCM tank. Experimental procedure and operating parameters are also defined at the same time. Finally, experimental measurements and data acquisition including thermocouples and weight sensor are represented.

5.2 Main Experiment Model Design and Test Rig Set-up

5.2.1 Experiment Model Design

As shown in literature review before, thermochemical energy storage system can be applied for some long term heating or cooling fields due to their specific properties. In practical implementation, high thermal storage density, acceptable space requirements and low associate costs will be considered at details design stage. Figure 5.1 shows a proposed and acceptable seasonal energy storage system. In order to satisfy the house heating demand, a large volume of materials is required, which therefore has a high mass. An ideal place is proposed to set them in foundation of a building. Meanwhile, a high thermal resistance and good air tightness for adsorbents installation are required to reduce heat loss for long term energy storage.

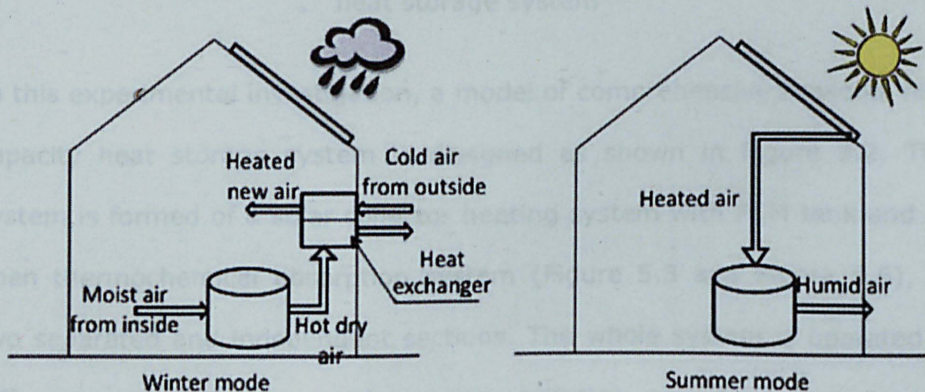


Figure 5.1 Schematic view of the proposed seasonal energy storage system

A common type evacuated tube solar collector is integrated in the roof of the building. This solar collector is connected with an air to air fan coil heat exchanger, which transfers the heat energy to thermochemical foundation. With chemical reaction (dehydration process) occurring and moisture removing, thermal energy can be stored in a stable state for a long time.

When space heating is required in winter, thermal energy will be generated through receiving moisture from internal zones (hydration process).

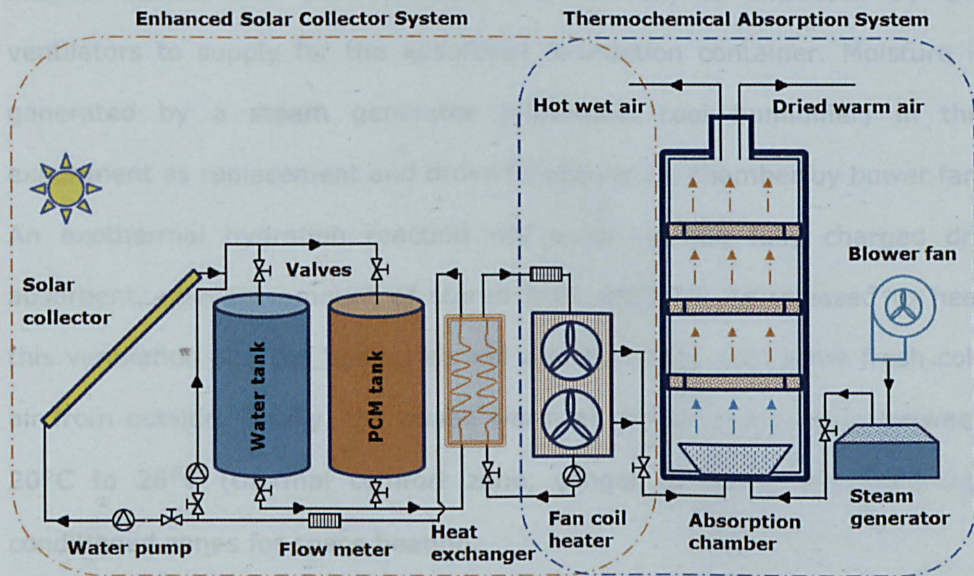


Figure 5.2 Schematic diagram of a comprehensive seasonal high capacity heat storage system

In this experimental investigation, a model of comprehensive seasonal high capacity heat storage system is designed as shown in Figure 5.2. This system is formed of a solar collector heating system with PCM tank and an open thermochemical absorption system (Figure 5.3 and Figure 5.6), as two separated and independent sections. The whole system is operated in different modes between winter and summer periods (charging and discharging stages). In the charging stage, solar energy captured by the roof-integrated evacuated tube solar collectors will be transferred and stored in water or PCM tank, and passed to the adsorbent foundation. An endothermic dehydration reaction occurs as the adsorbent is heated under high temperature (around 70°C). The generated water vapour will be carried out from the foundation container of the building by hot circulation air from fan coil heater. The thermal energy can be stored in a stable

situation as it is absolute dry of thermochemical materials. In the discharging mode, as a reversing process, some humid air from different internal zones, like shower room and kitchen, is extracted by the ventilators to supply for the adsorbent foundation container. Moisture is generated by a steam generator (ultrasonic cool humidifier) in this experiment as replacement and drove to absorption chamber by bower fan. An exothermal hydration reaction will occur on the fully charged dry absorbent, relevant amount of stored heat will then be released to heat this ventilation air. The heated air will also be mixed with some fresh cold air from outside. Finally, the mixed warm air under temperature between 20°C to 26°C (thermal comfort zone, çengel, 1998) is circulated into conditioned zones for space heating.

5.2.2 Experiment Rig Set-up

5.2.2.1 Enhanced Solar Collector Heating System

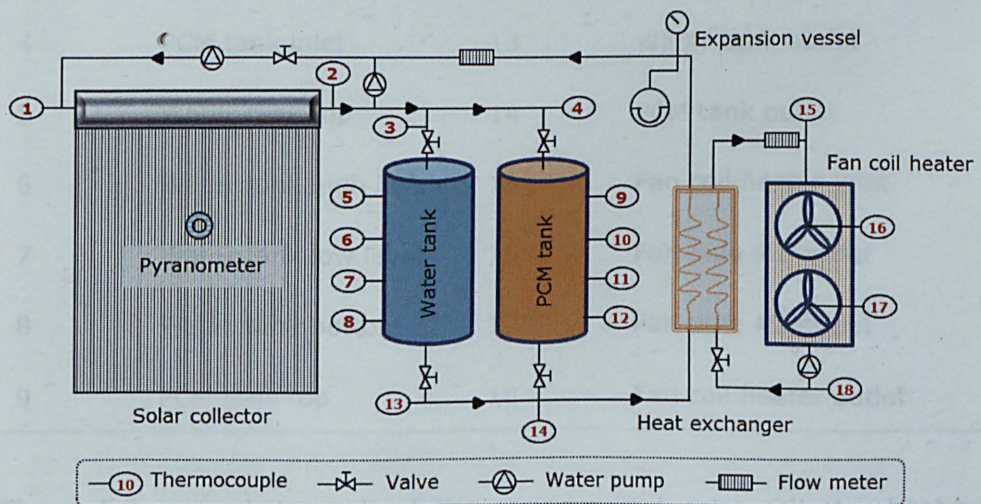


Figure 5.3 Schematic diagram of solar collector heating system with PCM

In this section, a full and enhanced solar collector heating system is introduced and investigated as shown in Figure 5.3 and Table 5.1. This

experimental system consists of a 3m² DF100 type vacuum tube collector, a 45 litres coiled hot water tank, a 45 litre coiled PCM storage tank incorporating 42kg of PCM (Paraffin RT58), a 5kW heat exchanger, a 5kW fan coil heat exchanger, a circulation pump and piping systems (for the continuous circulation of water as the heat transfer fluid), gate (ball) valves, a data logger and a computer to record and analyse measured temperature data. Eighteen thermocouples are employed to record temperature change in the system. Table 5.1 shows details description of thermocouples position in the system.

Table 5.1 Description of thermocouples position

Number	Thermocouple Position	Number	Thermocouple Position
1	Solar collector inlet	10	PCM tank high level
2	Solar collector outlet	11	PCM tank low level
3	Water tank inlet	12	PCM tank bottom
4	PCM tank inlet	13	Water tank outlet
5	Water tank top	14	PCM tank outlet
6	Water tank high level	15	Fan coil heater inlet
7	Water tank low level	16	Fan pipe #1 outlet
8	Water tank bottom	17	Fan pipe #2 outlet
9	PCM tank top	18	Fan coil heater outlet

Figure 5.4 is a photograph of the experimental solar collector heating system testing rig with water and PCM tank in the laboratory, which is built according to Figure 5.3. This experimental system has been designed in accordance with the operational principles of solar assisted heating and the possibility of employing PCMs in place of water in solar heating systems for

building applications. A DF100 vacuum tube collector has been selected for generating heat due to its efficiency (approximately 83.2% as given by manufacture), which is thought to be suitable for northern European countries with solar radiation levels (an average of 800W/m^2).

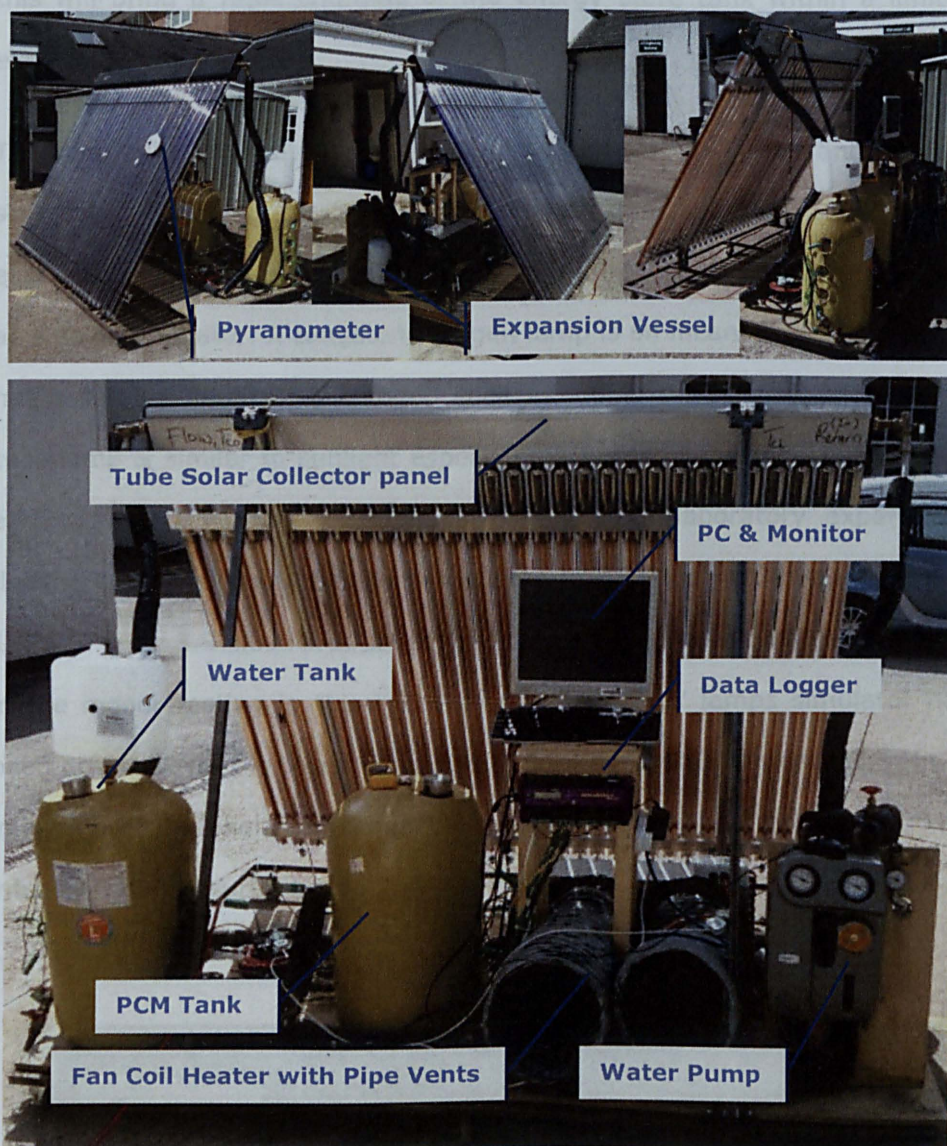


Figure 5.4 Solar collector heating system rig with water and PCM tank

As shown in Figure 5.4, the system contains a standard water pump, a 3m^2 solar collector (30 vacuum tubes), and two 45 litres storage containers (water and PCM). Normally, for store tank sizing, 35 litres per square

meter of a solar collector is a standard quantity of thermal storage advised in the UK (David, 2012). Following this guideline the total quantity for this size of collector will equate to approximately 105 litres. However, the amount used on the rig in this research is about half this value. Therefore, this will bring a rapid charging of the energy store tank within a limited experimental time.

The solar collector heating system has two test stages, indoor and outdoor stages. The outdoor testing follows sunny days' periods of high sun exposure. For the indoor testing, the tungsten halogen lamps are employed as a solar simulator. A tungsten halogen lamp is an incandescent lamp that has a small amount of a halogen such as iodine or bromine added. This type lamp is similar to sunlight especially in terms of thermal radiation. In early 1979, McMillan and Peterson conducted a laboratory experiment dealing with solar simulation with tungsten halogen quartz lamps (McMillan, 1979). Figure 5.5 illustrates about 4m² tungsten halogen lamps frame used in the indoor testing in this research. A 25 x 400W lamps simulator has been arranged for the experiment with a light control dimmer to control the intensity of the light in order to obtain the required irradiation. The intensity is measured using the CMP 3 pyranometer with sensitivity of $17.99 \times 10^{-6} \text{ V/Wm}^{-2}$.

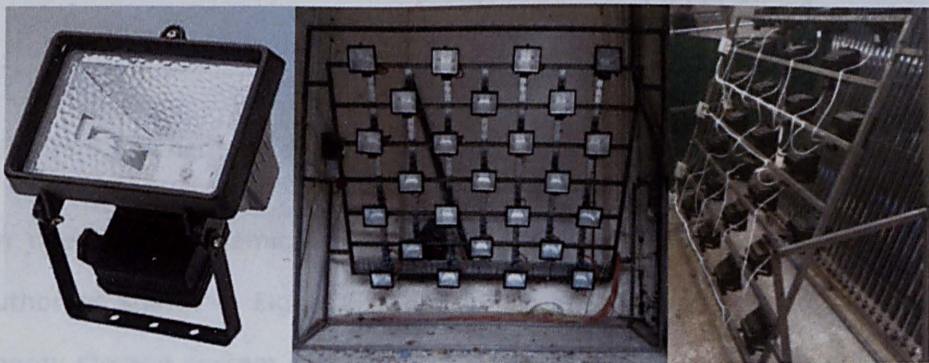


Figure 5.5 Tungsten halogen lamps used as a solar simulator

5.2.2.2 Open Thermochemical Energy Storage System

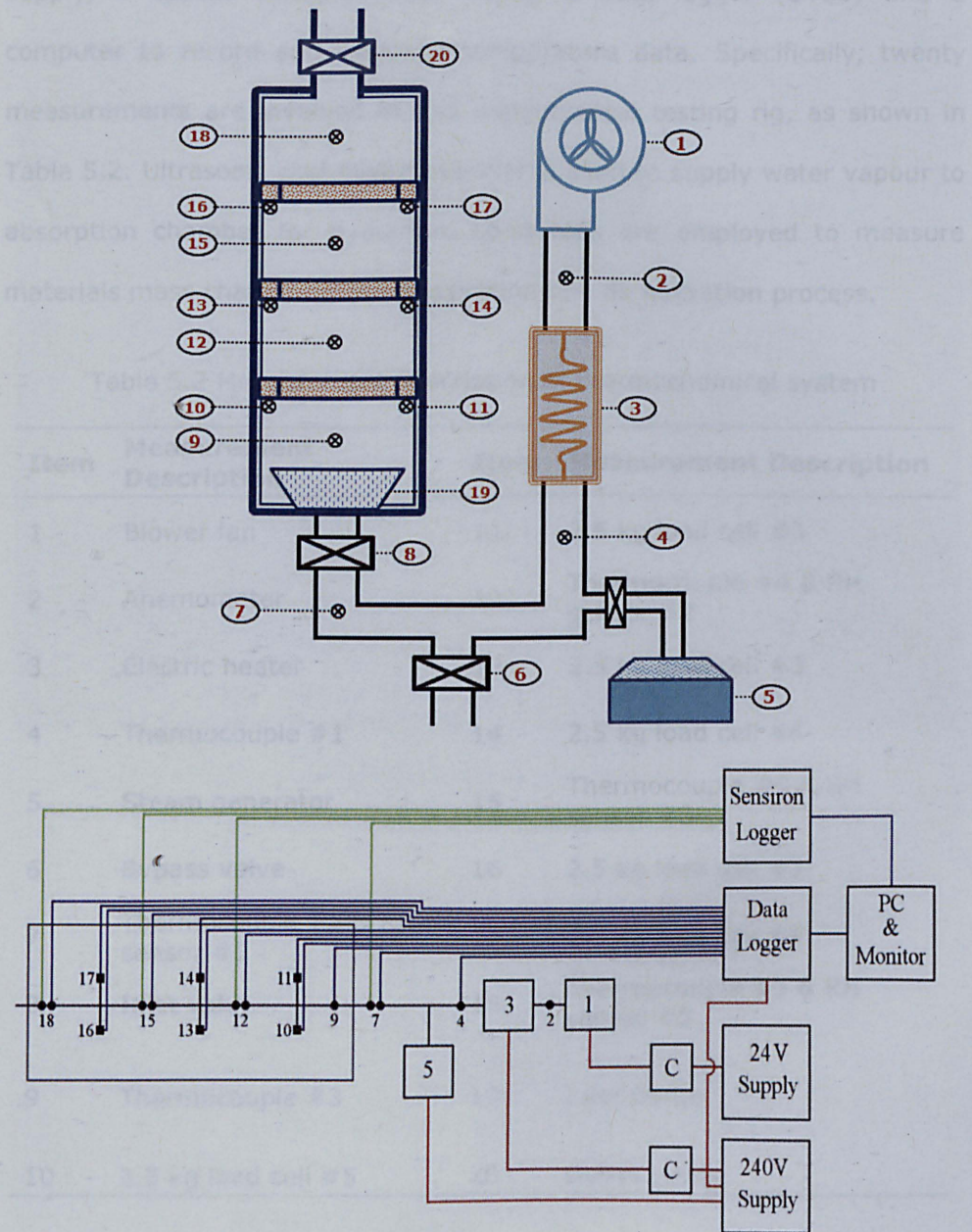


Figure 5.6 Schematic diagram of the system with measurement locations

An open thermochemical energy storage system has been designed by author as shown in Figure 5.6 and Table 5.2. The open thermochemical energy storage system consists of a blower fan, an electric heater, a 3.78 litre steam generator (ultrasonic cool humidifier), six weight sensors/load

cells (range: 0 ~ 2.5kg), a relative humidity sensor, a 24V DC power supply, a special designed inlet baffle, a data logger (DT80) and a computer to record and measure temperature data. Specifically, twenty measurements are involved in this experimental testing rig, as shown in Table 5.2. Ultrasonic cool mist humidifier is used to supply water vapour to absorption chamber for hydration. Load cells are employed to measure materials mass change between hydration and de hydration process.

Table 5.2 Measurement description of thermochemical system

Item	Measurement Description	Item	Measurement Description
1	Blower fan	11	2.5 kg load cell #5
2	Anemometer	12	Thermocouple #4 & RH sensor #2
3	Electric heater	13	2.5 kg load cell #3
4	Thermocouple #1	14	2.5 kg load cell #4
5	Steam generator	15	Thermocouple #5 & RH sensor #3
6	By-pass valve	16	2.5 kg load cell #1
7	Thermocouple #2 & RH sensor #1	17	2.5 kg load cell #2
8	Inlet valve	18	Thermocouple #5 & RH sensor #3
9	Thermocouple #3	19	Inlet Baffle
10	2.5 kg load cell #5	20	Outlet valve

The thermochemical energy storage system test rig in this research is shown in Figure 5.7 with relevant measurements labels. Figure 5.8 is showing inside details of the thermochemical absorption chamber with air flow baffle and three absorbent trays with 1.2mm meshed bottom. Moreover, Figures 5.9 and 5.10 give more details of the internal dimension about absorption chamber and air flow baffle.

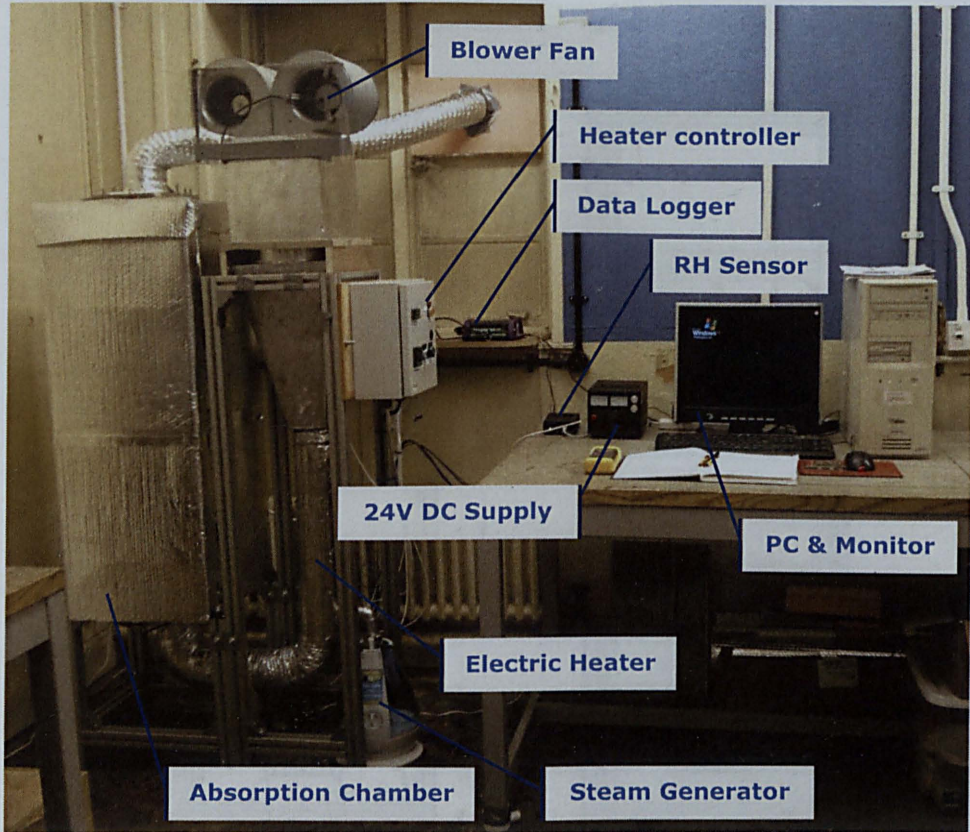


Figure 5.7 Open thermochemical energy storage system testing rig

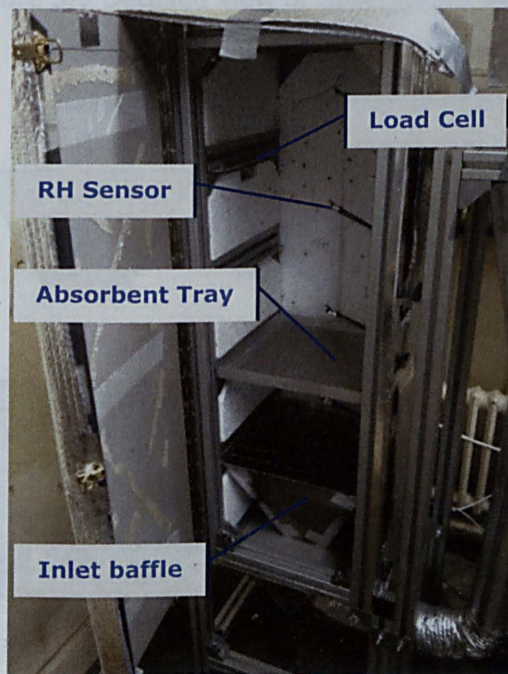


Figure 5.8 Testing absorption chamber with air flow baffle

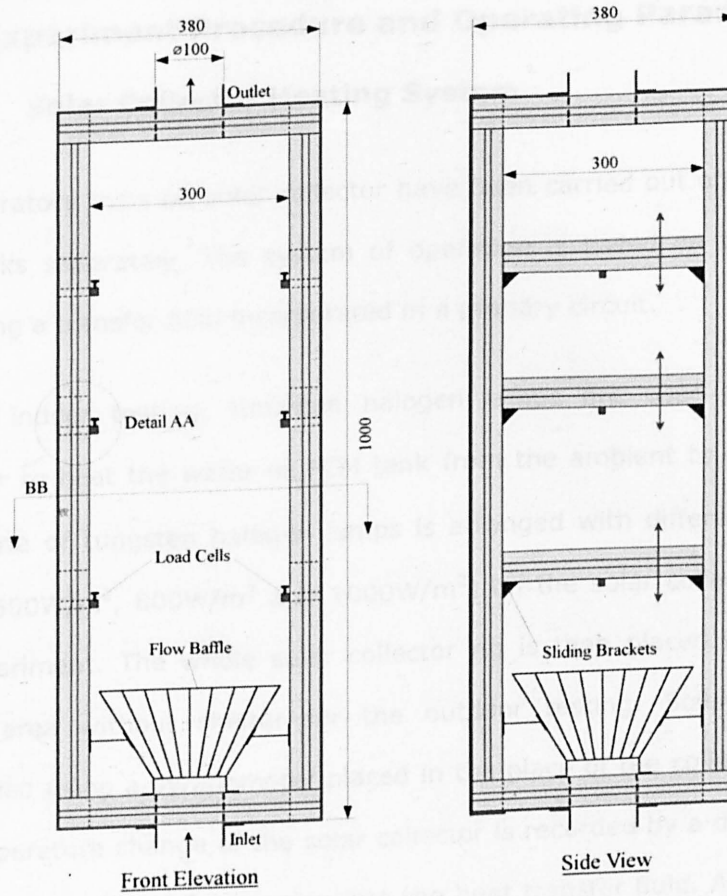


Figure 5.9 Detailed view of absorption chamber

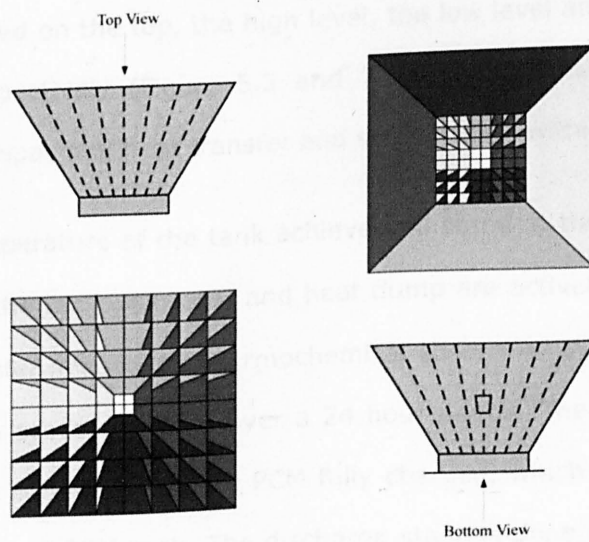


Figure 5.10 Detailed view of air flow baffle

5.3 Experiment Procedure and Operating Parameters

5.3.1 Solar Collector Heating System

The laboratory tests on solar collector have been carried out on water and PCM tanks separately. The system of operation is based on transferring heat using a transfer fluid incorporated in a primary circuit.

For the indoor testing, tungsten halogen lamps are used as a solar simulator to heat the water or PCM tank from the ambient to over 70°C. The frame of tungsten halogen lamps is arranged with different average power (600W/m², 800W/m² and 1000W/m²) on the solar collector during this experiment. The whole solar collector rig is then placed in an open outside area without shelter for the outdoor testing. Solar power is determined using a pyranometer placed in the place of the collector tubes. The temperature change of the solar collector is recorded by a data logger, which monitors energy absorption into the heat transfer fluid. At the same time, with inlet and outlet temperatures of water or PCM tank increasing, it is to monitor energy absorption into the tank. There are four thermocouple detectors placed on the top, the high level, the low level and the bottom of the tank, respectively (Figure 5.3 and Table 5.1). These detectors will monitor any impacts of heat transfer and stratification within the tank.

When the temperature of the tank achieve and stand at the required value (over 70°C), the fan coil heater and heat dump are activated to discharge tank and transfer heat to the thermochemical absorption system. Normally, the whole test procedure lasts over a 24 hour period. The charging of the tanks is about 8 hours to insure PCM fully charged, which can be checked by temperature of PCM tank. The discharge stage is done overnight where heat can be discharged from the store tank to room temperature.

5.3.2 Open Thermochemical Energy Storage System

In order to evaluate the performance of this thermochemical absorption system, a series of tests have been conducted at the laboratory, University Of Nottingham, the procedures of which has been described above. The basic equipment involved at this stage and the way it is set up is illustrated diagrammatically in Figures 5.6 to 5.10 and Table 5.2. The testing procedure is as follows:

- a)** Dry the materials for 24hrs at 115°C (silica gel, activated carbon and vermiculite) or 250°C (Zeolite 13X) in an experimental oven
- b)** Weigh the tray with mesh without material on an experimental scale
- c)** Weigh the tray with mesh and material to get the dry mass of the sample
- d)** Place the tray in the chamber and seal the door. Make sure the tray is not touching any of the walls in the chamber
- e)** Start the blower fan
- f)** Start logging from the data logger and relative humidity sensor at the same time. (Don't start the loggers before the chamber is sealed)
- g)** Start the humidity generator
- h)** When mass, temperature and relative humidity reach a steady state then;
- i)** Turn off and isolate the humidity generator
- j)** Switch on the heater and set at required temperature range (60°C, 80°C, 100°C or 120°C)
- k)** When mass, temperature and relative humidity again reach a steady state, then reduce the heater temperature to 22°C

- l)** When the temperature and relative humidity reach ambient condition (22°C) at a steady state, then switch off the heater
- m)** Repeat cycle from stage **f)** if required
- n)** At the end of cycling:
 - Stop the data logger and relative humidity sensor at the same time, save the data logged and then clear the loggers
 - Ensure the heater is switched off and then switch off the fans
 - Unseal the chamber and remove the tray
 - Weigh the tray

5.4 Experiment Measurements and Data Acquisition

5.4.1 Instrumentation and Measurements

The favourable performance of the system is based upon the accuracy of instruments employed and also methods of measurement. Core performance indicators for the high capacity heat storage system include operating temperatures, relative humidities, materials weight change rates and air flow rates.

5.4.1.1 Temperature Measurement

In order to achieve a reasonable accuracy in temperature measurements, type K thermocouple and data taker (DT80) have been employed through whole testing process, as shown in Figure 5.11. Type K thermocouple is the most common general purpose thermocouple with a sensitivity of approximately 41 $\mu\text{V}/^\circ\text{C}$. Type K thermocouple has a temperature range between -50°C and 250°C with a tolerance of $\pm 1.5^\circ\text{C}$. It is particularly suitable for high pressure, high vacuum or high vibration applications. The data taker DT80 is a smart data logger that provides an extensive array of

features that allow it to be used across a wide variety of applications. All type k thermocouples are connected with this DT80 data logger.



(a): Type K thermocouple

(b): Data taker DT80

Figure 5.11 Temperature measurements

For reference temperatures control, RS 53II digital thermometer (as shown in Figure 5.12) is used to ensure and calibrate all sensors probably and normally working. RS 53II digital thermometer has a wide temperature range between -200°C and 1375°C with an accuracy of about $\pm 0.3\%$ and resolution of 0.1°C .



Figure 5.12 RS 53II digital thermometer

5.4.1.2 Solar Radiation Measurement

In solar collector heating system testing section, the solar or light intensity is measured by a Pyranometer CMP 11 supplied by Kipp & Zonen, as shown in Figure 5.13. It has sensitivity of $9.66 \times 10^{-6} \text{ V/W.m}^{-2}$ with 1% of

temperature dependence of sensitivity. Directional error (up to 80°C with 1000 W/m² beam) is less than 10 W/m².

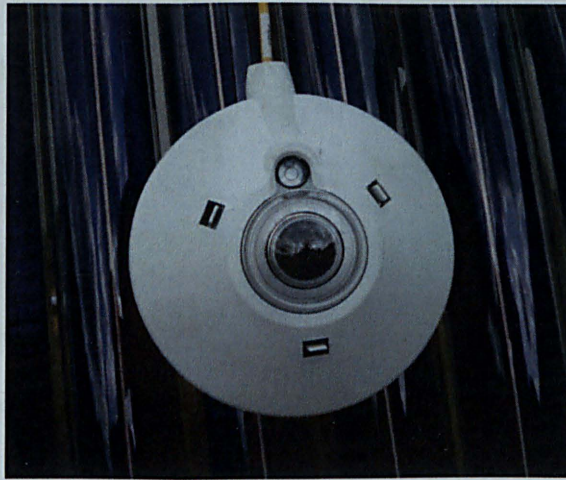
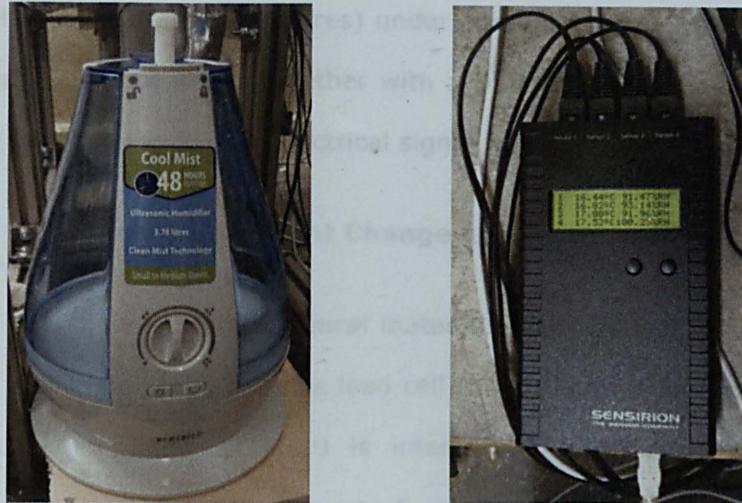


Figure 5.13 CMP11 Pyranometer (Kipp & Zonen)

5.4.1.3 Relative Humidity Measurement

Ultrasonic cool mist humidifier is used as a steam generator to supply enough water vapour to absorption chamber for thermochemical energy storage testing. This type humidifier can supply about 18°C water vapour by using Ultrasonic technology. It has a 3.8 litre water tank with visible water level indicator, as shown in Figure 5.14 (a). Relative humidity is measured by using evaluation kit EK-H4, which combines an easy-to-use plug-and-play system for sensor evaluation with a data logging equipment for simultaneous recording of humidity and temperature. Normally, the evaluation kit EK-H4 has four digital channels for different type humidity and temperature sensors, as shown in Figure 5.14 (b). Connected to a digital humidity sensor type SHT21, evaluation kit EK-H4 can give relative humidity operating range 0~100%RH and temperature operating range between -40°C and 125°C.



(a): Ultrasonic cool humidifier (b): RH evaluation kit EK-H4

Figure 5.14 Steam generator and relative humidity evaluation kit (EK-H4)

5.4.1.4 Measuring the Pressures

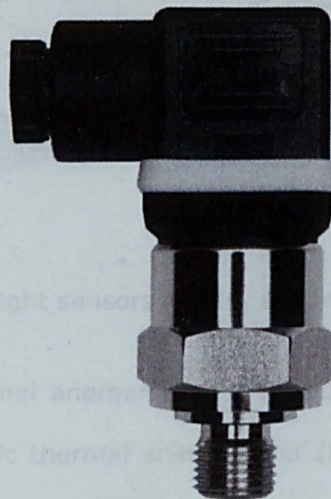


Figure 5.15 Jumo Midas pressure transmitter (type 401001)

Pressure transmitters are used for measuring the relative pressure in liquids and gases. Figure 5.15 is showing a pressure transmitter (type 401001) supplied by the Jumo Midas. This type pressure transmitter is a multipurpose, high performance stainless steel device with pressure range

from -1 to 5 bars (gauge pressures) under operating temperature between -20°C and 125°C. It works together with a DT80 data logger because the pressure is converted into an electrical signal.

5.4.1.5 Measuring Weight Change and Air Flow Rates

In order to measure thermochemical materials mass change during testing process, a single point low profile load cell (S220) is employed to measure weight change. Load cell S220 is intended for applications requiring accurate measurement of forces up to 5.4kg force, as shown in Figure 5.16. It has a -40°C to 150°C operating temperature and temperature effect on output is less than 0.03% reading. Six load cells S220 are used in absorption chamber in this research.

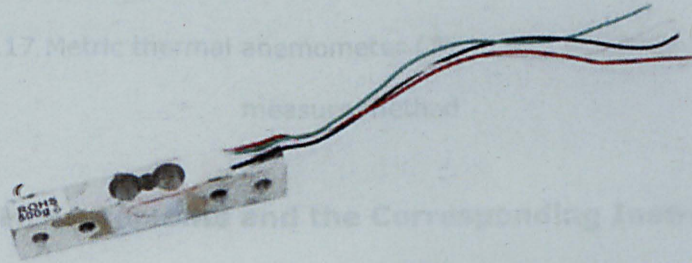


Figure 5.16 Weight sensors (S220, single point Load Cell)

For air flow rates, thermal anemometer is introduced to this experiment. Figure 5.17 shows metric thermal anemometer (type 405-V1) supplied by Testo and its five points measuring method, which is suitable for testing the air flow speed in fan coil duct. This mini-anemometer has a rapid response sensor for detecting the minute changes in air velocity such as inlet and outlet of duct. It reads air velocity (m/s) and temperature (°C) and calculates volume flow in cubic meters per hour. Its velocity range is 0 to 10 m/s with accuracy of about ± 0.1 m/s and air velocity resolution of 0.01 m/s.

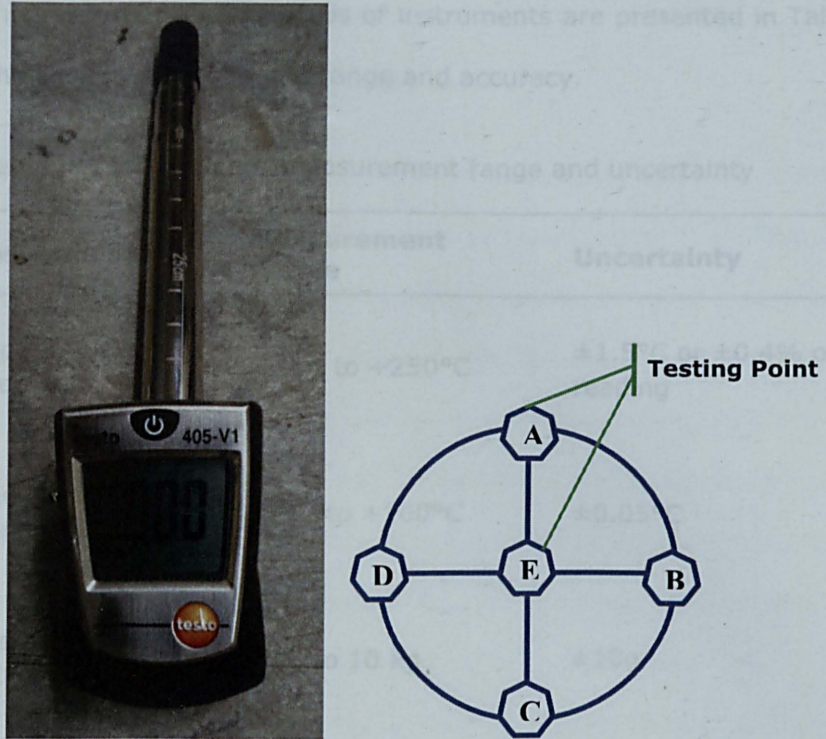


Figure 5.17 Metric thermal anemometer (Testo 405 V1) and five points' measure method

5.4.2 Measurements and the Corresponding Instruments

In laboratory tests, measurement errors and extrapolated uncertainties always occur. There are two types of errors associated with an experiment result as precision and accuracy. The precision errors are related to the random error distribution associated with a particular experiment. The accuracy errors are related to the existence of systematic errors. The object of a good experiment is to minimize both precision and accuracy errors by careful calibration of instruments. A given experiment usually has one type of errors dominant, and the experimenter devotes the most effort toward reducing that one. Taking multiple measurements helps reduce uncertainties. Figures 5.11 to 5.17 are showing some relevant instruments.

used in this research. All the details of instruments are presented in Table 5.3, which includes measurement range and accuracy.

Table 5.3 Instruments' measurement range and uncertainty

No.	Instruments	Measurement Range	Uncertainty
1	Type K thermocouple	-50°C to +250°C	±1.5°C or ±0.4% of reading
2	Thermostat heater (Grant SV200)	+5°C to +100°C	±0.05°C
3	Weigh Scales (Kern ECB 10K10)	0 kg to 10 kg	±10g
4	Thermal Imaging Scanner (Fluke TiS)	-20°C to +100°C	±5°C or 5 % of reading
5	Digital thermometer (RS 53II)	-200°C and 1375°C	+0.8°C or ±0.3% of reading
6	Pyranometer (Kipp & Zonen CMP11)	285 nm to 2800 nm	10W/m ² or ±1.0% of reading
7	Relative humidity kit (Sensirion EK-H4)	0 ~ 100% RH & -40°C and +125°C	±2.0% RH & ±0.3°C
8	Pressure transmitter (Jumo Midas 401001)	-1 bar to +5 bar	±0.3% of reading
9	Weight sensor (Load cell S220)	0 kg to 5.4 kg	±0.03% of reading
10	Thermal anemometer (Testo 405-V1)	0 m/s to +10 m/s & -20°C to +150°C	0.3 m/s or ±5% of reading & ±0.5°C

5.4.3 Instruments Calibration

5.4.3.1 Calibration of Thermocouples

Temperatures change is one of key factors to investigate the performance of the thermochemical energy storage system. Calibration of the type K thermocouples has been carried out by using a water tank and a standard mercury thermometer as shown in Figure 5.18. The method is based on a fixed-point temperature calibration. Grant thermostat heater (SV200) is used to heat the water tank to some temperature. Thirty thermocouples and one standard mercury thermometer are located at the same depth in the water tank. The actual water temperature is about 50.40°C measured by the mercury thermometer. The calibration results from the thirty thermocouples are shown in Figure 5.19, which shows excellent consistency within a maximum difference of 0.4% approximately of mercury thermometer's reading.

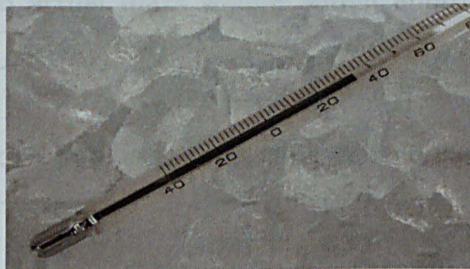


Figure 5.18 A standard mercury thermometer

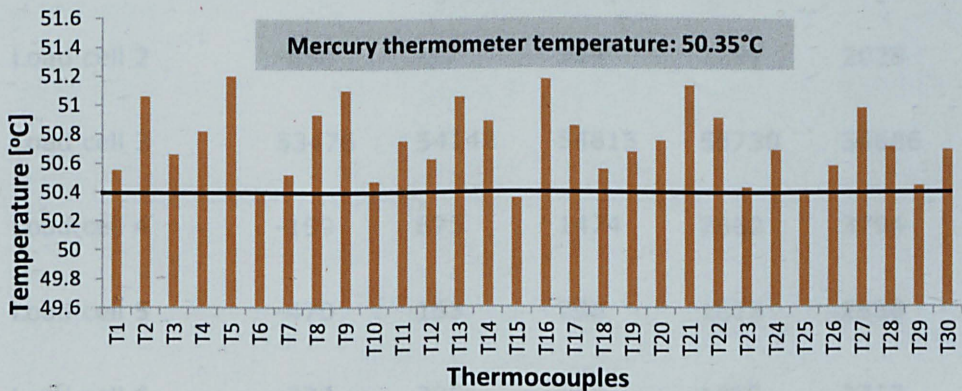


Figure 5.19 Temperature calibration of type K thermocouple

5.4.3.2 Calibration of Weight Sensors (Load Cells)

A weight sensor is an ideal device to measure weight change of materials to investigate thermochemical materials' absorption capacity. A weight sensor is a type of transducer which reads an initial amount of force or weight, and then converts this force into an electrical signal. Compared with any others precise measurement devices, calibration of a weight sensor are an exact science. Calibration of load cells is conducted step by step in this research. Six single point low profile load cells (S220) are installed in the absorption chamber as shown in Figure 5.9. Each load cell has a special and original reading value different from others. Table 5.4 is showing load cells reading values under different mass weights. Figure 5.20 plots out the data of Table 5.4, which implies relevant linear trend equations. Based on these equations, actual value of load cells can be calibrated and calculated, as shown in Table 5.5. These actual calibrated values are close to actual mass weight within approximately $\pm 0.03\%$ of accuracy.

Table 5.4 Weight sensors original reading value under different weights

Weight sensor	0g	315g	631g	1084g	1537g
Load cell 1	-566	-26	529	1298	2102
Load cell 2	-550	-17	524	1297	2028
Load cell 3	53476	54142	54815	55730	56686
Load cell 4	-159	675	1474	2662	3794
Load cell 5	-470	153	790	1672	2538
Load cell 6	-232	396	984	1838	2712

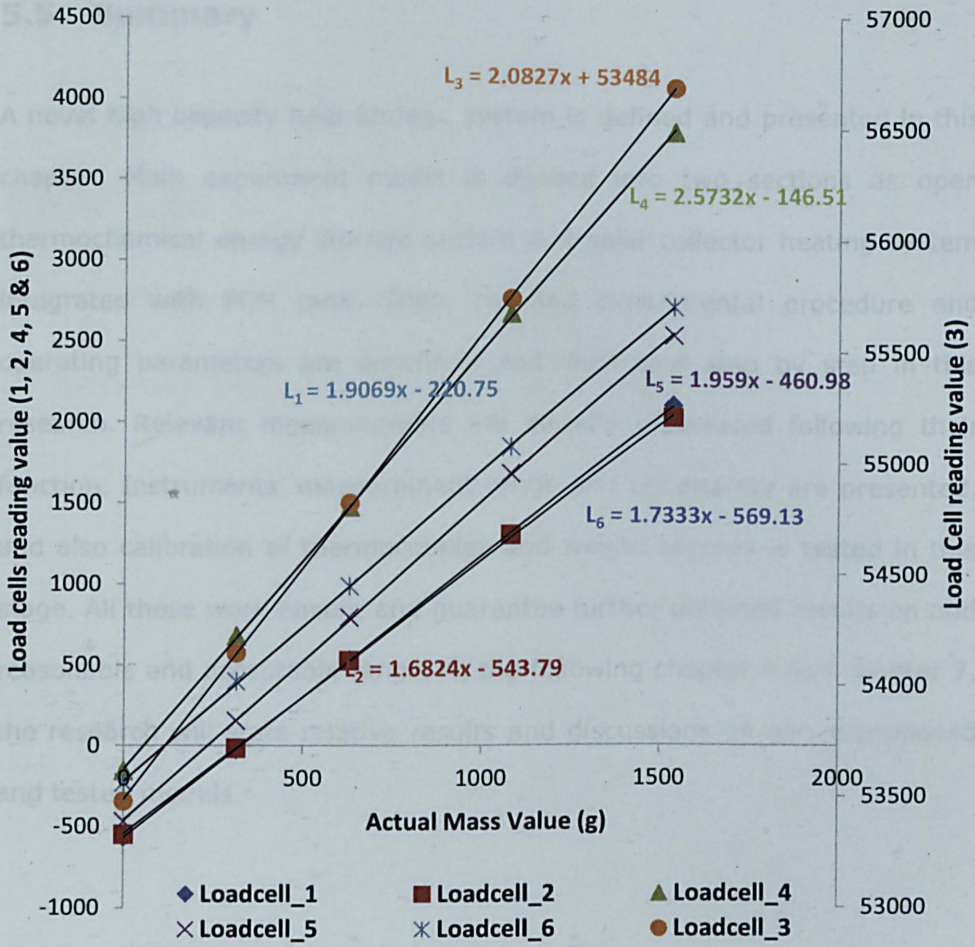


Figure 5.20 Calibration of six weight sensors (Load cell S220)

Table 5.5 Weight sensors actual calibrated value under different weights

Weight sensor	0g	315g	631g	1084g	1537g
Load cell 1	1.81	313.35	633.55	1077.21	1541.07
Load cell 2	-3.69	313.12	634.68	1094.15	1528.64
Load cell 3	-3.84	315.94	639.08	1078.42	1537.45
Load cell 4	-4.85	319.26	629.76	1091.45	1531.37
Load cell 5	-4.60	313.42	638.58	1088.81	1530.87
Load cell 6	-5.90	323.43	631.78	1079.63	1537.97

5.5 Summary

A novel high capacity heat storage system is defined and presented in this chapter. Main experiment model is divided into two sections as open thermochemical energy storage system and solar collector heating system integrated with PCM tank. Then, detailed experimental procedure and operating parameters are described and illustrated step by step in this research. Relevant measurements are already introduced following their function. Instruments' measurement range and uncertainty are presented, and also calibration of thermocouples and weight sensors is tested in this stage. All these work ensure and guarantee further obtained results on and reasonable and acceptable range. At the following chapter 6 and chapter 7, the research will state relative results and discussions on above proposed and tested models.

CHAPTER 6

Experiment Results and Discussions on Enhanced Solar Collector System

6.1 Introduction

Experiment results of the direct flow evacuated tube solar collector heating system is discussed and analysed in this chapter, which works with water and PCM storage tank. Tungsten halogen lighting is used for indoor testing and natural solar radiation is for outdoor testing. Numerical analysis and comparison of water and PCM tank system is also stated on the basis of properties of PCMs. Efficiency analysis method is utilised to evaluate the performance of the novel fan coil heating pipes system which is powered by the solar collector integrated with a PCM storage tank.

6.2 Experiment Results on Solar Collector Heating System

6.2.1 Solar Collector System Dimensioning

The final version solar collector system consists of a 3.0m² (30 tubes) Kingspan DF100 vacuum tube collector, a 45 litres water tank, a 45s litre PCM storage tank incorporating 42kg of Paraffin RT58, a 5kW heat exchanger and a 5kW fan coil heat exchanger. As described in Chapter 3 and 5, Kingspan DF100 is a very common glass-metal direct flow evacuated tube solar collector with approximate 83.2% efficiency, which consists of a row of solar tubes and a highly insulated manifold. Heat transfer fluid is circulated in a coaxial manner through the manifold and tubes. More detailed specifications of DF100 show in Table 3.4, which is from the manufacturer. The tungsten halogen lamps are employed as a solar simulator for indoor testing. Figure 6.1 shows temperature change within the water tank under 1000W/m² light radiation.

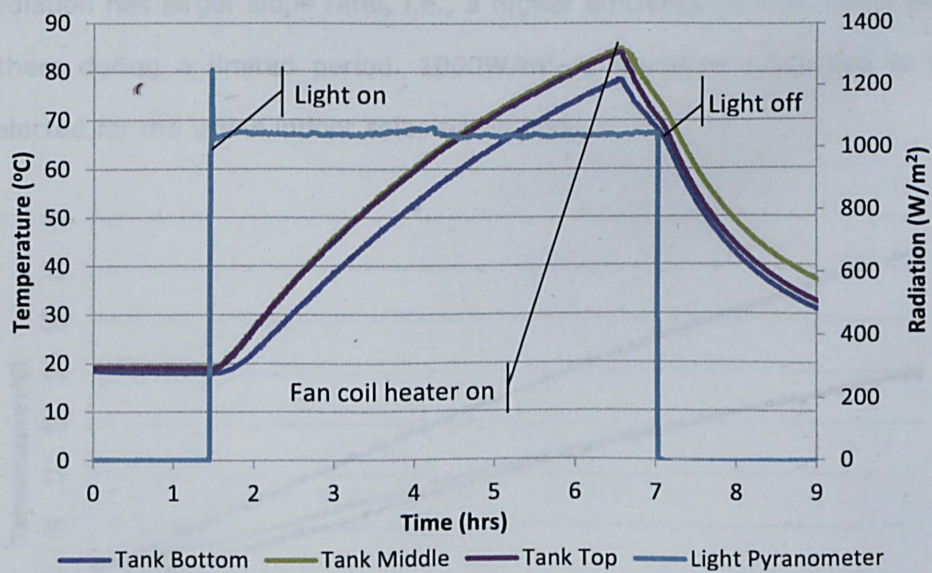


Figure 6.1 Temperatures change in water tank under light radiation

As can be seen, the internal temperature starts increasing when the tungsten lamp is on, and reaches its peak point (about 84°C) when the fan

coil heater is on. After that, the temperature starts dropping and sharply decreases when the lamp is turned off in which stored tank heat energy is transferring to fan oil heater. It takes approximately 5.5 hours to heat water to over 80°C from 20°C under 1000W/m² light radiation. This linear trend of temperature change is very common for this evacuated tubes solar collector system for both indoor lamps light and outdoor solar.

6.2.1.1 Selection of Radiation Intensity for Solar System

In order to test this proposed solar collector system, some parameters should be selected up and fully understood. Radiation intensity is the first key factor to determine the efficiency of a solar system. The line trend of temperature change in water tank under different radiations (600W/m², 800W/m² and 1000W/m²) has been studied in this research and the result is illustrated in Figure 6.2. It is obvious that the line of 1000W/m² light radiation has larger slope ratio, i.e., a higher efficiency to heat water than others during a limited period. 1000W/m² is therefore confirmed to be selected for the whole indoor solar simulation.

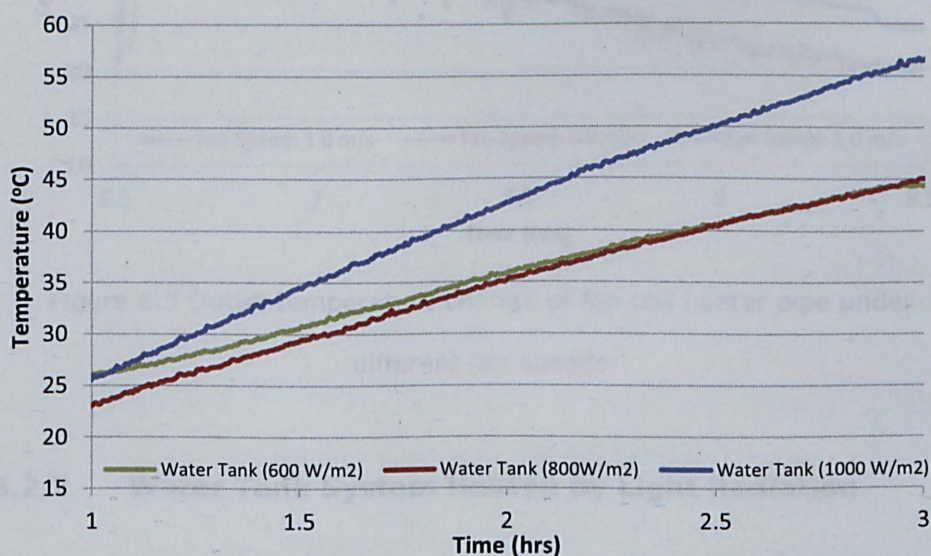


Figure 6.2 Temperatures change in water tank under different radiations

6.2.1.2 Effect of Fan Speed on Heating Temperature

The fan speed of fan coil heater is another significant parameter to affect heat output of the solar system. Three types fan speed (1.0m/s, 3.0m/s and 5m/s) have been tested as shown in Figure 6.3 in this research, which implies that 3.0m/s is the most appropriate fan speed with higher thermal output than others. The reason for this is that 5.0m/s is too fast for heat exchange in which too much room temperature is mixed and produce lower output temperature than 3.0m/s one. Meanwhile, 1.0m/s is quite slow and lower powerful to for heat exchange (even with a fluctuated linear trend). Therefore, the fan speed is locked at 3.0m/s through the whole testing progress and process.

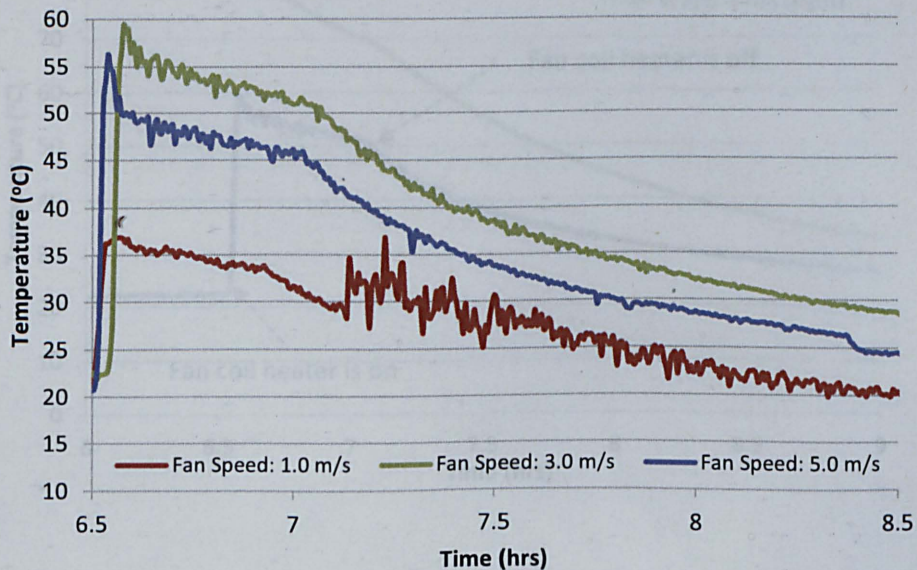


Figure 6.3 Outlet temperature change of fan coil heater pipe under different fan speeds

6.2.2 Water Tank System Heated by Light Radiation

The indoor testing rig employs the tungsten lamps rig as a solar simulator. Temperature in the water tank is heated up to 84°C after about 5.5 hours

(one hour free stand before testing) under $1000\text{W}/\text{m}^2$ light radiation. At this point, the fan coil heater, relevant pump and valves are all turned on. Figure 6.4 presents temperatures change of fan pipe outlet and water tank under light radiation. It can be seen that the outlet temperature of fan pipe suddenly jumps up to 60°C when the fan coil heater starts working, and then slowly decrease to about 50°C within half an hour. The outlet temperature gradually drops to the original value (around 21°C) in three hours after the fan coil heater is turned off. The dry hot air, heated by the fan coil heater, is at the same time delivered to the absorption chamber through a diameter of 0.30 meter hose under 3.0 m/s speed.

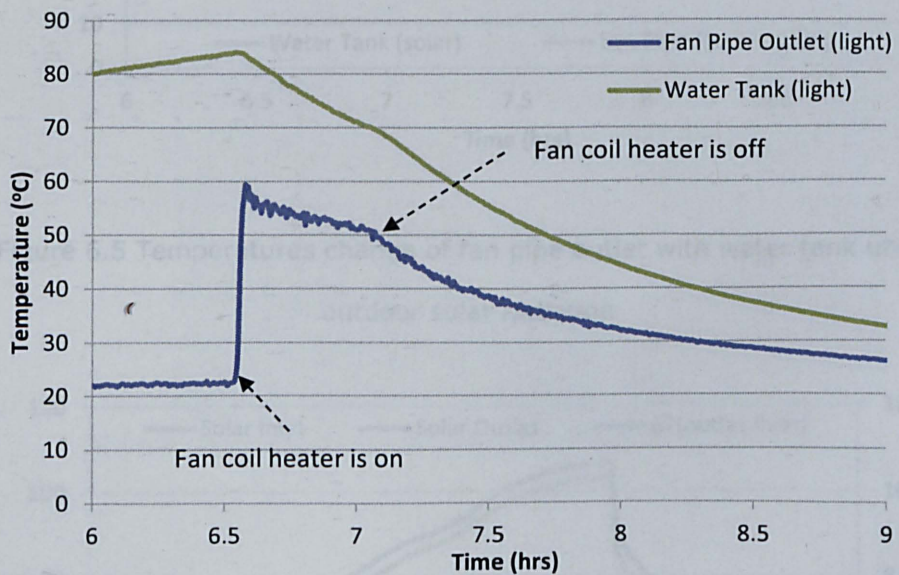


Figure 6.4 Temperatures change of fan pipe outlet with water tank under indoor light radiation

6.2.3 Water Tank System Heated by Solar Energy

Figure 6.5 reveals temperatures change of fan pipe outlet with water tank under outdoor solar radiation. Very similar linear trends can be observed as

shown in Figure 6.4. The difference is that the outdoor solar radiation can service a longer time (approximately 1 hour) for proposed outlet temperature (over 50°C) than the indoor light one.

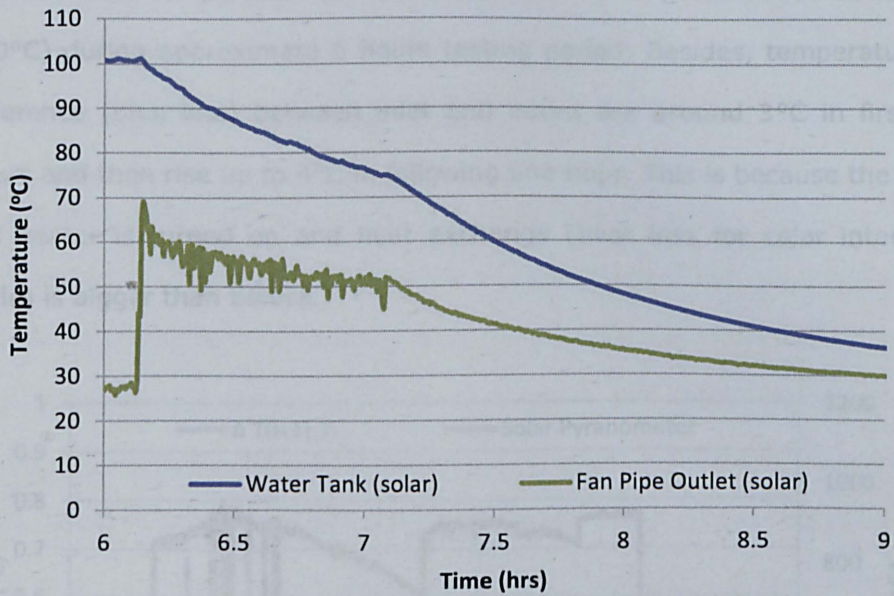


Figure 6.5 Temperatures change of fan pipe outlet with water tank under outdoor solar radiation

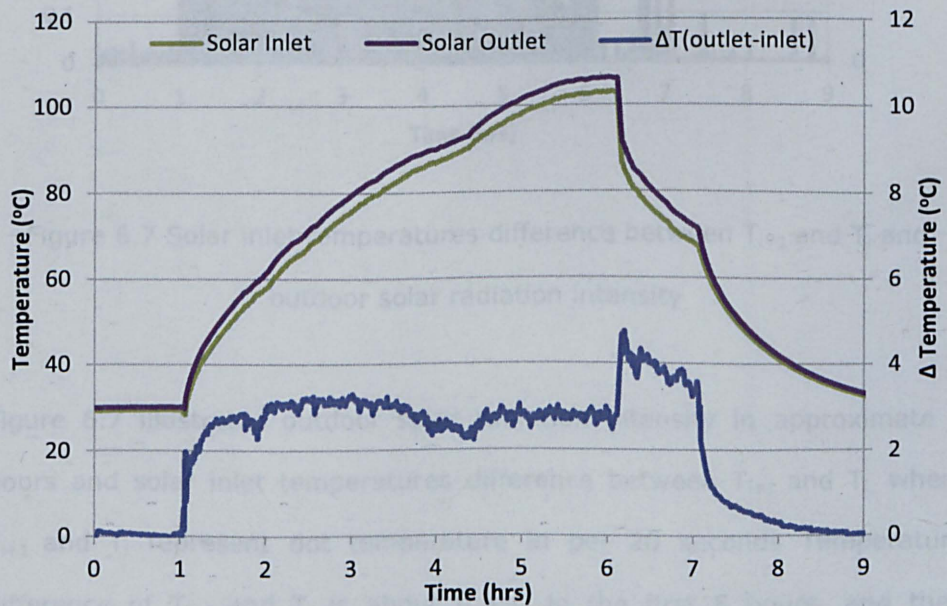


Figure 6.6 Solar collector inlet and outlet temperatures change

Figure 6.6 shows the internal inlet and outlet temperatures change of the solar collector and their difference under a water flow rate of 11.0 l/min. The maximum outlet temperature exceed 100°C and peak at about 106°C, and the inlet temperature difference is over 70°C (from about 30°C to 100°C) during approximate 6 hours testing period. Besides, temperatures difference (blue line) between inlet and outlet are around 3°C in first 5 hours and then rise up to 4°C in following one hour. This is because the fan coil heater is turned on and heat exchange (heat loss for solar internal cycle) is bigger than before.

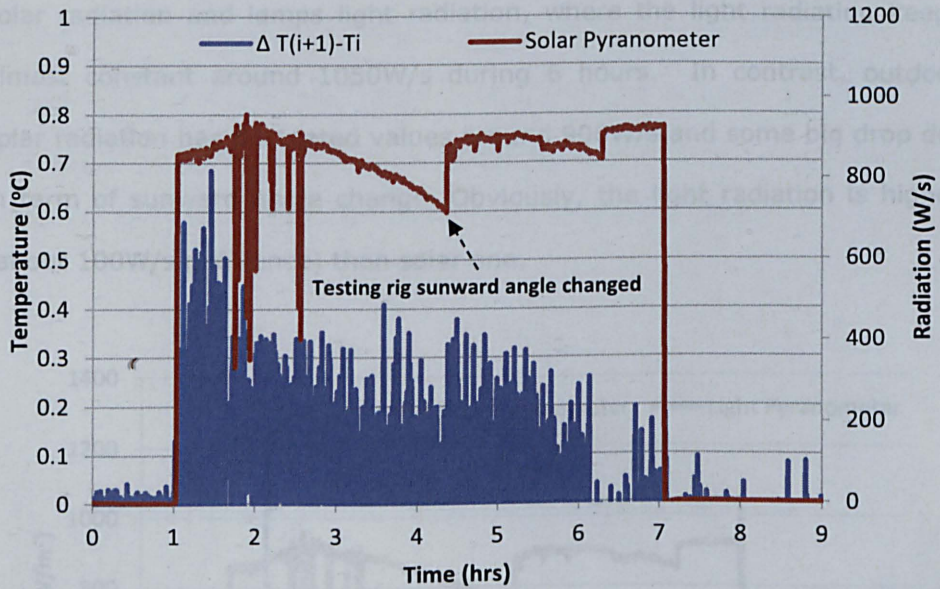


Figure 6.7 Solar inlet temperatures difference between T_{i+1} and T_i and outdoor solar radiation intensity

Figure 6.7 illustrates outdoor solar radiation intensity in approximate 6 hours and solar inlet temperatures difference between T_{i+1} and T_i , where T_{i+1} and T_i represent dot temperature in per 20 seconds. Temperature difference of T_{i+1} and T_i is about 0.3°C in the first 5 hours, and then decreases to less than 0.1°C in the last one hour when fan coil heater is on.

It also can be seen that the testing day is a mostly sunny day and radiation are around 900W/s with a drop point (about 720W/s) due to testing rig sunward angle changed.

6.2.4 Comparison of the Light Radiation and Solar Energy on Water Tank Systems

To compare temperatures change of the water tank system with solar and light energy, it is manifest to study the difference of outdoor solar radiation and indoor lamps light radiation. Figure 6.8 shows detailed different data of solar radiation and lamps light radiation, where the light radiation keeps almost constant around 1050W/s during 6 hours. In contrast, outdoor solar radiation has fluctuated values around 900W/s and some big drop dot in term of sunward angle change. Obviously, the light radiation is higher (about 100W/s difference) than solar one.

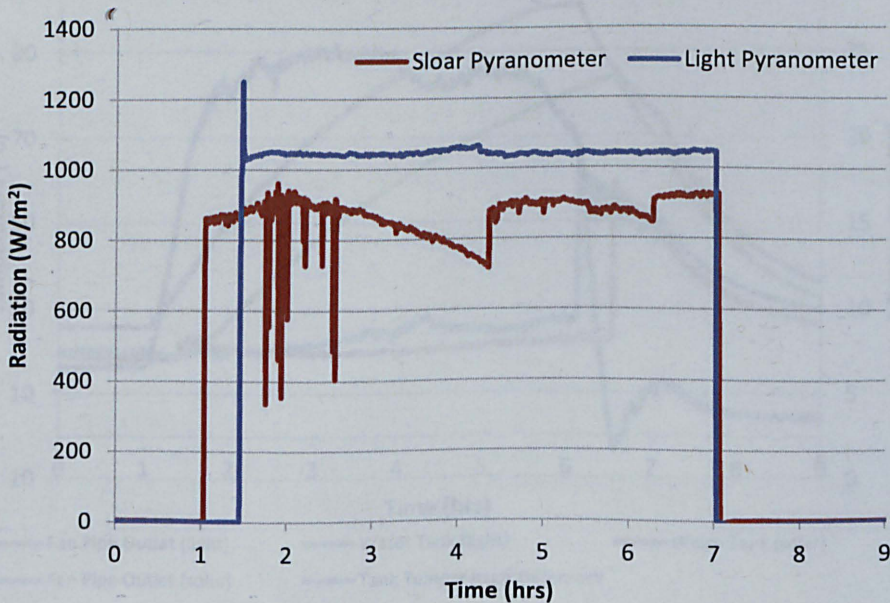


Figure 6.8 Comparison of outdoor solar and indoor lamps light radiation

Figure 6.9 illustrates full curves graph of water tank internal temperatures and fan pipe outlet temperatures change under different radiations. During about 5 hours, water tank is heated up to 100°C from 25°C by solar radiation and 85°C from 20°C by light radiation respectively. More exactly, solar heated water tank has a higher temperature than the light heated one within the same time period although average solar radiation has a lower value around 900W/s than light radiation about 1050W/s (Figure 6.8). Temperature difference of two heated water tanks is about 25°C as the dark blue line shown in Figure 6.9, because Tungsten lamps light radiation has a lower efficiency (about 70%) compared with solar radiation. As a matter of fact, this situation affects final pipes outlet temperature from fan coil heater in last one hour. More exactly, fan pipes outlet of solar water tank can provide over 50°C (light blue line) air flow over one hour, longer than only half hour of the light heated (red line) water tank.

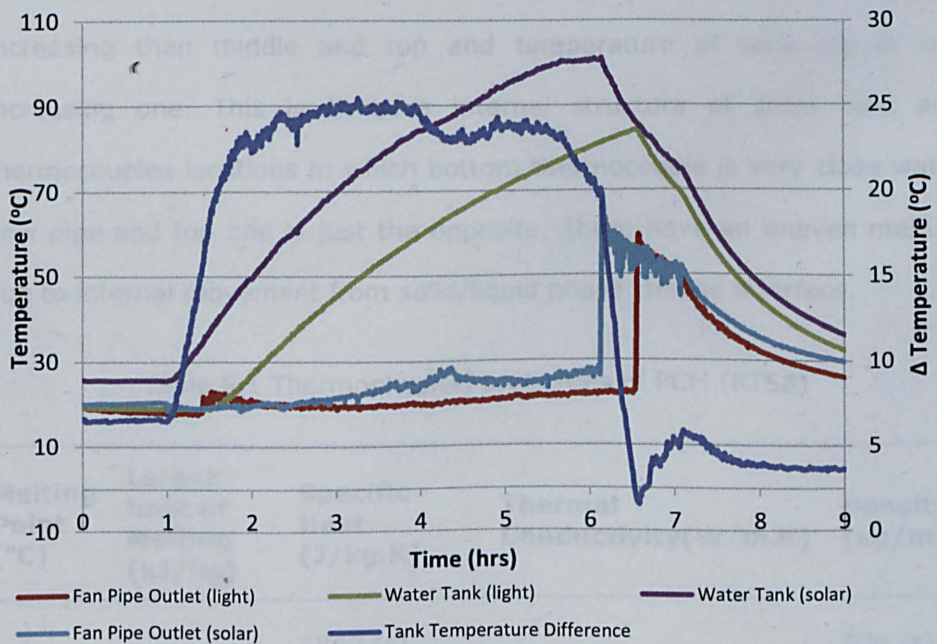


Figure 6.9 Water tank internal temperatures and fan pipe outlet temperatures change under different radiations

6.3 Experiment Results on Solar Collector Heating System with PCM

6.3.1 PCM Tank System Heated by Light Radiation

As mentioned before, PCM tank is connected to the solar collector rig in parallel with water tank. Table 6.1 lists the thermophysical properties of the RT58 PCM employed in this solar collector experiment. In PCM tank cycle, water tank is always closed. Figure 6.10 represents PCM tank temperatures' change with 1000W/s light radiation. When Tungsten halogen lamps are on, the internal temperatures of PCM tank (represented by tank middle, dark blue line) start increasing rapidly in the first two hours (2~4 in Figure 6.10), and remain stable around 60°C when PCM reaches its melting point. Internal temperatures start increasing again after another two hours when PCM is fully charged (totally about 4 hours). Meanwhile, it can be seen that Temperature of tank bottom is firstly increasing than middle and top and temperature of tank top is last increasing one. This is because internal structure of store tank and thermocouples locations in which bottom thermocouple is very close water flow pipe and top one is just the opposite. There have an uneven melting due to internal movement from solid/liquid phase change interface.

Table 6.1 Thermophysical properties of PCM (RT58)

Melting Point (°C)	Latent heat of Melting (kJ/kg)	Specific Heat (J/kg.K)	Thermal Conductivity(W/m.K)	Density (kg/m ³)
58	179	1800 (s) 2400 (l)	0.2	900 (s) 760 (l)

Source (Agyenim, 2012)

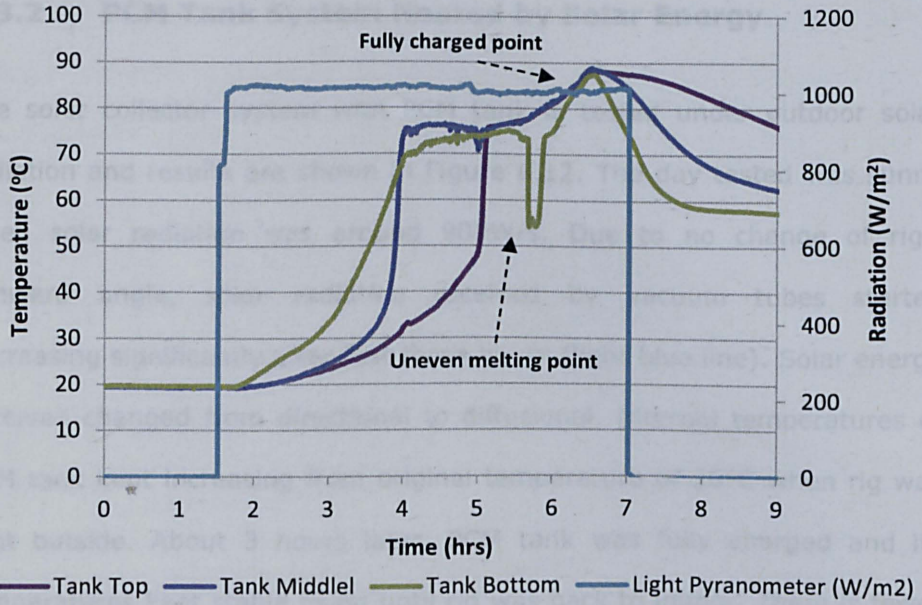


Figure 6.10 PCM tank temperatures change by light radiation

In the next stage, when the fan coil heater is on, dry high temperature air is blown out through pipes. Figure 6.11 reveals fan pipe outlet temperature is over 50°C and maintains about one hour, which is a similar to that of the water tank.

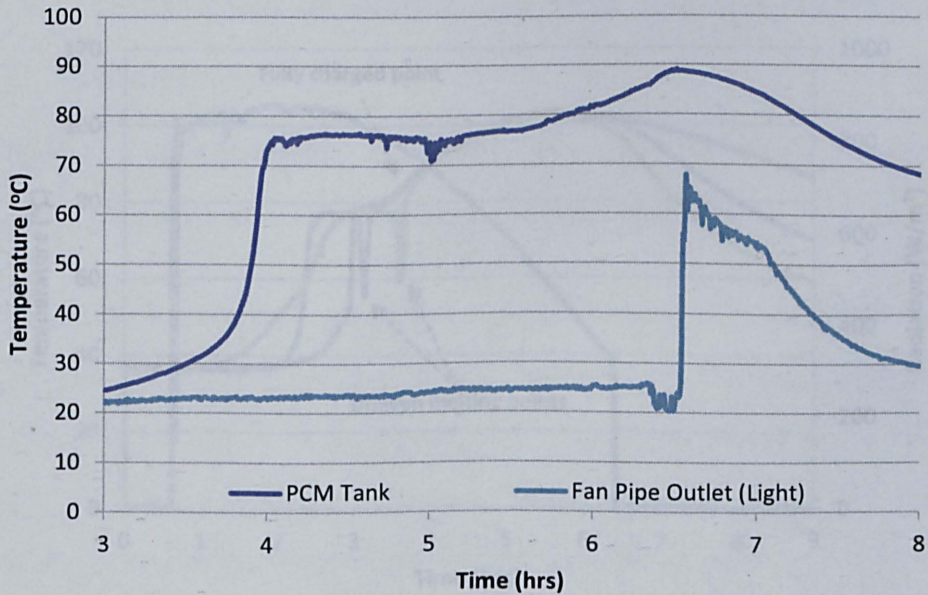


Figure 6.11 Fan pipe outlet temperatures change by light radiation

6.3.2 PCM Tank System Heated by Solar Energy

The solar collector system with PCM tank is tested under outdoor solar radiation and results are shown in Figure 6.12. The day tested was sunny when solar radiation was around 900W/s. Due to no change of rig's sunward angle, solar radiation received by vacuum tubes started decreasing significantly after first three hours (light blue line). Solar energy received changed from directional to diffusional. Internal temperatures of PCM tank kept increasing from original temperature of 36°C when rig was sent outside. About 3 hours later, PCM tank was fully charged and its temperatures kept stable rising until rig was back to indoor. There is fewer one hour than light radiation to charge PCM tank, which mean solar radiation is more efficiency to heat store tank than light one. The maximum internal temperature of the PCM tank was also approximate 105°C, very similar with sunward angle manual changed as shown in Figure 6.7. That is to say solar diffusion can also heat PCM tank to a target temperature as direct one.

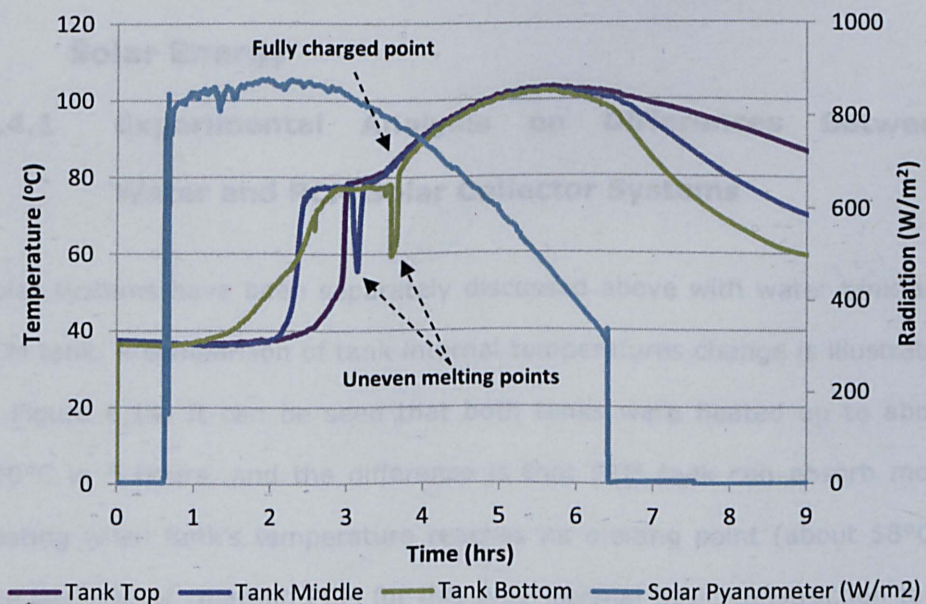


Figure 6.12 PCM tank temperatures change by solar radiation

Figure 6.13 shows one of testing results on fan pipe outlet temperatures change with PCM tank under sunlight radiation, which has a similar linear trend as water tank.

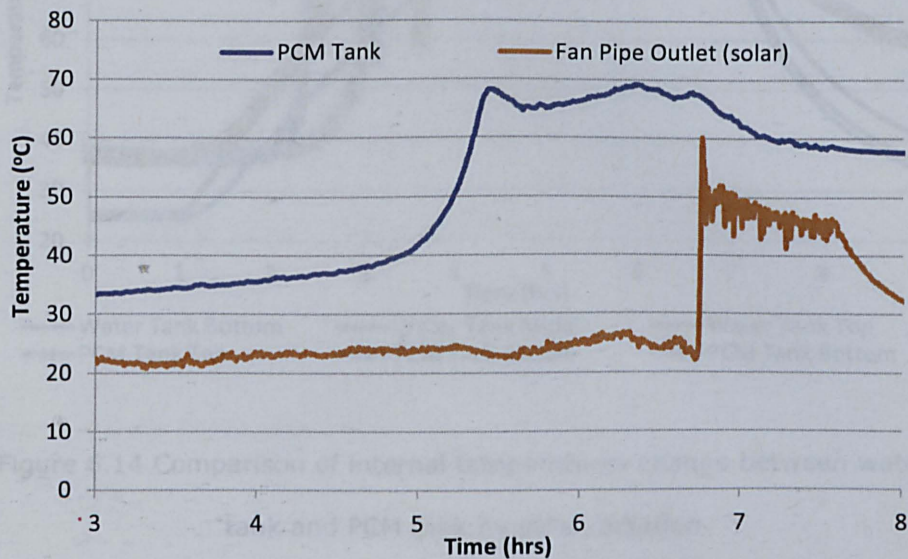


Figure 6.13 Fan pipe outlet temperatures change with PCM tank by solar radiation

6.4 Comparison of Water and PCM System Heated by Solar Energy

6.4.1 Experimental Analysis on Differences Between Water and PCM Solar Collector Systems

Solar systems have been separately discussed above with water tank and PCM tank. A comparison of tank internal temperatures change is illustrated in Figure 6.14. It can be seen that both tanks were heated up to about 100°C in 5 hours, and the difference is that PCM tank can absorb more heating when tank's temperature reaches its melting point (about 58°C). The duration of charging PCM for this type internal basic construction tank is over 2 hours.

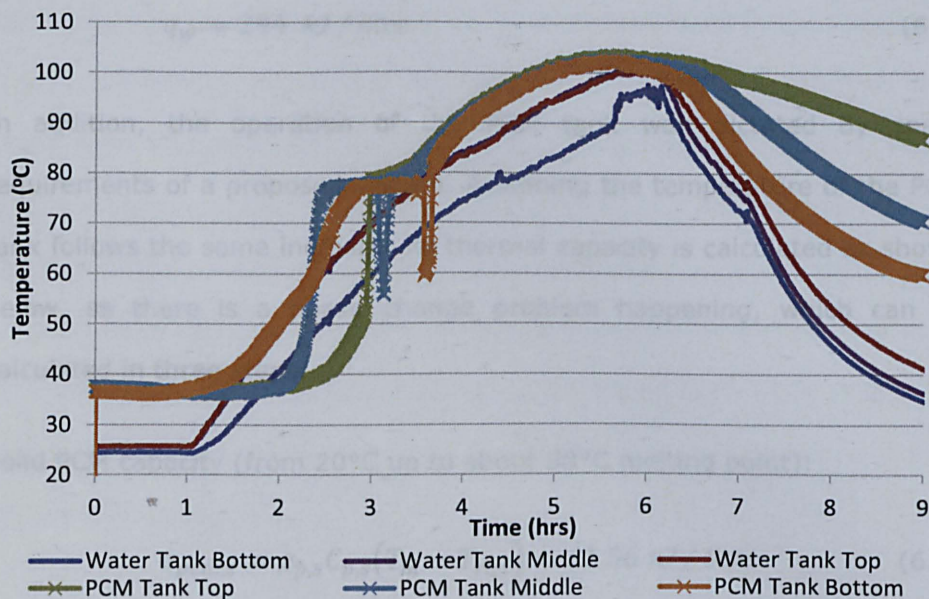


Figure 6.14 Comparison of internal temperatures change between water tank and PCM tank by solar radiation

For the PCM tank system, the theoretically maximum quantity of energy contained in 42kg PCM is calculated by:

$$Q_{pcm} = m_p [C_{p,l}(T_{fin} - T_m) + \lambda + C_{p,s}(T_m - T_{ref})] \quad (6.1)$$

For normal water tank system, the energy contained in a 45 litres water tank is written as:

$$Q_w = \rho_w V_w C_w (T_{fin} - T_{ref}) \quad (6.2)$$

Based on the thermophysical properties given in Table 6.2 and water's properties, assuming a 70°C increase in temperature from inlet 20°C to 90°C in both 45 litres tanks, the calculations associated with this are as follows:

Water capacity for 20°C to 90°C:

$$q_w = 294 \text{ kJ / litre} \quad (6.3)$$

In addition, the operation of the PCM tank was dictated by space requirements of a proposed system. Assuming the temperature of the PCM tank follows the same increase, its thermal capacity is calculated as shown below, as there is a phase change problem happening, which can be calculated in three steps.

Solid PCM capacity (from 20°C up to about 58°C melting point):

$$q_{pcm,s} = \rho_{p,s} C_{p,s} (T_m - T_{ref}) = 61.56 \text{ kJ / litre} \quad (6.4)$$

Capacity of the phase change:

$$q_{pcm,m} = \rho_{p,s} H_p = 161.10 \text{ kJ / litre} \quad (6.5)$$

Liquid PCM capacity (from 58°C to 90°C):

$$q_{pcm,l} = \rho_{p,l} C_{p,l} (T_{fin} - T_m) = 58.37 \text{ kJ / litre} \quad (6.6)$$

Therefore, the total PCM capacity:

$$q_{pcm} = q_{pcm,s} + q_{pcm,m} + q_{pcm,l} = 281.03 \text{ kJ / litre} \quad (6.7)$$

To sum up, the total amount of energy that can be stored in a 42kg PCM RT58 is 12.65MJ compared to 13.23MJ for same volume of water. As known, the size of DF100 vacuum tube collector is based on the amount of PCM that can be melted. An average of solar availability of 800W/m² (for northern European countries), with a collector efficiency of 83.2%, the size of the collector to melt 42kg PCM with 5 hours heating time has been determined to be 3m². In line with these calculations, it has been decided that in order to establish a baseline set of results that all future research

can be compared against, the size of the PCM tank used in this testing rig is set to be the same as that of the water tank. Therefore identical 45 litres tanks, with standard coils are used in both experimental sections. Figure 6.15 shows comparison of fan pipe outlet temperatures change between water and PCM tanks under outdoor solar radiation. Upon completion it can be seen water tank store capacity is bigger than PCM one in term of basic tank model. It also can be concluded that latent heat base PCM RT58 material is not suitable or cannot be directly used within current solar systems by its speciality.

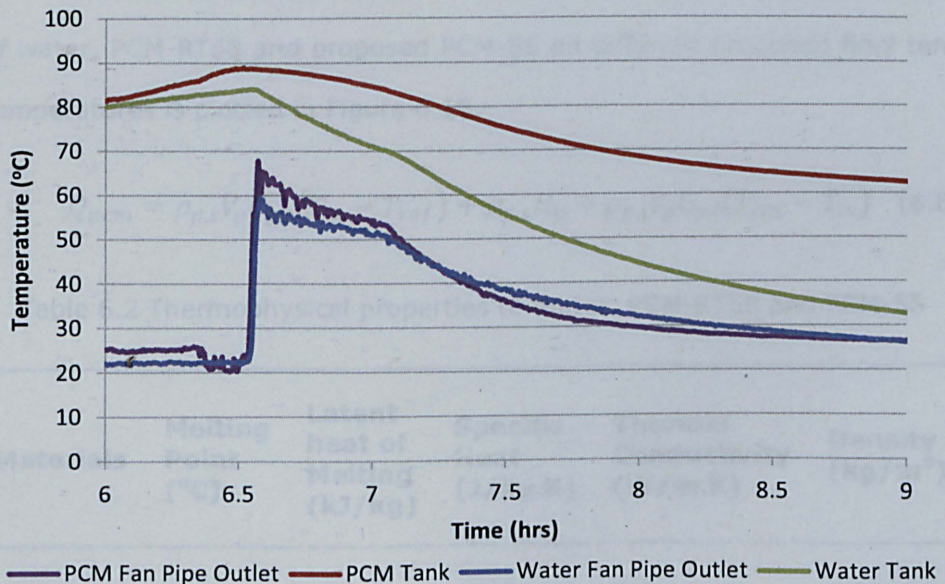


Figure 6.15 Comparison of fan pipe outlet temperatures change between water tank and PCM tank by solar radiation

6.4.2 Mathematical Analysis on Heating Storage Capacities of Water and Proposed PCM Solar Collector Systems

In the case of above experimental results discussion, numerical analysis method can be used to select and propose appropriate PCM for this system

in current available market. Table 6.2 gives more details about thermophysical properties of water, PCM (RT58) and proposed PCM-55. As known, materials thermal conductivities will change along with temperature change. These kinds of changes are ignored in this mathematical simulation due to limited effect on modelling results. A normal size of water tank is 45 litres and the PCM tank is defaulted as 42 litres. Tank reference temperature (T_{ref}) is set from 0°C, final tank targeted temperature is assumed between 0°C and 100°C. Based on above Eq. (6.2) and below Eq. (6.8), relevant parameters can be calculated out in term of relative data and Table 6.2's data information. Therefore, a comparison of heating gain of water, PCM-RT58 and proposed PCM-55 on different proposed final tank temperatures is plotted in Figure 6.16.

$$Q_{pcm} = \rho_{p,s}V_pC_{p,s}(T_m - T_{ref}) + \rho_{p,s}H_p + \rho_{p,l}V_pC_{p,l}(T_{fin} - T_m) \quad (6.8)$$

Table 6.2 Thermophysical properties of Water, PCM-RT58 and PCM-55

Materials	Melting Point (°C)	Latent heat of Melting (kJ/kg)	Specific Heat (J/kg.K)	Thermal Conductivity (W/m.K)	Density (kg/m ³)
Water	-	-	4200	0.6	1000
PCM-RT58	58	179	1800 (s)	0.2	900 (s)
			2400 (l)		760 (l)
			3060 (s)		1392 (s)
PCM-55	56.5	241.6	3310 (l)	0.65	1279 (l)

Source (Agyenim, 2010 and 2012)

Firstly, Figure 6.16 is clearly showing that heating gain of PCM RT58 tank is less than that of water tank, although PCM RT58 absorbs and stores more latent heating after its melting point, which has the same result as experimental testing. It is evident that the heating storage capacity of the proposed PCM-55 tank is better than those of both PCM RT58 and water. Before its melting point (56.5°C), PCM-55 tank has the same or tiny less value as water tank. After its melting point and absorbed huge latent solar heating energy from sun, heating gain of PCM-55 tank jumps up and is dramatically better than those of water and PCM RT58 tank.

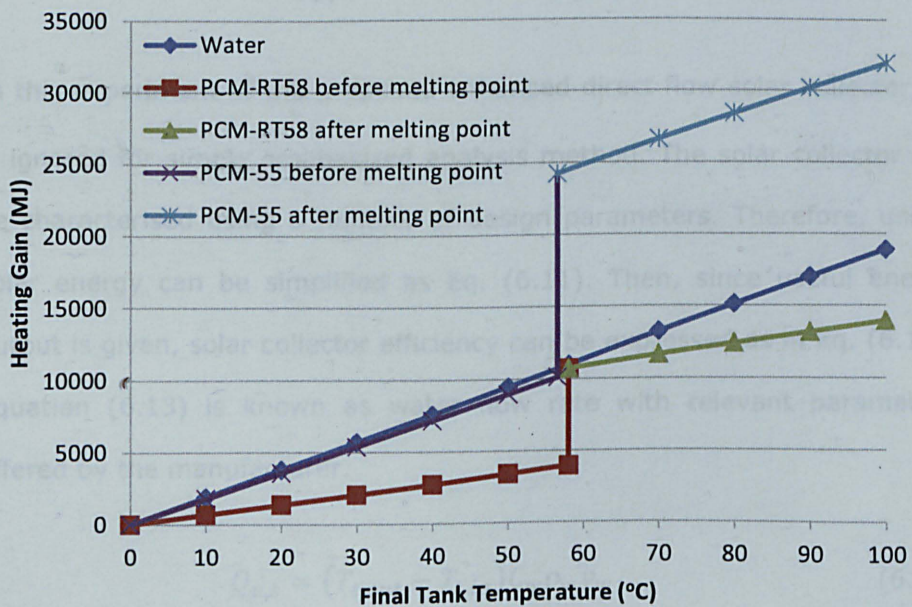


Figure 6.16 Heating gain comparison of water, PCM-RT58 and PCM-55 on different final tank temperatures

6.5 Analysis on Efficiency of Solar Collector Heating System

As known, DF100 is a direct flow solar collector with up to 83.2% efficiency. For DF100 solar collector, the overall energy balance per unit collector at a steady state conditions can be expressed as:

$$Q_u = Q_i - Q_l \quad (6.9)$$

Where, Q_u represents useful energy, Q_i is input energy and Q_l is heat loss. The average solar collector efficiency (η) of the system over a period of time is the ratio of useful energy delivered by the collector during a specified time period to the incident solar radiation on the collector during the same time period (Struckmann 2008 and omer 2009), which can be written as:

$$\eta_s = \frac{\int Q_{u,s} \cdot dt}{A_s \int G \cdot dt} \quad (6.10)$$

In this experiment of the proposed enhanced direct flow solar collector, Q_l is ignored for simple emphasized analysis method. The solar collector can be characterised using a number of design parameters. Therefore, useful solar energy can be simplified as Eq. (6.11). Then, since useful energy output is given, solar collector efficiency can be expressed as in Eq. (6.12). Equation (6.13) is known as water flow rate with relevant parameters offered by the manufacturer.

$$Q_{u,s} = (T_{t,out} - T_{t,in}) C_w \rho_w v_w \quad (6.11)$$

$$\eta_s = \frac{(T_{t,out} - T_{t,in}) C_w \rho_w v_w}{A_s G} \quad (6.12)$$

$$v_w = \frac{3C_{count}}{3600K_{pump}} \quad (6.13)$$

Useful energy output of a fan coil heater can be simplified as Eq. (6.14). Fan coil heater efficiency can therefore be written as Eq. (6.15). Equation (6.16) is known as air flow rate of heating pipes.

$$Q_{u,f} = (T_{f,out} - T_{air})C_a\rho_a v_a \quad (6.14)$$

$$\eta_f = \frac{(T_{f,out} - T_{air})C_a\rho_a v_a}{A_s G} \quad (6.15)$$

$$v_a = v_{count} A_f \quad (6.16)$$

6.5.1 Efficiency Change of Solar Collector System in a Sunny Day

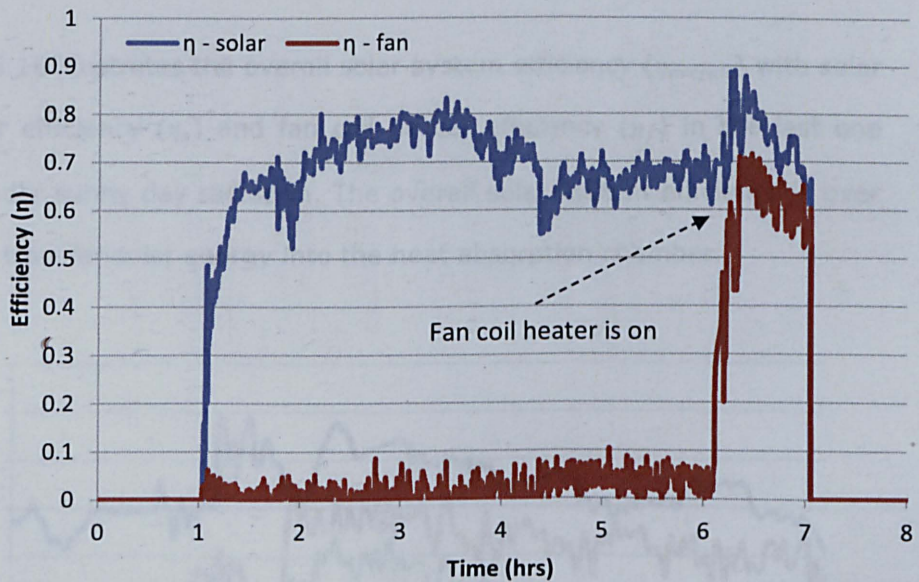


Figure 6.17 Solar collector efficiency (η_s) and fan coil heater efficiency (η_f) in a sunny day

Figure 6.17 illustrates solar collector efficiency (η_s) and fan coil heater efficiency (η_f) in outdoor sunny day testing. When solar heating systems is delivered out for testing, solar collector efficiency starts increasing and obtains a value of around 70% in first half an hour. Then, it starts

fluctuating between 60% and 80% in the following 5 hours. The efficiency of fan heater suddenly and rapidly rises when the fan coil heater and relevant instruments start working. It peaks at 71% and then slowly decreases to about 55% in one hour. At the same time, solar collector efficiency goes up slightly to 88% in term of a bigger heat exchange than before (heat loss increasing for solar internal cycle).

Finally, the overall efficiency ($\eta_{overall}$) of the whole solar collector system is given as:

$$\eta_{overall} = \eta_s \eta_f \tag{6.17}$$

Figure 6.18 illustrates the overall solar system efficiency ($\eta_{overall}$) with solar collector efficiency (η_s) and fan coil heater efficiency (η_f) in the last one hour under sunny day radiation. The overall solar system efficiency is over 50% to transfer solar energy into the heat absorption chamber.

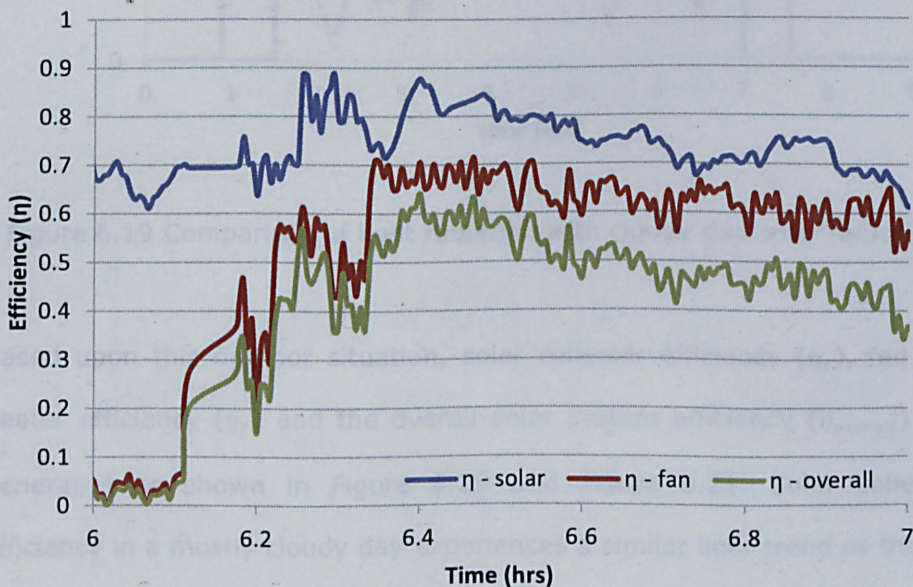


Figure 6.18 Solar collector efficiency (η_s), fan coil heater efficiency (η_f) and overall solar system efficiency ($\eta_{overall}$) in a sunny day

6.5.2 Efficiency Change of Solar Collector System in a Mostly Cloudy Weather

On the other hand, this solar collector system is also tested under mostly cloudy day radiation. A comparison of light radiation with cloudy day solar radiation is given in Figure 6.19, which shows cloudy day solar radiation dramatically fluctuated and changed between 60W/s to 950W/s and average value of radiation was below 400W/s.

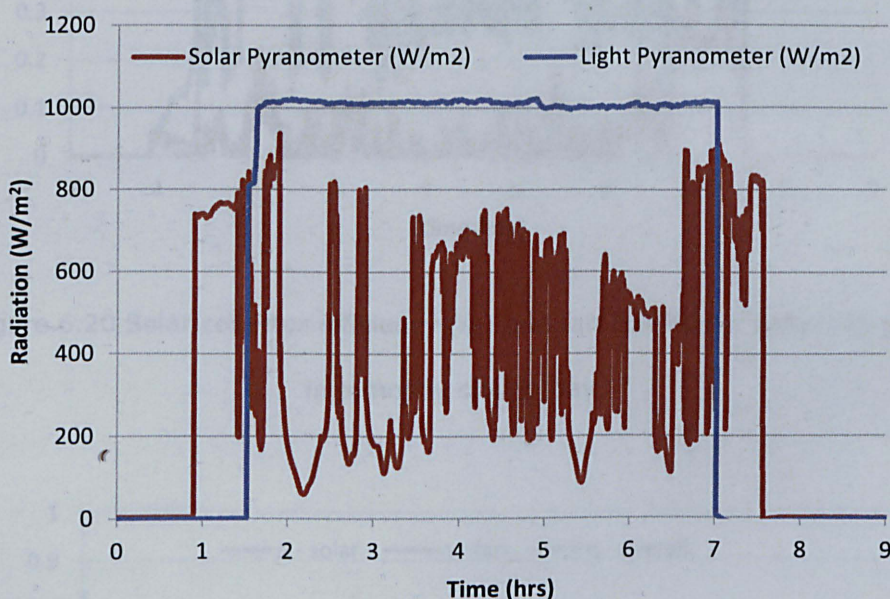


Figure 6.19 Comparison of light radiation with cloudy day solar radiation

Based upon this outdoor situation, solar collector efficiency (η_s), fan coil heater efficiency (η_f) and the overall solar system efficiency ($\eta_{overall}$) are generated as shown in Figure 6.20 and Figure 6.21. Solar collector efficiency in a mostly cloudy day experiences a similar liner trend as that of outdoor solar radiation and its average value is about 40%. When fan coil heater is on for one hour heating, fan coil heater efficiency is around 25%. As a consequence, the overall solar system efficiency is about only 10%

under mostly cloudy weather, which is significantly lower than in a sunny day.

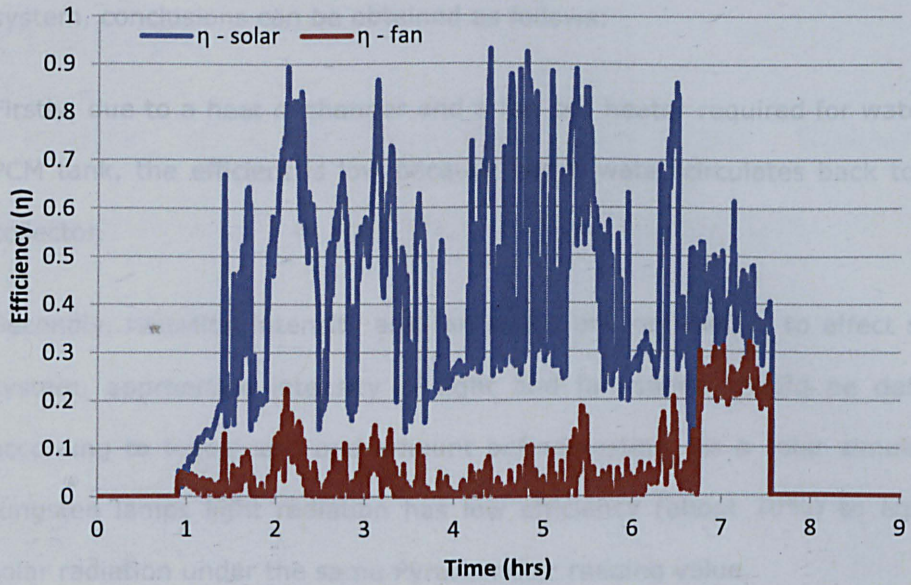


Figure 6.20 Solar collector efficiency (η_s) and fan coil heater efficiency (η_f) in a mostly cloudy day

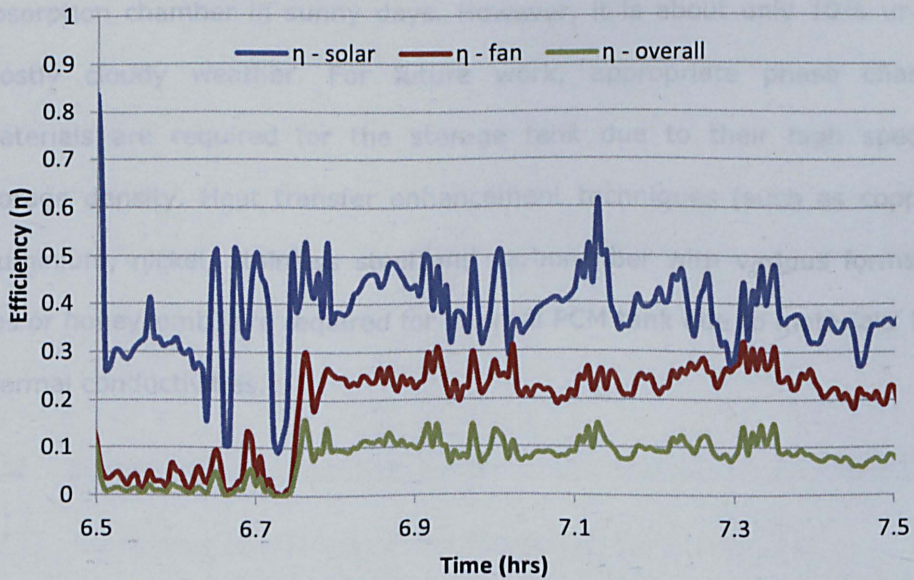


Figure 6.21 Solar collector efficiency (η_s), fan coil heater efficiency (η_f) and overall solar system efficiency ($\eta_{overall}$) in a mostly cloudy day

6.6 Summary of Results and Conclusion

Based upon above results and discussions on the proposed solar collector system, conclusions can be obtained as follows:

Firstly, due to a heat exchanger and a fan coil heater required for water or PCM tank, the efficiency is low because warm water circulates back to the collector.

Secondly, radiation intensity and fan speed are key factors to affect solar system, appropriate intensity of light and fan speed should be defined according to tubes' size and amount before testing. As a solar simulator, tungsten lamps light radiation has low efficiency (about 70%) to equate solar radiation under the same Pyranometer reading value.

Finally, the system can supply over 50°C heating energy and PCM tank can supply a higher output temperature than water tank. The overall solar system efficiency is over 50% to transfer solar energy into the heat absorption chamber in sunny days. However, it is about only 10% under mostly cloudy weather. For future work, appropriate phase change materials are required for the storage tank due to their high specific storage density. Heat transfer enhancement techniques (such as copper, aluminium, nickel, stainless steel and carbon fiber with various forms of fins or honeycomb) are required for internal PCM tank due to materials' low thermal conductivities.

CHAPTER 7

Results and Discussions on the Seasonal Thermochemical Energy Storage System

7.1 Introduction

Generally, a thermochemical energy storage cycle includes three main processes as charging, storing and discharging process. Based on experiment test rig on thermochemical energy storage (Figure 5.6, Figure 5.7 and Figure 5.8), the thermochemical absorption system has been investigated and divided into a hydration heating generation and a dehydration process in this chapter. Comparison results between simulation and experimentation is also illustrated in this stage.

7.2 Experiment Results on Thermochemical Absorption Systems for Hydration Heat Generation

7.2.1 Evaluation of Proposed Thermochemical Materials

7.2.1.1 Silica Gel (SiO_2 , white)

Silica gel is a granular, vitreous, porous form of silicon dioxide made synthetically from sodium silicate. Its molecular formula is SiO_2 . It is a naturally occurring mineral that is purified and processed into either granular or beaded form with colours (white, yellow and blue). As a desiccant or absorbent, it has an average pore size of 2.4 nanometres and has a strong affinity for water molecules. Equation 7.1 shows simple silica gel and water's reversible physico-chemical reaction. Figure 7.1 shows white type silica gel and its weight tray.

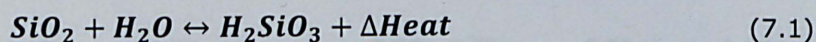


Figure 7.1 Weight of silica gel (SiO_2 , white granular) tray

At the first stage of hydration process, several silica gel trays are directly put into chamber after mass weight. Water vapour steam is generated and powered up into chamber by ultrasonic cool mist humidifier and blower fan, respectively. The speed of blower fan is set the same value as that of fan coil heater, 3.0 m/s. Table 7.1 shows weight lists of silica gel and water during this testing process, based on water absorption ratio of silica gel can be calculated as shown in Figure 7.2.

Table 7.1 Weight of silica gel and water during hydration process

Silica Gel (unit: g)	M ₁ : tray +Material	M ₂ : tray + material +water	M ₃ : tray	M ₄ : material	M ₅ : material + water	M ₆ : water
1 T-01	0.65	0.76	0.33	0.32	0.43	0.11
T-02	0.64	0.74	0.34	0.30	0.40	0.10
2 T-03	0.93	1.16	0.31	0.62	0.85	0.23
3 T-01	1.23	1.38	0.33	0.90	1.05	0.15
T-02	1.12	1.29	0.34	0.78	0.95	0.17

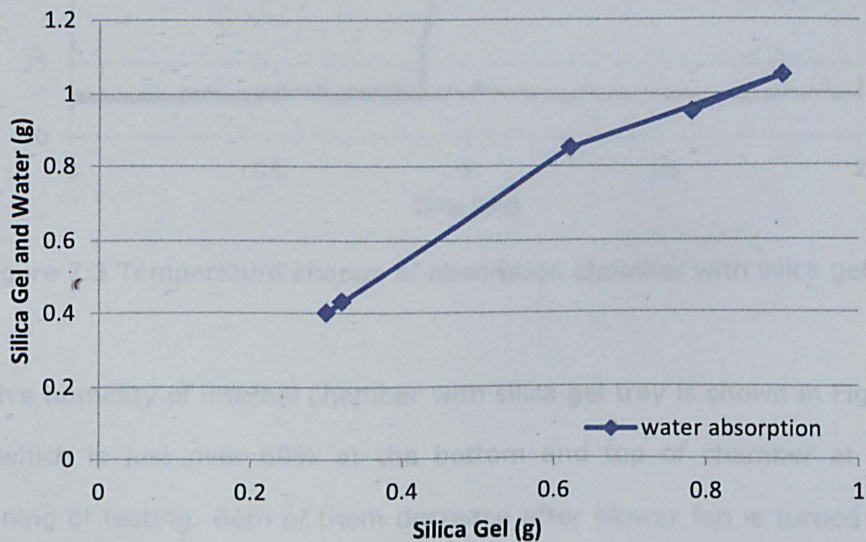


Figure 7.2 Water absorption of silica gel (SiO₂)

Figure 7.3 shows outlet temperature change of the absorption chamber with silica gel tray. At the beginning of testing, internal chamber and ambient temperatures maintain the similar value about 23°C. Internal chamber temperature suddenly jumps up to 30°C from 23°C when the blower fan is powered up and ultrasonic humidifier is closed. The main reason for this is that ambient air holds a certain amount of water vapour,

and hydration heat is released and temperature rises up when hydration of silica gel and water occurs. Approximate ten minutes, the temperature of chamber outlet dramatically jumps up again and reaches its peak point approximately 48°C in five minutes when ultrasonic humidifier is powered up. Chamber outlet temperature starts slowly decreasing after peak point.

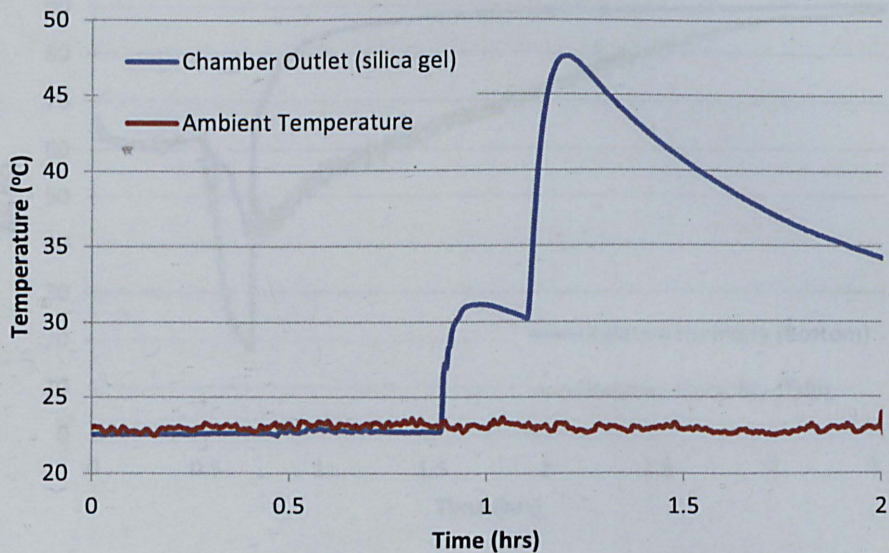


Figure 7.3 Temperature change of absorption chamber with silica gel

Relative humidity of internal chamber with silica gel tray is shown in Figure 7.4, which is just over 60% at the bottom and top of chamber at the beginning of testing. Both of them decrease after blower fan is turned on, and relative humidity of the chamber top is even down to about 19%. Ten minutes later, relative humidity of the chamber bottom jumps up to 80% and relative humidity of the chamber top starts slowly increasing when ultrasonic humidifier is on. Difference relative humidity at bottom and top of the chamber is about 30%, which maintains during hydration process nearly 2 hours. Humidity of the top of chamber reaches the same value as the bottom one (around 90%) after the steam generator is turned on and works for 3 hours.

A comparison of temperature change and relative humidity change of silica gel chamber are plotted in Figure 7.5. Temperature and humidity experience an opposite change, when temperature is rapidly increasing; humidity is steeply decreasing before it saturates.

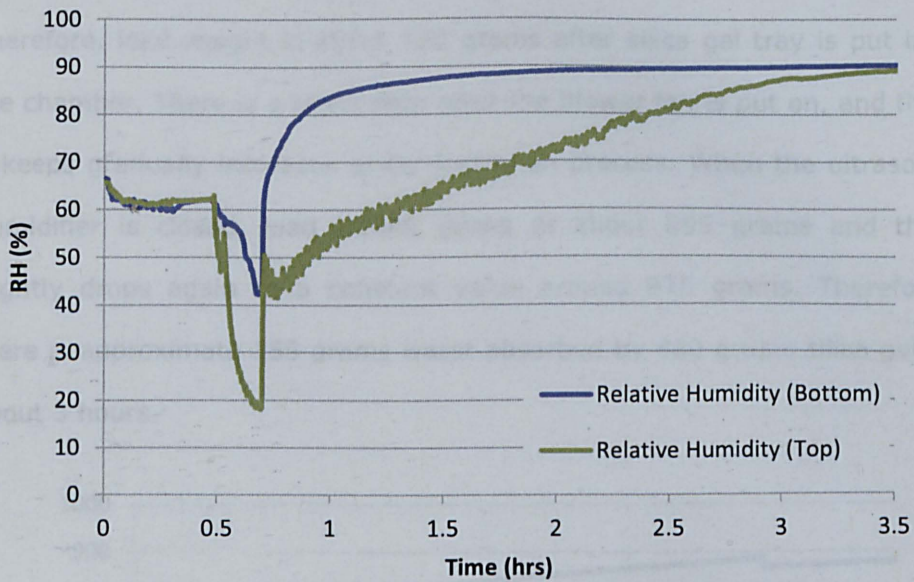


Figure 7.4 Relative humidity change of internal chamber with silica gel

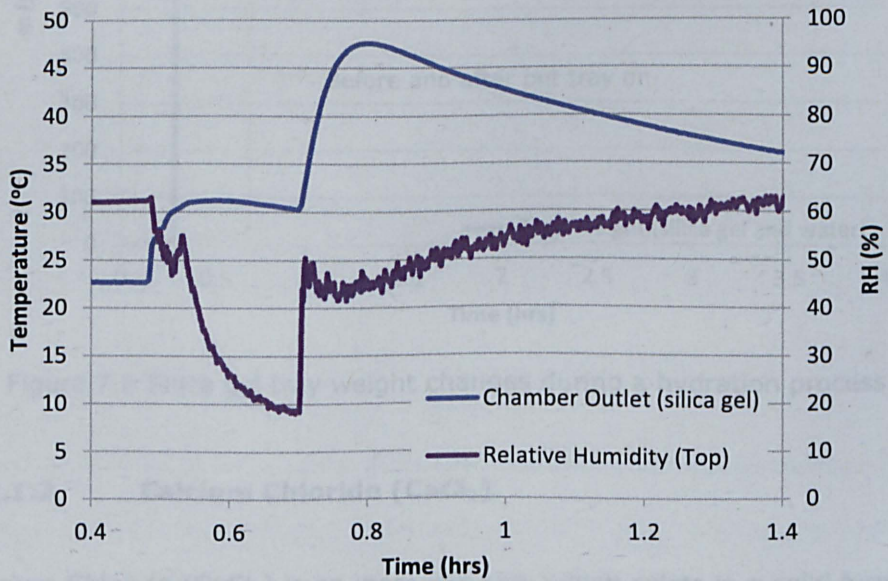


Figure 7.5 Comparison of temperature and relative humidity change of silica gel chamber

Weight change is a key factor to investigate thermochemical material's absorption capacity. Weight sensors are employed to measure relative mass changes. Figure 7.6 is a sample of silica gel tray weight change during a hydration process. Weight value is already calibrated to its actual value. In this case, tray weight is 320 grams and silica gel is 400 grams. Therefore, load weight is about 720 grams after silica gel tray is put into the chamber. There is a slight drop after the blower fan is put on, and then it keeps gradually increases under hydration process. When the ultrasonic humidifier is closed, load weight peaks at about 895 grams and then slightly drops again to a constant value around 875 grams. Therefore, there is approximate 155 grams water absorbed by 400 grams silica gel in about 3 hours.

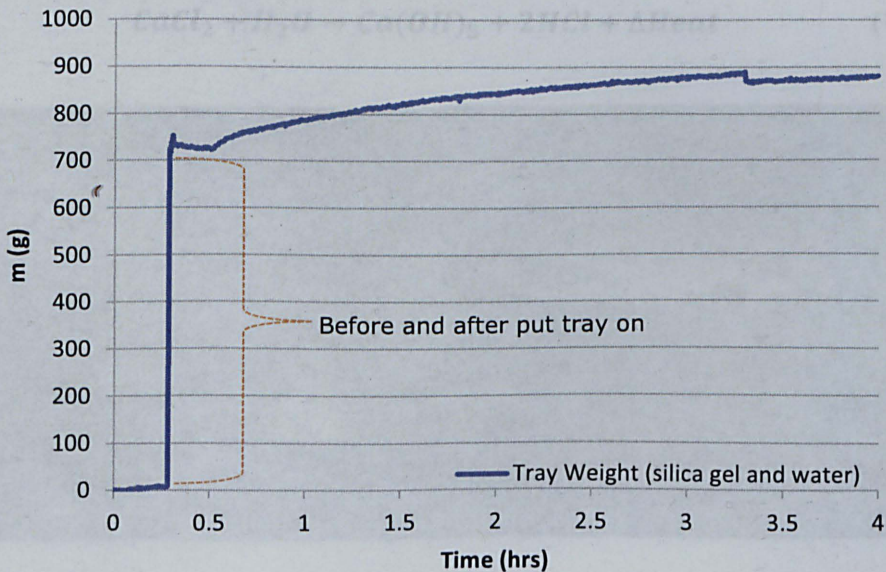


Figure 7.6 Silica gel tray weight changes during a hydration process

7.2.1.2 Calcium Chloride (CaCl_2)

Calcium Chloride (CaCl_2) is an inorganic salt, which exists in a solid form or as a liquid solution. Solid calcium chloride is a white, crystalline substance in the form of flake, granule or powder. Depending on the crystallized

water contents, it can be dehydrated or anhydrous. Liquid calcium chloride is a colourless liquid. Due to its exothermic properties, ability to attract moisture from the air and surroundings and dissolve at a very low temperature, calcium chloride is widely used in snow and ice melting, dust control, oil and gas drilling, moisture-absorbing, accelerator for concretes, etc. Equation 7.2 shows chemical reaction on hydrolysis of calcium chloride with water. Figure 7.7 shows calcium chloride tray and set-up in the chamber. It can be seen that mass tray has changed into some kind of mixture with liquid and solid after calcium chloride absorbs some water. As mentioned in Chapter 5, absorbent tray has a 1.2mm meshed bottom. Therefore, calcium chloride is not suitable as an ideal absorbent in this experimental rig.

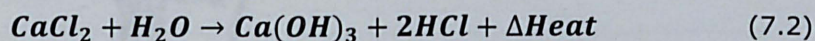


Figure 7.7 Weight of calcium chloride (CaCl_2) tray

Figure 7.8 illustrates relative humidity change of internal chamber with calcium chloride tray. When blower fan, top and bottom valves are opened, both of top outlet and bottom inlet humidity rapidly decrease. Top outlet humidity reaches its bottom at about 28% from 61% under calcium

chloride's absorbing function. Top and bottom humidity both have a slight rise and remain constant for 10 minutes at approximate 40% and 55%, respectively, after ultrasonic humidifier is on. Then, bottom inlet humidity sharply jumps up over 85% and top outlet dramatically increases to catch up the bottom one. Difference of bottom and top relative humidity is not bigger than that of silica gel. Within 1 hour, top humidity reaches the same value as bottom one around 90%.

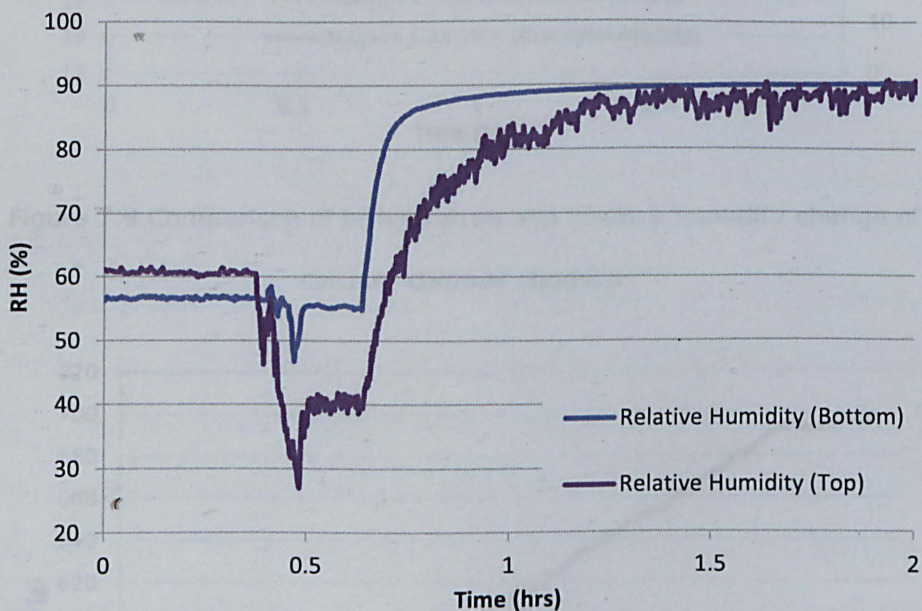


Figure 7.8 Relative humidity change of chamber with calcium chloride

A comparison of internal temperature change and relative humidity change of calcium chloride chamber is plotted in Figure 7.9. At the beginning of testing, chamber's internal temperature suddenly jumps up to 30°C from 21°C, and then gradually increases and reaches its peak at 35°C. Internal temperatures and humidity of absorption chamber experience a nearly opposite change during the hydration process. After that, humidity starts sharply increasing under constant water vapour supplying by the ultrasonic humidifier.

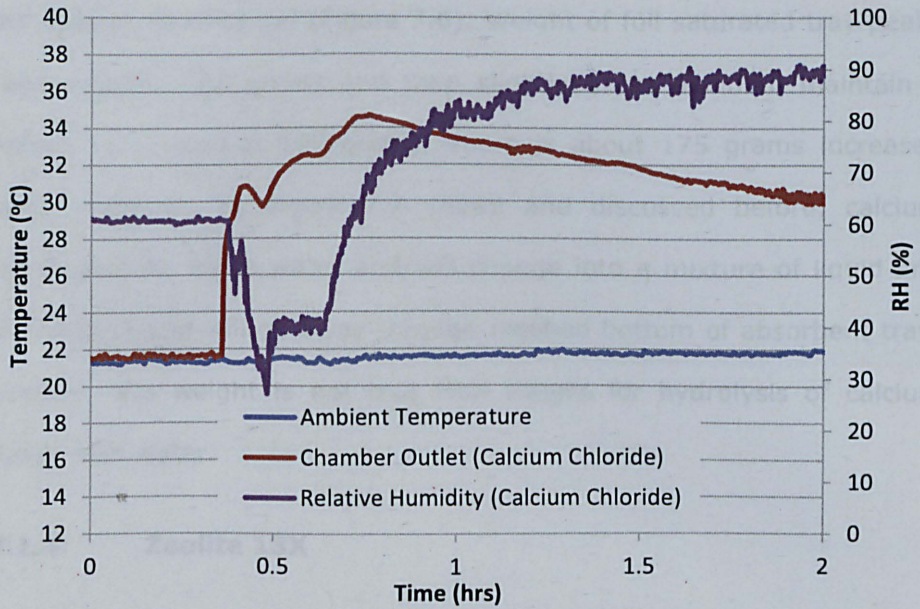


Figure 7.9 Comparison of temperature and relative humidity change of calcium chloride chamber

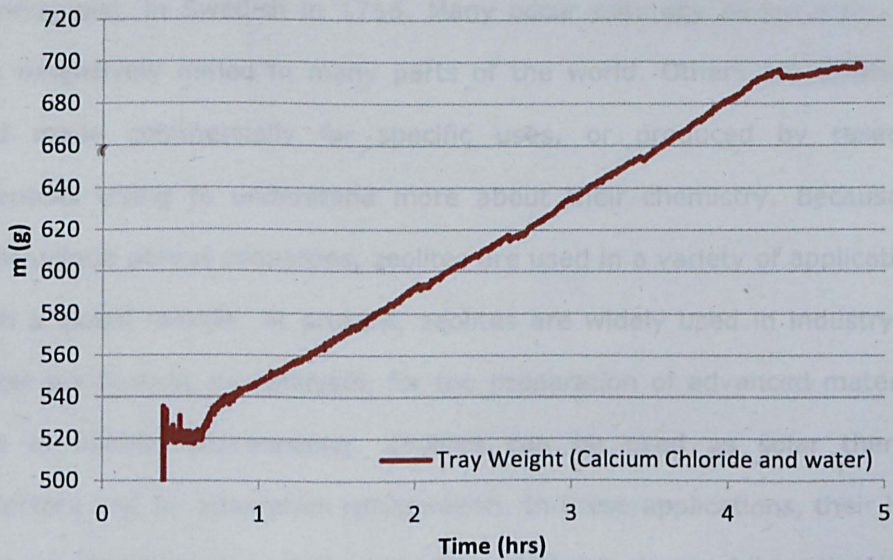


Figure 7.10 Calcium chloride tray weight change during hydration process

Figure 7.10 shows calcium chloride tray weight change accompanying with water vapour absorbed. As can be seen, the empty sample tray weight is 320 grams and calcium chloride is 200 grams. It is 520 grams when the full tray is set up into the chamber. It experiences an almost similar linear

trend change as silica gel (Figure 7.6). Weight of full saturated tray peaks at approximate 700 grams and then slightly drops again to maintain a constant value around 695 grams. There is about 175 grams increased weight. However, as Figure 7.7 shows and discussed before, calcium chloride absorbs some water and will change into a mixture of liquid and solid. Some liquid will go away through meshed bottom of absorbent tray. Therefore, this weight is not true final weight for hydrolysis of calcium chloride with water.

7.2.1.3 Zeolite 13X

Zeolites are microporous crystalline solids with well-defined structures. Generally they contain silicon, aluminium and oxygen in their framework. The term zeolite was originally coined by Axel Fredrik Cronstedt, a mineralogist, in Swedish in 1756. Many occur naturally as minerals, and are extensively mined in many parts of the world. Others are synthetic, and made commercially for specific uses, or produced by research scientists trying to understand more about their chemistry. Because of their unique porous properties, zeolites are used in a variety of applications with a global market. At present, zeolites are widely used in industry for water purification, as catalysts, for the preparation of advanced materials and in nuclear reprocessing. Zeolites can be used as solar thermal collectors and for adsorption refrigeration. In these applications, their high heat of adsorption and ability to hydrate and dehydrate while maintaining structural stability is exploited. Zeolite 13x is now readily available as commercial molecular sieves. Chemical formula of zeolites 13x can be expressed as $\text{Na}_2\text{O} \cdot \text{Al}_2\text{O}_3 \cdot (2.8 \pm 0.2)\text{SiO}_2 \cdot (6\sim7)\text{H}_2\text{O}$, and its linear formula is $\text{Na}_{86}[\text{AlO}_2]_{86}(\text{SiO}_2)_{106}] \cdot x\text{H}_2\text{O}$. Figure 7.11 shows white granular sample zeolite 13x and its full tray weight.



Figure 7.11 Weight of full zeolite 13x (white granular) tray

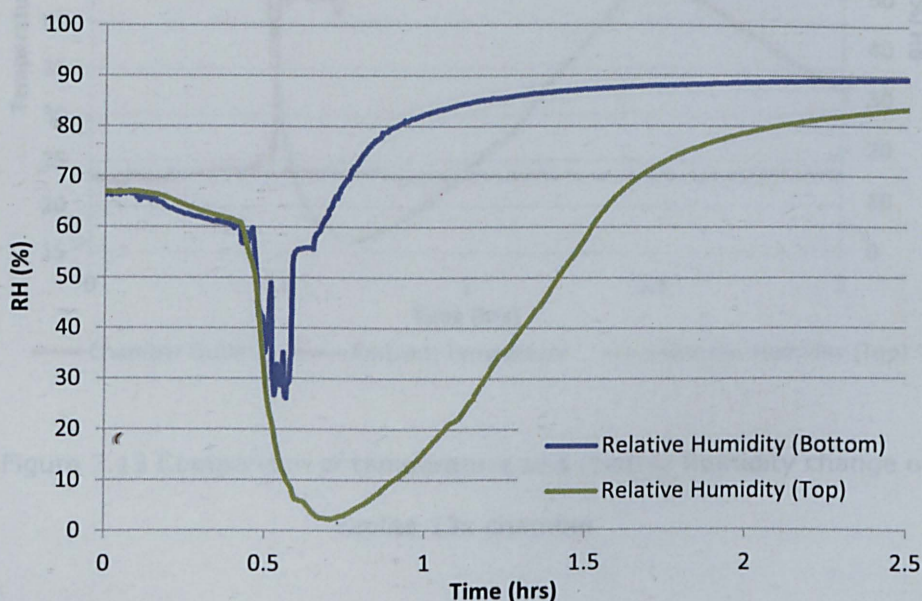


Figure 7.12 Relative humidity change of internal chamber with zeolite 13x

Internal relative humidity change of chamber with zeolite 13x is charted in Figure 7.12. Both of top outlet and bottom inlet humidity steeply decrease after top and bottom valves and blower fan are opened. Top outlet humidity reaches to almost 0% from 67% within about ten minutes in term of a really huge ability of zeolite 13x to absorb moisture than silica gel and calcium chloride. Bottom inlet humidity has a significant rise to over 80% from 30% after cool humidifier is on. At the same time, top outlet humidity

starts slowly increasing. Difference of bottom and top relative humidity is over 70% significantly larger than those of former absorbents. Internal humidity reaches a constant value around 90% after steam generator starts working for about 3 hours.

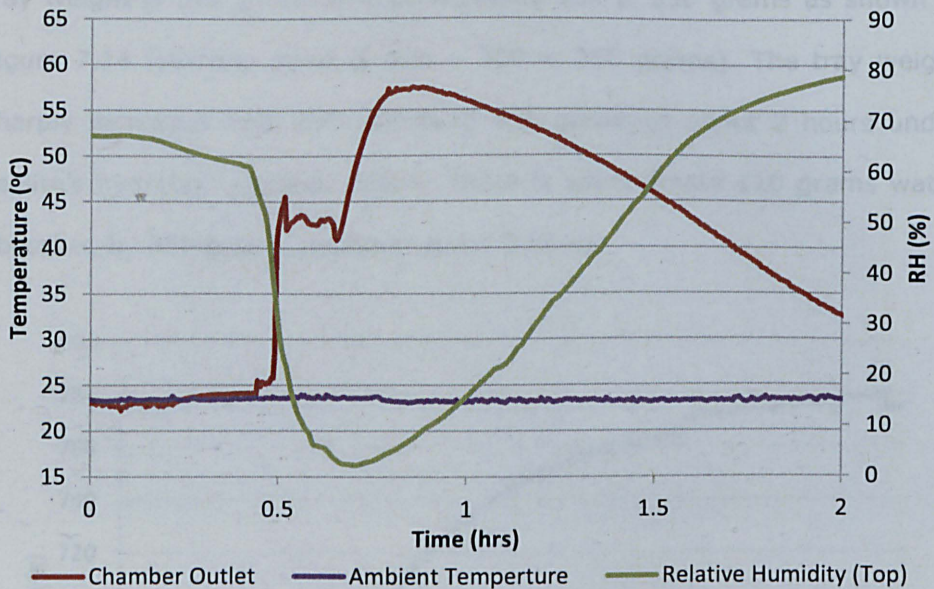


Figure 7.13 Comparison of temperature and relative humidity change of zeolite 13x chamber

In Figure 7.13, internal temperature change and relative humidity change of zeolite 13x chamber is clearly represented. Internal chamber temperature suddenly jumps up to about 45°C from 22°C when inlet and outlet valves, fan are opened. It remains around 45°C for approximate 15 minutes after the steam generator is on. It jumps up again and reaches peak at 58°C, which is also the highest point among all absorbents discussed. At the same time, humidity of absorption chamber experiences an opposite change and bottoms its lowest point during the hydration process. After that, internal humidity starts increasing gradually and

internal temperature starts decreasing slowly, both achieve a constant state within 2 hours.

Tray weight change of zeolite 13x during the hydration testing process can be charted as shown in Figure 7.14. As mentioned before, empty sample tray weight is 320 grams and pure zeolite 13x is 350 grams as shown in Figure 7.14 (starting point of $670 - 320 = 350$ grams). The tray weight sharply increases from 670 grams to 780 grams in about 2 hours under zeolite's hydration process. Finally, there is approximate 110 grams water absorbed by 350 grams zeolite in about 2 hours.

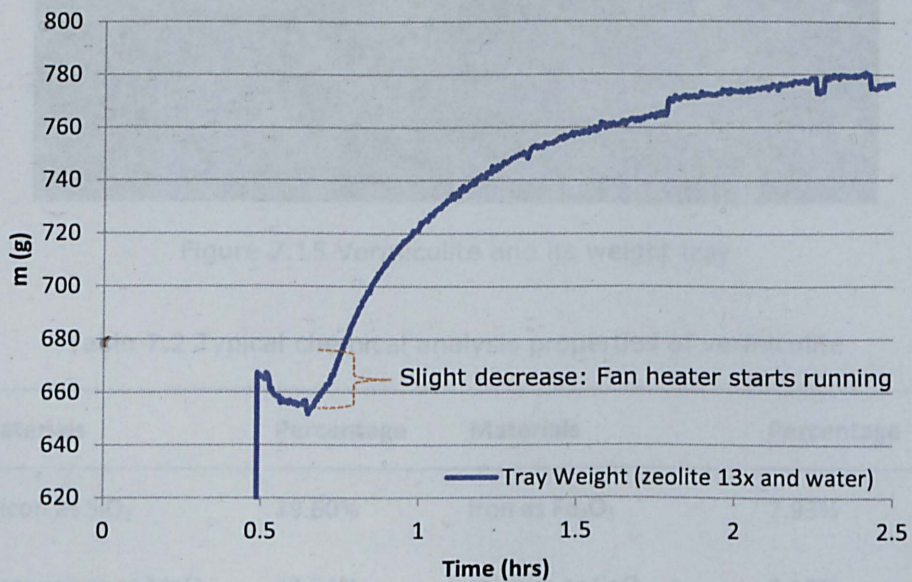


Figure 7.14 Zeolite 13x tray weight change during the hydration process

7.2.1.4 Vermiculite

Vermiculite is a hydrous and silicate mineral. Vermiculite is classified as a phyllosilicate and that expands greatly when heated. Exfoliation occurs when the mineral is heated sufficiently, and the effect is routinely produced in commercial furnaces. Vermiculite is formed by weathering or

hydrothermal alteration of biotite or phlogopite. Large commercial vermiculite mines currently exist in Russia, South Africa, China, and Brazil. In general, product of vermiculite is a grade of exfoliated vermiculite having a controlled particle size distribution. Figure 7.15 shows the proposed and tested vermiculite and its weight tray in this research. Table 7.2 supplies typical chemical analysis properties of vermiculite.



Figure 7.15 Vermiculite and its weight tray

Table 7.2 Typical chemical analysis properties of vermiculite

Materials	Percentage	Materials	Percentage
Silicon as SiO ₂	39.60%	Iron as Fe ₂ O ₃	7.93%
Magnesium as MgO	23.54%	calcium as CaO	2.12%
Aluminium as Al ₂ O ₃	9.22%	Titanium as TiO ₂	1.02%
Potassium as K ₂ O	6.11%	Fluorine as F	0.62%

Sources from the manufacturer: Dupre Minerals Ltd (UK).

Figure 7.16 describes relative humidity change of internal chamber with vermiculite. At this stage, blower fan, top and bottom valves and ultrasonic humidifier are opened at the same time. It can be seen that bottom inlet relative humidity significantly increases and top outlet relative humidity

steeply decreases. Bottom inlet humidity reaches its constant value over 90% from about 55% in less than half an hour. Top outlet reaches its bottom at about 35% and then gradually increases to catch up outlet one in very shorter time compared with zeolite and silica gel.

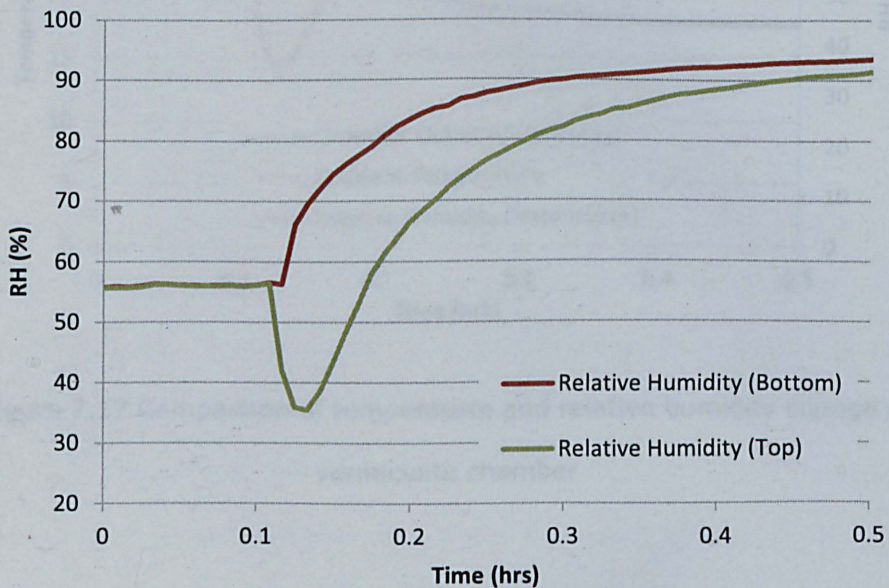


Figure 7.16 Relative humidity change of internal chamber with vermiculite

Comparison on temperature change and relative humidity change of vermiculite chamber is revealed in Figure 7.17. Internal temperature of vermiculite chamber rapidly rises up to 37°C from about 22°C when all devices (fans, valves and humidifier) of testing rig are set on. After that internal temperature suddenly decreases to meet temperature of water vapour generated by cool humidifier (normally around 18°C) in less than half an hour. The fundamental reason for this is that absorption capacity of vermiculite is not very high and mass amount of vermiculite is not enough to meet this chamber size. At the same time, relative humidity of chamber experiences an opposite change as discussed and shown in above Figure 7.16.

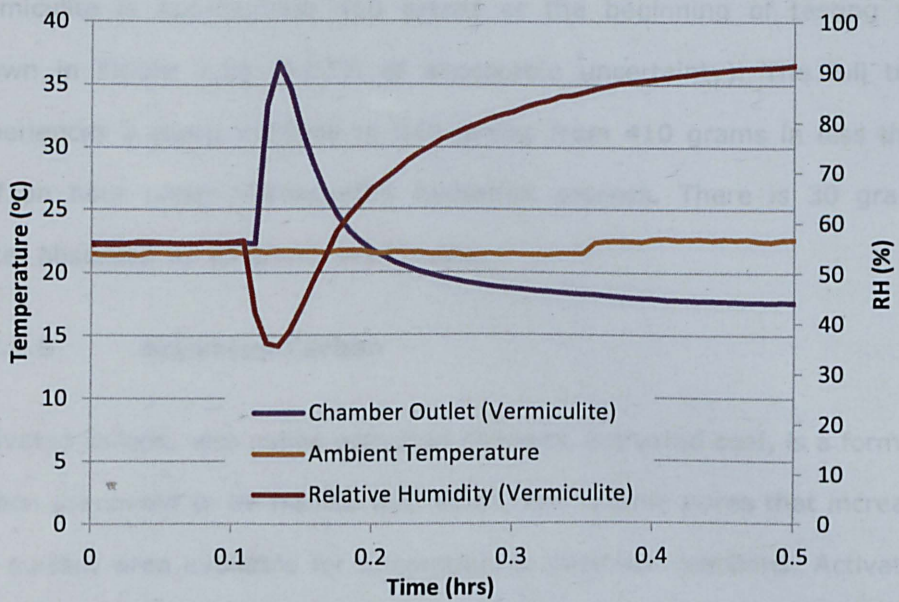


Figure 7.17 Comparison of temperature and relative humidity change of vermiculite chamber

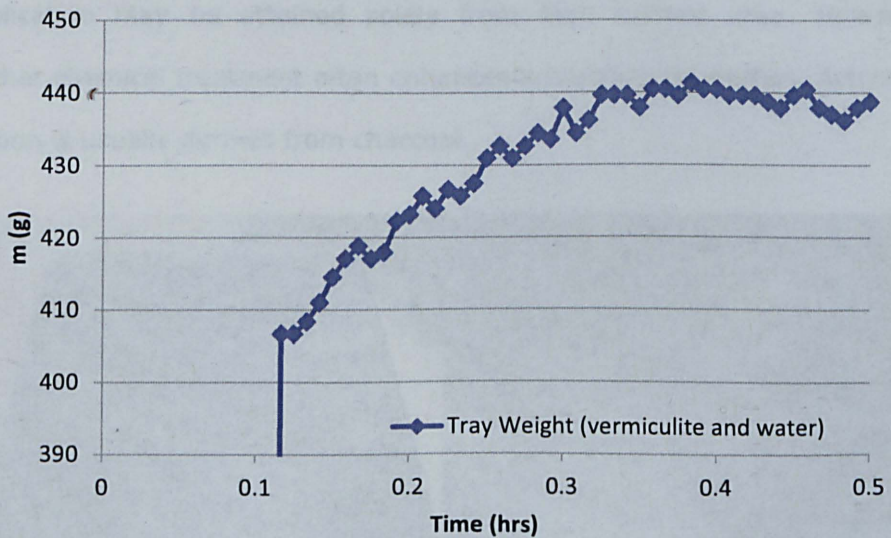


Figure 7.18 Vermiculite tray weight change during the hydration process

Vermiculite tray weight change during the hydration testing process is plotted as shown in Figure 7.18. Empty sample tray weight is 320 grams and pure vermiculite involved is 90 grams. Therefore, the tray weight of

vermiculite is approximate 410 grams at the beginning of testing (as shown in Figure 7.18, 0.03% of acceptable uncertainty). The full tray experiences a sharp increase to 440 grams from 410 grams in less than half an hour under vermiculite's hydration process. There is 30 grams water absorbed by 90 grams vermiculite.

7.2.1.5 Activated Carbon

Activated carbon, also called activated charcoal, activated coal, is a form of carbon processed to be riddled with small, low volume pores that increase the surface area available for adsorption or chemical reactions. Activated carbon is usually derived from charcoal. Due to its high degree of micro porosity, just one gram of activated carbon has a surface area in excess of 500m^2 , as determined by adsorption isotherms of carbon dioxide gas at room or 0.0°C temperature. An activation level sufficient for useful application may be attained solely from high surface area. However, further chemical treatment often enhances adsorption properties. Activated carbon is usually derived from charcoal.



Figure 7.19 Activated carbon and its weight tray

Granular activated carbon has a relatively larger particle size compared to powdered activated carbon and consequently, presents a smaller external

surface. Granulated carbons are used for water treatment, deodorization and separation of components of flow system and also in rapid mix basins. Figure 7.19 illustrates granular sample activated carbon and its full tray weight.

It can be seen from Figure 7.20, internal relative humidity change of activated carbon is clearly charted by bottom inlet and top outlet. It can be seen that both inlet and outlet relative humidity have a sharp drop from 50% and 30% to about 20% after blower fan, top and bottom valves are turned on. Ten minutes later, the cool humidifier also starts working, resulting in that bottom inlet humidity suddenly and steeply jumps up to 55% and then keeps increasing. Top inlet humidity also starts gradually going up. Difference of inlet and outlet humidity is around 10% during this change. It is noted that the duration of hydration process of activated carbon is similar to that of vermiculite in less than half an hour.

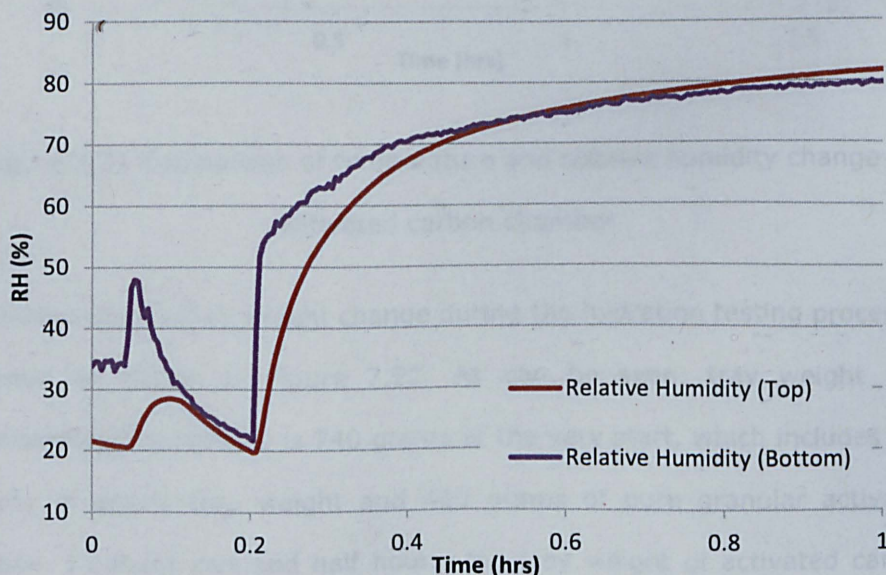


Figure 7.20 Relative humidity change of with activated carbon

Figure 7.21 describes a comparison on temperature change and relative humidity change of activated carbon chamber. In the first place, internal

chamber temperature rapidly increases to 27°C from 22°C when blower fans and valves are open and remains stable before cool humidifier is on. And then, internal temperature jumps up again to its peak point about 32°C and starts slowly reducing to meet cool humidifier's original temperature of 18°C in 2 hours. At the same time, relative humidity has a reversed liner trend change as shown in Figure 7.21.

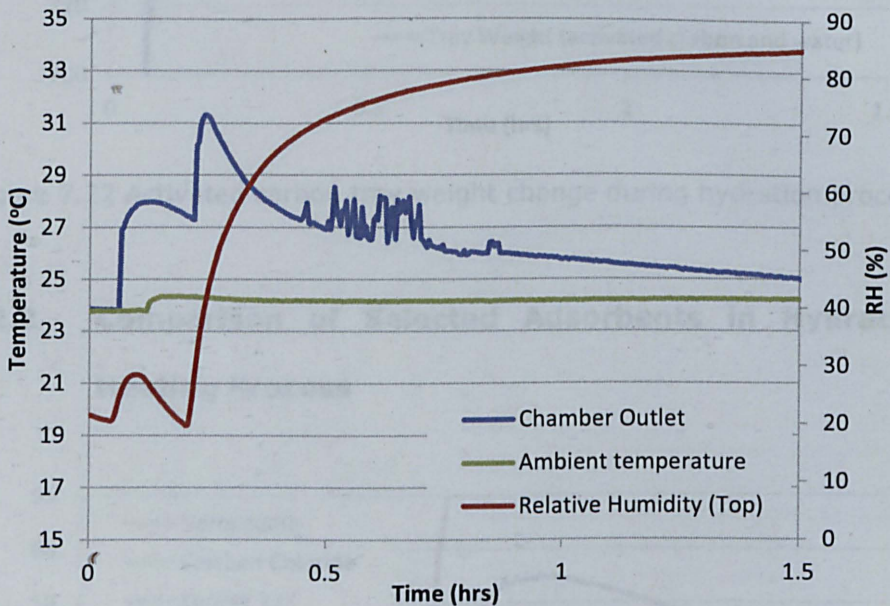


Figure 7.21 Comparison of temperature and relative humidity change of activated carbon chamber

Activated carbon tray weight change during the hydration testing process is charted as shown in Figure 7.22. As can be seen, tray weight with activated carbon initially is 740 grams at the very start, which includes 320 grams of empty tray weight and 420 grams of pure granular activated carbon. In about one and half hours, the tray weight of activated carbon and water rises up to 820 grams from 740 grams during this absorption process. Approximate 80 grams water is absorbed by 420 grams activated carbon.

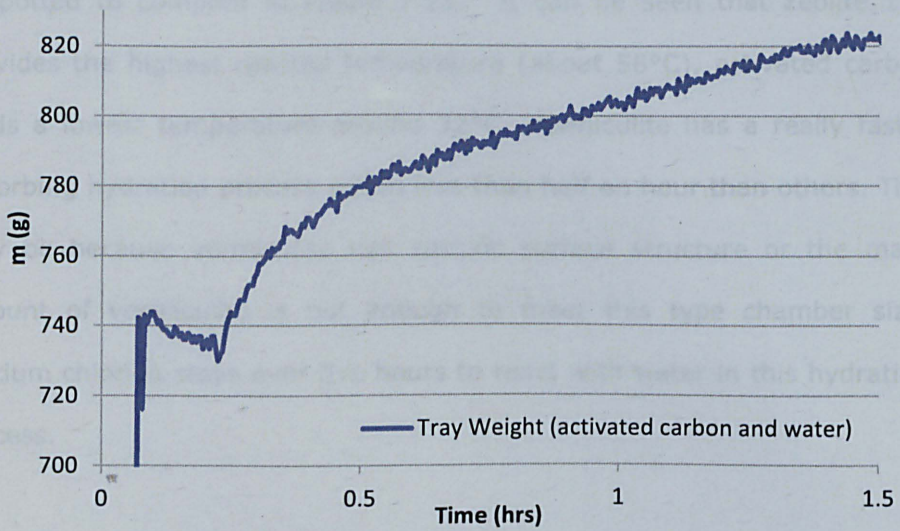


Figure 7.22 Activated carbon tray weight change during hydration process

7.2.2 Comparison of Selected Adsorbents in Hydration Heating Process

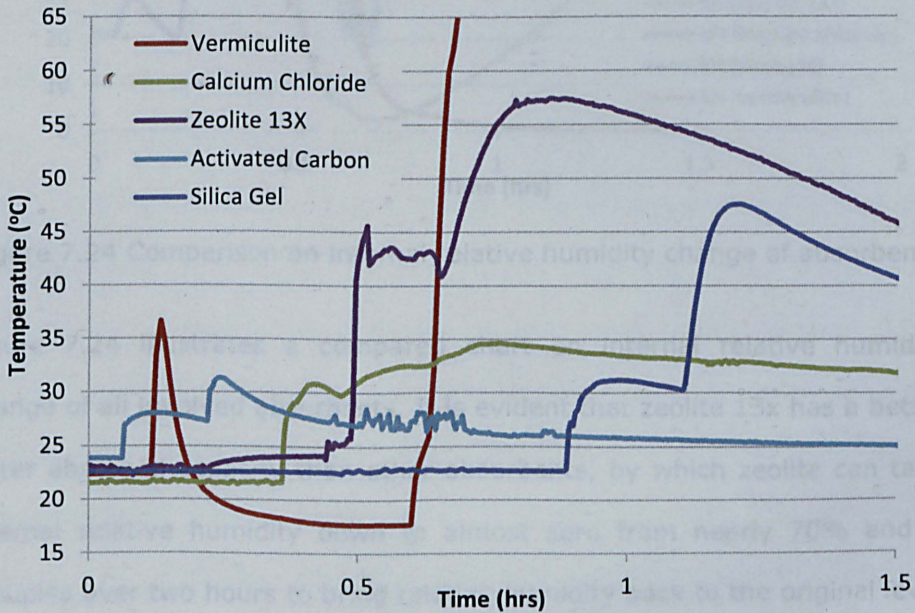


Figure 7.23 Comparison on internal temperature change of absorbents

Based on research above individual absorbents' properties discussed and analysed, internal temperature change of all investigated absorbents can

be potted to compare in Figure 7.23. It can be seen that zeolite 13x provides the highest reacted temperature (about 58°C), activated carbon holds a lowest temperature around 32°C. Vermiculite has a really faster absorbing hydration process within less than half an hour than others. This may be because vermiculite has specific surface structure or the mass amount of vermiculite is not enough to meet this type chamber size. Calcium chloride stays over five hours to react with water in this hydration process.

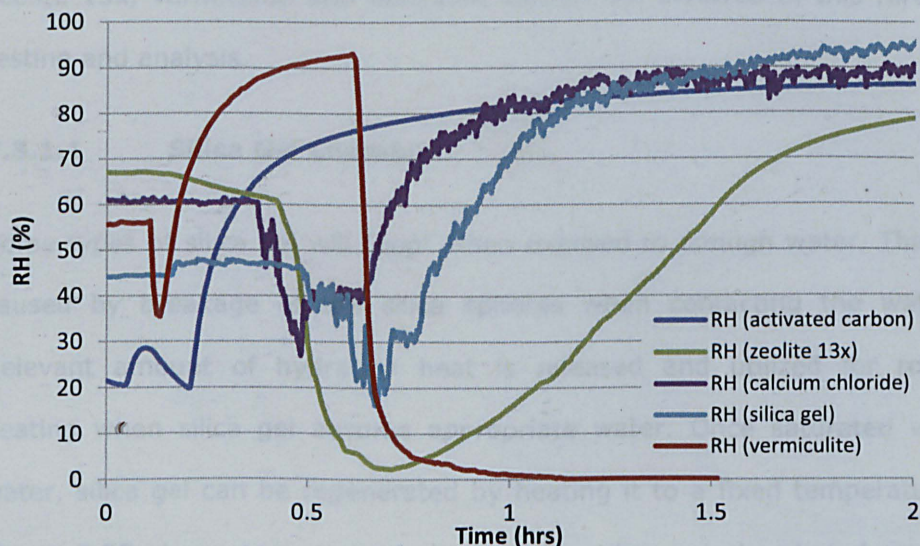


Figure 7.24 Comparison on internal relative humidity change of absorbents

Figure 7.24 illustrates a compared chart on internal relative humidity change of all involved absorbents. It is evident that zeolite 13x has a better water absorbed capacity than other absorbents, by which zeolite can take internal relative humidity down to almost zero from nearly 70% and it occupies over two hours to bring relative humidity back to the original level. Compared with others, activated carbon holds the lowest ability to absorb water vapour and vermiculite has the shortest reaction time with water. Silica gel and calcium chloride give similar linear trend change during this whole hydration process.

7.3 Experiment Results on Dehydration Process of Thermochemical Energy Storage System Regeneration

7.3.1 Investigation on Thermochemical Energy Storage System with Different Absorbents

Investigation in this chapter is focusing on materials dehydration process for thermochemical energy storage system regeneration, where silica gel, zeolite 13x, vermiculite and activated carbon are involved in this further testing and analysis.

7.3.1.1 Silica Gel Chamber

Some types of silica gel will "pop" when exposed to enough water. This is caused by breakage of the silica spheres when contacting the water. Relevant amount of hydration heat is released and utilized for room heating when silica gel absorbs appropriate water. Once saturated with water, silica gel can be regenerated by heating it to a fixed temperature. Figure 7.25 shows temperature change of a silica gel chamber during a hydration and dehydration process. At the beginning, room temperature and internal temperature maintain at the same values around 23°C. Internal inlet temperature drops down to about 18°C and internal outlet temperature jumps up to 35°C after cool humidifier's open. Approximate five hours later, internal outlet and inlet temperature hold the same value around 18°C. Hydration process finishes, and mass, relative humidity and temperature reach a steady state. Furthermore, the humidity generator is turned off and isolated, and Fan heater is switched on and set at 100°C. Inlet temperature suddenly jumps up to over 75°C and outlet temperature also rapidly increase to catch up the inlet one. When inlet and outlet

temperature have almost same values and again reach a steady state, heater is switched off and isolated. This whole cycle of hydration and dehydration takes approximate half day time. On the second cycle, in order to make a comparison on dehydration temperatures, fan heater's target temperature is reduced to 80°C. It can be seen, after that, temperatures experience a similar linear trend as shown in Figure 7.25. Specifically, there are three type turnover points, point-one means humidifier is turn on, point-two means fan heater is turn on and humidifier is turn off, point-three means fan heater is turn off.

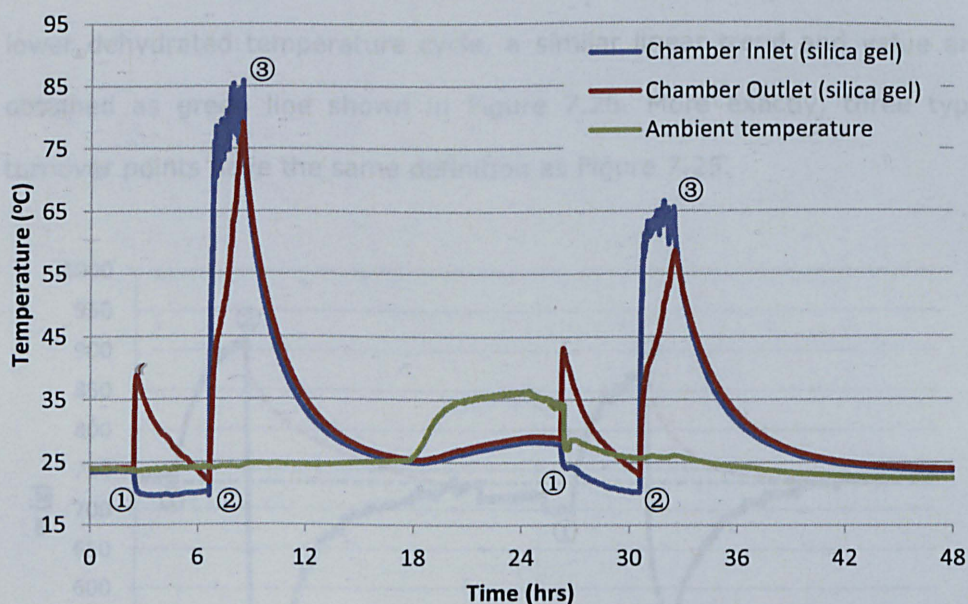


Figure 7.25 Temperature change of silica gel chamber during a hydration and dehydration process

Figure 7.26 illustrates weight change of the silica gel tray during a hydration and dehydration process, in which weight is measured by load cells S220. Due to switching on the humidifier, tray weight starts significantly rising up when inlet relative humidity is increasing. Tray weight reaches its peak point (about 900 grams from 740 grams) when

inlet and outlet temperature hold a steady state. In the dehydration process, tray weight dramatically and sharply drops and bottoms out 460 grams, which seems something is wrong, but actually not. The main reason for this load cell change phenomenon is that, physical metal property of load cell changes with temperature and high temperature has an important effect on load cell's ability to re-zero and output. Red dash lines are showing actual tray weight change because water absorbed by silica gel is heated and blew out via the fan heater. In the first cycle, when the internal temperature recovers to the room temperature, tray weight stays in its steady state, which is the same value as original one. During the second lower dehydrated temperature cycle, a similar linear trend and value are obtained as green line shown in Figure 7.26. More exactly, three type turnover points have the same definition as Figure 7.25.

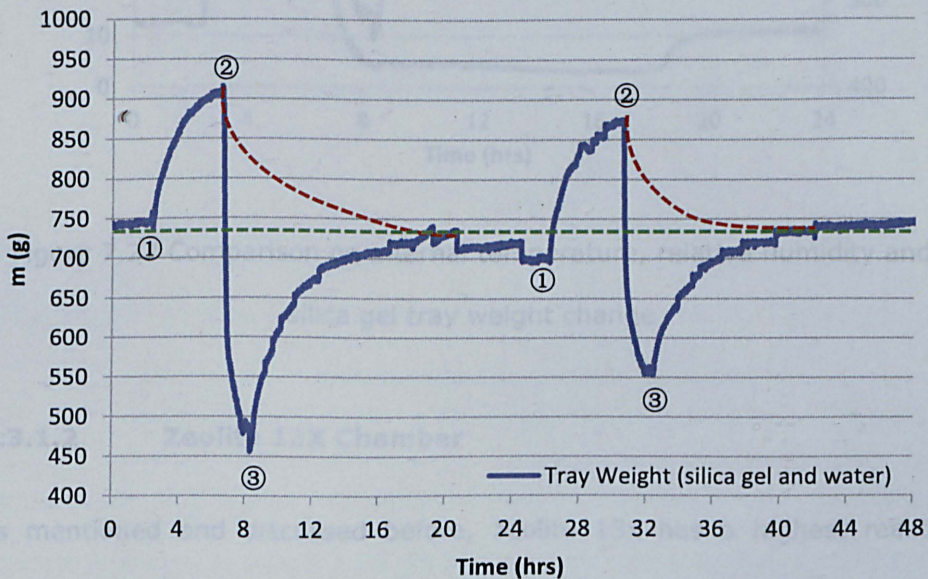


Figure 7.26 Weight change of silica gel chamber during a hydration and dehydration process

A comparison among internal temperature change, relative humidity change and silica gel tray weight change is potted in Figure 7.27. Internal

space of silica gel chamber is dry with approximate 12% RH before testing. When the humidifier is switched on, tray weight, internal relative humidity and outlet temperature start increasing. When the fan heater is on, both tray weight and relative humidity decrease dramatically. After that, internal space maintains at a dry state again, in which the relative humidity stays at a flat value around 12% RH.

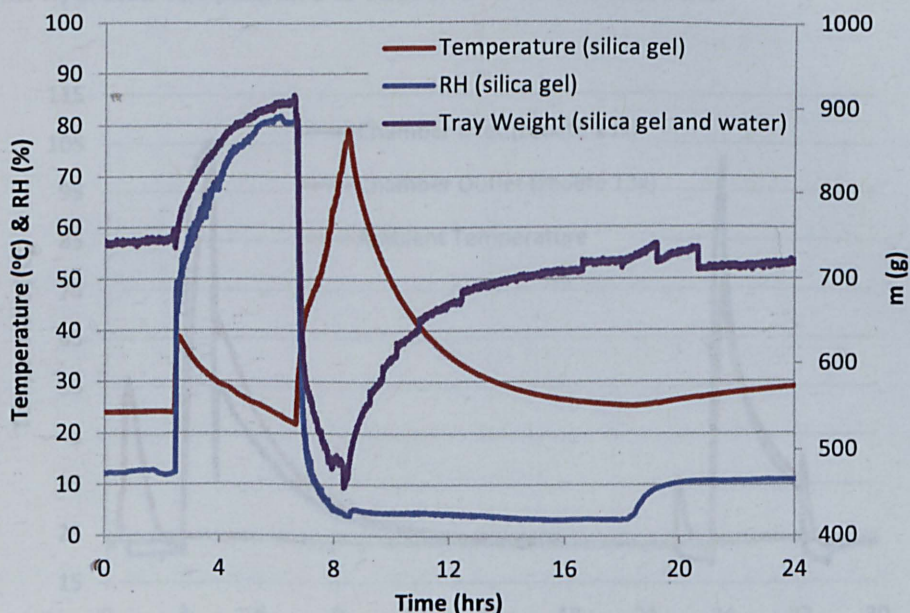


Figure 7.27 Comparison on internal temperature, relative humidity and silica gel tray weight change

7.3.1.2 Zeolite 13X Chamber

As mentioned and discussed before, zeolite 13x has a highest reacted temperature and better water absorbed capacity than others. Figure 7.28 shows temperature change of a zeolite 13x chambers during its hydration and dehydration process. When humidifier is on, internal inlet temperature drops down to about 18°C and internal outlet temperature jumps up to over 55°C. Internal outlet and inlet temperatures reach a steady state after

about two hours, when the humidity generator is turned off and isolated, and fan heater is switched on and set at 100°C. Inlet and outlet temperatures reach another steady state within one hour and the heater is then switched off and isolated. In the first cycle, hydration and dehydration process takes about a half day time. In the second cycle, the fan heater's target temperature is reduced to 80°C. It can be seen that the maximum outlet hydrated temperature is about 35°C at this moment.

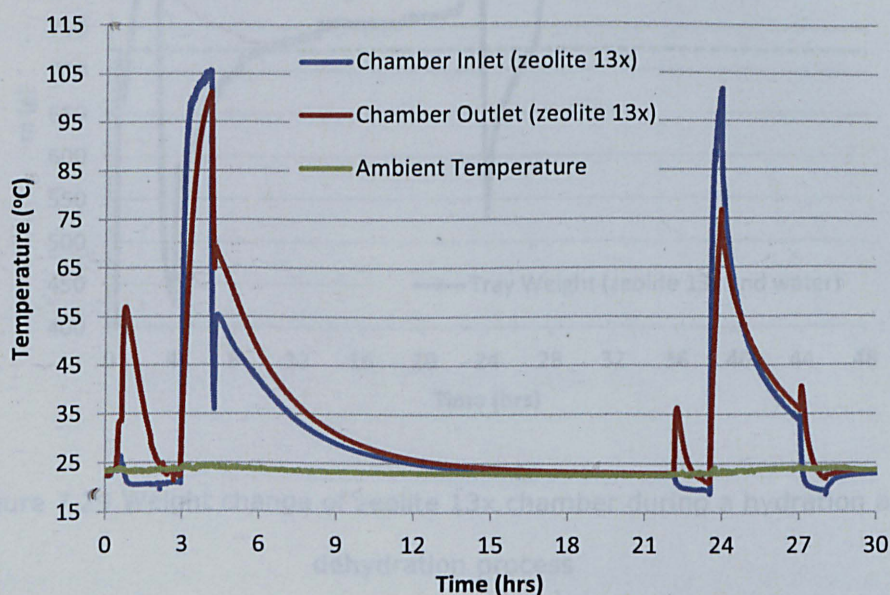


Figure 7.28 Temperature change of zeolite 13x chamber during a hydration and dehydration process

Based on foregoing evaluation on various zeolite hydration process (as studied in Section 7.1) vermiculite has a very short reaction time with Zeolite 13x tray weight change during the hydration and dehydration process is shown in Figure 7.29. In the first testing cycle, tray weight starts rapidly increasing and reaches its peak point at 840 grams from 700 grams when inlet and outlet temperatures hold a steady state. On dehydration process, red dash lines are showing suppositional and actual tray weight change complying with water loss. When the internal temperature recovers to the room temperature, tray weight stays in a steady state, which is the

same value as original one and means zeolite 13 is totally dried. On the contrast, zeolite 13x tray weight returns to a really high value around 820 grams (as orange line shown in Figure 7.29) after the second lower temperature 80°C cycle, which means that 80°C heating temperature cannot dehydrate zeolite 13x at this condition stage.

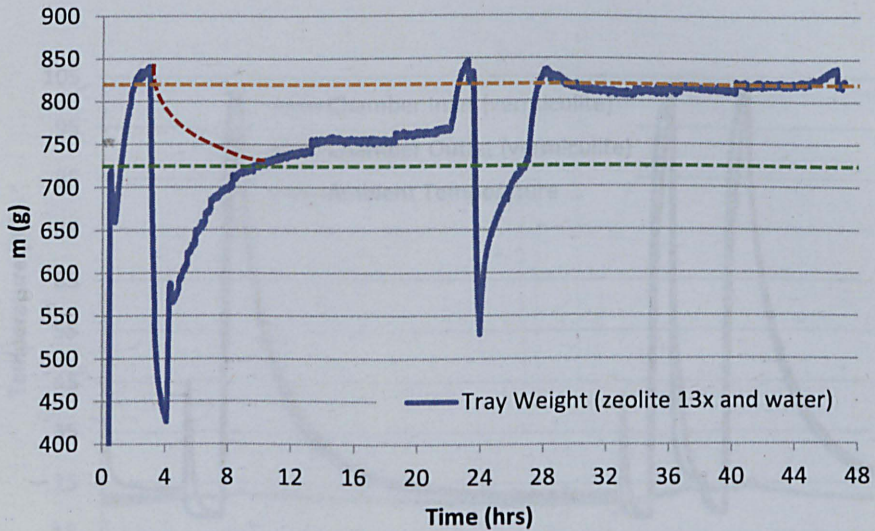


Figure 7.29 Weight change of zeolite 13x chamber during a hydration and dehydration process

7.3.1.3 Vermiculite Chamber

Based on foregoing evaluation on vermiculite's hydration process (as studied in Section 7.2), vermiculite has a very short reaction time with water, less than half an hour. Specifically, Figure 7.30 reveals more details on vermiculite chamber temperature change during three cycle's hydration and dehydration process. In the first cycle, internal outlet temperature sharply jumps up to about 45°C and both internal outlet and inlet temperatures reach 18°C a steady state within a short time (2 hours). Then, the humidity generator is turned off and isolated and the fan heater

is switched on at 100°C. The first cycle process takes up a half day time. In the second cycle, the fan heater is under the same target temperature (100°C). As can be seen, the second cycle has a similar liner trend as the first one. When both inlet and outlet temperatures reach the target value, the heater is switched off and the cool humidifier is switched on immediately, which means the third cycle testing is starting.

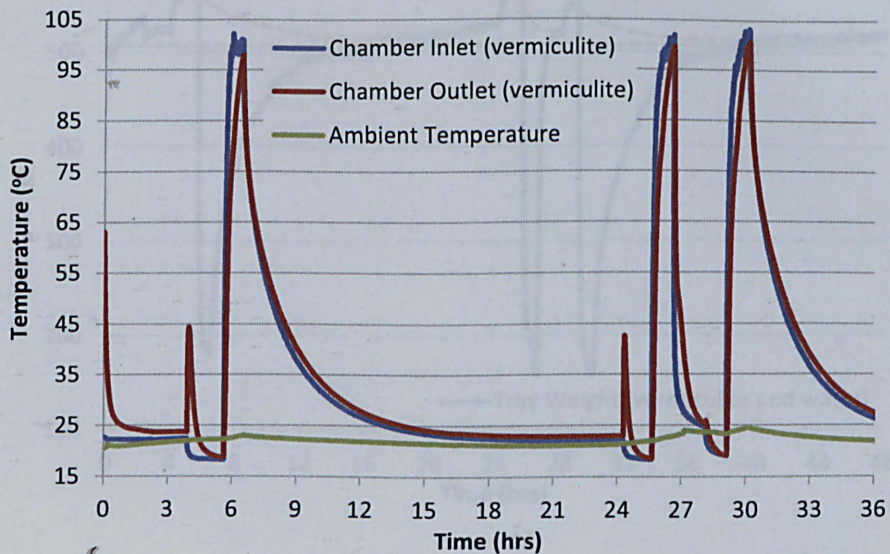


Figure 7.30 Temperature change of vermiculite chamber during hydration and dehydration processes

7.3.1.4 Activated Carbon Chamber

Figure 7.31 illustrates vermiculite weight change during three cycle's hydration and dehydration process. At the beginning of the first cycle, tray weight starts gradually increasing and peaks at about 560 grams from 500 grams when inlet and outlet temperatures reach a steady state. In the dehydration process, tray weight sharply drops to its bottom value as original blue line shown in Figure 7.31. Actually, red dash lines are showing suppositional tray weight change complying with water loss. Vermiculite tray weight returns to the same value as original tray weight when the internal temperature recovers to room temperature (about 23°C), which

means vermiculite is totally dried. Green and red dash lines in Figure 7.31 point out that there is no change on the vermiculite tray weight after three dehydration processes under current heater temperature. This implies show that fast model (short duration) recycle is possible for this designed absorption chamber.

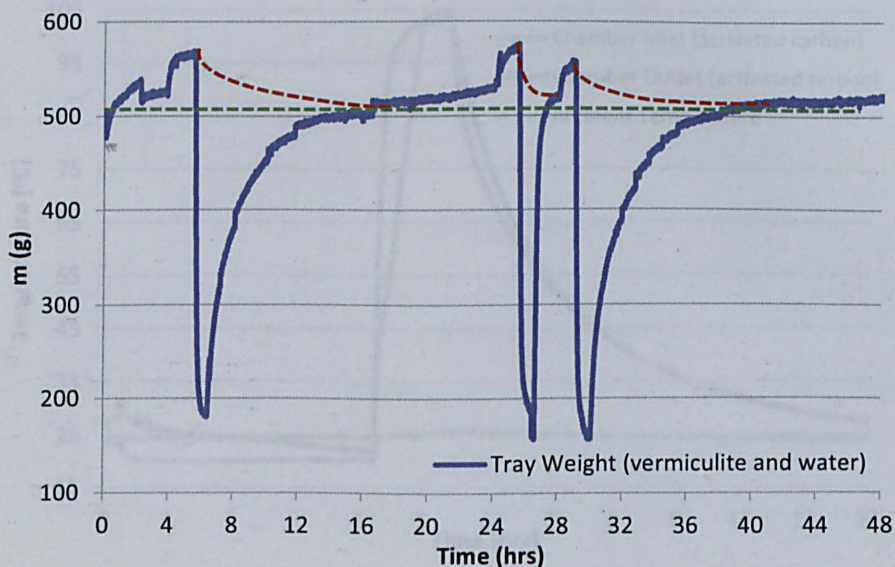


Figure 7.31 Weight change of vermiculite chamber during hydration and dehydration process

7.3.1.4 Activated Carbon Chamber

Activated carbon is a type of charcoal that has been treated with oxygen to open up millions of tiny pores between the carbon atoms. Laboratory tests in this research show that activated carbon has a lower capacity to absorb water vapour than others. Figure 7.32 shows internal temperature change of the activated carbon chamber during hydration and dehydration process. Inlet temperature starts decreasing and outlet temperature starts increasing when humidifier and top and bottom valves are all full opened. Difference of inlet and outlet temperatures is around 10°C in the hydration

process, which lasts over four hours. After that, testing process enters a dehydration cycle when heater is switched on and humidifier is switched off. Approximate one hour later, both inlet and outlet temperatures achieve their steady states at around 100°C, which means all water absorbed by activated carbon has been evaporated.

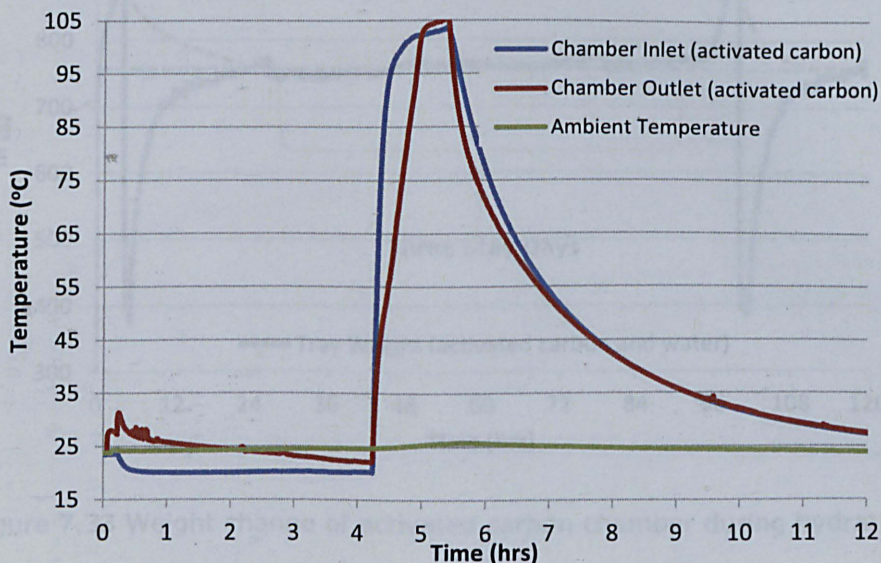


Figure 7.32 Temperature change of activated carbon chamber during hydration and dehydration process

Figure 7.33 illustrates tray weight change of the activated carbon during hydration and dehydration cycle in five days. In the first cycle, tray weight starts significantly rising up when inlet relative humidity is increasing. Activated carbon tray weight reaches peak point 900 grams from 740 grams when inlet and outlet temperatures achieve a steady state. In the dehydration process, tray weight suddenly and sharply drops and gets back to its original value in approximate 18 hours. After that, top and bottom valves are full closed and the whole system stays free for over 72 hours (three days). Then, the second cycle is powered on; the same linear trend and parameter values are obtained as green and red dash lines shown in

Figure 7.33. During this full five days testing, there was no leakage in the absorption chamber, which as a proof brings an avenue to this seasonal long term thermochemical energy storage system.

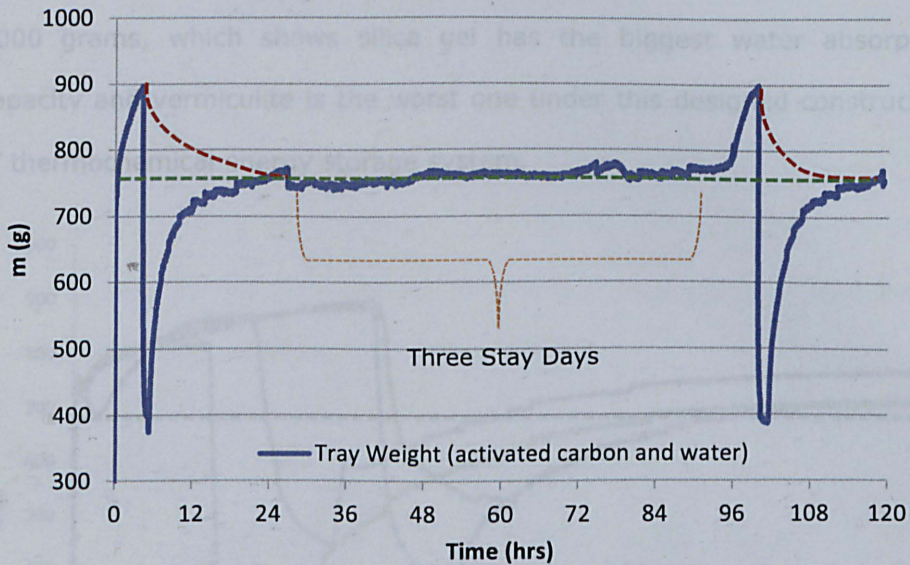


Figure 7.33 Weight change of activated carbon chamber during hydration and dehydration process

7.3.2 Comparison of Thermochemical Energy Storage System with Different Absorbents

Based upon all investigation and results above, Figure 7.34 summarises a comparison of hydrated and dehydrated mass change of different absorbents of equal tray weight. It can be seen that all absorbents are able to achieve requirements of the seasonal thermochemical energy storage system, which is to absorb water vapour and enter a saturated state when the stored heat is released. Then, saturated absorbents experience a reverse endothermic charging process under a proposed heater temperature. It is also illustrated that the weight of all absorbents with the tray nearly returns back to its original value after one cycle of discharging

and charging process, i.e., 720 grams (320 grams empty tray plus 300 grams absorbents) as black dash line in Figure 7.34. A notable exception is zeolite 13x due to its highest charging temperature as discussed before. Figure 7.35 reveals water absorption ratios of these absorbents per pure 1000 grams, which shows silica gel has the biggest water absorption capacity and vermiculite is the worst one under this designed construction of thermochemical energy storage system.

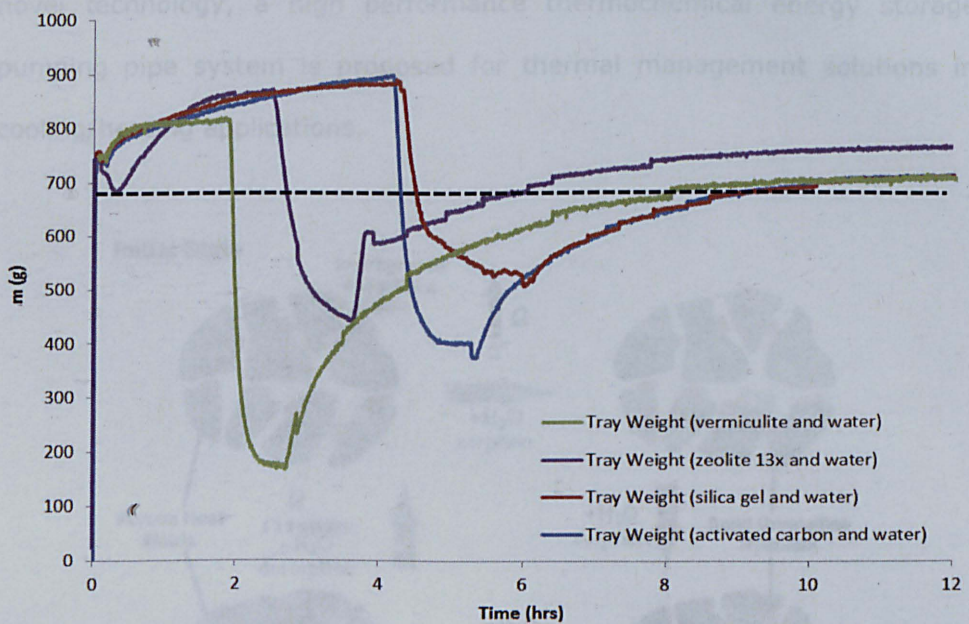


Figure 7.34 Comparison on hydrated and dehydrated mass change of absorbents of an equal tray weight

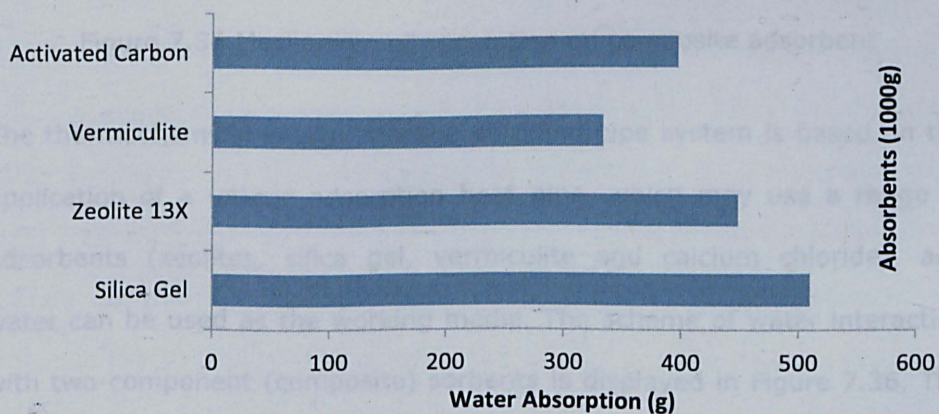


Figure 7.35 Water absorption ratios of absorbents (1000g)

7.4 Comparison of Simulation and Experimentation on Thermochemical Materials Energy Storage Systems

7.4.1 Principles for Thermochemical Energy Storage Pumping Pipe System

A novel cooling and heating energy storage system was presented and patented by the University of Nottingham (Riffat, 2000). In respect of this novel technology, a high performance thermochemical energy storage pumping pipe system is proposed for thermal management solutions in cooling/heating applications.

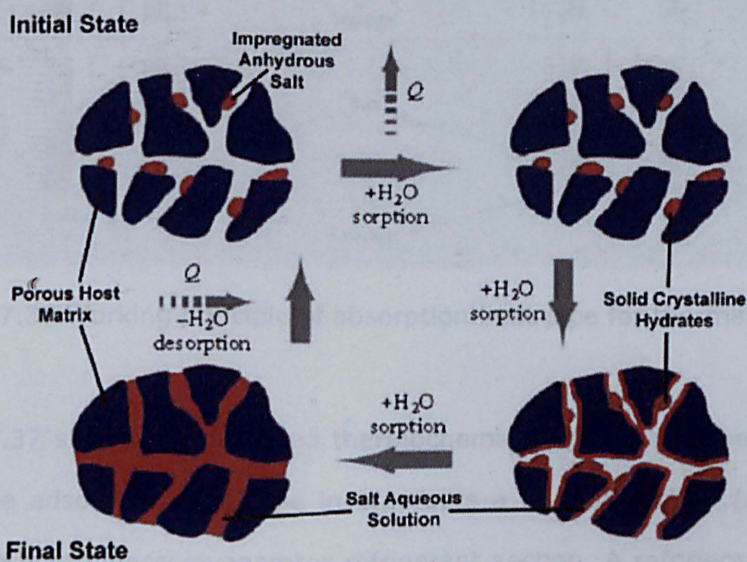


Figure 7.36 Mechanism of adsorption on composite adsorbent

The thermochemical energy storage pumping pipe system is based on the application of a unique adsorption heat pipe, which may use a range of adsorbents (zeolites, silica gel, vermiculite and calcium chloride), and water can be used as the working media. The scheme of water interaction with two-component (composite) sorbents is displayed in Figure 7.36. The main mechanisms of water sorption taking place on a composite sorbent

"salt inside a porous host matrix" are: (1) a solid absorption (or a chemical reaction, 10~15% of the total sorption), and (2) a liquid absorption (approximate 80% of the total sorption). In addition, heterogeneous adsorption on the matrix surface is responsible for 3~4% and can be neglected.

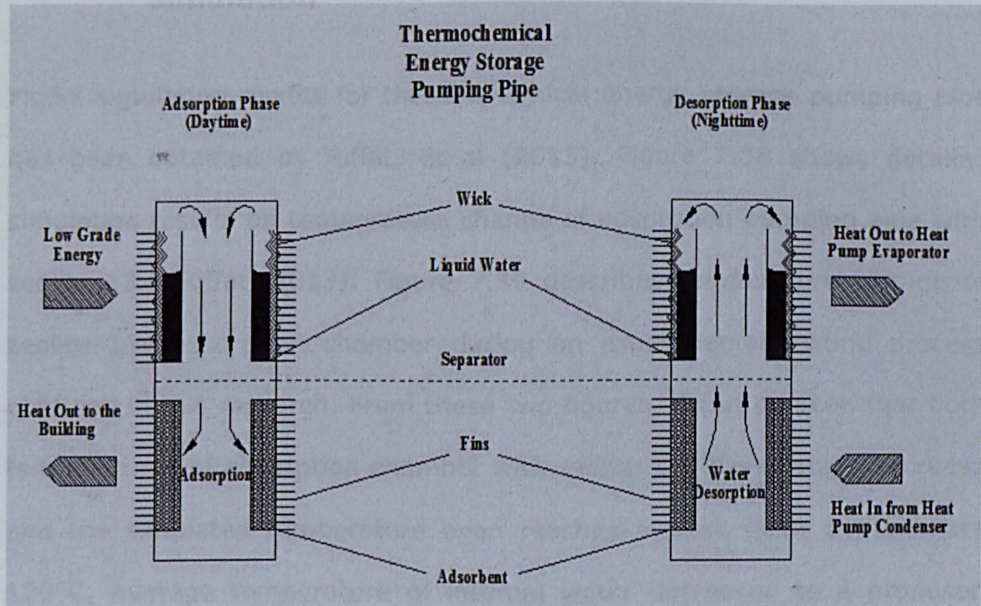


Figure 7.37 Working principle of absorption heat pipe for thermal storage

Figure 7.37 shows the proposed thermochemical energy storage pumping pipe. The adsorption heat pipe incorporates a reactor section (adsorbent bed) and a condenser/evaporator refrigerant section. A refrigerant vapour (e.g., water) can be transported in the pipe with minimal pressure drop when a temperature difference is formed between the heat source and the sink. The adsorbent material can be incorporated in the lower part of the heat pipe while the refrigerant receiver/wick structure can be placed at the top part of the pipe. This configuration can improve the heat transfer and enhance the overall performance of the energy storage system, compared with a bulky heat exchanger with packed adsorbent. Heat is stored at night

when the adsorbent is re-generated with a heat input from a thermal source such as a heat pump. During the day, the stored heat is released due to adsorption of vapour on the adsorbent (Riffat, 2013).

7.4.2 Results Discussion on Experimentation and Simulation

Model simulation results for thermochemical energy storage pumping pipe has been obtained by Riffat, et al (2013). Figure 7.38 shows detailed simulation results on temperature change of adsorption pumping pipe with zeolite 13x (Riffat, 2013). Figure 7.39 describes temperature change of zeolite 13x absorption chamber during an experimental testing process obtained in this research. From these two figures, it can be seen that both temperatures of absorption chamber with zeolite 13x have rapidly increase and the simulated temperature even reaches a peak point approximate 120°C. Average temperature of internal water decreased to a proposed cooling required thermal range in simulation, which means that thermochemical materials can be used for both cooling and heating purposes. Simulation and laboratory experiment were in different work conditions, the former was well sealed and under a lower pressure (round 0.025 bar) whilst the latter was under a room pressure (normally, 1.0 bar). Therefore, the simulation result has a much higher final temperature than the experimental one. Taking into account of the complexity of processes in cooling and heating system, the agreement of simulation and experimentation is satisfactory, thus the lumped numerical model is acceptable and significant for preliminary investigation of this scaled seasonal thermochemical energy storage system.

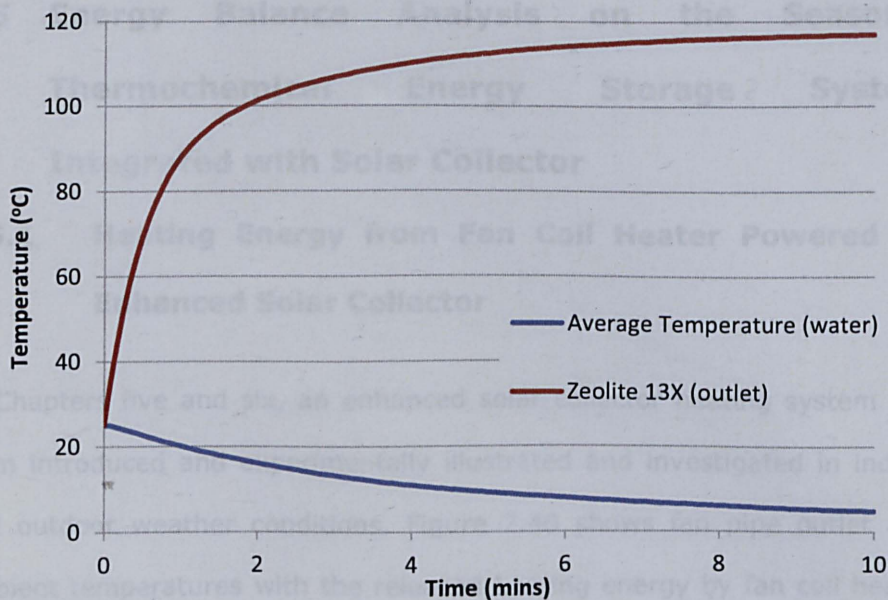


Figure 7.38 Simulation on temperature change of adsorption pumping pipe with zeolite 13x (Riffat, 2013)

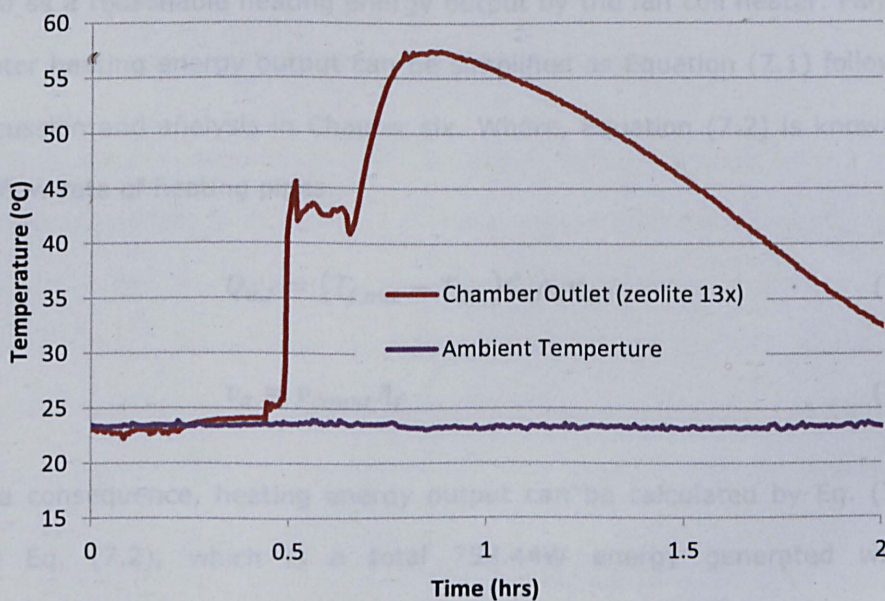


Figure 7.39 Temperature change of zeolite 13x absorption chamber during experimental testing

7.5 Energy Balance Analysis on the Seasonal Thermochemical Energy Storage System Integrated with Solar Collector

7.5.1 Heating Energy from Fan Coil Heater Powered by Enhanced Solar Collector

In Chapters five and six, an enhanced solar collector heating system has been introduced and experimentally illustrated and investigated in indoor and outdoor weather conditions. Figure 7.40 shows fan pipe outlet and ambient temperatures with the released heating energy by fan coil heater in a PCM store tank solar collector system. As can be seen, fan pipe outlet temperature is over 50°C for approximate half an hour, which is proposed to be the minimum temperature for absorbents endothermic dehydration reaction. An acceptable temperature range of over 50°C is shown in Figure 7.40 as a reasonable heating energy output by the fan coil heater. Fan coil heater heating energy output can be simplified as Equation (7.1) following discussion and analysis in Chapter six. Where, Equation (7.2) is known as air flow rate of heating pipes.

$$Q_{u,f} = (T_{f,out} - T_{air})C_a\rho_a v_a \quad (7.1)$$

$$v_a = v_{count}A_f \quad (7.2)$$

As a consequence, heating energy output can be calculated by Eq. (7.1) and Eq. (7.2), which is a total 752.44W energy generated within approximate half an hour over 50°C. The power of this PCM tank solar collector system is then obtained to be 0.75 kWh (about 0.42 kWh during a testing day).

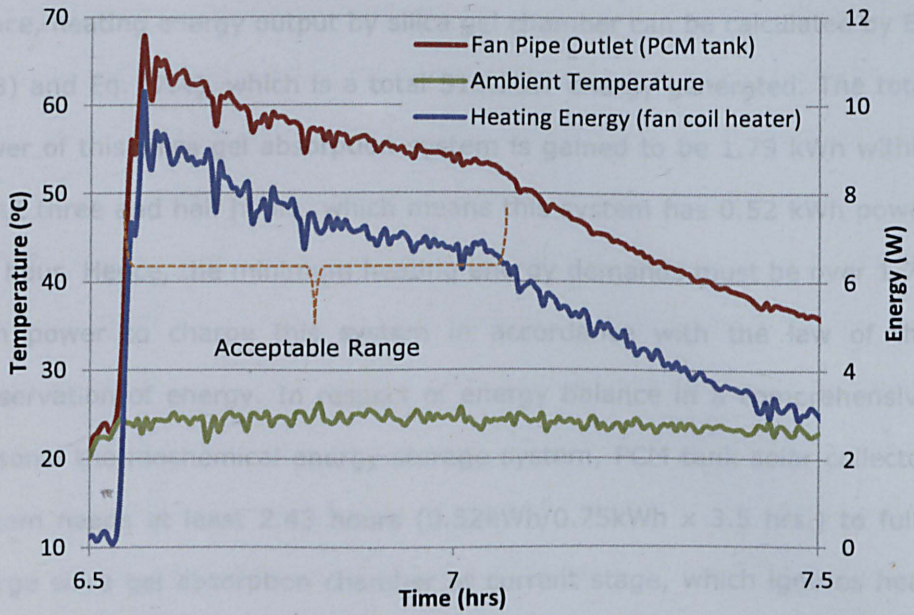


Figure 7.40 Fan pipe outlet and ambient temperature with heating energy from PCM tank solar collector system

7.5.2 Heating Energy Demand on Endothermic Dehydration Process of Absorbents

As well known, absorbents are releasing heating energy during their exothermic hydration discharging process. Figure 7.41 represents silica gel chamber outlet and ambient temperature change within four hours, and heating energy output from the absorption chamber system. Absorbents chamber heating energy output can be simplified and governed as Equation (7.3). Equation (7.4) is known as air flow rate of internal absorption chamber.

$$Q_{u,ac} = (T_{ac,out} - T_{air})C_a\rho_a v_{ac} \quad (7.3)$$

$$v_{ac} = v_{count}A_{ac} \quad (7.4)$$

Hence, heating energy output by silica gel chamber can be calculated by Eq. (7.3) and Eq. (7.4), which is a total 515.23W energy generated. The total power of this silica gel absorption system is gained to be 1.79 kWh within about three and half hours, which means this system has 0.52 kWh power per hour. Hence, the minimum heating energy demands must be over 1.79 kWh power to charge this system in accordance with the law of the conservation of energy. In respect of energy balance in a comprehensive seasonal thermochemical energy storage system, PCM tank solar collector system needs at least 2.43 hours ($0.52\text{kWh}/0.75\text{kWh} \times 3.5 \text{ hrs.}$) to fully charge silica gel absorption chamber at current stage, which ignores heat loss occurring during the energy delivery.

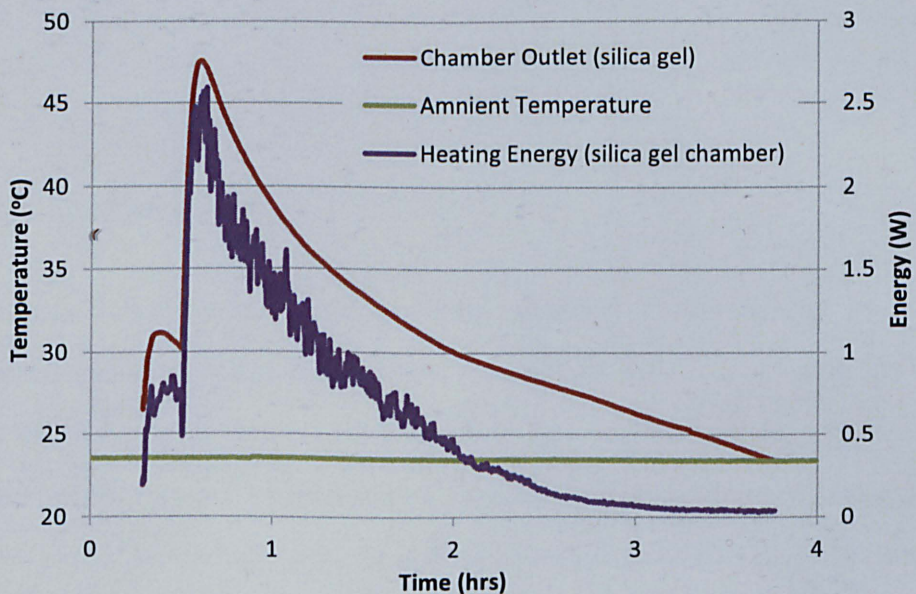


Figure 7.41 Silica gel chamber outlet and ambient temperatures change with heating energy from absorption chamber system

7.6 Summary of Results and Conclusion

To sum up, five types of thermochemical materials (silica gel, calcium chloride, zeolite 13x, vermiculite and activated carbon) have been

evaluated in their hydration heating processes. Results imply that zeolite 13x holds the highest reacted temperature (over 58°C) and vermiculite has a fast absorbing hydration duration (less than half an hour). Furthermore, four types materials have been involved in the reverse dehydration endothermic reaction. Silica gel holds the biggest water absorbed capacity and vermiculite has worse water absorption than others under this designed construction of thermochemical energy storage system. Taking into account the complexity of processes in cooling and heating systems, numerical simulation results show the same trend with experimentation data. Both investigations and results are acceptable and significant for this preliminary evaluation of the scaled seasonal thermochemical energy storage system.

CHAPTER 8

Economic, Environmental Analysis and Recommendation

8.1 Introduction

A simple economic and environmental analysis is represented in this chapter, including sensitivity analysis methods of net present value (NPV) and internal rate of return (IRR), which is derived from previous chapters of literature review, methodologies, results and discussions studies on novel seasonal thermochemical energy storage system integrated with solar collectors. Intelligent transpired solar collector system is introduced as future work to replace current conventional solar collector.

8.2 Economic and Environmental Analysis

8.2.1 Economic Analysis

The previous sections have shown that seasonal high capacity heat storage system integrated with solar collector is intelligent and suitable for home

and commercial applications from the technique view. However, the economic aspect is also a crucial factor that affects the application of this technology. A preliminary economic analysis of this combined system has been carried out in order to understand its commercial viability.

8.2.1.1 Capital Cost Comparison with Conventional Heating System of Household

According to Dimplex's (www.dimplex.co.uk) 2013 report about UK retro fit and new household of running cost assumptions, annual space heating load and hot water heating for a typical new built four bedroom detached house are approximately 11302.33kWh and 4437.30kWh, respectively (UK House, 2013). Specifically, house building details is as follows:

Occupants: 4, floor area: 120m², specific heat loss: 45W/m², annual operating hours: 1800 (75days), efficiency of gas boiler: 86%, average price of electricity: 15.32p/kWh and gas: 4.64p/kWh (Carbon, 2013).

Based on these data, annual running cost of space heating and hot water for a new built four bedroom detached house are 609.80 pounds and 263.35 pounds (plus 10% electric supplementary), respectively, which are both based on conventional gas heating system.

In terms of above result and requirements, a full size 3 kW seasonal high capacity heat storage integrated solar collector system integrated with a 3.5 kW solar collector has been proposed and economic analysed in the following section. Table 8.1 illustrates subentry detailed calculation of the capital cost of this 3 kW novel system. The whole system is assumed to have an operation life span of 20 years and maintenance cost of 2%. Its capital cost can be calculated by summing up the prices of the system components, taking into account the appropriate sale profit and value

added tax (VAT, 20%). It should be noted that the unit costs of the system components are quoted from the selected product catalogue. In order to illustrate a direct cost comparison between this novel system and the conventional systems, the costs of the system components in different currencies have been converted to British pounds. It can be concluded that the initial expense of the prototype system is £7034.83.

Table 8.1 Calculation of the capital cost of a 3 kW seasonal high capacity heat storage system integrated with evacuated solar collector

System Components	Unit Cost (including materials and equipment costs) (£)	Quantity	Cost (£)
Evacuated solar collector (thermomax DF100)	1871.82	(30)	1871.82 (Kingspan, 2013)
Thermomax Collector Fix Kit	98.80	1	98.80 (Kingspan, 2013)
Water/PCM Tank	185.93	1	185.93 (PCM, 2013)
PCM (RT 58)	7.36	50kg	368.00 (PCM, 2013)
Flat Plate Heat Exchanger	35.99	2	71.98 (PCM, 2013)
Fan Coil Unit Heater	105.38	1	105.38 (Wang, 2011)
Transport Lines	3.65	10m	36.50 (Wang, 2011)
Water piping	3.65	20m	73.00 (Wang, 2011)
Absorbents Chamber	200.00	1	200.00 (PCM, 2013)
Absorbents (Synthesis)	30.00	75kg	2250.00 (PCM, 2013)
Inverter and Meter	150.00	1	150.00 (Wang, 2011)
Total Cost (excluding labour) (£)			5411.41
VAT (20% of profit) (£)			1082.28
Labour (assume 10% total cost) (£)			541.14
Total Capital Cost of Prototype (£)			7034.83

8.2.1.2 Estimation of the Cost Payback Period and Life Cycle Cost Saving

Based on discussions with solar collector system manufactures and absorbents suppliers, it is assumed that mass production can reduce the total capital cost by a factor of 0.5. Hence, proposed and renewed total capital cost of a commercial system: $£7034.83 \times 0.5 = £3517.42$. As mentioned before, annual operating time is 1800 hours and a proposed full size system heating output is 3 kW. Therefore, over the heating period the system provides $1800 \times 3 = 5400$ kWh. It is assumed that the seasonal thermochemical energy storage system is used to provide supplementary heating to the existing conventional heating system. Therefore, the heating load that is supposed to be provided by the existing system will be reduced significantly via this novel system.

$$\text{Reduction in heating load} = 11302.33 - 5400 = 5902.33\text{kWh} \quad (8.1)$$

$$\text{Revised gas heating cost} = (5902.33 \times 0.0464) / 0.86 = £318.46 \quad (8.2)$$

This combined system is integrated with a high efficiency solar collector, which can also be used as a hot water supplement. Normally, it can provide up to 70% (data from manufactures: Kingspan, 2013) of household annual hot water needs. Given its summer season absorbents heating function, it is assumed that about 35% of annual hot water load can be covered by this integrated solar collector system.

$$\text{Reduction in hot water load} = 4437.30 \times 0.65 = 2884.25\text{kWh} \quad (8.3)$$

$$\text{Revised hot water cost} = (2884.25 \times 0.0464) / 0.86 \times 1.1 = £171.18 \quad (8.4)$$

Hence, new annual running cost of space heating and hot water:

$$\text{New gas system cost} = 318.46 + 171.18 = \text{£}489.64 \quad (8.5)$$

The savings made using the thermochemical energy storage system are:

$$\text{Cost of novel system saved} = (609.80 + 263.35) - 489.64 = \text{£}383.51 \quad (8.6)$$

$$\text{Therefore, the payback period} = 3517.42 / 383.51 = \mathbf{9.17 \text{ years}} \quad (8.7)$$

In consideration of 20 years system life span, it is therefore attractive to use this novel system in both household and commercial building.

Furthermore, sensitivity analysis methods of the net present value (NPV) and internal rate of return (IRR) are introduced to evaluate this proposed novel system. Both NPV and IRR are primarily used in capital budgeting, the process by which companies determine whether a new investment or expansion opportunity is worthwhile. Given an investment opportunity, a firm needs to decide whether undertaking the investment will generate net economic profits or losses for the company in terms of NPV and IRR.

Net present value (NPV) is a formula used to determine the present value of an investment by the discounted sum of all cash flows received from the project. The formula for the discounted sum of all cash flows can be rewritten as equation (8.8):

$$NPV = -C_0 + \frac{C_1}{(1+r)} + \frac{C_2}{(1+r)^2} + \dots + \frac{C_i}{(1+r)^i} = -C_0 + \sum_{i=1}^T \frac{C_i}{(1+r)^i} \quad (8.8)$$

Where, $-C_0$: initial investment, C_i : running cost (cash flow), r : annual market discount rate, i : time (1~20 years); relevant input parameters shows in Table 8.2.

In the equation (8.8), the $-C_0$ is the capital cost of system, which is a negative cash flow showing that money is going out as opposed to coming

in. Considering that the money going out is subtracted from the discounted sum of cash flows coming in, the net present value would need to be positive in order to be considered a valuable investment.

Table 8.2 List of input parameters of heat storage system

Input parameters	Value	Units
Capital cost	3517.420	£
Gas inflation rate (Carbon, 2013)	7	%
Annual market discount rate (Wu, 2014)	8	%
Annual heating load	5400	kWh
Annual hot water	1553.055	Kwh
Price of gas	0.0464	£/kWh

Table 8.3 The net present value (NPV) analysis method calculation

Year	NPV	C_i
1	-3218.7	322.6218
2	-2922.74	345.2053
3	-2629.52	369.3696
4	-2339.02	395.2255
5	-2051.21	422.8913
6	-1766.06	452.4937
7	-1483.55	484.1683
8	-1203.66	518.06
9	-926.358	554.3242
10	-651.626	593.1269
11	-379.437	634.6458
12	-109.769	679.071
13	157.4029	726.606
14	422.1006	777.4684
15	684.3474	831.8912
16	944.166	890.1236
17	1201.579	952.4322
18	1456.608	1019.102
19	1709.276	1090.44
20	1959.605	1166.77

Table 8.3 shows the net present value during 20 years system service period, which can be seen that NPV stands positive value in 13th year. Therefore, it is worth to invest this novel project whatever is in household or commercial building in consideration of its 20 years system life span.

On the other hand, internal rate of return (IRR) is the discount rate often used in capital budgeting that makes the net present value of all cash flows from a particular project equal to zero.

Generally speaking, the higher a project's internal rate of return, the more desirable it is to undertake the project. As such, IRR can be used to rank several prospective projects a firm is considering. Assuming all other factors are equal among the various projects, the project with the highest IRR would probably be considered the best and undertaken first. IRRs can also be compared against prevailing rates of return in the securities market (annual market discount rate). If a firm can't find any projects with IRRs greater than the returns that can be generated in the financial markets, it may simply choose to invest its retained earnings into the market.

Therefore, based on equation (8.8), internal rate of return (IRR) can be obtained when net present value (NPV) equals to zero, see equation (8.9).

$$NPV = 0 = -C_0 + \frac{C_1}{(1+R)} + \frac{C_2}{(1+R)^2} + \dots + \frac{C_i}{(1+R)^i} = -C_0 + \sum_{i=1}^T \frac{C_i}{(1+R)^i} \quad (8.9)$$

Where, R : internal rate of return (IRR), C_0 : initial investment, C_i : running cost (cash flow), i : time (1~20 years);

Then, IRR can be calculated out (**IRR=13.6%**). This value of IRR is bigger than the required rate of return (annual market discount rate, 8%), which means this system is desirable in term of 20 years system life span.

8.2.2 Environmental Analysis

The UK aims to reduce carbon dioxide (CO₂) emissions by 80 per cent below 1990 levels by 2050. To help make it happen, we should all aim to achieve a low carbon footprint. This novel solar system is a green, renewable combined system and can reduce carbon dioxide emissions. To investigate the environmental benefit of utilizing solar energy instead of conventional source of energy, the different emission of per unit energy is a key factor to estimate and compare a novel solar system with a conventional gas or electric system. The analysis has been carried out based on the UK guidelines for companies reporting on greenhouse gas emissions. Equation 8.8 and 8.9 for converting gas or electricity to CO₂ are given as follows:

$$\text{Carbon Dioxide Emission (kg} \cdot \text{CO}_2/\text{year)} = \text{Electricity (kWh/year)} \times 0.517 \quad (8.8)$$

$$\text{Carbon Dioxide Emission (kg} \cdot \text{CO}_2/\text{year)} = \text{Gas (kWh/year)} \times 0.185 \quad (8.9)$$

Where, CO₂ conversion factor is 0.517 for electricity and 0.185 for gas (Carbon, 2013). Therefore, the savings amount of carbon dioxide emission is calculated as follow:

Carbon dioxide emission by gas:

$$= (5400 + 4437.30 \times 0.35) \times 0.185 = \mathbf{1286.32 \text{ kg}} \quad (8.10)$$

Carbon dioxide emission by electricity:

$$= 4437.30 \times 0.35 \times 0.1 \times 0.517 = \mathbf{80.29 \text{ kg}} \quad (8.11)$$

Therefore, total saving amount of carbon dioxide emission from this novel solar energy based renewable and sustainable system is up to 1366.61 kg per year.

8.3 Recommendation

8.3.1 Intelligent Transpired Solar Collector System

A simple, efficient and cost effective solar technology is known as a transpired solar collector. Transpired solar collectors were invented in the mid-1980s by John Hollick and Rolf Peter as a method of using solar radiation to preheat ventilation air for buildings (Hollick, 1994 and Kutscher, 1996). The first transpired solar collector system in the UK was installed in 2006 on the south wall of a single storey industrial building (CA Group, 2009). In 2011, Hall et al presented a full review of research into transpired solar collector technology, examining its thermal performance, the different construction types, annual energy performance, and international experiences.

More precisely, the transpired solar collector is an air preheating system as shown in Figure 8.1. Sunlight strikes and warms a south facing vertical wall. Heat is transferred to ventilation air as it passes through tiny holes or slits in the wall. The result is a model of simplicity and efficiency. These systems conservatively collect 60~70 percent of the incident solar energy. During the heating season, the system not only collects solar energy but also recaptures wall heat loss. During the cooling season, collector bypass vents can be opened allowing the wall to dump heat, thus reduce cooling loads. This technology is ideally suitable for buildings that have a south-facing wall near with access to the building ventilation system. The

collector surface is generally corrugated steel or aluminium and can be any dark colour.

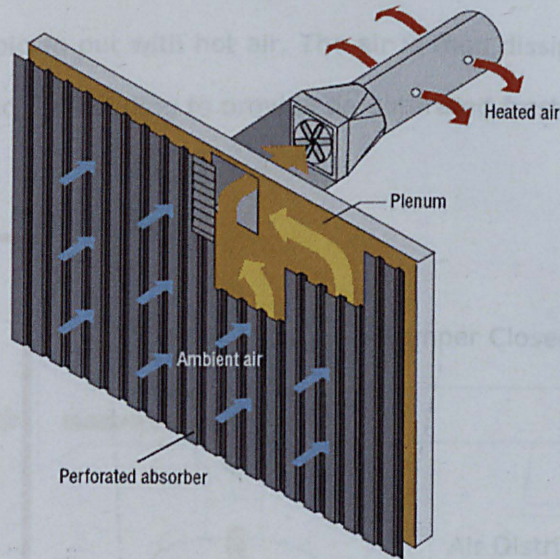


Figure 8.1 Schematic of working principle of a transpired solar collector

8.3.2 Seasonal Thermochemical Heat Storage System Integrated with Transpired Solar Collector

Based on above introduction and illustration to transpired solar collector, a seasonal thermochemical heat storage system integrated with a transpired solar collector has been proposed as shown in Figures 8.2 and 8.3, in which the system is seasonally divided into cooling and heating modes.

8.3.2.1 Summer Season Cooling Mode (charging cycle)

For summer season operating mode, the working mechanism is shown in Figure 8.2. Specifically, a transpired solar collector is normally setup on a south-facing wall integrated with insulated and cavity wall. In this charging cycle, the transpired solar collector is employed to heat air and a network

of dampers and ductwork to distribute air into the absorption chamber in which the adsorbent is stored. The internal absorption chamber configuration allows for the charging (dehydration) of the adsorbents in which water is blown out with hot air. The air is then dissipated externally, or if needed, into the building to provide de-saturated fresh ventilation air.

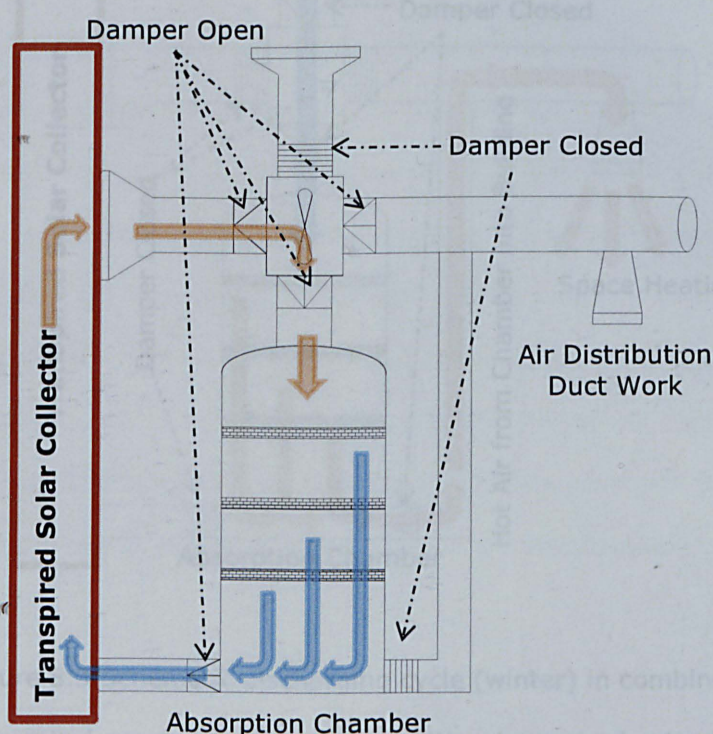


Figure 8.2 Schematic charging cycle (summer) in combined thermochemical energy storage system with a transpired solar collector

8.3.2.2 Winter Season Heating Mode (discharging cycle)

Figure 8.3 illustrates the working mechanism of winter season heating mode. During this discharge (hydration) mode process, internal moisture laden air from within the building (such as shower room or kitchen) is recirculated through the ductwork system into absorption chamber. As the adsorbent is discharged (water adsorbed by the adsorbent), the internal air

recirculation is heated and distributed into the internal environment to provide space heating.

8.4 Summary

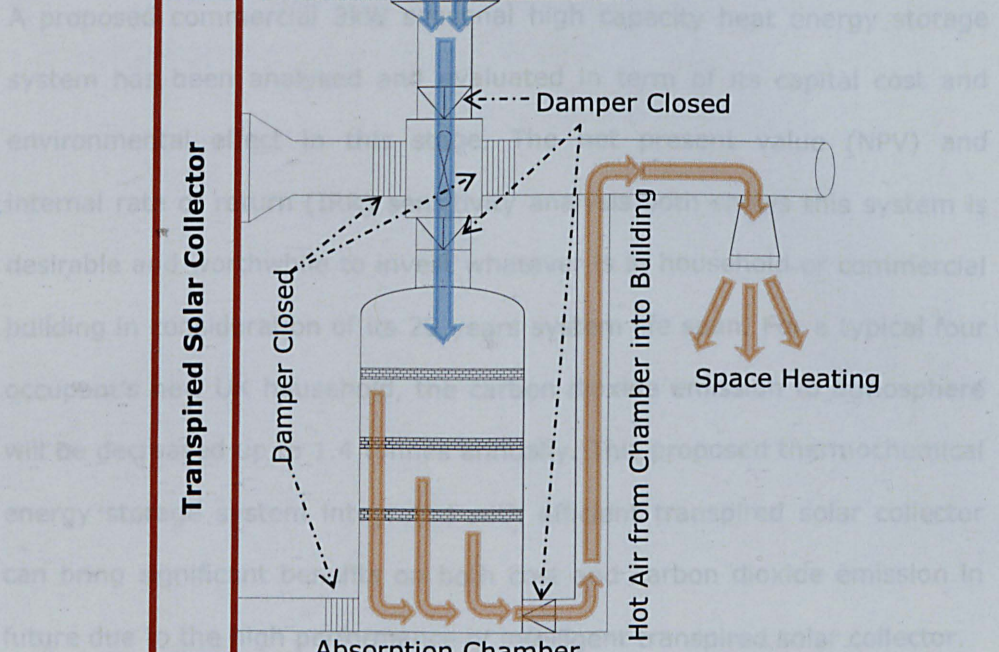


Figure 8.3 Schematic discharging cycle (winter) in combined thermochemical energy storage system with a transpired solar collector

Whilst the configuration of absorption and transpired solar collector is simple, a detailed design along with computation modelling will be required to ensure adequate flow distribution throughout the system, which promises accurate and complete adsorption in future work. Currently, transpired solar collectors are only installed on south facing facades in order to capture low-lying winter sun. The proposed thermochemical absorption system will enable transpired solar collectors' installation onto roof of buildings with unsuitable southerly aspects. This implies a

significantly great market share on renewable heat generation along with large CO₂ offsetting.

8.4 Summary

A proposed commercial 3kW seasonal high capacity heat energy storage system has been analysed and evaluated in term of its capital cost and environmental effect in this stage. The net present value (NPV) and internal rate of return (IRR) sensitivity analysis both shows this system is desirable and worthwhile to invest whatever is in household or commercial building in consideration of its 20 years system life span. For a typical four occupant's new UK household, the carbon dioxide emission to atmosphere will be decreased up to 1.4 tonnes annually. This proposed thermochemical energy storage system integrated with efficient transpired solar collector can bring significant benefits on both cost and carbon dioxide emission in future due to the high performance of intelligent transpired solar collector.

CHAPTER 9

Conclusions and Future Work

9.1 Summary of the Work

The aims of the research described in this thesis is to design, produce and evaluate a high performance, low-cost seasonal high capacity heat energy storage system, which can be integrated with a solar collector used for buildings heating sector. The whole system has been designed and tested in lab intending to provide a satisfactory heating source for rooms with compensating huge heating loads. Firstly, comprehensive literature review has been carried out on the following aspects: existing PCMs, thermochemical energy storage technologies. Particular emphasis has been put on their thermal application and complex heat transfer process due to the study of methods (analytical, numerical and experimental). Besides, investigation has been conducted on relevant preliminary experiments and simulation, which involves properties and characteristics of PCMs,

thermochemical materials, temperature controlled cold chamber and absorption cooling system. After the investigation above, a novel solar heating system has been tested and evaluated to power and dry a proposed thermochemical absorption system. This heating system is a modified direct flow evacuated tube solar collector with PCM tank integrated with a fan coil heat exchanger. Lastly, the proposed seasonal thermochemical energy storage system is divided into hydration heating generation and dehydration process to investigate and discuss three processes of charging, storing and discharging. At the end of research, a brief economic and environmental analysis and recommendations have been conducted and stated on the basis of this research.

9.2 Conclusions

9.2.1 Temperature Controlled High Capacity Heat Energy Storage System

Basic investigation on properties and characteristics of PCMs show that each material has special melting point, melting and solidifying time, and specific storage density. A test on building device tank with PCM reveals that materials can maintain a considerable high internal temperature of system in a low temperature ambient.

The proposed seasonal thermochemical materials storage system can not only reduce space heating cost in winter but also avoid overheating in summer, which derives from simulation modelling on passive house (Nottingham House). The modelling results show that a certain amount of potential thermochemical materials can meet house annual heating load and roof space is enough for solar panels to heat and dry materials.

On assessments of temperature controlled TCC chamber through PCMs, relative and essential conclusions can be drawn and summarized as follows: (a). TCC chamber is capable of maintaining a constant internal temperature of 2°C ~ 8°C even at an ambient high temperature over 30°C; (b). Original TCC chamber can keep internal temperature between 2°C ~ 8°C for 24 hours in terms of capacity of PCM (MC20) packs; (c). Basic TCC chamber appears weak in cooling a high level internal position of a space (temperatures increase to over 8°C). Therefore, the internal construction integrated with PCM is a key factor for further assessment, (d). Additional same size PCM packs can enhance the cooling capacity of TCC chamber and extend approximately duration of internal temperatures (2°C ~ 8°C) two days. Integrating thermal controlled chamber system with PCM is an importantly viable concept not only for shipping of chilled or hot food, pharmaceutical products but also for cooling or heating applications in buildings and industry.

Preliminary experiments have been carried out on a novel closed thermochemical energy storage pumping pipe system and fast adsorption cooling technique. There are some challenges and barriers that need to be addressed. Due to system fully closed under quite lower internal pressure, it will bring more difficulties to apply this technology for building devices. On the other hand, the adsorbents vessel side has quite high temperature (over 50°C) after hydration reaction. This heat must be removed into the ambient or temporarily stored by some methods, such as heat sink and adsorbent own thermal capacity, which potentially supplies a good idea for a heating system in winter room as a renewable energy strategy. On the other hand, materials have different thermal capacities, so lithium nitrate and silica gel have shown different heating temperatures. Adsorbents selection, development, and optimization is an important subject for

further works. Their feasibility may depend on the price and availability of materials marketing. Comparatively speaking, the simplest method is to use more adsorbents in cooling system. However, if cheap materials are available, it should be most attractive. The composite adsorbent is easy to prepare, inexpensive and can be scaled up in future.

9.2.2 PCMs Enhanced Solar Collector Heating System

A direct flow evacuated solar collector with enhanced PCM tank integrated with a fan coil heat exchanger has been characteristically tested. Firstly, due to fan coil heat exchanger required for water or PCM tank, the system is less efficient because of warm water circulates back to the collector. Secondly, radiation intensity and fan speed are key factors for solar collector heating system. Therefore, appropriate intensity of light and fan speed should be defined according to tubes' size and amount before tests. As a solar simulator, light radiation of tungsten lamps has a low efficiency (approximately 70%) to equate solar radiation under the same Pyranometer reading value.

Besides, store capacity of water tank is bigger than that of PCM RT58 in terms of basic tank model. It can be concluded that latent heat base PCM RT58 materials is not suitable or cannot be directly used within current solar systems. On the other hand, results of mathematical analysis have shown that heating storage capacity of proposed PCM-55 tank is better than those of PCM RT58 and water. Therefore, material selection will significantly influence the efficiency and capacity of thermal storage system.

Finally, experiment results show that the system can supply heating energy of over 50°C and PCM tank can supply a higher output temperature with a longer duration than water tank. The efficiency of enhanced solar collector

heating system is over 50% to transfer solar energy into heat absorption chamber in sunny days. However, the efficiency is only 10% in mostly cloudy weather.

9.2.3 Open Thermochemical Energy Storage System

In experiments on open thermochemical materials storage system, five types of thermochemical materials (silica gel, calcium chloride, zeolite 13x, vermiculite and activated carbon) have been evaluated on their hydration heating processes. Experiment results show that zeolite 13x holds the highest reacted temperature (over 58°C) and vermiculite has the fast absorbing hydration duration (less than half an hour). It is also shown that calcium chloride has changed into a mixture with liquid and solid after absorbing some water. As a result, this liquid goes away through meshed bottom of absorbent tray. That is to say some material cannot be used in the current model design and material selection is an important element to this system.

Furthermore, there are four types of materials involved in reverse dehydration endothermic reaction. Silica gel holds the biggest water absorbed capacity and vermiculite has worse water absorption than others under this designed construction of high capacity heat storage system. More importantly, considering the complexity of processes in cooling and heating system, numerical simulation results show the same linear trend as experimentation data. Both investigations are acceptable and significant for this preliminary evaluation of this scaled seasonal thermochemical energy storage system.

9.2.4 3kW Solar-Driven High Capacity Heat Storage System

A proposed 3kW solar-driven seasonal high capacity heat energy storage system has been described and analysed on economic and environmental effects. For a new household with a typical UK running cost (assuming heating load: 11302kWh and hot water: 4437kWh), estimation of capital cost of the proposed system is approximate 7035 pounds. This value can be decreased to around 3517 pounds, assuming mass production can reduce the total capital cost by a factor of 0.5. Based on these estimation and assumption, the payback period of the proposed system is about nine years in consideration of twenty years system life span. More importantly, there is up to 1366.61kg per year of total saving amount of carbon dioxide emission through employing this novel combined system. Therefore, this proposed system is very attractive to the market and a very promising application in both household and commercial buildings.

9.3 Potential Improvements and Future Work

The research has studied the complex and integrated process of the novel high capacity heat storage system powered by solar collector. As it is well known, both solar collector heating system and open thermochemical absorption system, which have been tested, work well independently. In combined mode of solar collector and thermochemical absorption system, solar energy captured by evacuated tube collector will be transferred to thermochemical absorption system in the charging stage, dehydration reaction occurs and water will be driven out from materials and thermal energy is stored. In the discharging mode, as a reversing process, moisture

from a steam generator is driven to absorption chamber by bower fan. The stored heat will then be released to heat space.

Therefore, the performance of a combination mode of these two systems should be investigated in future. The long term performance, stability and reliability of the whole combined system should also be evaluated on-site over a one-year monitoring period.

For the solar collector system, appropriate PCMs are required for storage tank due to their specific storage densities. Heat transfer techniques should be improved for internal PCMs tank due to low thermal conductivities of materials (such as copper, aluminium, nickel, stainless steel and carbon fiber with various forms of fins or honeycomb). For the thermochemical absorption system, materials selection, synthesis and optimisation are still crucial challenges and barriers that for which further research should be carried out to meet basic requirement of seasonal storage at low temperature ($\leq 70^{\circ}\text{C}$). Furthermore, the transpired solar collector, a simple, efficient and cost effective solar technology, has been proposed and recommended to drive seasonal thermochemical energy storage system instead of current evacuated solar collector in future.

However, both technical and economical questions on this seasonal thermochemical energy storage system have yet to be fully answered in practice. More research and development work as well as large scale demonstration projects are required to prove the viability and long term performance of novel high capacity heat storage systems.

REFERENCES

A

Abedin AH, Rosen MA, 2011a, *Closed and open thermochemical energy storage: Energy-and exergy-based comparisons*, Energy, doi:10.1016/j.energy.2011.06.034

Abedin AH, Rosen MA., 2011b, *Assessment of a closed thermochemical energy storage using energy and exergy methods*. Applied Energy, doi:10.1016/j.apenergy.2011.05.041

Abedin Ali Haji, 2010, *Master Thesis: Thermochemical Energy Storage Systems: Modelling, Analysis and Design*, University of Ontario, Institute of Technology.

Abhat A. 1983, *Low temperature latent heat thermal energy storage: heat storage materials*. Solar Energy 30, Issue 4, 313–332.

Agyenim Francis, 2007, PhD Thesis: *The development of medium temperature thermal energy storage for cooling applications*, University of Ulster.

Agyenim F., Eames P. and Smyth M., 2009, *A comparison of heat transfer enhancement in a medium temperature thermal energy storage heat exchanger using fins*, Solar Energy 83, 1509-1520.

Agyenim Francis, Hewitt N., Eames P. and Smyth M., 2010a, *A review of materials, heat transfer and phase change problem formulation for latent heat thermal energy storage systems (LHTESS)*, Renewable and Sustainable Energy Reviews 14, 615-628.

Agyenim F, Eames P, Smyth M., 2010b, *Heat transfer enhancement in medium temperature thermal energy storage system using a multitube heat transfer array*. Renewable Energy 35, 198–207.

Agyenim Francis, et al, 2011, *Experimental study on the melting and solidification behaviour of a medium temperature phase change storage material (Erythritol) system augmented with fins to power a LiBr/H₂O absorption cooling system*, Renewable Energy 36, 108-117

Agyenim Francis, Hewitt Neil, 2012, *Experimental investigation and improvement in heat transfer of paraffin PCM RT58 storage system to take advantage of low peak tariff rates for heat pump applications*, The International Journal of Low-Carbon Technologies 2012, 1-11, doi:10.1093/ijlct/cts041.

Ahmad Maha, Bontemps Andre', et al, 2006, *Thermal testing and numerical simulation of a prototype cell using light wallboards coupling vacuum isolation panels and phase change material*, Energy and Buildings 38, 673–681

Akhilesh R., Narasimhan Arunn, Balaji C., 2005, *Method to improve geometry for heat transfer enhancement in PCM composite heat sinks*, International Journal of Heat and Mass Transfer 48, 2759–2770.

Alam M et al., 2011, *Vacuum Insulation Panels (VIPs) for building construction industry – A review of the contemporary developments and future directions*, Applied Energy (2011), doi:10.1016/j.apenergy.2011.04.040.

Alexiades V. and Solomon AD., 1993, *Mathematical modelling of melting and freezing processes*. USA: Hemisphere.

Aristov, Y.I., et al., 2010, *Reallocation of adsorption and desorption times for optimisation of cooling cycles*, International Journal of Refrigeration (2010), doi:10.1016/j.ijrefrig.2010.07.019

Arkar C. and Medved S., 2007, *Free cooling of a building using PCM heat storage integrated into the ventilation system*, Solar Energy 81, 1078–1087

Atul Sharma, V.V. Tyagi, C.R. Chen, D. Buddhi, 2009, *Review on thermal energy storage with phase change materials and applications*, Renewable and Sustainable Energy Reviews, Issue 13, 318–345.

Aveyard R. and Haydon D.A., 1973, *An introduction to the principles of surface chemistry*. CUP Archive, 1973.

Ayompe L.M., et al, 2011, *Comparative field performance study of flat plate and heat pipe evacuated tube collectors (ETCs) for domestic water heating systems in a temperate climate*, Energy 36, 3370–3378

Ayompe L.M., Duffy A., 2013, *Thermal performance analysis of a solar water heating system with heat pipe evacuated tube collector using data from a field trial*, Solar Energy 90, 17–28

Azpiazu, M. N., Morquillas, J. M., and Vazquez, A., 2003, *Heat Recovery from a Thermal Energy Storage based on the Ca(OH)₂/CaO Cycle*, Applied Thermal Engineering, 23(6), 733–741.

B

Balasubramanian Ganesh, et al, 2010, *Modeling of thermochemical energy storage by salt hydrates*, International Journal of Heat and Mass Transfer 53 (2010) 5700–5706

Baylin F., 1979, *Low temperature thermal energy storage: a state of the art survey*. Solar Energy Research Institute, USA, Golden, SERI/RR/-54-164.

Bales Chris, et al, 2005, *Thermal Properties of Materials for Thermochemical Storage of Solar Heat*, solar heating and cooling programme, international energy agency

Bales C, 2006, *Solar Energy Research Center (SERC). Chemical and sorption heat storage*. In: Proceedings of DANVAK seminar, DANVAK seminar (solar heating systems – Combisystems – heat storage).

Belén Zalba, et al, 2003, *Review on thermal energy storage with phase change: materials, heat transfer analysis and applications*, Applied Thermal Engineering 23, 251–283.

Boer RD, Haije W, Veldhuis J, Smeding S., 2004, *Solid sorption cooling with integrated storage: the SWEAT prototype*. In: 3rd international heat powered cycles conference—HPC 2004.

Brunner S, Simmler H, 2008, *In situ performance assessment of vacuum insulation panels in a flat roof construction*, Vacuum, Volume 82, Issue 7, 700.

C

Cabeza, L.F., 2005, *Storage Techniques with Phase Change Materials, Thermal energy storage for solar and low energy buildings, State of the art*, the IEA Solar Heating and Cooling Task 32, Seite 77-105

Cabeza, L.F., et al, 2011, *Materials used as PCM in thermal energy storage in buildings: A review*, Renewable and Sustainable Energy Reviews 15, 1675–1695

Caglar Ahmet, Yamalı Cemil, 2012, *Performance analysis of a solar-assisted heat pump with an evacuated tubular collector for domestic heating*, Energy and Buildings 54, 22–28

Carbon factor, 2013, <http://www.energysavingtrust.org.uk/Energy-Saving-Trust/Our-calculations#water>, for further details (accessed 30/10/2013)

CA Group, 2009, *The Solar Wall Perforated Transpired Solar Collector (pTSC)*. See <http://www.cagroupltd.co.uk/>, for further details (accessed 01/10/2013)

Carbonari A., et al, 2006, *Numerical and experimental analyses of PCM containing sandwich panels for prefabricated walls*, Energy and Buildings 38, 472–483

çengel Y, 1998, *Heat transfer-A practical approach*, Mc Graw Hill

Cerón Isabel, Neila Javier, Khayet Mohamed, 2011, *Experimental tile with phase change materials (PCM) for building use*, Energy and Buildings 43, 1869–1874

Chen Chao, et al, 2008, *A new kind of phase change material (PCM) for energy-storing wallboard*, Energy and Buildings 40, 882–890

Crozat G., et al, 1988, *Systems de gestion de L'énergie thermique bases sur des reaction solid-gaz*, Pompes Chaleur Chimiques de Hautes Performances, 2(5), 310-319.

D

- Darkwa, K, 2000, *Thermochemical energy storage in inorganic oxides: an experimental evaluation*, Applied Thermal Engineering 18(6), 387-400
- Darkwa K., Ianakiev A., O'Callaghan P.W., 2006, *Modelling and simulation of adsorption process in a fluidised bed thermochemical energy reactor*, Applied Thermal Engineering 26 (2006) 838-845
- Dincer Ibrahim, 2002a, *Thermal energy storage as a key technology in energy conservation*, Int.J. Energy Res, 26 (7), 567-588.
- Dincer I. and M.A. Rosen, 2002b, *Thermal energy storage systems and applications*, John Wiley & sons, London, 1st Ed, 51-55, 83-152, 335-406.
- Dincer I. and M.A. Rosen, 2010, *Thermal energy storage, systems and applications*, John Wiley & sons, Ltd., London, 2nd Ed, 483-570.
- Ding Yate, Riffat Saffa, 2012, *Thermochemical Energy Storage Technologies for Building Applications: a State-of-the-art Review*, The International Journal of Low-Carbon Technologies 2012, 1-11, doi:10.1093/ijlct/cts004.
- Duffie J. and Beckmann W. A., 1991, *Solar engineering of thermal processes*, John Wiley and Sons, New York, 414-418, 506-507.
- David Tetlow, Francis Agyenim, 2012, *Investigation to standardise thermal performance of a novel domestic UK solar thermal storage with the inclusion of PCM*, 11th International Conferences on Sustainable Energy Technologies (SET-2012), 2-5 September, Vancouver, Canada, ISBN: 0-9781236-1-2

E

- EDSL TAS, Empirical Validation, 2013, Available from: <http://edsl.net/main/Software/Designer/Validation.aspx> (accessed: August.12.2013).
- El-Dessouky H, Al-Juwayhel F., 1997, *The effectiveness of a thermal energy storage system using phase change materials*. Energy Conversion Management; 38(6):601-17.
- Essen Van M, Zondag AH, Schuitema R, van Helden WGJ, Rindt CCM., 2008, *Materials for thermochemical storage: characterization of magnesium sulfate*. In: Proceedings of the Eurosun 2008, 1st international conference on solar heating, cooling and buildings.
- Essen van V.M., H.A. Zondag, J.C. Gores, L.P.J. Bleijendaal, M. Bakker, R. Schuitema, W.G.J. van Helden, Z. He, C.C.M. Rindt, 2009, *Characterization of MgSO₄ hydrate for thermochemical seasonal heat storage*, J. Solar Energy Eng.-Trans. ASME 131 (4). 041014.

Ettouney Hisham M., et al 2004, *Heat transfer enhancement by metal screens and metal spheres in phase change energy storage systems*, Renewable Energy 29, 841–860

Evacuated solar collector, 2013, *Solar collector: Heat Pipe and Direct Flow* <http://www.intelligentenergysolutions.com/journal/2008/03/solar-collectors-heat-pipe-vs-direct-flow/> (accessed: August 20, 2013).

E

Fadhel M.I., Sopian K., Daud W.R.W., 2010, *Performance analysis of solar-assisted chemical heat-pump dryer*, Solar Energy 84, 1920–1928

Fadhel M.I.; Sopian K., Daud W.R.W., Alghoul M.A., 2011, *Review on advanced of solar assisted chemical heat pump dryer for agriculture produce*, Renewable and Sustainable Energy Reviews 15, 1152–1168

Fan Liwu and Khodadadi J.M., 2011, *Thermal conductivity enhancement of phase change materials for thermal energy storage: A review*, Renewable and Sustainable Energy Reviews 15, 24–46

Fricke J., Heinemann U. and Ebert H.P, 2008, *Vacuum insulation panels - From research to market*, Vacuum, Volume 82, Issue 7, 680-690.

Fujimoto S., Bilgen E., Ogura H., 2002, *CaO/Ca(OH)₂ chemical heat pump system*, Energy Conversion and Management 43, 947–960

Fujioka k., et al, 1998, *Measurement of effective thermal conductivity of CaCl₂ reactor beds used for driving chemical heat pumps*, J. Chem. Eng. Japan, 31, 266-272

Fukai J, Hamada Y, Morozumi Y, Miyatake O., 2002, *Effect of carbon-fibre brushes on conductive heat transfer in phase change materials*. Heat and Mass Transfer 45:4781–92.

G

Garg HP, Mullick SC, Bhargava AK., 1985, *Solar thermal energy storage*. Dordrecht: Reidel Publishing Company.

George A., 1989, *Hand book of thermal design*. In: Guyer C, editor. Phase change thermal storage materials. McGraw Hill Book Co.

Ghommem Mehdi, et al, 2011, *Release of stored thermochemical energy from dehydrated salts*, International Journal of Heat and Mass Transfer 54, 4856–4863

Glembin J., Rockendorf G., Scheuren J., 2010, *Internal thermal coupling in direct-flow coaxial vacuum tube collectors*, Solar Energy 84, 1137–1146

Goldstein R.J., et al, 2010, *Heat transfer - A review of 2005 literature*, International Journal of Heat and Mass Transfer 53, 4397–4447

Gustafsson Mari, Bo He, Setterwall Fredrik, 1998, *Paraffin waxes and their mixture as phase change materials (PCMs) for cool storage in district cooling system*. IEA Annex Turkey 10, 45–56.

H

Hadorn J-C, editor. 2005, *Thermal energy storage for solar and low energy buildings—state of the art*. Lleida, Spain: Servei de Publicacions de la Universitat de Lleida.

Halford C.K. and Boehm R.F., 2007, *Modeling of phase change material peak load shifting*, Energy and Buildings 39, 298–305

Halime ö. Päksoy, 2007, *Thermal energy storage for sunsustainable energy consumption - Fundamentals, case studies and design*, Springer, Mathematics, Physics and chemistry Vol. 234.

Hamada Y, Ohtsu W, Fukai J., 2003, *Thermal response in thermal energy storage material around heat transfer tubes: effect of additives on heat transfer rates*. Solar Energy, 75:317–28.

Hamdan MA, Elwerr FA. 1996, *Thermal energy storage using phase change material*. Solar Energy 56(2), 183–9.

Hanneman et al., 1974, *Closed loop chemical systems for energy transmission, conversion and storage*. Proc. 9th Intersoc. Energy Convers. Engng Conf. ASME, pp. 435–441.

Hans Simmler, et al, 2005, *Vacuum Insulation Panels - Study on VIP-components and Panels for Service Life Prediction of VIP in Building Applications (Subtask A)*, High Performance Thermal Insulation, IEA/ECBCS, 4.

Harald Mehling and Luisa F. Cabeza, 2008, *Heat and cold storage with PCM—an up to date introduction into basics and applications*, Springer Verlag Berlin Heidelberg, 1-8, 13-52, 105-204, 217-256.

Hastings R and Wall M., 2007, *IEA Energy Conservation in Buildings & Community Systems Programme*, editors. Sustainable solar housing: exemplary buildings and technologies. Earthscan.

Hauer, A., 2002, *Thermal Energy Storage with Zeolite for Heating and Cooling Applications*, Proc. 3rd Workshop of Annex 17 ECES IA/IEA, 1-2 October, Tokyo, Japan.

Hauer A., 2007a, *Sorption theory for thermal energy storage*. In: Thermal energy storage for sustainable energy consumption. Netherlands: Springer; pp. 393–408.

Hauer, A., and Lavemann, E., 2007b, *Open Absorption Systems for Air Conditioning and Thermal Energy Consumption, Thermal Energy Storage for Sustainable Energy Storage*. Netherlands: Springer, pp. 429-444.

-
- Hauer, A., 2008, *Sorption Storage for Solar Thermal Energy - Possibilities and Limits*. Proc. Eurosun 2008: 1st International Conference on Solar Heating, Cooling and Buildings, Lisbon, Portugal.
- Heim Dariusz and Clarke J. A., 2004, *Numerical modelling and thermal simulation of PCM-gypsum composites with ESP-r*, Energy and Buildings 36, 795-805
- Hodgson, Peter E., 2010, *Energy, the Environment and Climate Change*, Imperial College Press, London, 1-2.
- Hollick JC, 1994, *Unglazed solar wall air heaters*. Renewable Energy 5: 415-421.
- Hongois S, Stevens P, Coince A-S, Kuznik F, Roux J-J., 2008, *Thermochemical storage using composite materials*. In: Proceedings of the Eurosun 2008, 1st international conference on solar heating, cooling and buildings.
- Houghton, J.T., Ding, Y., etc, 2001, *Climate change 2001: the scientific basis*, the press syndicate of the university of Cambridge, UK, 2.
- Henze RH, Humphrey JAC., 1981, *Enhanced heat conduction in phase-change thermal energy storage devices*. Heat Mass Transfer; 24:459-74.
- Herrick S, Golibersuch DC, 1978, *Quantitative behavior of a new latent heat storage device for solar heating/cooling systems*. In: General International Solar Energy Society Conference.

I

- Ibáñez Manuel, et al, 2005, *An approach to the simulation of PCMs in building applications using TRNSYS*, Applied Thermal Engineering 25, 1796-1807
- Ibáñez Manuel, et al, 2006, *Modelization of a water tank including a PCM module*, Applied Thermal Engineering 26, 1328-1333
- Iammak K, Wongsuwan W, Kiatsiriroj T., 2004, *Investigation of modular chemical energy storage performance*. In: The joint international conference on sustainable energy and environment (SEE).
- Inglezakis VJ, Pouloupoulos S., 2006, *Adsorption on exchange and catalysis: design of operations and environmental applications*. Elsevier.
- Ismail K.A.R. and Moraes R.I.R., 2009, *A numerical and experimental investigation of different containers and PCM options for cold storage modular units for domestic applications*, International Journal of Heat and Mass Transfer 52, 4195-4202

J

Jason Makansi and Jeff Abboud, 2002, *Energy Storage, the missing link in the electricity value chain*, the Energy Storage Council, 3-8, 13, 16.

Jeremy Butterfield, 2003 *Collins English Dictionary, complete and unabridged*, HarperCollins, 6th Ed.

K

Kawasaki H, Watanabe T, Kanzawa A., 1999, *Proposal of a chemical heat pump with paraldehyde depolymerization for cooling system*. Applied Thermal Engineering, 19 (2):133-43.

Kato, Y., N. Yamashita and Y. Yoshizawa, 1993, *Study of chemical heat pump with reaction system of magnesium oxide/water*, Kagaku Kogaku Ronbunshu, 19 (6), Japan, 1213-1216.

Kato Yukitaka, Takahashi Fu-uta, Watanabe Akihiko, Yoshizawa Yoshio, 2001, *Thermal analysis of amagnesium oxide/water chemical heat pump for cogeneration*, Applied Thermal Engineering 21, 1067-1081

Kato Yukitaka, Yamashita Norimichi, Kobayashi Kei, Yoshizawa Yoshio, 1996, *Kinetic study of the hydration of magnesium oxide for a chemical heat pump*, Applied Thermal Engineering 16(11), 853-862

Kato Y., 2007, *Chemical energy conversion technologies for efficient energy use*. In: Thermal energy storage for sustainable energy consumption. Netherlands: Springer; pp. 377-91.

Kato Yukitaka, Takahashi Rui, Sekiguchi Toshiya, Ryu Junichi, 2009, *Study on medium-temperature chemical heat storage using mixed hydroxides*, International Journal of Refrigeration, 32(4), 661-666

Kauranen Pertti, et al, 2010, *Temperature optimisation of a diesel engine using exhaust gas heat recovery and thermal energy storage (diesel engine with thermal energy storage)*, Applied Thermal Engineering 30, 631-638

Kenneth Goodier, 1961, *Making and using an expanded plastic*, New Scientist 240, Quickfit and Quartz Ltd, 706.

Kenneth R. Berger and Bruce Welt, 2002, *A Brief History of Packaging*, Institute of Food and Agricultural Sciences, University of Florida, USA.

Kim Tae S., et al., 2011, *Reactivity enhancement of chemical materials used in packed bed reactor of chemical heat pump*, Progress in Nuclear Energy, doi:10.1016/j.pnucene.2011.05.013

Kingspan, 2013, Kingspan Renewables Ltd, a division of Kingspan Group Plc. <http://www.kingspansolar.co.uk/products/16/df100.aspx> (accessed: August 20, 2013).

Kuninari Araki, et al, 2009, *Optimization about multilayer laminated film and getter device materials of vacuum insulation panel for using at high temperature*, journal of materials processing technology 209, 271–282

Kutscher CF, 1996, *Transpired solar collector systems: a major advance in solar heating*. Proceedings of the 19th World Energy Engineering Congress, Atlanta, GA, 6–8 November

Kuznik Frédéric, Virgone Joseph, Johannes Kevyn, 2010, *Development and validation of a new TRNSYS type for the simulation of external building walls containing PCM*, Energy and Buildings 42, 1004–1009

Kwon Jae-Sung, et al, 2009, *Effective thermal conductivity of various filling materials for vacuum insulation panels*, International Journal of Heat and Mass Transfer 52, 5525–5532.

L

Lahmidi H., Mauran S., Goetz V., 2006, *Definition, test and simulation of a thermochemical storage process adapted to solar thermal systems*, Solar Energy 80, 883–893

Lamberg Piia, 2004, *Approximate analytical model for two-phase solidification problem in a finned phase-change material storage*, Applied Energy 77, 131–152

Lane GA and Glew DN, 1975, *Heat of fusion system for solar energy storage*. In: Proceedings of the workshop on solar energy storage subsystems for the heating and cooling of buildings. Virginia: Charlottesville; 43–55.

Levy M., Levitan R., Rosin H., Rubin R., 1993, *Solar energy storage via a closed-loop chemical heat pipe*, Solar Energy, 50 (2), 179–189

Liu Hui, N'Tsoukpoe K. Edem, Le Pierres Nolwenn, Luo Lingai, 2011, *Evaluation of a seasonal storage system of solar energy for house heating using different absorption couples*, Energy Conversion and Management 52, 2427–2436

Liu Z, Sun X, Ma C., 2005, *Experimental investigations on the characteristics of melting processes of stearic acid in an annulus and its thermal conductivity enhancement by fins*. Energy Conversion and Management; 46: 959–69.

Lucelia Taranto Rodriguesa, Mark Gillottb, David Tetlowc, 2013, *Summer overheating potential in a low-energy steel frame house in future climate scenarios*, Sustainable Cities and Society 7 (2013) 1–15

M

Mandelis A, Christofides C., 1993, *Physics and chemistry and technology of solid state gas sensor devices*, illustrated ed., New York: Wiley-Interscience

Mark Zimmermann, et al, 2001, *High performance thermal insulation - vacuum insulated products (VIP)*, International Energy Agency, EMPA, January 22-24.

Mauran S., Lahmidi H., Goetz V., 2008, *Solar heating and cooling by a thermochemical process First experiments of a prototype storing 60 kW h by a solid/gas reaction*, Solar Energy 82, 623-636

Maurice Barakat, 2003, *Transit packaging and temperature-controlled packaging issues*, Business Briefings Ltd, USA.

Mbaye M., Aidoun Z., Valkov V. and Legault A., 1998, *Analysis of chemical heat pumps chps basic concepts and numerical model description*, Applied Thermal Engineering 18, 131-146

McMillan J.A., Peterson E.M., 1979, *Solar simulation with tungsten-halogen quartz lamps and optical filters*, Solar Energy, Volume 22, Issue 5, 467-469

Morrison G.L., 2001, *Solar collectors, Solar Energy: The State of the art, international Solar Energy Society (ISES) Position Papers*, James and James Publishers, London, 145-221.

Murat Kenisarın, Khamid Mahkamov, 2007, *Solar energy storage using phase change materials*, Renewable and Sustainable Energy Reviews, 11, 1913-1965.

N

Nam Jinmoo, Ko Johan, Ju Hyunchul., 2011, *Three-dimensional modelling and simulation of hydrogen absorption in metal hydride hydrogen storage vessels*. Applied Energy (2011), doi:10.1016/j.apenergy.2011.06.015

Nayak K.C., Saha S.K., Srinivasan K., Dutta P., 2006, *A numerical model for heat sinks with phase change materials and thermal conductivity enhancers*, International Journal of Heat and Mass Transfer 49, 1833-1844

NEDO, 1993, *the New Energy and Industrial Technology Development Organization (NEDO)*, in 1993, final report for the project of super heat pump and energy interated system.

Nemanic V, 1995, *Vacuum insulating panel*, Elsevier Science Ltd, Vacuum, volume 46, 839 - 842.

Ng KW, Gong ZX, Mujumdar AS., 1998, *Heat transfer in free convection-dominated melting of a phase change material in a horizontal annulus*. Heat Mass Transfer 25(5), 631-40.

Nkwetta Dan Nchelatebe, et al, 2013, *Experimental performance evaluation and comparative analyses of heat pipe and direct flow augmented solar collectors*, Applied Thermal Engineering 60, 225-233

Norton B., 1992, *Solar energy thermal technology*, Spring-Verlag London Limited, 118-147

N'Tsoukpoe K. Edem, Liu Hui, Le Pierre` s Nolwenn, Luo Lingai, 2009, *A review on long-term sorption solar energy storage*, Renewable and Sustainable Energy Reviews 13, 2385–2396

O

OECD/IEA, 2007, *Renewables in global energy supply*, An IEA fact sheet, International Energy Agency (IEA), France, part 1.

OECD/IEA, 2012, *Key world energy statistics 2012*, International Energy Agency (IEA), France, 30.

Office de la Langue Française (OLF). *Grand Dictionnaire Terminologique*. Québec, Canada. www.olf.gouv.qc.ca.

Ogura H., et al, 1991, *Thermal conductivity analysis of packed bed reactor with heat transfer fin for Ca(OH)₂/CaO chemical heat pump*, Kagaku-kogaku Ronbunshu, 17(5), 916-923.

Ogura Hironao, Yamamoto Tetsuya, Kage Hiroyuki, 2003, *Efficiencies of CaO/H₂O/Ca(OH)₂ chemical heat pump for heat storing and heating/cooling*, Energy 28, 1479–1493

Omer Siddig, 2009, *Solar thermal systems design exercise - part 3*, renewable energy technology 2, handout 2009-2010, 8-9

P

PCM products, 2013, http://www.pcmproducts.net/Phase_Change_Material_Products.htm, ((accessed 30/12/2013)).

Perry, Robert H. and Green, Don W., 1984, *Perry's Chemical Engineers' Handbook*, eighth ed., McGraw-Hill Professional Publishing.

Phalguni Mukhopadhyaya, 2006, *High Performance Vacuum Insulation Panel - Research Update from Canada*, Global Insulation Magazine, 9-15.

Posern K., Kaps C., 2008, *Humidity controlled calorimetric investigation of the hydration of MgSO₄ hydrates*, J. Therm. Anal. Calorim. 92 (3) (2008) 905–909.

Posern K., Kaps Ch., 2010, *Calorimetric studies of thermochemical heat storage materials based on mixtures of MgSO₄ and MgCl₂*, Thermochemica Acta 502, 73–76

R

Ravikumar M. and Srinivasan Pss., 2008, *Phase change material as thermal energy storage material for cooling of building*, Journal of Theoretical and Applied Information Technology

Richard T. Bynum Jr., 2001, *Insulation handbook*, the McGraw-Hill Companies, Inc. 21-28, 214.

Riffat S.B., 2000, *UK Patent, Publication No. GB2347202, Heat Transfer Device*, University of Nottingham, 2000.

Riffat S.B., Omer S.A. and Ma Xiaoli, 2001, *A novel thermoelectric refrigeration system employing heat pipes and a phase change material: an experimental investigation*, *Renewable Energy* 23, 313–323

Riffat Saffa, Su Yuehong, Ding Yate, 2013, *Thermochemical cooling system based on adsorption pumping pipe*, *The International Journal of Low-Carbon Technologies* 2013, 1-7, doi:10.1093/ijlct/ctt055.

Robak C. W., Bergman T. L., Faghri A., 2011, *Enhancement of latent heat energy storage using embedded heat pipes*, *International Journal of Heat and Mass Transfer* 54, 3476–3484

Roland Caps, et al, 2008, *Quality control of vacuum insulation panels: Methods of measuring gas pressure*, Elsevier Ltd., *Vacuum* 82, 691–699

Ruben Baetens, et al, 2010, *Vacuum insulation panels for building applications: A review and beyond*, *Energy and Buildings* 42 (2010), 147–172.

S

Sapienza Alessio, Glaznev Ivan S., Santamaria Salvatore, Freni Angelo, Aristov Yuriy I., 2012, *Adsorption chilling driven by low temperature heat: New adsorbent and cycle optimization*, *Applied Thermal Engineering* 32, 141-146

Sari A, Kaygusuz K., 2002, *Thermal and heat transfer characteristics in a latent heat storage system using lauric acid*. *Energy Conversion and Management* 43, 2493–507.

Sharma SD, Kitano H, Sagara K, 2004, *Phase change materials for low temperature solar thermal applications*. *Res Rep Fac Eng Mie Univ*, Vol. 29, 31–64.

Sharonov V.E., Aristov Yu.I., 2008, *Chemical and adsorption heat pumps: Comments on the second law efficiency*, *Chemical Engineering Journal* 136, 419–424

Solomon A. D., 1979, *Melt time and heat flux for a simple PCM body*, *solar energy* 22, 251-257.

Soteris A. Kalogirou, 2003, *The potential of solar industrial process heat applications*. *Applied Energy* 2003; 76:337–61.

Soteris A. Kalogirou, 2004, *Solar thermal collectors and applications*, *Progress in Energy and Combustion Science* 30 (2004) 231–295

Soutullo S., Juan C. San, Heras M.R., 2011, *Comparative study of internal storage and external storage absorption cooling systems*, *Renewable Energy* 36, 1645-1651

Srivastava NC, Eames IW., 1998, *A review of adsorbents and adsorbates in solidvapour adsorption heat pump systems*. Applied Thermal Engineering, 18(9-10):707-14.

Stach H., Mugele J., Janchen J., Weiler E., 2005, *Influence of cycle temperatures on the thermochemical heat storage densities in the systems water/microporous and water/mesoporous adsorbents*, Adsorp.-J. Int. Adsorp. Soc. 11 (3-4) 393-404.

Stitou D, et al., 2011, *Experimental investigation of a solid/gas thermochemical storage process for solar air conditioning*, Energy (2011), doi:10.1016/j.energy.2011.07.029

Struckmann F., 2008, *Analysis of a flat-plate solar collector*, 2008 MVK160 Heat and Mass Transport, Project Report, Lund Sweden, 8th May 2008.

I

Tahat M.A., Babus'Haq R.F., O'Callaghan P.W., Probert S.D., 1995, *Performance of an integrated thermochemical heat pump/energy store*, Thermochemica Acta 255, 39-47

Tan F.L., et al, 2009, *Experimental and computational study of constrained melting of phase change materials (PCM) inside a spherical*, International Journal of Heat and Mass Transfer 52, 3464-3472

Tang Runsheng, Gao Wenfeng, Yu Yamei, Chen Hua , 2009, *Optimal tilt-angles of all-glass evacuated tube solar collectors*, Energy 34, 1387-1395

Taube M., et al., 1980, *Opportunities and limitations for the use of ammoniated salts as a carrier for thermochemical energy storage*, Int. Seminar on Thermochemical Energy Storage , Stockholm, PP. 349-369.

Tay NHS et al, 2011, *Experimental investigation of tubes in a phase change thermal energy storage system*. Applied Energy, doi:10.1016/j.apenergy.2011.05.026

Tamainot-Telto Z., and Critoph R.E., 2001, *Monolithic carbon for sorption refrigeration and heat pump applications*, Applied Thermal Energy, 21(1), 37-52

Tenpierik M, Cauberg H., 2006, *Vacuum insulation panel: friend or foe*, Proceeding of 23rd conference on passive and low energy architecture, Geneva, Switzerland.

Tian Y., Zhao C.Y., 2013, *A review of solar collectors and thermal energy storage in solar thermal applications*, Applied Energy 104, 538-553

U

UKHouse,2013,http://www.dimplex.co.uk/assets/Downloads_Documents/Running_Cost_Assumptions.pdf, UK household Running Cost Assumptions, for further details (accessed 30/10/2013)

V

Van de Voort I.M., 2007, *Master Thesis: Characterization of a thermochemical storage material*, Eindhoven University of Technology

Visscher, K., Veldhuis, J.B.J., Oonk, H.A.J., Van Ekeren, P.J., Blok, J.G., 2004, *Compacte chemische seizoensopslag van zonnearmte* ECN-C-04-074

Visscher K, Veldhuis JBJ., 2005, *Comparison of candidate materials for seasonal storage of solar heat through dynamic simulation of building and renewable energy system*. In: Proceedings of the ninth international building performance simulation association.

W

WBGU, 2012, *World in Transition, towards sustainable energy systems*, Earthscan, London.

Walter Soroka, 2010, *Fundamentals of Packaging Technology*, Institute of Packaging Professionals, 4th Ed.

Wang Cheng, Zhang Peng and Wang Ruzhu, 2008, *Review of Recent Patents on Chemical Heat Pump*, Recent Patents on Engineering, 2, 208-216, Bentham Science Publishers Ltd.

Wang Zhangyuan, 2011, PhD Thesis: *Investigation of a Novel Façade-Based Solar Loop Heat Pipe Water Heating System*, University of Nottingham.

Wang LW, Wang RZ, Oliveira RG., 2009 *A review on adsorption working pairs for refrigeration*. Renewable and Sustainable Energy Reviews, 13(3):518-34

Wang Y, Amiri A, Vafai K., 1999, *An experimental investigation of the melting process in a rectangular enclosure*. Heat and Mass Transfer; 42: 3659-72.

Wettermark G., et al., 1979, *Storage of heat, A survey of efforts and possibilities*, Swedish Council for Building Research.

Wongsuwan W., Kumar S., Neveu P., Meunier F., 2001, *A review of chemical heat pump technology and applications*, Applied Thermal Engineering 21, 1489-1519

Wu Huijun, Wang Shengwei, Zhu Dongsheng, Ding Yunfei, 2009, *Numerical analysis and evaluation of an open-type thermal storage system using composite sorbents*, International Journal of Heat and Mass Transfer 52, 5262-5265

Wu Liuren, 2014, <http://faculty.baruch.cuny.edu/lwu/3000/Chapter6.ppt>, (accessed 20/05/2014)

X

Xiao Wei, Wang Xin, Zhang Yinping, 2009, *Analytical optimization of interior PCM for energy storage in a lightweight passive solar room*, Applied Energy 86, 2013–2018

Z

Zhang Dahai, Fung Alan S., Siddiqui Omar, 2007, *Numerical studies of integrated concrete with a solid-solid phase change material*, 2nd Canadian Solar Buildings Conference, Calgary, June 10 – 14

Zhao C.Y., Lu W., Tian Y., 2010, *Heat transfer enhancement for thermal energy storage using metal foams embedded within phase change materials (PCMs)*, Solar Energy 84, 1402–1412

Zhao C.Y., Wu Z.G., 2011, *Heat transfer enhancement of high temperature thermal energy storage using metal foams and expanded graphite*, Solar Energy Materials & Solar Cells 95, 636–643

Zhang Wei, 2010, PhD Thesis: *A solar powered ejector air conditioning system for Mediterranean climate*, University of Nottingham, 7–15.

Zhuang Chun-long, et al, 2010, *Validation of Veracity on Simulating the Indoor Temperature in PCM Light Weight Building by EnergyPlus*, Lecture Notes in Computer Science, Volume 6328/2010, 486–496,

APPENDICES

Appendix I: Water Pump Flow Meter Reference K Factor

Calibration Report

Serial Number:	OG41922	Job Number:	12897
Meter Size:		Save File Name:	OG41922
Bearing Type:	St.Steel/Peek	LtModel Number:	OG4 St.Steel
Sensor PN/SN:		Meter Tag:	OG4-SU5-VRT-B
Ambient Temperature:	20.00 °C	End Fittings:	3/4" BSP
		Sensor Type:	Reed Switch
		Sensor Output:	Pulse
		Meter Density:	0.998 kg/l

Meter Rate (l/min)	Meter Frequency (Hz)	Meter K-factor (p/lit)	Meter Pressure (bar)
2.4890	4.78375	115.32	5.52
9.3260	17.98721	115.72	5.52
15.9915	30.67998	115.11	5.52
23.0917	44.10099	114.59	5.52
30.2577	57.64399	114.31	5.52
36.4307	69.32169	114.17	5.52
40.5282	76.98822	113.98	5.52
49.9087	94.63302	113.77	5.52

Calibrator Inv #:	Calibrated By:	S. Sweet
Recal Date:	Date:	10/04/2012
Procedure:	Certified By:	

Traceability:

Notes:

Maximum Operating Temperature 150oC.

Appendix II: Water Absorption of Thermochemical Materials

Materials	Tray & Absorbent (g)	Absorbent (g)	Absorbent & Water (g)	Water (g)	Water Absorption (1KG)
Silica Gel	720	400	604	204	510.00
Zeolite 13X	690	350	507	157	448.57
Vermiculite	520	200	256	56	280.00
Activated Carbon	740	400	559	159	397.50

Appendix III: the Basic Parameters Applied to Calculation

Parameters	Value	Parameters	Value
C_w	4.2 kJ/kg.K	C_a	1.01 kJ/kg.K
ρ_w	1.0 kg/m ³	ρ_a	1.07 kg/m ³
A_s	3.0 m ²	V_{count}	3.0 m/s
K_{pump}	115.72 p/lit	A_f	0.07 m ²